



HAL
open science

Nanotechnologie et assemblages collés : étude des performances mécaniques d'un adhésif dopé par des nanocharges

Sabrine Khammassi

► **To cite this version:**

Sabrine Khammassi. Nanotechnologie et assemblages collés : étude des performances mécaniques d'un adhésif dopé par des nanocharges. Matériaux et structures en mécanique [physics.class-ph]. ENSTA Bretagne - École nationale supérieure de techniques avancées Bretagne, 2021. Français. NNT : 2021ENTA0021 . tel-04457303

HAL Id: tel-04457303

<https://theses.hal.science/tel-04457303v1>

Submitted on 14 Feb 2024

HAL is a multi-disciplinary open access archive for the deposit and dissemination of scientific research documents, whether they are published or not. The documents may come from teaching and research institutions in France or abroad, or from public or private research centers.

L'archive ouverte pluridisciplinaire **HAL**, est destinée au dépôt et à la diffusion de documents scientifiques de niveau recherche, publiés ou non, émanant des établissements d'enseignement et de recherche français ou étrangers, des laboratoires publics ou privés.

PHD THESIS

ECOLE NATIONALE SUPERIEURE
DE TECHNIQUES AVANCEES BRETAGNE

ECOLE DOCTORALE NO. 602
Engineering Sciences
Speciality: *Mechanics of Solids, Materials, Structures and Surfaces*

By **Sabrina KHAMMASSI**

Nanotechnology and bonded joints: An investigation of the mechanical performance of an adhesive doped with nanofillers

Thesis presented and defended in Brest on 14 / 12 / 2021

Research Unit : Institut de Recherche Dupuy de Lôme – UMR CNRS 6027

Jury panel:

Defending reporters :

Michel POTIER-FERRY
Redouane ZITOUNE

Professeur, LEM3, Université Lorraine, Metz
Professor, Université Paul Sabatier, Toulouse

Examiners:

Adil BENAARBIA
Francisco CHINESTA
Mohamed ELMANSORI
Bruno MORTAIGNE
Daniela PLACHA

Associate Professor, Arts et Métiers, Metz
Professor, Arts et Métiers, Paris
Professor, Arts et Métiers ParisTech ENSAM, Metz
Materials Specialist, Délégation générale pour l'armement (DGA)
Professor, VSB, Technical University of Ostrava, Rép. Tchèque

Thesis supervisor:

Mostapha TARFAOUI

Professor, ENSTA Bretagne, Brest

Acknowledgments

First and foremost, I would like to thank Allah Almighty for His grace, mercy, and help in every step of this project, because without Him, it wouldn't have been possible to complete this work successfully. After His grace, I hereby acknowledge the valuable support and guidance of my supervisor, Pr. Mostapha TARFAOUI from ENSTA Bretagne. I would like to wholeheartedly pay my respect and show my gratitude, as without their support, guidance, trust, and assistance this work would not be presented in this form. Specifically, constant encouragement, insights, thoughtful guidance, and the timely advice of Pr. Tarfaoui have helped me greatly in achieving my ambition and in taking on greater challenges. His inquiries always encouraged me to seek out higher quality and his advice guided me through hard times and helped me finish tasks within the allocated time.

I would also like to send my deepest regards to ENSTA Bretagne institute for accepting me for this great opportunity and for providing me with a platform to conduct my research and convert my dream into reality. In continuity, I would like to thank the technical staff and lab engineers, especially Frederic MONTEL, Raphaël PONCIN, and Sébastien BOURCHIS, who assisted me throughout my experimental procedures and with whom I worked as a team to overcome any hurdles that could have halted my research.

I would also like to acknowledge the patience and support of my father Ali KHAMMASSI and my mother Fatma REZGUI, who supported me to fulfill my dream and who believed in me. They supported me throughout my whole student life and in my career. They dreamed of this goal with me and being a Ph.D. doctorate is as equally their achievement as it is mine.

I would like to give thanks to all my colleagues Hamza BEN YAHIA, Yumna QURESHI, and Manel CHIHI, for their support and encouragement.

General introduction

Chapter I: State of The Art

I. State of the Art	30
I.1 Introduction	32
I.2 Adhesives.....	39
I.3 Types of Adhesives	41
I.3.1 Reactive acrylic-based adhesives	42
I.3.2 Polyurethane adhesives	42
I.3.3 Epoxy-based adhesives	42
I.4 Adhesively-bonded structures	43
I.4.1 Surface treatments	43
I.4.2 Interphase concept.....	44
I.5 Types of adhesively-bonded joints, their benefits and limitations	45
I.5.1 Metal to metal bonding	45
I.5.2 Bonding composite to composite	45
I.5.3 Composite to metal bonding	48
I.6 Parameters that affect the performance of bonded joints	50
I.6.1 Surface preparation	50
I.6.2 Adhesive bond configuration	51
I.6.2.1 Joint parameters.....	51
I.6.2.2 Adhesive layer thickness	52
I.6.2.3 Overlap length	53
I.6.3 Environmental factors	53
I.6.3.1 Moisture.....	53
I.6.3.2 Temperature.....	54
I.7 Characterization of mechanical properties	54
I.8 Enhancement of adhesive performance	54
I.8.1 Z-pining.....	55

I.8.2	Stitching	58
I.8.3	Adding inter-adherent glass fibers	63
I.9	Adhesive enhancement	64
I.9.1	The principle of nanocomposite	65
I.9.1.1	Matrix	66
I.9.1.2	Nanodimensional phase	66
I.9.1.3	Carbon Black (CB)	67
I.9.1.4	Metallic powder	68
I.9.1.5	Graphene Nanoplatelets (GNPs)	69
I.9.1.6	Graphite	69
I.9.1.7	Diamond	70
I.9.1.8	Fullerene	70
I.9.1.9	Carbon nanotubes (CNTs)	70
I.9.1.10	Single-walled nano-tube (SWCNT)	72
I.9.1.11	Multiplied walled nanotubes (MWCNTs)	73
I.9.2	Influences of Nanofillers on adhesive performances	74
I.9.2.1	Metallic Nanoparticles	74
I.9.2.2	Carbon nanotubes (CNT)	75
I.9.2.3	Graphene and Fullerene	79
I.9.3	Effects of the excess amount of nanofillers on adhesives	82
I.10	Conclusion	85
II.	Methodology	88
II.1	Introduction	89
II.2	Resin	89
II.3	Nanoparticles	91
II.3.1	Carbon nanotubes (CNTs)	91
II.3.2	Graphene	92
II.3.3	Carbon Black	95
II.3.3.1	Particle Size	96
II.3.3.2	Structure	97
II.3.3.3	Surface Chemistry	98
II.3.3.4	Aggregate Size	98

II.3.3.5	Aggregate Shape.....	99
II.4	Dispersion and implementation of nanofiller-doped adhesive resin	99
II.4.1	Graphene and Carbon Black dispersion	100
II.4.2	CNT dispersion with planetary agitators.....	102
II.5	Homogeneity optimization via DIGIMAT	104
II.5.1	Clustering	104
II.5.2	Cluster size distribution.....	105
II.6	Microstructural study.....	106
II.6.1	Differential Scanning Calorimetry (DSC).....	106
II.6.2	Micro-indentation.....	108
II.7	Mechanical Characterization of Nanocomposites	111
II.7.1	Static tests: Mechanical test bench – INSTRON	111
II.7.2	Compression Test.....	115
II.8	Study of the dynamic behavior of nanocomposites.....	117
II.9	Conclusion	125
III.	Physico-chemical properties	128
III.1	Introduction	129
III.2	Thermal properties.....	129
III.3	Mechanical properties on a local scale	132
III.3.1	CNTs/ DGEBA epoxy nanocomposite	136
III.3.2	GNPs/DGEBA epoxy nanocomposite	141
III.3.3	CBs/DGEBA epoxy nanocomposite	145
III.3.4	Comparative analysis with different nanoparticles (CNTs/ GNPs /CBs) reinforced DGEBA adhesive.....	151
III.4	Conclusion	155
IV.	Quasi-static properties.....	159
IV.1	Introduction	160
IV.2	Tensile Test.....	160

IV.2.1	CNT-reinforced DGEBA adhesive nanocomposite	162
IV.2.2	GNP-reinforced DGEBA adhesive nanocomposite	165
IV.2.3	CB reinforced DGEBA adhesive nanocomposite	167
IV.2.4	Comparison analysis	169
IV.3	Compression test.....	172
IV.3.1	CNT reinforced DGEBA epoxy nanocomposite.....	174
IV.3.2	GNP reinforced DGEBA epoxy nanocomposite.....	178
IV.3.3	CB reinforced DGEBA epoxy nanocomposite	182
IV.3.4	Comparative analysis	185
IV.4	Conclusion	188
V.	Dynamic behavior of adhesive doped with nanofillers.....	191
V.1	Introduction	192
V.2	Overview	192
V.3	Influence of nanofillers CNTs, CBs, GNPs on the dynamic velocity of nanocomposites based DGEBA adhesive	195
V.4	Effects of CNTs, GNPs, CBs on DGEBA adhesive Nanocomposites': Dynamic Behavior.....	198
V.4.1	Strain rate sensitivity	199
V.4.2	Stress-strain behavior	204
V.4.3	Comparison analysis	212
V.5	Conclusion.....	227
VI.	Fracture resistance of a nanofiller-doped adhesive for bonded joints	230
VI.1	Introduction	232
VI.2	Surfaces treatments.....	233
VI.3	Experimental procedure.....	236
VI.4	Analytical calculation of strain energy release rate for Mode I (G_I).....	237
VI.4.1	MBT 1 (Modified Beam Theory 1).....	237
VI.4.2	MBT 2 (Modified Beam Theory 2).....	238

VI.4.3	CBBM (Compliance Based Beam Method).....	238
VI.4.4	CC (Compliance Calibration Method)	239
VI.5	Analytical calculation of Strain energy release rate for Mode II (G_{II})	239
VI.5.1	Simple Beam Theory (SBT).....	239
VI.5.2	Timoshenko Beam Theory (TBT).....	240
VI.6	DCB Testing	241
VI.6.1	DCB Test Samples	241
VI.6.2	DCB test results.....	243
VI.6.3	Bonded joints with neat DGEBA adhesive	244
VI.6.4	Graphene nanoplatelets (GNP) reinforced adhesive for bonded joints.....	246
VI.6.5	Carbon nanotubes (CNT) reinforced adhesive for bonded joints	248
VI.6.6	Fracture surface analysis	252
VI.6.6.1	Fracture surface analysis of CNT reinforced adhesive for bonded joint	256
VI.6.6.2	Fracture surface analysis of GNP reinforced adhesive for bonded joint	259
VI.6.6.3	Comparative analysis of the surface roughness parameters	261
VI.7	ENF Testing.....	262
VI.7.1	ENF Test Samples	262
VI.7.2	Experiment results.....	264
VI.7.3	Comparative analysis	270
VI.8	Numerical investigation using cohesive zone models	274
VI.8.1	Modeling	275
VI.8.2	. Conclusion.....	283

List of Figures

General introduction

Chapter I: State of The Art

Figure 1: Bonded joint revolution	18
Figure 2: Areas of application for bonded joints.....	19
Figure 3: Bonded Joint Composition	20
Figure 4: Adhesively-bonded joint on Helicopter blades.....	20
Figure 5: Adhesively-bonded joint on LEAP (Leading Edge Aviation Propulsion) engine....	21
Figure 6: Naval structure adhesive-bonded joint example.....	21
Figure 7: Naval structure degradation	22
Figure 8: Aeronautical structure degradation.....	23
Figure 9: Aeronautical structure degradation.....	25
Figure I.1: Boat Structure [3]	33
Figure I.2: Riveted joints belong to boat structure [4]	33
Figure I.3: Bonded Joint.....	34
Figure I.4: Composite damage after bearing failure [5].....	34
Figure I.5: Welding joint belong boat structure [6]	35
Figure I.6: Different types of welding.....	35
Figure I.7: Laser welding	35
Figure I.8: Adhesively-bonded joint belong boat structure [11].....	36
Figure I.9: Adhesively-bonded joint	38
Figure I.10: Stress concentration in the bonded joint [22].....	39
Figure I.11: Identification of hybrid joints	39
Figure I.12: Wetting surfaces with adhesive	41
Figure I.13: Adhesive bonding metal to metal	45
Figure I.14: Composite single lap joint	47
Figure I.15: Various failure modes possible with bonding composite to composite [55]	48
Figure I.16: A typical hybrid joint specimen [5].....	49
Figure I.17: Load applicated on hybrid joint.....	50
Figure I.18:Adhesive variety according to the Stress/Strain link.....	51
Figure I.19: Cleavage or peel owing to an impact (or static).....	51
Figure I.20 : Modifications to basic lap joint	52
Figure I.21 : Examples of good and bad designs	52
Figure I.22: SLJ reinforced with Z-pinning	56
Figure I.23: Load vs displacements with different Z-pins' diameters	56
Figure I.24: Load vs displacements with different Z-pins' spacing	56
Figure I.25: Influence of pinned structure on the moisture absorption	57
Figure I.26: Schematic representation of the different steps of toughening processes with the z-pin method.....	57
Figure I.27: SEM micrographs of the delamination around z-pin reinforcements [97].....	58
Figure I.28: Specimen of 3D stitched woven composites [106]	58

Figure I.29: EMAA stitch bridging the delamination crack in the composite (The stitches consist of poly (ethylene-co-(methacrylic acid)) (EMAA) filament)	59
Figure I.30: Effect of the unstitched and stitched adhesive-bonded joint on the evolution mode I interlaminar fracture toughness [102]	59
Figure I.31: Influence of thread pretension on the peel stress distributions	59
Figure I.32: Influence of stitch density on the peel stress distributions	59
Figure I.33: Difference in strain energy release and stitch stress vs delamination length between unstitched and stitched specimens.....	60
Figure I.34: Damaged stitched specimen for out-of-plane tests [113].....	62
Figure I.35: Crack owing to the stitching thread.....	62
Figure I.36: Porous microstructure of EMAA stitch.....	62
Figure I.37: Influence of stitching on the bending stress-time curve for shifted BLJ samples [98]	63
Figure I.38: Sample of the joint with fiber [8]	64
Figure I.39: Incorporation of fiber [8].....	64
Figure I.40: Type of failure with including glass fiber [8].....	64
Figure I.41: Fracture toughness values for a variety of nanofillers.....	67
Figure I.42: Carbon Black particle (CB) [122]	68
Figure I.43: Carbon Black structures [122].....	68
Figure I.44: Multilayer Graphene.....	69
Figure I.45: Buckyball.....	70
Figure I.46: Morphology of random distribution of nanotubes with epoxy matrix [128].....	71
Figure I.47: Single-walled nano-tubes (CNT).....	73
Figure I.48: Kind types of Single-walled Carbon [122].....	73
Figure I.49: multi-walled carbon nanotubes (MWCNTs)	74
Figure I.50: Influence of adding 3% of Carbon Nanotube (CNT) on the adhesive strength [144]	76
Figure I.51: CNT+PVP	77
Figure I.52: Mechanical proprieties of the epoxy adhesive reinforced with the CNT & PVP	77
Figure I.53: Deviation of a micro crack in the reinforced adhesive layer with MWCNTs [14]	78
Figure I.54: Distribution of MWCNT on the fracture surface [27]	78
Figure I.55: SEM image of the distribution of multi-walled carbon nanotubes in the epoxy adhesive.....	78
Figure I.56: Influence of adding 1% Carbon Nanotube, Graphene, and Fullerene onto a different type of adhesive.....	80
Figure I.57: Influence of CNT and GONR on the adhesive performances.....	81
Figure I.58: Influence of different percentages of the nanofillers in the epoxy adhesive on the lap shear strengths	82
Figure I.59: Agglomerated at the level of an adhesive layer with 0.8 wt% of MWCNTs [14]	83
Figure I.60: The progress of the fracture surface with different percentages of CNT in Epoxy showed by SEM image ((a) 0.2% CNT, (b) 0.5% CNT, (c) 1 % CNT and (d) 2% CNT) [13]	83
Figure I.61: The progress of the fracture surface with different percentages of CNT in Epoxy showed by SEM image ((a) 0.2%NGP, (b) 0.5%NGP, (c) 1% GNP and (d) 2%NGP) [13] ...	84

Figure I.62: The progress of the fracture surface with different percentages of CNT in Epoxy showed by SEM image((a) 0.2% CNH, (b) 0.5% CNH, (c) 1% CNH and (d) 2% CNH) [13]	84
Figure I.63: STEM micrographs of adhesive reinforced with 2wt.% CNT & PVP.....	84
Figure I.64: STEM micrographs of adhesive reinforced with 3wt.% CNT & PVP.....	84

Chapter II: Methodology

Figure II.1: Reaction of epichlorohydrin (chloro-1-epoxy-2.3-propane) and bisphenol A (diphyllopropane).....	90
Figure II.2: Relationship structure properties	90
Figure II.3: (a) Single-walled carbon nanotube and (b) multi-walled carbon nanotube	92
Figure II.4: (a) The structure of graphene (b) Large pieces placed on SiO ₂ wafer prepared by "Sellotape method"	93
Figure II.5: Graphene derived nanoparticles: (a) Graphene oxide (GO), (b) Fluorographene, (c) Graphene Nanoplatelets (GNP).....	95
Figure II.6: Spherical CB Structure.....	96
Figure II.7: Carbon Black Particle Dimension Comparison	97
Figure II.8: Carbon Black Structure	97
Figure II.9: surface area Comparison of diverse particles structures [50]	98
Figure II.10: Manufacturing CBs-GNP-reinforced DGEBA epoxy nanocomposite	101
Figure II.11: Manufacturing CNT-reinforced DGEBA epoxy nanocomposite	103
Figure II.12: Simulation of dispersion modes of CB-GNP-CNT nanofillers in DGEBA Adhesive using DIGIMAT	105
Figure II.13: DSC machine	107
Figure II.14: DSC sample preparation steps	107
Figure II.15: Micro-indentation machine	108
Figure II.16: Steps of surface sample preparation.....	110
Figure II.17: Indentation depths expression	111
Figure II.18: Tensile test with INSTRON machine	114
Figure II.19: Compression test under INSTRON machine	116
Figure II.20: Split HOPKINSON bar apparatus.....	117
Figure II.21: Schematic description of the Hopkinson bar device	118
Figure II.22: Principle of wave propagation, Lagrange diagram (the length of the sample is exaggerated to show the reverberation of the waves in the sample)	119
Figure II.23: Schematic description of the punching effect during dynamic compression using Hopkinson bar	125

Chapter III: Physico-chemical properties

Figure III.1: Glass transition temperature for reinforced DGEBA epoxy nanocomposite (a) CNTS (b) GNPS S (c) CB.....	130
Figure III.2: Micro-indentation tests on neat DGEBA adhesive sample	134
Figure III.3: Repeatability of the load-displacement response of micro-indentation test on CNT-reinforced DGEBA adhesive nanocomposite sample	135
Figure III.4: Repeatability of the load-displacement response of micro-indentation test on GNP-reinforced DGEBA adhesive nanocomposite sample	135

Figure III.5: Repeatability of the load-displacement response of micro-indentation test on CB-reinforced DGEBA adhesive nanocomposite sample	136
Figure III.6: Influence of CNTs nanofillers on the mechanical performance of the DGEBA adhesive.....	137
Figure III.7: Variation of micromechanical properties of CNTs/DGEBA nanocomposite ...	140
Figure III.8: Print Indentations of Vickers microhardness for CNT/DGEBA nanocomposite	141
Figure III.9: Influence of GNPS S nanofillers on the mechanical performance of the DGEBA adhesive.....	142
Figure III.10: Variation of micromechanical properties of GNPs /DGEBA nanocomposite	144
Figure III.11: Print Indentations of Vickers microhardness for GNPs /DGEBA nanocomposite	145
Figure III.12: Influence of CBs nanofillers on the mechanical performance of the DGEBA adhesive.....	146
Figure III.13: Variation of micromechanical properties of CB/DGEBA nanocomposite.....	147
Figure III.14: Print Indentations of Vickers microhardness for CBs/DGEBA nanocomposite	149
Figure III.15: Comparison of the load-displacement curve for reinforced DGEBA with nanofillers (CNT, GNP, CB) under different mass fraction	151
Figure III.16: Comparison of the different micromechanical properties for reinforced DGEBA with nanofillers (CNT, GNP, CB) under a different mass fraction.....	152

Chapter IV: Quasi-static properties

Figure IV.1: Dumbbell sample of neat DGEBA epoxy nanocomposite under tensile test	161
Figure IV.2: Test reproducibility of (a) the neat adhesive and (b) 1wt.% CB/DGEBA under tensile test.....	162
Figure IV.3: Stress-strain curves of carbon nanotube-reinforced composite under different wt.% for uniaxial tensile tests.....	163
Figure IV.4: Stress-strain curves of Graphene reinforced adhesive nanocomposite under different wt.% for uniaxial tensile tests.....	165
Figure IV.5: Stress-strain curves of carbon black reinforced adhesive nanocomposite under different wt.% for uniaxial tensile tests.....	168
Figure IV.6: Stress-strain comparison curves of different categories of reinforced adhesive nanocomposite under different wt.% for uniaxial tensile tests	170
Figure IV.7: Diagram of Young modulus progress of different categories of reinforced adhesive under uniaxial tensile tests	171
Figure IV.8: Carbon black, Carbon nanotube, Graphene, 0D, 1D, and 2D materials.....	171
Figure IV.9: Stress-strain curves of neat DGEBA epoxy nanocomposite for uniaxial compressive.....	172
Figure IV.10: Test reproducibility of (a) the neat adhesive and (b) 1wt.% CBs/DGEBA adhesive under compressive test	173
Figure IV.11: SEM images of neat DGEBA epoxy nanocomposite.....	174
Figure IV.12: Surface Photographic images of neat DGEBA epoxy nanocomposite after compression.....	174

Figure IV.13: Stress-strain curves of carbon nanotube-reinforced composite under different wt.% for uniaxial compressive tests	176
Figure IV.14: Surface Photographic images of CNTs/DGEBA epoxy nanocomposite with different wt.% after compression	177
Figure IV.15: SEM images of CNTs/DGEBA adhesive nanocomposite.....	178
Figure IV.16: Stress-strain curves of Graphene reinforced composite under different wt.% for uniaxial compressive tests	179
Figure IV.17: Surface photographs of GNP/DGEBA epoxy nanocomposite with different wt.% after compression	181
Figure IV.18: Photographs of GNP reinforced DGEBA adhesive nanocomposite samples (5wt.% GNP loading) before and after the compressive tests.....	182
Figure IV.19: Stress-strain curves of Carbon Black-reinforced adhesive nanocomposite under different wt.% for uniaxial compressive tests	183
Figure IV.20: Surface photographs of CB/DGEBA adhesive nanocomposite with different wt.% after compression	185
Figure IV.21: Stress-strain comparison curves of different categories of reinforced adhesive nanocomposite under different wt.% for uniaxial compressive tests	187
Figure IV.22: Diagram of Young modulus progress of different categories of reinforced adhesive under uniaxial compressive tests	187
Figure IV.23: Deformation and failure progress of different 1wt.% (CNT/GNP/CB) reinforced adhesive under compressive test	188

Chapter V: Dynamic behavior of adhesive doped with nanofillers

Figure V.1: Strain Rate vs. Strain of CNTs/DGEBA, GNPs/DGEBA, CBs/DGEBA under 4 bar impact pressure.....	193
Figure V.2: Test reproducibility under 1.5bar, Neat adhesive	195
Figure V.3: The Velocity –time curves of CNT-reinforced DGEBA epoxy nanocomposite for different impact pressure	196
Figure V.4: The Velocity –time curves of GNP-reinforced DGEBA epoxy nanocomposite for different impact pressure	197
Figure V.5: The Velocity–time curves of CB-reinforced DGEBA epoxy nanocomposite for different impact pressure	198
Figure V.6: The Strain rate–time curves of CNT-reinforced DGEBA epoxy nanocomposite for different impact pressure	200
Figure V.7: The Strain rate–time curves of GNP-reinforced DGEBA epoxy nanocomposite for different impact pressure	202
Figure V.8: The Strain rate–time curves of CB-reinforced DGEBA epoxy nanocomposite for different impact pressure	203
Figure V.9: Strain rate vs Pressure for CNTs/DGEBA, GNPs/DGEBA, CBs/DGEBA	204
Figure V.10: Stress-strain curves of the CNT-reinforced DGEBA epoxy nanocomposite for different impact pressure	205
Figure V.11: Stress-strain curves of the GNP-reinforced DGEBA epoxy nanocomposite for different impact	207

Figure V.12: Stress-strain curves of the CB-reinforced DGEBA epoxy nanocomposite for different impact pressure	207
Figure V.13: Max Stress vs Pressure for CNTs/DGEBA ; GNPs/DGEBA; CBs/DGEBA... ..	209
Figure V.14: High-speed photographs of dynamic compression experiment of the CNT-reinforced DGEBA adhesive sample under 4bar impact pressure	210
Figure V.15: High-speed photographs of dynamic compression experiment of the GNP-reinforced DGEBA adhesive sample under 4bar impact pressure	211
Figure V.16: High-speed photographs of dynamic compression experiment of the CB-reinforced DGEBA adhesive sample under 4bar impact pressure	212
Figure V.17: Microscopic observation of a specimen for 4wt.% CNT reinforced DGEBA epoxy nanocomposite.....	215
Figure V.18: Strain rate-time curves of CNTs/DGEBA, GNPs/DGEBA, CBs/DGEBA nanocomposite, 1wt.%	216
Figure V.19: Strain rate-time curves of CNTs/DGEBA, GNPs/DGEBA, CBs/DGEBA nanocomposite, 2wt.%	217
Figure V.20: Strain rate-time curves of CNTs/DGEBA, GNPs/DGEBA, CBs/DGEBA nanocomposite, 5wt.%	218
Figure V.21: Strain rate and Max Stress vs Impact Pressure for neat adhesive and adhesive doped with nanofillers	220
Figure V.22: Stress vs strain curves for neat adhesive and adhesive doped with 1 wt.% nanofillers.....	221
Figure V.23: Stress vs strain curves for neat adhesive and adhesive doped with 2 wt.% nanofillers.....	222
Figure V.24: Stress vs strain curves for neat adhesive and adhesive doped with 5 wt.% nanofillers.....	223

Chapter VI: Fracture Resistance of a nanofiller-doped adhesive for a bonded joint

Figure VI.1: Aluminum surface treatment	235
Figure VI.2: Composite surface treatment	235
Figure VI.3: Manufacture of composite/composite bonded joints.....	235
Figure VI.4: Manufacture of bonded aluminum/aluminum joints	236
Figure VI.5: Modes of crack propagation in the material	237
Figure VI.6: Dimensions of double cantilever beam (DCB) specimen, Mode I.....	242
Figure VI.7: Mode I test with DCB specimen using INSTRON machine	243
Figure VI.8: Crack propagation in a bonded joint (DCB - Mode I).....	243
Figure VI.9: Force-displacement curves of bonded joints with neat DGEBA adhesive.....	244
Figure VI.10: Energy release rate G_I based on the crack propagation (R curve) of bonded (a) Aluminum (b) Composite joints with neat DGEBA adhesive	245
Figure VI.11: Force-displacement curves of bonded joints with DGEBA adhesive doped with 1wt.% and 2wt.% GNPs	247
Figure VI.12: Energy release rate G_I based on the crack propagation (R curve) of bonded joints with DGEBA adhesive doped with 1wt.% and 2wt.% GNPs	247

Figure VI.13: Diagram of progress initial and critical Energy release rate (J/m^2) of bonded joint with DGEBA adhesive doped with 1wt.% and 2wt.% GNPs	248
Figure VI.14: Force-displacement curves of bonded joints with DGEBA adhesive doped with 1wt.% and 2wt.% CNTs	249
Figure VI.15: Energy release rate G_I based on the crack propagation (R curve) of bonded joints with DGEBA adhesive doped with 1wt.% and 2wt.% CNTs	250
Figure VI.16: Diagram of progress initial and critical Energy release rate G_I (J/m^2) under DCB bonded joint with CNT-reinforced DGEBA adhesive	250
Figure VI.17: Proposed mechanism for the strengthening and toughening of adhesive joints	251
Figure VI.18: Adhesive joint interaction with adherent materials at a high mass fraction of reinforced nanofillers	254
Figure VI.19: Wetting of the surface	254
Figure VI.20: Illustration of mechanical coupling between two substrates	255
Figure VI.21: Representation of the failure modes of the adhesive joint[353]	255
Figure VI.22: Fracture surfaces of DCB specimens Aluminum and Composite bonded with neat DGEBA adhesive	256
Figure VI.23: Fracture surfaces of DCB specimens bonded with CNT reinforced DGEBA adhesive under a different mass fraction	258
Figure VI.24: RVE showing CNT pull out under loading test.....	259
Figure VI.25: Fracture surfaces of Aluminum/Aluminum and Composite/Composite bonded joints with GNP-reinforced DGEBA adhesive	260
Figure VI.26: Energy release rate (J/m^2) for aluminum/aluminum and composite/composite bonded joints with DGEBA adhesive doped with nanofillers	261
Figure VI.27: Energy release rate (J/m^2) progress among CNT/DGEBA adhesive and GNPs/DGEBA adhesively-bonded joint.....	262
Figure VI.28: Dimensions of Notched Flexure specimen (ENF), Mode II.....	263
Figure VI.29: ENF specimen for mode II bonding characterization.....	264
Figure VI.30: Force-displacement curves of ENF specimens bonded joints with neat DGEBA adhesive	265
Figure VI.31: Force-displacement curves of ENF specimens bonded with DGEBA adhesive doped with CNTs	266
Figure VI.32: Force-displacement curves of ENF specimens bonded with DGEBA adhesive doped with GNPs	267
Figure VI.33: Energy release rate G_{II} based on the crack propagation of ENF specimens of bonded joints with DGEBA adhesive doped by GNPs	267
Figure VI.34: Diagram of progress initial and critical Energy release rate G_{II} (N/mm) of ENF specimen of bonded joints with DGEBA adhesive doped by GNPs.....	268
Figure VI.35: Energy release rate G_{II} based on the crack propagation of ENF specimens bonded with CNT-reinforced DGEBA adhesive under 1wt.% and 2wt.%	269
Figure VI.36: Diagram of progress initial and critical Energy release rate G_{II} (N/mm) of ENF bonded joint with CNT-reinforced DGEBA adhesive	269
Figure VI.37: CNT deformation during bending loading	270

Figure VI.38: Comparison analysis Force-displacement curves of ENF specimens of bonded joints with CNTs/DGEBA and GNPs/DGEBA adhesive	271
Figure VI.39: Comparison analysis energy release rate (R- curves) of ENF specimens of bonded joints with CNTs/DGEBA and GNPs/DGEBA adhesive	272
Figure VI.40: Diagram showing the Energy release rate GII difference of ENF samples bonded joint and with GNPs/DGEBA and CNTs/DGEBA adhesive (N/mm)	272
Figure VI.41: Diagram showing the Energy release rate GII difference of ENF-aluminum bonded joint and ENF-Composite bonded joint with GNPs/DGEBA and CNTs/DGEBA adhesive	273
Figure VI.42: Finite element model of a double cantilever beam test	276
Figure VI.43: Finite element model of end notched flexure test.....	276
Figure VI.44: Mesh employed in the FE simulation and cohesive thickness element size ...	277
Figure VI.45: Adherent Composite laminated structure simulated with Texgen and Digimat	278
Figure VI.46: Damage of joints, DCB model	280
Figure VI.47: Damage of joints, ENF model	280
Figure VI.48: Comparison of numerical and experimental force-displacement curves for DCB tests.....	282

General Conclusio

List of Tables

General introduction

Chapter I: State of The Art

Table I.1: Mechanical properties of CNT in a different orientation	72
Table I.2: Carbon nanotube proprieties	74

Chapter II: Methodology

Table II.1: The different composition ratios of CB-GNP-CNT reinforced DGEBA epoxy nanocomposites	103
--	-----

Chapter III: Physico-chemical properties

Table III.1: Different thermal parameters of reinforced DGEBA nanocomposite sample	132
Table III.2: Micromechanical properties of CNT/DGEBA nanocomposite sample	138
Table III.3: Micromechanical properties of GNPS S /DGEBA nanocomposite sample.....	143
Table III.4: Micromechanical properties of CB/DGEBA nanocomposite sample.....	146
Table III.5: Different micromechanical properties of reinforced DGEBA nanocomposite sample.....	150
Table III.6: Indenter surface area of different reinforced DGEBA nanocomposite under a different mass fraction.....	155

Chapter IV: Quasi-static properties

Table IV.1: Evolution of the CNTs/adhesive nanocomposites mechanical properties	163
Table IV.2: Evolution of the GNPs/adhesive nanocomposites mechanical properties	166
Table IV.3: Evolution of the CBs/adhesive nanocomposites mechanical properties	168
Table IV.4: Evolution of the CNTs/ Adhesive nanocomposites mechanical properties.....	176
Table IV.5: Evolution of the GNPs/ Adhesive nanocomposites mechanical properties.....	180
Table IV.6: Evolution of the CBs/Adhesive nanocomposites mechanical properties	184

Chapter V: Dynamic behavior of adhesive doped with nanofillers

Table V.1: Dynamic mechanical properties of neat DGEBA adhesive under different impact pressure.....	213
Table V.2: Dynamic mechanical properties of reinforced DGEBA adhesive under different impact pressure.....	214
Table V.4: Dynamic mechanical parameters for neat adhesive and adhesive doped with nanofillers under 1.5 bar.....	224
Table V.5: Dynamic mechanical parameters for neat adhesive and adhesive doped with nanofillers under 2 bar.....	225

Table V.6: Dynamic mechanical parameters for neat adhesive and adhesive doped with nanofillers under 4 bar.....	226
---	-----

Chapter VI: Fracture Resistance of a nanofiller-doped adhesive for a bonded joint

Table VI.1: Composite properties	234
Table VI.2: Aluminum properties	234
Table VI.3: Energy release rate (J/m^2) under adhesive bonded Aluminum and Composite joint	252
Table VI.4: Energie release rate (N/mm) under adhesively-bonded Aluminum and Composite joint under ENF sample.....	274
Table VI.5: Composite properties	278
Table VI.6: CNTs/DGEBA properties	278
Table VI.7: GNPs/DGEBA properties	278
Table VI.8: Cohesive parameters of GNPs/DGEBA adhesively-bonded composite joint	278
Table VI.9: Cohesive parameters of GNPs/DGEBA adhesively-bonded aluminum joint	279
Table VI.10: Cohesive parameters of CNTs/DGEBA adhesively-bonded composite joint ..	279
Table VI.11: Cohesive parameters of CNTs/DGEBA adhesively-bonded aluminum joint...	279

General Conclusion

General Introduction

Background and motivation

Adhesively bonding is an old assembly technique that has always existed in nature, even in very severe environments. From ancient times, people used this technique to assemble tools and build. A significant revolution occurred in the 1930s and 1940s with the advent of metal/metal bonding in the aeronautical and marine sectors, associated with the discovery of polyepoxide resins, Figure 1. Nowadays, bonding has spread to all areas of everyday life; it can meet the most diverse specificities and is still a source of progress in many industry sectors.

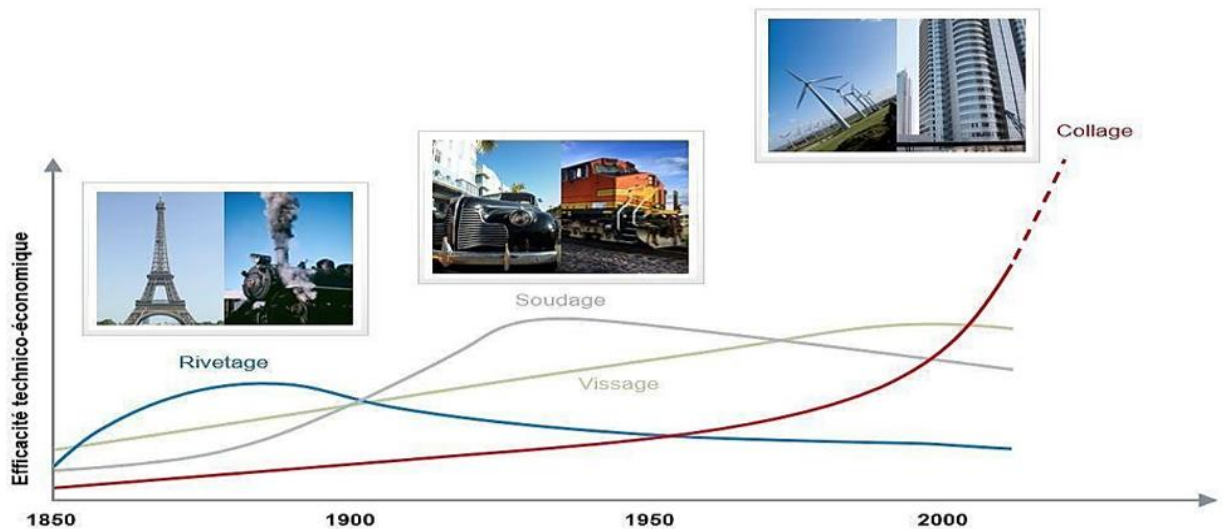


Figure 1: Bonded joint revolution

Adhesively-bonded joints are becoming increasingly popular. Advances in science have made adhesive bonding a preferred technique for high mechanical performance bonded structures, particularly in the marine, aeronautical and automotive sectors, Figure 2.



Figure 2: Areas of application for bonded joints

This technique makes it possible to reduce the weight of structures compared with conventional techniques such as riveting or welding, and hence avoid machining operations that are potentially damaging for assembly (drilling and heating in particular). Furthermore, an adhesively-bonded joint must be carefully manufactured under suitable conditions, Figure 3.

This technique is commonly used in aeronautics to assemble sandwich panels, fuselage panels, landing gear doors and hatches, flight control surfaces or helicopter blades, Figures 4 and 5. Adhesive bonding is used in the railway industry to assemble door panels on honeycomb structures, among other uses. Adhesive bonding is used in the naval structure to assemble parts whose gaskets must be sealed (junctions between wheel passages and engine compartments, floor gaskets, petrol trap, etc.), Figure 6.

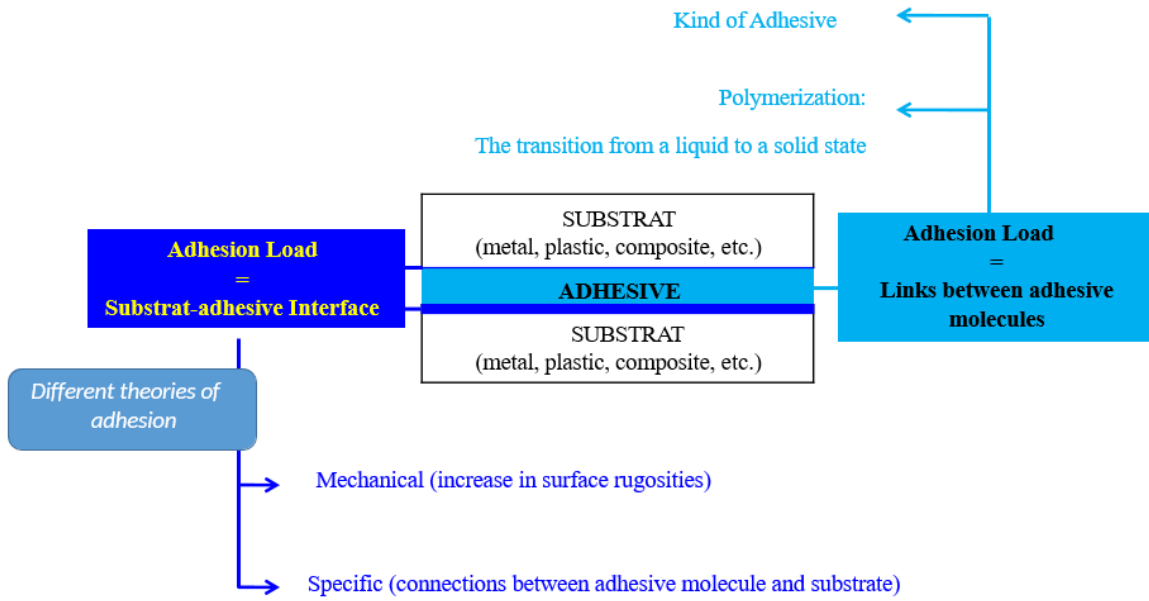


Figure 3: Bonded Joint Composition

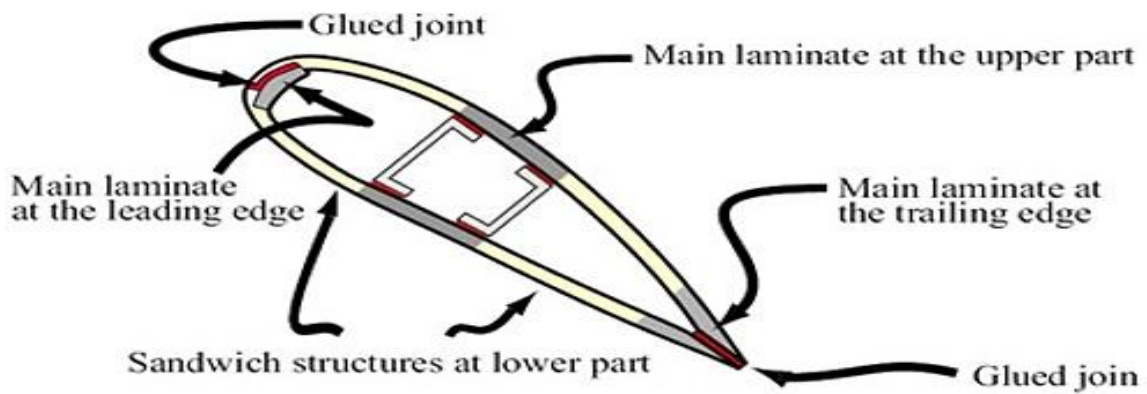


Figure 4: Adhesively-bonded joint on Helicopter blades

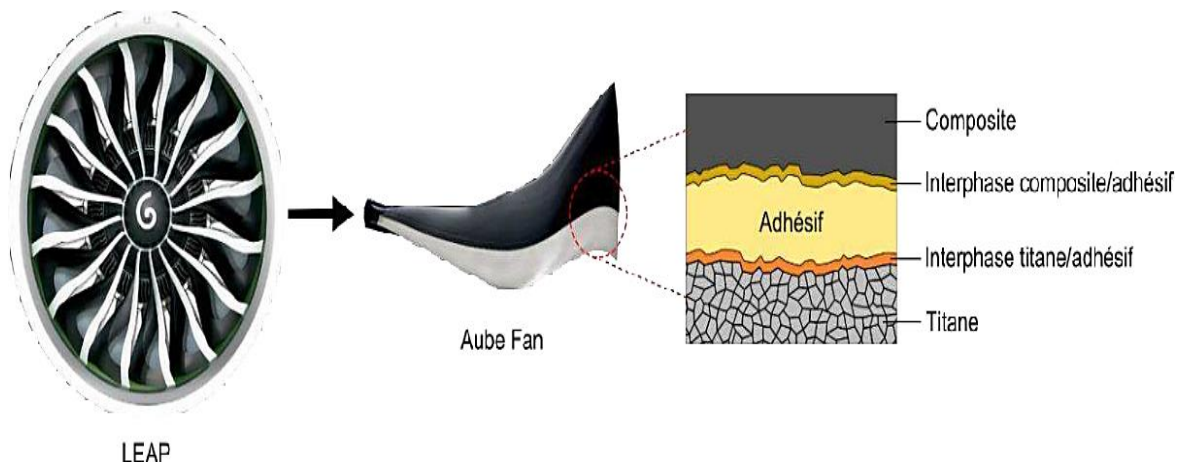


Figure 5: Adhesively-bonded joint on LEAP (Leading Edge Aviation Propulsion) engine

This widespread use inevitably necessitates the need to size bonded links in the face of severe environments generated during crashes, as well as high-speed impacts from all types of projectiles (micrometric space debris on satellites, safety of components against ballistic attacks). Mechanical stresses are associated with rapid dynamics, and indeed, shock waves are generated and then propagate through the structures. The induced strain rates range from 10^5 s^{-1} to 10^7 s^{-1} depending on the type of stress, Figure 7.

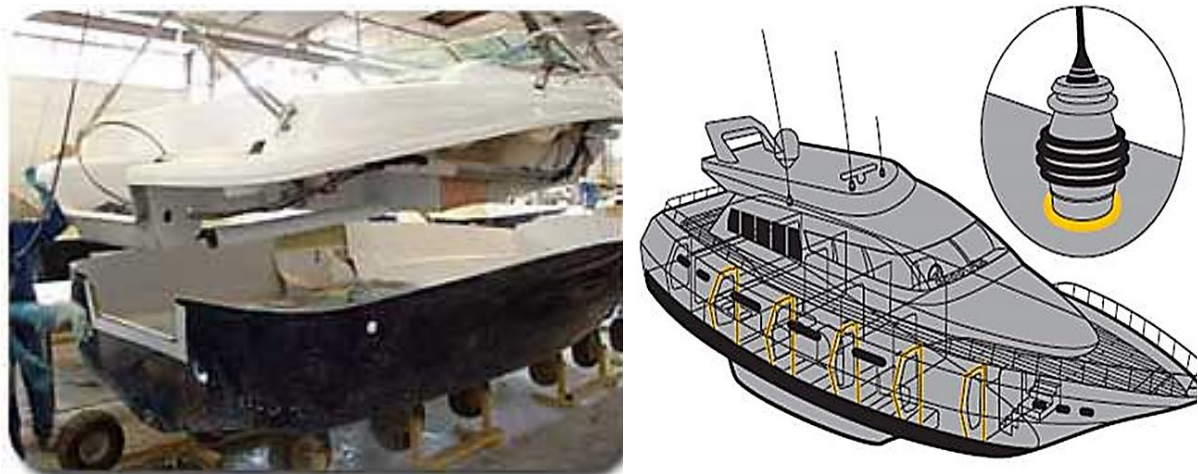


Figure 6: Naval structure adhesive-bonded joint example

The incumbent mechanical demands are found in the domain of fast dynamics, and shock waves are generated and spread throughout the structures. However, one of the most significant issues is controlling the aging of connected joints. The external factor constraints that these materials experience cause a weakening of intrinsic adhesive properties, as well as of interface adhesion properties, resulting in the degradation of assemblies. This issue is particularly prevalent in the maritime, aeronautical, and automotive industries, where the loss of adhesion of adhesive connections in environmental conditions and mechanical crashes presents a major stumbling block for structural assembly technology, Figures 7 and 8.



Figure 7: Naval structure degradation



Figure 8: Aeronautical structure degradation

Nonetheless, the issue of increasing the joint's usage interval remains a significant scientific challenge. There have been other suggestions such as using a multi-adhesive junction. However, this notion has demonstrated its limitations, allowing for the development of new concepts such as a joint with properties that are maintained along the length of the encased surface.

Problematic

Adhesively-bonded joints, which tend to quickly become unavoidable, must not present any risk to humans and their environment, whether during their implementation, their use, or even during their recycling process.

The solution proposed in the present thesis is to develop a new generation of adhesives by incorporating different types of nanofillers into an adhesive epoxy and quantifying the generated nanocomposites' mechanical performance under different types of loading. Creating a nanocomposite reinforced with nanofillers allows the mechanical, chemical, and thermal properties to change. However, this evolution of polyepoxide matrices has degrees which are

dependent on the type of nanofillers, their mass fraction, their dispersion, their sizes, their shapes, and their molecular interactions with the adhesive matrix.

Objectives

This thesis aims to gain a better understanding of the solicitation and shock response of adhesive assemblies of millimeter thicknesses by paying particular attention to the influence of the nature of the adhesive used on the fracture mechanisms.

We have chosen to test bonding made with commercial polymer materials, with an epoxy resin representing the response characterizing a thermosetting polymer. As part of this thesis, we will try to answer the following questions:

- How does the nature of the adhesive affect the behavior of the bonded joint?
- Will the damage occur at the interfaces and/or in the adhesive layer?
- What will be the breakage thresholds under different stresses?

This thesis's main goal is to gain a better understanding of the behavior and flaws of the neat adhesive and the reinforced adhesive under mechanical tasks that are similar to those induced by external environments and develop mechanical abilities. This research has focused on determining which nanofillers are the most effective and suitable for improving the adhesive.

The main goal of this project is to improve adhesive behavior in order to create a more rigid and lightweight structure. This research work will first focus on the mechanisms that govern the mechanical behavior of materials used for the assembly of structures, which are the neat and doped adhesives. Then, we will try to evaluate the adhesive performances of these materials in two types of bonded joints: aluminum/aluminum; and composite/composite. Figure 9 provides a summary diagram of the adopted procedure.

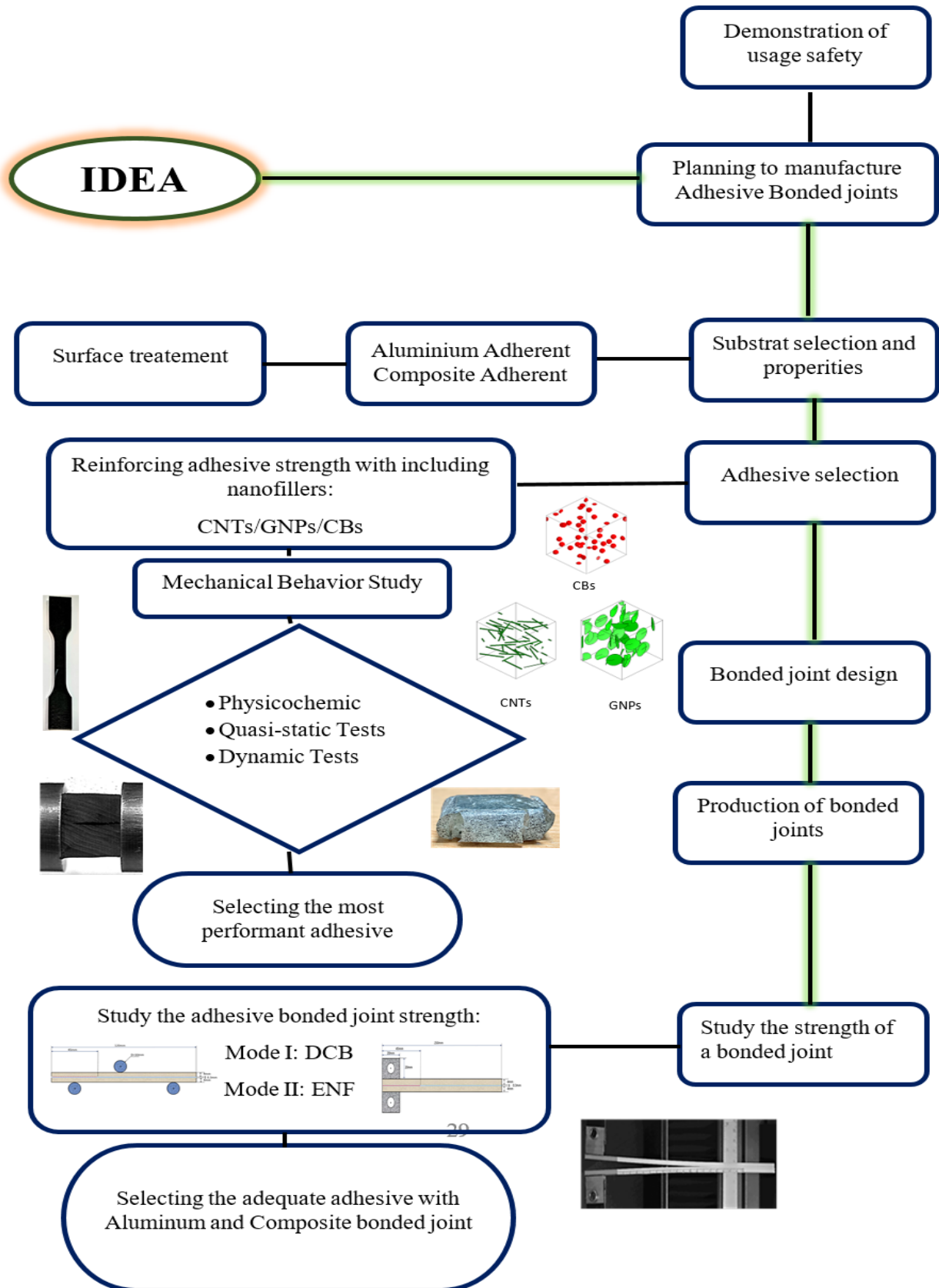


Figure 9: Aeronautical structure degradation

Summary of thesis outline

This thesis is divided into six parts:

The **first chapter** is devoted to a bibliographic study, in which the main adhesion mechanisms as well as some generalizations about adhesion will be covered. Next, the effect of external factors on adhesive adhesion and the various ruptures caused by this exposure will be discussed. Finally, the various techniques that have been used to improve the durability of the bonded joints in harsh environments will be considered.

The **second chapter** is devoted to selecting an adhesive and the types of nanofillers to be used. A descriptive study was conducted to clarify the technique of fabricating nanocomposites (adhesive doped by nanofillers). The nanocomposites are elaborated with a Polyepoxide DGEBA network that is doped with various nanofillers (carbon nanotubes (CNT), carbon black (CB), and graphene nanoplatelets (GNP) in various mass fractions (0, 1, 2, and 5%). This chapter will be dedicated to the implementation and microstructural description of nanocomposites in a separate section. The microstructure will be described using numerical approaches in conjunction with the Digimat software. After the description of the studied materials, we present the various experimental protocols for the characterization of nanocomposites under static and dynamic loading.

In the **third chapter**, we proceed to determine the physicochemical and local mechanical properties of the materials as a function of the type and mass fraction of the nanofillers. We'll study the effect of the types of nanofillers on the glass transition temperature, as well as different fractions of mass. Using the Differential Scanning Calorimetry (DSC), the glass transition temperature will be determined. These experiments will allow us to track the evolution of the glass transition temperature at macroscale levels. For local mechanical properties, we will evaluate the influence of nanofiller types and sizes on elastomeric material properties using

micro indentation tests. The use of test instrumentation allows us to determine the Poisson coefficient and to track the effectiveness of various types of nanofillers on the Young modulus, hardness, rigidity, and other material properties. This chapter will also examine how microstructure parameters (nanofillers size, distribution, and intermolecular distances) influence the measured properties.

The **fourth chapter** is devoted to the quasi-static experimental investigation of the Polyepoxide DGEBA network doped with various nanofillers (carbon nanotubes, carbon black, graphene nanoplatelets) with various mass fractions (0, 1, 2 and 5wt.%). Using the INSTRON device, an experimental study was carried out to investigate the static behavior of nanocomposites CNTs/DGEBA, GNPs/DGEBA, and CBs/DGEBA under a constant 1mm/min solicitation speed. The goal here is to identify the nanofillers that have the most impact on the improvement of mechanical properties of the adhesive, as well as the parameters that cause the adhesive to degrade.

The **fifth chapter** focuses on dynamic experimental studies on nanocomposite networks such as CNTs/DGEBA, GNPs/DGEBA, and CBs/DGEBA with various mass fractions (0, 1, 2, 5wt.%). An experimental study was carried out to investigate the dynamic behavior using the Split-Hopkinson Pressure Bar (SHPB) device. Furthermore, these dynamic compression tests were carried out at three different impact pressures, respectively 1, 2, and 4 bar, in order to examine the rigidity and energy absorption capacity of these reinforced nanocomposites in greater detail while selecting the best nanofillers.

The **sixth chapter** considers the investigation and implementation of a new concept of doped adhesive joint that transfers major technical functions between different constituents of a bonded structure under various nanofillers and mass fractions. This section entails putting the linear elastic fracture mechanics tests, such as the Double Cantilever Beam Test (DCB) for mode I and the End Notched Flexure Test (ENF) for mode II, into action to characterize the

mechanical behavior of adhesively-bonded joints under different conditions. Another section will show how to use ABAQUS to model DCB and ENF tests using the finite element method with implementing the cohesive law. The numerical models were validated by correlating them with the experimental results.

To **conclude**, we will go over the main points of this research, such as microstructure observation, the doping of adhesive epoxy with nanofillers and its sensitivity to the nature and size of the nanofillers, physical and mechanical properties, and comparison between experimental results from various nanocomposite structures. In addition to this, we will compare the performance of different adhesives at the level of bonded joints and see which ones are the most efficient.

Chapter I: State of the Art

I. State of the Art

Summary

I. State of the Art	30
I.1 Introduction	32
I.2 Adhesives.....	39
I.3 Types of Adhesives	41
I.3.1 Reactive acrylic-based adhesives	42
I.3.2 Polyurethane adhesives	42
I.3.3 Epoxy-based adhesives	42
I.4 Adhesively-bonded structures	43
I.4.1 Surface treatments	43
I.4.2 Interphase concept.....	44
I.5 Types of adhesively-bonded joints, their benefits and limitations	45
I.5.1 Metal to metal bonding	45
I.5.2 Bonding composite to composite	45
I.5.3 Composite to metal bonding	48
I.6 Parameters that affect the performance of bonded joints	50
I.6.1 Surface preparation	50
I.6.2 Adhesive bond configuration	51
I.6.3 Environmental factors	53
I.7 Characterization of mechanical properties	54
I.8 Enhancement of adhesive performance	54
I.8.1 Z-pining.....	55
I.8.2 Stitching	58
I.8.3 Adding inter-adherent glass fibers	63

I.9	Adhesive enhancement	64
I.9.1	The principle of nanocomposite	65
I.9.2	Influences of Nanofillers on adhesive performances	74
I.9.3	Effects of the excess amount of nanofillers on adhesives	82
I.10	Conclusion	85
II.	Methodology	88
II.1	Introduction	89
II.2	Resin	89
II.3	Nanoparticles	91
II.3.1	Carbon nanotubes (CNTs).....	91
II.3.2	Graphene	92
II.3.3	Carbon Black.....	95
II.4	Dispersion and implementation of nanofiller-doped adhesive resin	99
II.4.1	Graphene and Carbon Black dispersion	100
II.4.2	CNT dispersion with planetary agitators.....	102
II.5	Homogeneity optimization via DIGIMAT	104
II.5.1	Clustering	104
II.5.2	Cluster size distribution.....	105
II.6	Microstructural study.....	106
II.6.1	Differential Scanning Calorimetry (DSC).....	106
II.6.2	Micro-indentation.....	108
II.7	Mechanical Characterization of Nanocomposites	111
II.7.1	Static tests: Mechanical test bench – INSTRON	111
II.7.2	Compression Test.....	115
II.8	Study of the dynamic behavior of nanocomposites.....	117
II.9	Conclusion	125

I.1 Introduction

In recent years, significant research is going on to achieve lightweight structures especially through structural assemblies that ensure high specific strength for applications such as aerospace, marine, civil and automobile industries. Generally, an assembled structure is composed of different materials joined together and the complexity of the structure increases by increasing the number of assembled parts as it is in the marine area, Figure I.1. The assembled parts ensure the transmission of load from one substrate to the other. Therefore, it is important to investigate the strength of this complex structure to confirm longer and better service life [1]. Different types of assembly techniques were used traditionally such as riveting, bolting, welding, etc. and each technique had its pros and cons based on structural (subtracts thickness, applied load, environmental conditions), design (weight, disassembly) or manufacturing (production time, drilling) constraints. Initially, the replacement of materials was considered to be the solution of having structures with better mechanical strength and structural reliability so, metals were replaced with composites. Indeed, composites had improved the mechanical behavior of the structural assembly with a reduction in the weight due to their excellent strength, resilience and damage tolerance with low weight but, it was still not the perfect solution due to their complex damage behavior such as delamination owing to the stress concentration round the holes of a rivet.

The bolted or riveted joints also known as “mechanical fasteners” are the most common methods of assembling two structures as it is employed in marine boat structure and are achieved by introducing a rivet or a bolt in the drill/hole of the respective assembled panels. The impact of stress concentrations in bolted joints can be decreased by installing a pre-load to produce the necessary frictional force because the durability of the assembly is directly related to the stresses localization around the hole of a fastener, Figure I.2.



Figure I.1: Boat Structure [3]



Figure I.2: Riveted joints belong to boat structure [4]

However, the flexibility of the fastener is also an important parameter which itself depends on the effort transferred by this fixation. The bolted/riveted joints are simple in installation, removable in case of repair; no prior surface preparations are needed and ensure easier load transfer in case of thicker specimens [1], [2]. At the same time, the drawbacks of this technique include more holes in the parts which can result in more stress concentration regions and an increase in the structure weight. Moreover, the increase in weight is more specific around the hole resulting in more strain concentration thus more crack formation. In the case of composite

material, the creation of the holes by drilling can cause delamination, Figure I.3, especially in the first ply and heat released by drilling can cause degradation of the matrix. In addition, corrosion is a crucial phenomenon that can cause the failure of the structure. Composite materials can cause galvanic corrosion of the bolts if the material of the fastener is not chosen carefully, for example, carbon fibers can degrade aluminum fasteners thus resulting in water infiltration into the fasteners [2], Figure I.4.

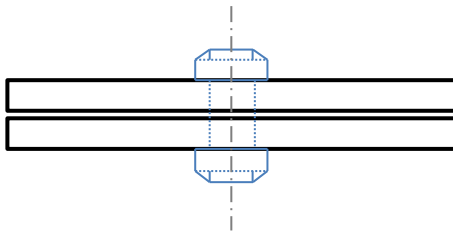


Figure I.3: Bonded Joint

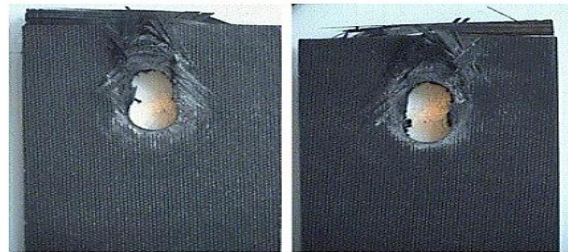


Figure I.4: Composite damage after bearing failure [5]

Welding is another traditional method of bonding two or more elements/materials, especially metals employed in marine areas as shown in Figure I.5. There are different kinds of welding joints such as butt, lap, corner, edge, tee welding, etc, Figure I.6. Moreover, there are different kinds of welding processes such as gas, arc, resistance, radiant energy and solid-state welding. The best welding technique to melt composite matrix is the radiant energy known as laser welding, Figure I.7. This method melts the composite matrix by heating and contact is formed by the solidification of the matrix after cooling. In addition, pressure is enforced to achieve good interaction between the surfaces.

The advantages of welding include better contact strength, no need for additional material, can be used in an open environment and has better significance in assembling small components. However, incorrect welding patterns can cause internal (slag inclusion, incomplete fusion, necklace cracking, incompletely filled groove or incomplete penetration) and external (weld crack, undercut, spatter, porosity, overlap, and crater) defects. Furthermore, the limitations of this technique include the creation of localized heat region which can cause weakening of

material in the vicinity of the welded zone thus, the heat dissipation on material especially in composite structures result in different damage modes such as matrix cracks, delamination, and rupture of fibers [7].



Figure I.5: Welding joint along boat structure [6]

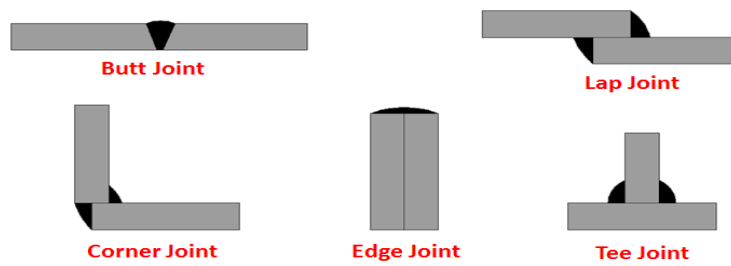
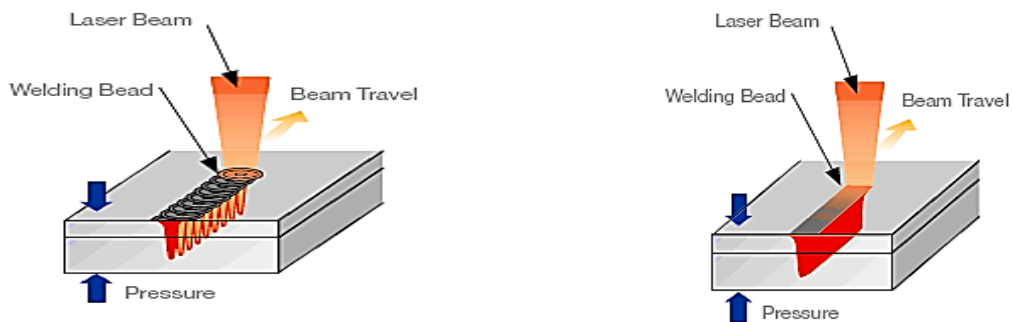


Figure I.6: Different types of welding



(a) In the case of pulse irradiation

(b) In the case of continuous irradiation

Figure I.7: Laser welding

So, traditional methods such as riveting, bolted joints and welding were proven not to be an efficient method to get a structure with better mechanical properties and behavior [1]. Hence, they had to get a method that can contribute to getting a more efficient and reliable bonded structure. Adhesively-bonded joints, Figure I.8, were then considered to be a significant technique to overcome the limitations of traditional joint methods. The adhesive joints are the most widely used due to their flexibility in manufacturing [8]. Adhesively-bonded joints have numerous applications such as in the area of aeronautics, electronics, automobile, sports, marine, ship design, oil and even in construction industries [9]. It is used as a replacement for the traditional mechanical fastening methods [10], due to providing substantial benefits.



Figure I.8: Adhesively-bonded joint belong boat structure [11]

Thus, there has been a significant increase in adhesively-bonded joints in all sectors particularly for repairing the damaged composite structures. The advantages of adhesively-bonded joints include method simplicity with the ability to join a variety of materials, better sealing ability, reduction in local stress concentration regions caused by the rivet or bolt holes, ensure uniform load and stress distributions with good mechanical vibration and fatigue resistance, reduction in weight with better strength to weight ratio [12], [13] and cost-effective method [1]. Thermal and electrical properties can also be achieved through adhesively-bonded joints which were not possible in other types of assemblies. Moreover, adhesively-bonded joints are considered to be

more advantageous for assembling composite structures because, without any hole/drill, the fibers stay continuous in composites, it ensures smooth surface finish without any surface irregularities and adhesive behaves like an insulator thus avoiding the galvanic coupling which eliminates the corrosion phenomenon, Figure I.9. However, like every other method, adhesively-bonded joints were not exempt from limitations and drawbacks. Adhesively-bonded joints have limitations such as large curing time, low temperature and humidity resistance (fragile to environmental conditions), non-removable and delicate surface preparation procedure required before bonding [14], a section of fabrication process and type of adherent used. Most of the adhesively-bonded joints lost their performance with a temperature higher than 200°C and don't facilitate the electrical properties between two surfaces due to their low electrical conductivity. Although the moisture absorption is inactive on the resin, adhesives have low humidity resistance and can cause weakening of bond to locate on the interface of adherent/adhesive. The adhesively-bonded joints have low peeling strength thus have the necessity frequent monitoring of structure [15]. Thickness of the adhesive bond plays a vital role in the overall mechanical behavior of the assembled structure. In addition, the existence of kissing bonds (caused by surface weakness or pollution) can cause severe damage to the strength of the bond formed [16]. Furthermore, adhesively-bonded joints may reduce the problem of stress concentration regions, but they are exempt from them. These stress concentration regions are created in the free edges of the bonding area as Tarfaoui demonstrated in his work [17], Figure I.10. To limit these stresses, additional treatment of the bonded joints is required such as tapering the adherent, modifying the lap-joint geometry by creating an adhesive fillet or by developing a hybrid double lap joint [18]–[21].

Hybrid joints consist of combining the adhesively-bonded joints with the mechanical fastening to benefit from the advantages of both techniques and minimizing their drawbacks [2] however, both techniques must work in synergy [23], Figure I.11. The addition of adhesive improves the

properties of individual mechanical fasteners so the total numbers of bolts/rivets can be decreased in the overall assembly. One of the key reasons is that the presence of bolt within the hybrid joint limits the propagation of the damage during the failure, thus avoid the detachment of the two adherents. Marannano *et al.* [20] studied the mechanical behavior of hybrid bonded/riveted joints of steel and aluminum rivets with adhesive experimentally and numerically. The results indicated an increase in mechanical behavior and fracture properties of about 20% under static loading and 45% under high cycle fatigue. This improvement in properties is due to the reduction in the stress concentration caused due to drilling by inserting the adhesive between the substrates, which also improved the fatigue resistance. Kelly and Stewart [24], [25] further confirmed in their study that adding the adhesive in a hybrid joint makes the structure more resistant and rigid than a simple bolted joint. Their results confirmed an increase of 40% in joint strength by using hybrid joints [26]. On the other side even with these enhancements in properties, the adhesively-bonded joints are more preferable to the hybrid joints because the appearance of holes within the composite structure results in the creation of stress concentration regions due to the fiber discontinuities within the structure. It decreases the strength of the structure in comparison with the joint because the removal of material during drilling and structure can give different properties under different conditions [27]. This is the reason why adhesively-bonded joints are more broadly applicable especially for composite structures.



Figure I.9: Adhesively-bonded joint

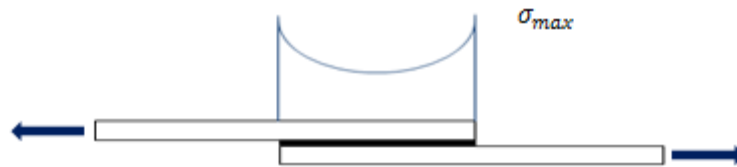
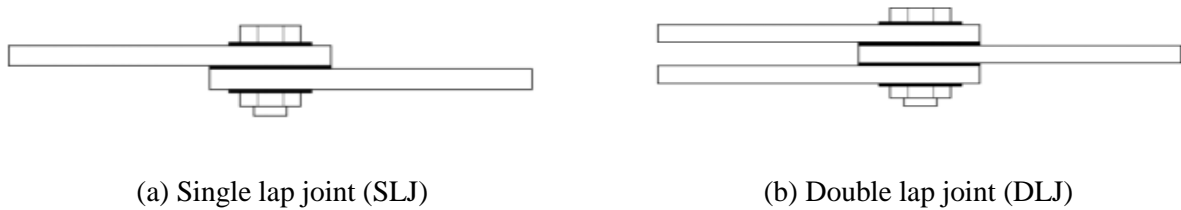


Figure I.10: Stress concentration in the bonded joint [22]



(a) Single lap joint (SLJ)

(b) Double lap joint (DLJ)

Figure I.11: Identification of hybrid joints

I.2 Adhesives

To sum up Adhesively-bonded is an old assembly technique that has always existed in nature, sometimes in very harsh environments. Since ancient times, man has used this technique for assembling tools and building. A major revolution took place from 1930 to 1940 with the appearance of metal/metal bonding in the aeronautics and marine sectors, associated with the discovery of polyepoxide resins. Today, assembly by bonding has extended to all areas of everyday life, responding to requirements and it is still a source of progress in many industry sectors.

Adhesives must be applied evenly onto the surface of the two substrates in such a way that it ensures thorough wetting to avoid entrapment of any air bubbles, Figure I.12. Adhesives can join complex shapes and two different materials without increasing the overall weight of the assembly [28]. In general, adhesive produces coherent and adapted results in comparison with traditional bonding methods. Moreover, modern adhesives have shown a large diversity of materials that facilitate the selection of an ideal adhesive bonding system according to a specific

application. For example, the selection of adhesive bonding materials can be made according to required properties such as flexibility/rigidity, environmental and thermal stability, chemical compatibility with the substrate material, economic and esthetic aspect, viscosity, and conductivities.

Advances in science have enabled bonding to become a preferred technique for the production of structural assemblies with high mechanical performances, particularly in the aeronautics and marine sectors. This technique makes it possible to reduce the weight of the structures compared with conventional techniques such as riveting or welding and avoid machining operations that are damaging for assembly (drilling and heating in particular).

Adhesives have many advantages in comparison to mechanical binding or thermal bonding such as welding, soldering, or brazing. For example, adhesives can join two dissimilar materials: two different metals with a different melting point or metal with composites. They can bond together heat-sensitive materials, surfaces of different geometric shapes with good fatigue resistance and sustain the reliability of the substrate. In addition, an adhesive joint does not deform and decolorize the substrates or form weld worm which may require secondary surface treatments such as crushing or painting. It ensures uniform stress distribution over a broader area, rather than just over a concentrated area. It has a sealing ability that protects the joint from corrosion, fluid penetration and thermal expansions [29], [30].

However, controlling the aging of bonded joints remains one of the main challenges. The environmental stresses on these materials result in a weakening of the intrinsic properties of the adhesive and the adhesion properties of the interface, causing damage to the assemblies. This problem is particularly acute in the aviation, marine and automotive sectors.

To date, numerous researchers [9], [31]–[38] have discussed the adhesively-bonded joints including the importance of adhesive materials and the parameters affecting the adhesive properties such as surface treatment, joint configuration, the importance of adhesive materials

[38], [39], geometrical specification, failure modes, fatigue strength [37], [40], bond repair [31], [32] and environmental durability [31], [33], [36]–[38], [41]. In the fabrication of adhesively-bonded joints, two main categories of activities must be performed accurately. These two categories are design activities such as materials selection, adhesive selection, design of the joint, etc., and manufacturing activities such as pre-treatment of surface, assembly, curing process and final inspection.

Moreover, the lack of dependable models to improve modelling for the mechanical behavior of these materials and predict the evolution of properties as a function of time is a definite handicap to make this technology accepted.

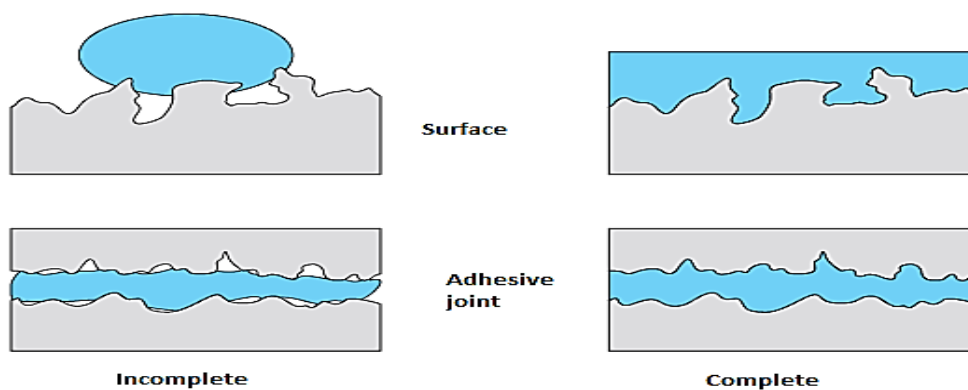


Figure I.12: Wetting surfaces with adhesive

I.3 Types of Adhesives

Several types of adhesives are available now-a-day and there are approximately 250,000 kinds of adhesive categories due to different domains, composition, properties etc. Adhesives can be classified by their chemical composition.

Among all these types of adhesives, acrylic-based adhesives, polyurethane and epoxy-based adhesives are most commonly used for adhesively-bonded joints. They are described in further detail below given their wide application range.

I.3.1 Reactive acrylic-based adhesives

Acrylic-based adhesives can bond a large variety of substrates. They are best known for their quick bonding process. But they can be very delicate to the surface preparation techniques similar to toughened adhesives. Moreover, the cyanoacrylate-based subfamily can have a rapid curing process when the moisture content in the air is high (they typically solidify within a second). However, these adhesives are brittle, and they are sensitive to creep and high temperatures. Because of this reason, they have limited use in bending or crash applications. Anaerobic, another type of acrylate adhesives can heal with the removal of oxygen content. These adhesives are generally used to secure and seal metallic structures to avoid loosening, leakage, and corrosion.

I.3.2 Polyurethane adhesives

These adhesives form a bond via a specific chemical reaction process and can be represented through single- or two-component systems. Polyurethane adhesives form a robust and resilient joint. They boast excellent thermal resistance as compared to different other adhesives. They offer vast applications in the field of construction, crash and as a sealant and can be used on a variety of substrate materials.

I.3.3 Epoxy-based adhesives

These types of adhesives have good bond strength, high mechanical performance, good chemical resistance, and a modest shrinkage rate. They do not generate volatiles during the curing process; thus, they demonstrate high tolerance to solvents, acids, bases, and salts. They demonstrate high durability for thermoplastic and thermosetting substrate materials. In general, their polymerization temperature ranges between 20 and 200°C. These adhesives have a wide range of applications due to their properties but their high price limits their use over large areas or in big quantities.

The thesis work presented here is devoted to the study of the most commonly used structural adhesives, namely polyepoxide resins. Its main objective is to better understand the behavior and weaknesses of these materials in the face of external factors for bonded assemblies made from these adhesives.

We therefore sought to model only the mechanical behavior of polyepoxide networks and how they behave during bonded assemblies against imposed mechanical impacts and to highlight the various factors that influence the evolution of the properties of the samples produced. Secondly, we worked on the development of a polyepoxide adhesive that improves the resistance to aging in ambient conditions by incorporating nanoparticles.

I.4 Adhesively-bonded structures

I.4.1 Surface treatments

Surface treatments are applied to increase the initial adhesion and durability of the bonded assemblies.

Among these are, firstly, mechanical treatments:

- Sandblasting via high-speed blasting of an abrasive powder (hard oxides, corundums or alumina) onto the substrate to be glued.
- Sanding abrasion, which involves sanding the surface with an abrasive coating.

There are also chemical treatments:

- Solvent degreasing, which uses hydrocarbon or chlorine derivatives to remove contaminants from the substrate surface.
- Saponification degreasing (a hydrolysis reaction of ester functions in a basic medium) causes a reaction with the animal and vegetable fats present on the surface of the substrate to obtain glycerin or soap which can be easily removed by rinsing [42].

- Emulsification degreasing, which emulsifies surface contaminants for suspension using products such as sodium silicates, tetraborates, etc., etc.).
- Chemical pickling to remove the oxide layer from metals. Acid treatment is carried out on iron and its alloys and treatment based on nitric or sulfuric acid in the case of stainless steel.
- The use of a primary silane, usually based on GPS, makes it possible to create links between the substrate and the adhesive at the interface.
- The surface treatment must be selected in line with the substrates to be glued, the adhesive used and the stresses to which the assembly will be subjected.

I.4.2 Interphase concept

Bonded assemblies are produced by coating the adhesive onto one or more substrates. The cross-linking reaction then occurs, resulting in the formation of a specific zone at the interface between the adhesive and the substrate called interphase. Indeed, the adsorption of certain components of the adhesive before complete crosslinking results in the formation of a property gradient between the adhesive and the metal substrate [30]. Other studies have also shown that migration of the amine hardener to the interface can occur, which can then subsequently be absorbed by the metal oxide at the surface [31]. A hardener defect is then induced at the center of the glue joint [32] and excess is induced at the interface. This excess causes the formation of interphase at the surface of the oxide. The lack of hardener within the adhesive leads to incomplete crosslinking, which may subsequently induce oxidation or hydrolysis phenomena during aging [33]. The glass transition temperature of the interphase is then different from that obtained at the core of the glue joint [34]. This zone has properties which differ from those of the materials constituting the assembly [35], [36]. The thickness of this zone depends on the substrates used, the surface treatment, the crosslinking cycle and, albeit to a lesser extent, on the viscosity of the adhesive [37]. In the case of aluminum substrates, this thickness varies from a few dozen microns to about 200 microns.

I.5 Types of adhesively-bonded joints, their benefits and limitations

I.5.1 Metal to metal bonding

Metals are well-known for their excellent strength and ductility, as well as for their melting and solidification capacities. Given these properties, they have wide area applications, whether as a single structure or as part of an assembly. There are numerous traditional methods to bond metal to metal substrates, but adhesive bonding demonstrates better joint properties with a reduction in the overall weight of the assembly. For example, this method is used to join reinforcing metal sheets integrated within the wing structure to avoid buckling. Adhesively-bonded joints play a vital role in low-weight metal structures such as aluminum than heavy metallic structures such as mild steel. However, the variation in the levels of oxides over the surface of substrate hinders metal-metal adhesive bonding and limits the application of this technique in metallic structures, Figure I.13.

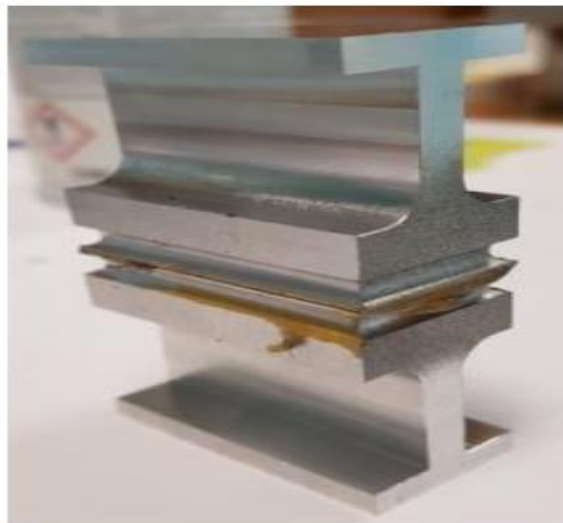


Figure I.13: Adhesive bonding metal to metal

I.5.2 Bonding composite to composite

Since antiquity, composite materials are being used in different areas to optimize the performance of conventional weapons and structures especially to reduce weight and increase

mechanical performance [43]. Their demand has been increased rapidly over the last few decades due to their supreme mechanical performance but at the same time, it also increases the cost of the structure. Moreover composites tend to show anisotropic behavior in rigidity and strength due to unidirectional fiber orientation which can increase the level of stress concentration regions or show weak intrinsic behavior in comparison to homogenous or isotropic behavior. In addition, they show complex damage behavior which further makes it essential to study in-depth the mechanical response of composite bonded joints and the damage evolution[44]. So, scientists developed the concept of using composite components assembled with the whole structure to make a compromise between good performance and low cost such as composite to composite or composite to metal. However, bonding composite-composite substrate is preferred over bonding composites with other materials such as metals, in order to avoid effects of dissimilarity in the mechanical behavior. In contrast, bonding composite to composite usually increases the overall strength of the structure, environmental resistance, and rigidity to weight ratio[45], [46]. This has increased assembly structures consisting of composite materials. Accordingly, the application of bonded joints has increased rapidly to replace the mechanical fasteners in composite structures, Figure I.14. Renewable marine energy conversion systems are one of the examples which have been making great progress by replacing components with composite materials such as in turbines [47]. Furthermore, in the field of transportation, composite materials are used to reduce weight which in return results in a reduction in energy consumption by increasing fuel efficiency [45], [46], [48]. For example, more than 50% of components used in airplanes are made from composites, which reduce the fuel consumption by up to 20% in comparison to the same size structure without composites. Furthermore, it is easier to repair the composite-composite bonded joint without compromising the reliability of the structure [49].

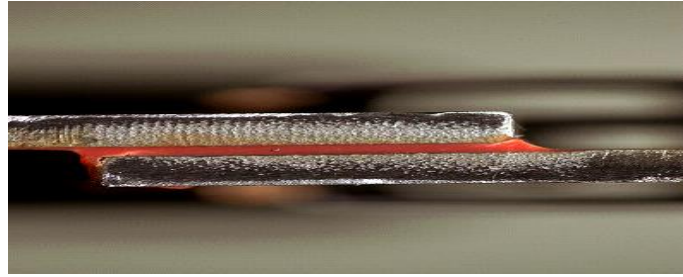


Figure I.14: Composite single lap joint

Although, composite-composite adhesive bonding shows better mechanical strength and performance, it is still not exempt from challenges which demand continuous research study to enhance their behavior and industrial applications. In the case of using composite as adherent, the external layer of the composites plays a vital role in adhesive joint strength. For example, complex damage behavior such as delamination or crack propagation of the external layer of unidirectional fiber composites can affect the interaction formed between the adherent-adhesive interface [50], [51]. Atkins *et al.* [52] studied the delamination of adherent surface and showed that the crack initiation took place in the overlap joint region due to high-stress concentration regions near the edges of the bonded joint. It was concluded that the delamination process was less sensitive in the adhesive bond region under the overlap area in a single lap joint (SLJ) than the inside of the adherent due to the high interlaminar stresses [53]. Another phenomenon known as the peel strength of adhesive bond plays a vital role in defining the strength of the structure. The high peel strength of adhesive bond can fail composite adherence under tension during the peel test. Various researchers had performed detailed studies to examine the peel strength of the adhesive and presented different approaches on how to decrease it such as an internal taper and an adhesive fillet [28]. These methods are difficult to fabricate but they can increase the interface stress failing bond before the failure of the structure. Neto *et al.* [28] presented a simpler and more effective method for increasing the interfacial stresses by using a ductile adhesive (Sika Forces 7888) and increasing the overlap area that confirmed a cohesive zone failure. Moreover, other than delamination of adherent, adhesive and cohesive failures,

critical failure modes that characterize the bonded composite joint systems include fiber-tear (failure only into the composite plate), light fiber-tear (failure occurs in the composite plate near the interface and can affect adhesive behavior), mixed failure (combination of two or more different failures) etc., Figure I.15. S.Sonia *et al.* thus demonstrated in their work that the macroscopic damage evaluates with increase of the pressure from 1 to 4 bar, corresponding to 210–713 s^{-1} strain rates. They verified that a significant damage can be appeared with the increase of strain rates [54].

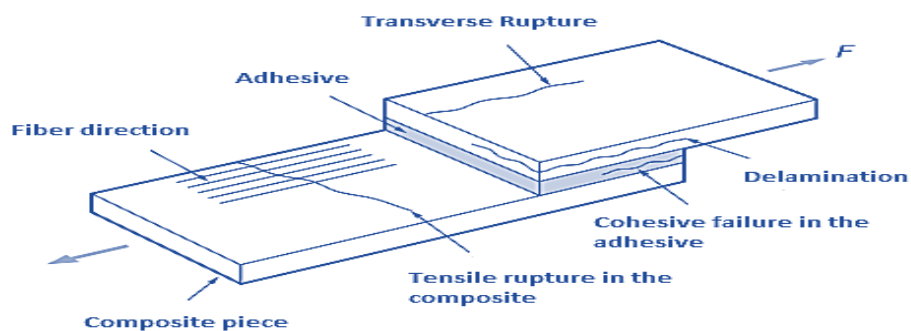


Figure I.15: Various failure modes possible with bonding composite to composite [55]

I.5.3 Composite to metal bonding

Various applications in the aerospace, automobile and marine sectors require the use of composite-metal bonded structures to compromise between better mechanical behaviors and costs. Previously, this process was carried out using traditional mechanical fasteners, described premature, which increased in stress concentration regions and complex damage behavior due to drilling holes, moisture entrapment and galvanic corrosion of not only fasteners but the metal substrate, Figure I.16 [56]. Initially, the thickness of the metal and composite substrate was increased to accommodate the concentration of holes and fasteners in the assembly, but it was a compromise on the weight of the structure not to mention other factors were still a concern. So, adhesively-bonded joints were preferred for this kind of assembly because adhesively-bonded joints separate one surface from another avoiding the effect of galvanic interaction,

improves the durability of the structure by eliminating the concept of holes and ensures good alignment and sealing behavior. It also avoids the differences in the thermal expansion coefficient composites and metals. It combines the high tensile strength of composites with the high shear strength of metals to achieve an efficient and cost-effective structure. Moreover, individual surface treatment of each substrate results in a suitable interfacial strength. These hybrid bonded joints had been in high demand in different areas, for example, high-speed ground transportation, horizontal stabilizers of aircraft and in tail sections of helicopters [57].



Figure I.16: A typical hybrid joint specimen [5]

However, the application of hybrid bonded joints is not simple and proved to pose different problems during the bonding process, Figure I.17. For example, it is critical that we understand the stress transformation behavior of both materials due to dissimilar mechanical behavior. Moreover, the adhesion system can be affected by environmental factors such as the presence of moisture can degrade the mechanical performance of metal by causing corrosion. They can also affect the bonding between the metal and adhesive, causing delamination and thus limiting their applications [58]. Moreover, various authors had verified that the bonding dissimilar materials could give rise to stress singularity at the intersection of the free edge and the interface [30]. Therefore, the selection of adhesives and joint geometry plays a crucial role in bonding two dissimilar materials. Erdogan and Ratwani [59] investigated a stepped-joint geometry to study the stress singularity phenomenon. They had demonstrated in their study that the adhesive

layer was locked as an isolated elastic medium between the adherents and the stress singularity at the end of the joint was eliminated.

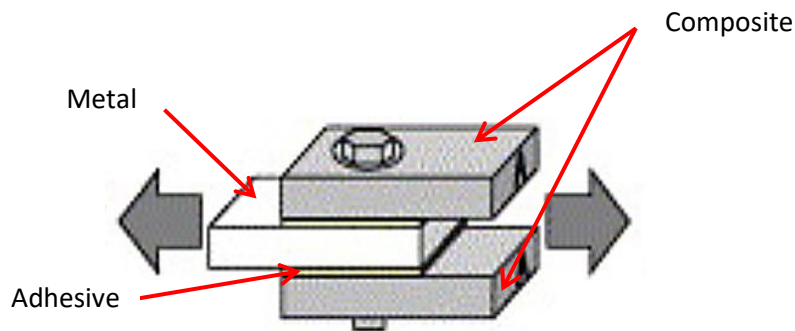


Figure I.17: Load applied on hybrid joint

I.6 Parameters that affect the performance of bonded joints

Different parameters have to be studied before and during the development of the bonded structure in order to achieve an excellent performance of the adhesively-bonded joints. The parameters which can affect the performance of the bonded assembly include material specifications (adhesive and adherent properties), manufacturing processes (surface preparation, etc.), geometric parameters (adhesive thickness, overlap length, fillet, and ply angle) and environmental factors. Some of these factors and how they affect the bonded joints are discussed briefly in this section

I.6.1 Surface preparation

During the manufacturing process, pre-treatment and surface treatment play a vital role in developing a strong and durable adhesive bond between the adherents. Pre-surface treatments ensure the elimination of all the surface irregularities and impurities such as lubricants, dust, and loose corrosion layers. A reliable surface must have good wettability, roughness, soundness, and solidity which can ensure homogeneity and adhesive conformity during the bonding process. Surface preparations improve bonded joint toughness, mechanical performance and ensure good bonding between even complex adherents. Diverse types of pre-

treatments ensure good surface preparation and are categorized into three groups: mechanical pre-treatments; chemical pre-treatments; and energetic pretreatments.

I.6.2 Adhesive bond configuration

I.6.2.1 Joint parameters

Adhesively-bonded joints can be load in shear, compression, tension, peel or cleavage which can generate defects like local stress concentration and, high peel stress. This is the reason that care must be taken in designing the bond joint design to ensure uniform distribution of stress. The selection of the appropriate adhesive is one factor that contributes to getting a suitable joint configuration and minimizing the peel load and cleavage, Figure I.18. Moreover, it can increase the cohesive strength of the entire bonded joint that's why it is important to choose the right adhesive and the right adhesive's parameters, Figure I.19.

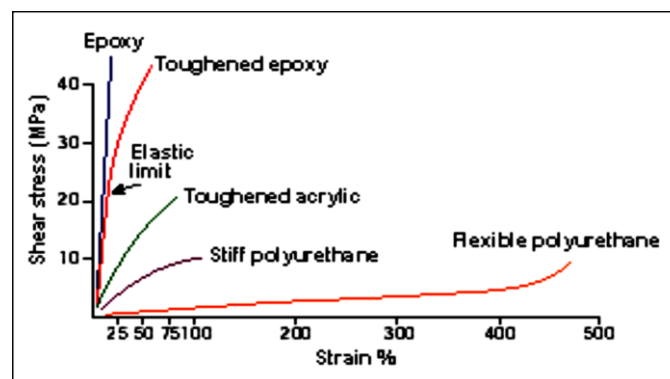


Figure I.18: Adhesive variety according to the Stress/Strain link

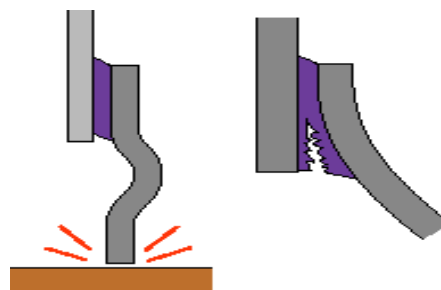


Figure I.19: Cleavage or peel owing to an impact (or static)

According to Figure I.19, the joint gradually broke while the peel stresses increased along the bond line as the load was increased. In this context, many researchers proposed different joint configurations to reduce this stress by modifying the joint geometry [60] or correcting the methods of forming bonded assemblies, Figures I.20 and I.21.

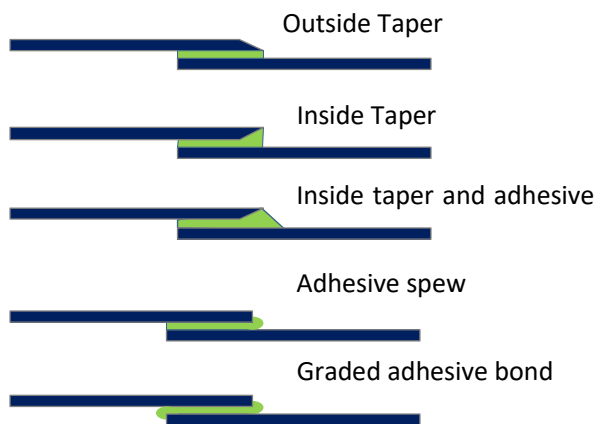


Figure I.20 : Modifications to basic lap joint

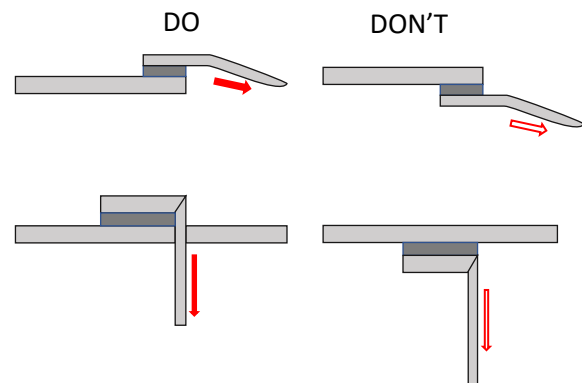


Figure I.21 : Examples of good and bad designs

I.6.2.2 Adhesive layer thickness

Adhesive layer thickness also plays an important role in bond strength and improper bond thickness can result in cohesion and adhesion failures [61]. Because of this reason, many researchers had conducted numerous studies on the effect of adhesive layer thickness on joint strength and concluded that the strength of joint increases with a thin adhesive layer. This decrease in strength can be due to more noticeable defects such as voids, micro cracks over the interface of bond lines [62]. Adams *et al.* [63] and Shah & Tarfaoui [64] further confirmed the phenomenon of a decrease in joint strength with an increase in the bond layer thickness due to the possibility of more defects. For example, a study was conducted on adhesive bonds formed by using elastomeric adhesives and showed that the strength of the joint decreased with an increase in adhesive thickness [65]. Grant *et al.* [66] showed in their study of single lap joints with mild steel that the augmentation of the adhesive thickness increased the bending moment which reduced the joint strength. Crocombe [67] discovered that the increase in thickness of the adhesive layer resulted in the fast-spreading of plasticity of the adhesive under the overlap.

Moreover, Lucas *et al.* [68] and Hunter-Alarcon *et al.* [69] showed in their respective studies that the increase of adhesive thickness can decrease the lap shear strength. They also showed in their studies that the manufacturing process of the adherent had no big influence on the applied adhesive thickness. However, Liao *et al.* [70] who worked with the ductile adhesive showed that the fracture toughness and energy of the joint was increased by increasing the thickness of bond in comparison with the brittle adhesives.

I.6.2.3 Overlap length

Overlap length is also a key factor in deciding joint strength. The perfect overlap length ensures good bonding between the adhesive and adherent. Currently, the strength of the joint increases with an increase in the overlap length to a certain limit. After that, it not only affects the joint strength but also affects the strength of the overall assembly.

I.6.3 Environmental factors

Generally, the strength and durability of the adhesively-bonded joints are affected by numerous environmental factors such as temperature, moisture absorption (humidity), fire and UV [29]. Among all these factors, moisture and temperature are the most important and common factors and are discussed in detail in this section.

I.6.3.1 Moisture

The moisture absorption can cause plasticization, swelling, crack propagation in the adhesive and various researchers confirmed the degradation of mechanical properties of adhesive occurs in the presence of humidity [71]–[76]. The moisture absorption mainly affects the interface of the bond and cause a decrease in their strength. The potential causes of the increase in the stresses consist of adhesive can be due to the reduction of adhesive toughening thus less stress relaxation [77].

I.6.3.2 Temperature

In designing the bonded joint, the variation of adhesive mechanical properties with temperature should be taken into consideration for example the stress-strain behavior or the change in toughness [78]–[80]. In general, the mechanical performance of adhesives increases by decreasing the working temperature because at higher temperatures the adhesive becomes soft and shows more viscoelastic behavior thus decreasing the durability of the structure [81].

I.7 Characterization of mechanical properties

The mechanical strength of polyepoxide arrays and bonded assemblies made from these materials are generally characterized by destructive testing. These studies establish laws of material behavior and define the conditions under which a broken structure.

There are two main types of mechanical tests:

- Mechanical tests to study cracking of material by causing cracking in a particular area. The mechanical strength is then mainly characterized by a variation in crack length or a crack propagation velocity over time. These include wedge cleavage and toughness tests.
- Mechanical tests stress the structure or material as a whole until it breaks. These are the tensile, double cantilever beam (DCB), shear, end notched flexure ENF (ENF), ARCAN tests, etc.
- Characterization of the mechanical properties can be carried out on solid adhesives or bonded assemblies.

I.8 Enhancement of adhesive performance

According to the above discussion, it is clearly understood that even though adhesively-bonded joints have an advantage over the traditional fastening techniques but, they are not exempt from limitations such as manufacturing, delamination at the interface, environmental factors. That is the reason why many researchers are working to ameliorate the performance of these joints by

indicating different significant ways such as surface treatment and adding other components to adhesive joints like stitching or z-pining for the bonded structures [14]. However, even these methods couldn't result in developing an excellent adhesively-bonded structure. During the past two decades, the development of nanotechnology and the introduction of nanofillers have revolutionized the properties of epoxies and adhesives and provided better solutions. Numerous publications over recent years had shown that adding nanofillers to the adhesive made it more resistant, reliable and resulted in the long service life of the structure. A variety of nanofillers, such as carbon nanotubes (CNTs) [82], [83], graphene, carbon black and metal and their derivatives nanoparticles [84] like alumina silicates [85], [86] were currently been used as additives in adhesives. It is a fact that adding nanofillers would increase the mechanical performance of the adhesive by increasing its strength and resistance to fracture but, after reaching some percentage limit, adding more nanofillers could result in a reduction of properties due to the factors such as agglomeration. So, it is vital to find the percentage threshold of adding these nanofillers in the adhesive to get the optimal bond. This area of study is still in the preliminary stage and has more room for investigation. This review paper presents a recent and concise overview about the adhesively-bonded joints summarizing the types of adhesives with their advantages and limitations then the different fabrication processes used specifically for adhesively-bonded joints, factors affecting their performance, their characterization methods, how to enhance their performance and then most importantly the advancement of these joints with nanotechnology.

I.8.1 Z-pining

Z-pining is a method in which short, steel pins at ± 45 angles are inserted through the thickness of the joint in the z-axis as reinforcements, Figure I.22. Huang *et al.* [87] investigated this method using rod-shaped pins for the first time to reinforce polymer laminates in 1978 and demonstrated that the bond strength for short beams was increased up to 73%. Furthermore,

Tao *et al.* [88] studied the effects of different parameters such as Z-pins' diameter, spacing and overlap length on the performance of ceramic matrix composite single lap joints. Their results showed an increase in the performance of bonded joints by increasing the diameter and reducing the spacing of Z-pins, Figures I.23 and I.24. Löbel *et al.* [89] demonstrated in their study that integrating z-pinning into CFRP double-lap joints ameliorate the tensile strength of the adhesive bond. Son *et al.* [90] and Ko *et al.* [91] investigated the use of stainless-steel and jagged pins respectively in their studies on single-lap joint specimens and were subjected to various environmental conditions, Figure I.25.

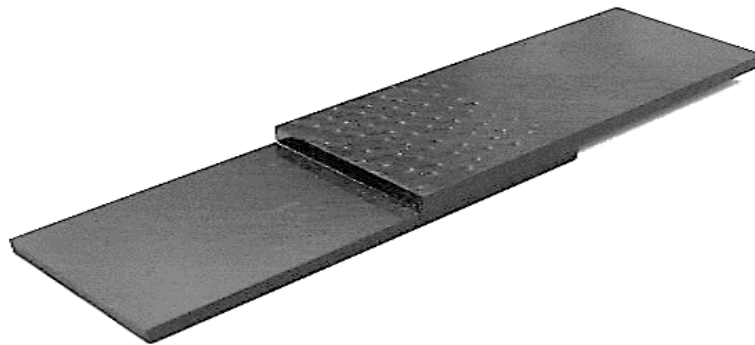


Figure I.22: SLJ reinforced with Z-pinning

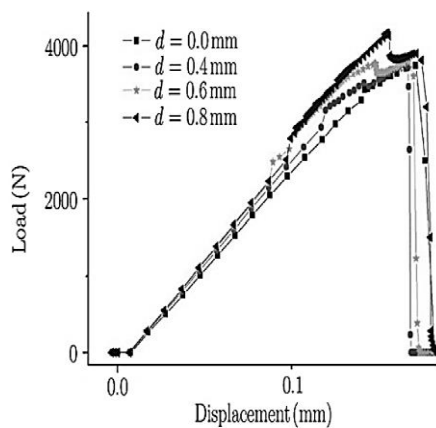


Figure I.23: Load vs displacements with different Z-pins' diameters

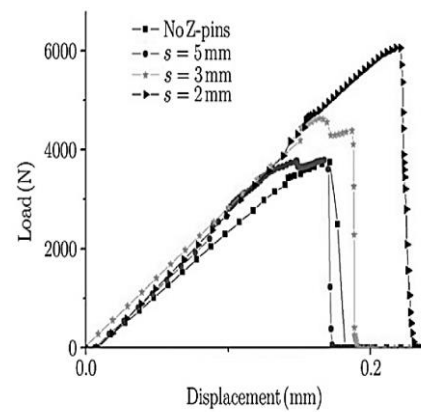


Figure I.24: Load vs displacements with different Z-pins' spacing

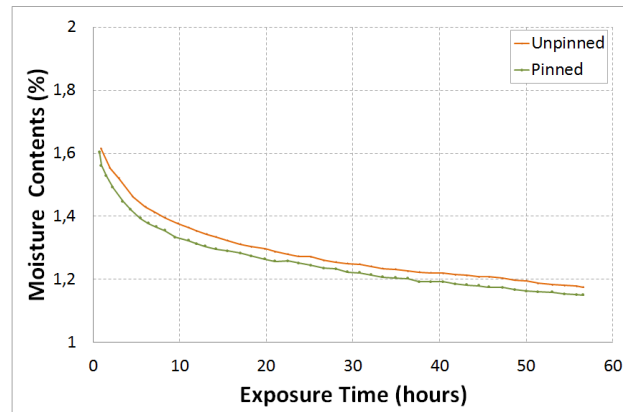


Figure I.25: Influence of pinned structure on the moisture absorption

Moreover, Chang *et al.* [92] had also shown in their study that z-pinning increased the tensile and fatigue of single-lap joint samples. Park *et al.* [93] examined the effect of z-pins on the tensile properties of adhesive bond through pull-off tests of T-joint samples and showed an increase in the mechanical properties. Chang *et al.* [94] further investigated the effect of z-pinning on polymer composite joints and showed in their results that thermal and damage tolerance of the bond was increased. However, this Z-pinning process is not so effective in retarding longer cracks and they also didn't appear to be good resisting for the crack initiation phenomenon [95], [96], Figure I.26, I.27.

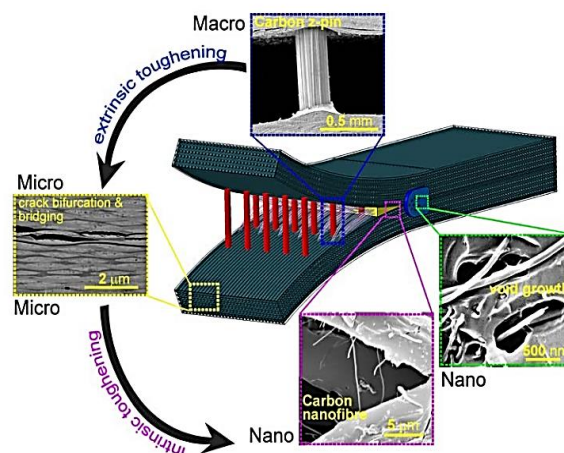


Figure I.26: Schematic representation of the different steps of toughening processes with the z-pin method

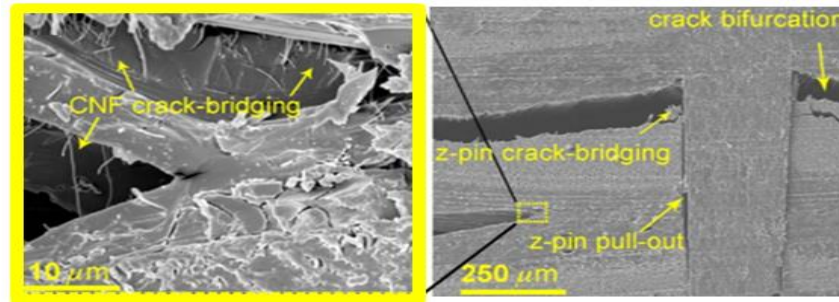


Figure I.27: SEM micrographs of the delamination around z-pin reinforcements [97]

I.8.2 Stitching

Stitching is a method in which the mechanical performance of the adhesive bond is increased because it behaves like a reinforcement material in the joint [98], Figure I.28. Many researchers have performed various studies to show the significance of stitching in single-lap adhesively-bonded joints and compared its fatigue resistance with other conventional assembling techniques [99]–[101]. Different studies showed that the stitching creates a large-scale bridge in the delamination zone thus increasing the fracture toughness and fatigue resistance of the materials [8], [102]–[104], Figure I.29. An example of the increase in fracture toughness of the materials due to stitching is shown in Figure I.30. However, the failure modes in a stitched specimen are mostly fiber breakage or pull-out [105]. This stitching process improves mechanical performance in the thickness direction of the joint by combining the performance of upper and lower adherents [105]. Beylergil *et al.* [8] explained in their investigation that stitching in the single-lap joint of composites decreased the peel and the shear stresses within the adhesive bond through-thickness direction [106].



Figure I.28: Specimen of 3D stitched woven composites [106]

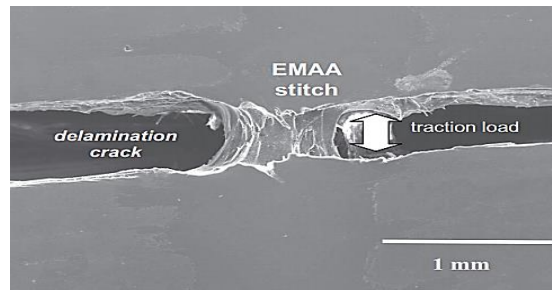


Figure I.29: EMAA stitch bridging the delamination crack in the composite (The stitches consist of poly (ethylene-co-(methacrylic acid)) (EMAA) filament)

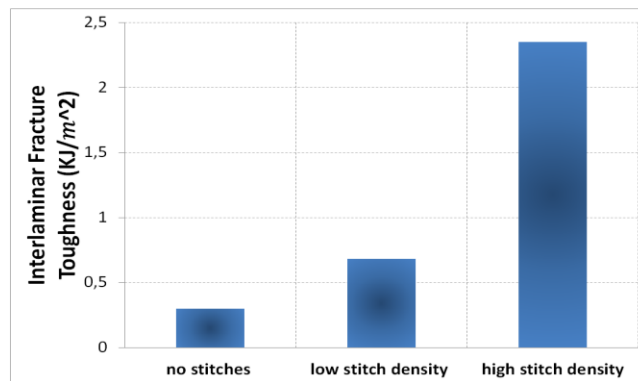


Figure I.30: Effect of the unstitched and stitched adhesive-bonded joint on the evolution mode I interlaminar fracture toughness [102]

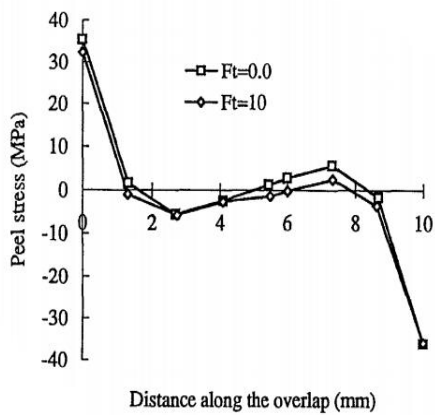


Figure I.31: Influence of thread pretension on the peel stress distributions

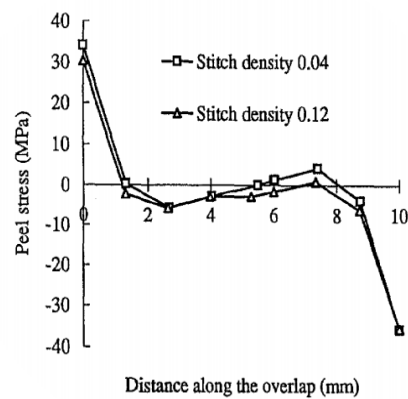


Figure I.32: Influence of stitch density on the peel stress distributions

In addition, many researchers also studied the transverse stitching method and showed how it also stops the delamination hence, increasing the fracture toughness [99]–[101], [103], [104],

[107], [108]. Tong *et al.* [100], [109] studied the phenomenon of transverse stitching of an adhesively-bonded composite joint and showed that the tensile strength was increased up to 40% and axial displacement was increased up to 25% in comparison with the unstitched specimens. Moreover, their results indicated that stitching of the double lap joint decreased the positive peel stress and stabilized the negative peel stress thereby improving the strength of the joint, Figure I.31, I.32. Stitching in a single lap joint also generates a positive effect and increases the fatigue resistance and fatigue life of the joint [110]. Even though stitching increases the mode I (G_I) values of the joint [111] but it has minimal effect on the mode II (G_{II}) energy which shows that stitching improves the tensile strength of the bond but does not improve the shear strength of the bond, Figure I.33.

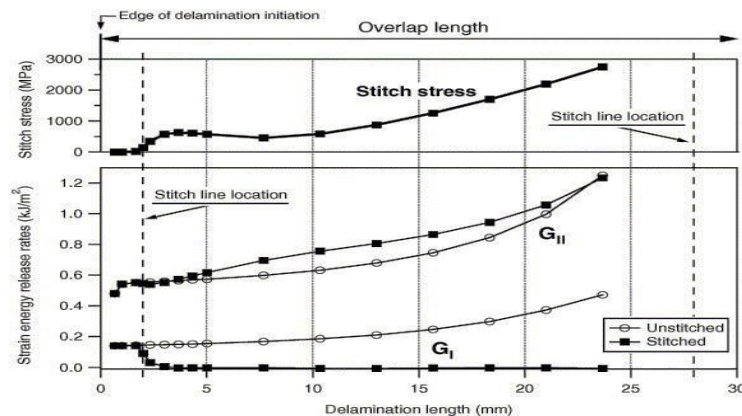


Figure I.33: Difference in strain energy release and stitch stress vs delamination length between unstitched and stitched specimens

Similarly, Beylergil *et al.* [8] conducted a similar study and showed that the stitching process on the composite joint increases the joint strength. Tong *et al.* [109] did the same study and showed that the stitching enhanced the tensile strength by 20% and displacement by 25% of single lap joint. They also confirmed in their investigation that stitching also improved the mode I and mode II fracture toughness of the adhesive joint. Furthermore, Tada and Ishikawa [159] demonstrated the effect of stitching on bonded carbon-fiber-reinforced polymer (CFRP)

laminates and showed in their results that stitching increased the damage tolerance of the material. It also limits the crack propagation phenomenon thus, delayed the final fracture.

Sawyer [99] studied the improvement of static failure strength of single lap joints of composites using stitching and stated an increase of fracture strength up to 38%. Velmurugan et al. [160] demonstrated in their study that stitching delayed the crack initiation and crack growth in cylindrical shells subjected to axial compression. Chung *et al.* [112] studied the effect of stitching techniques on the bond strength of CFRP and KFRP and showed an increase of 25% in the joint strength in their results. Moreover, they observed that the improvement in the bond strength due to the stitching phenomenon was influenced by the number of laminated layers. Some other factors can influence the efficiency of stitching on joint behavior subjected to bending load, for example, the notches made by the stitching technique in the overlap region could result in the propagation of fracture from the middle of the joint instead of the edge [98]. Jain *et al.* [100] confirmed in their study that the stitched adhesive joints achieved an improvement of 36.5% in fracture strength of thick SLJ specimens with 7 layers. Furthermore, I-fibers (glass fiber) were also used for stitching within the RTM (Resin Transfer Molding) single-lap joint samples which increased the fracture strength of the bond up to 34.6 - 68.0% in comparison to the samples without stitching [105].

However, the stitching method is affected by different parameters such as stitch rigidity, strength, thread type, diameter, stitching density, pattern, laminate thickness and the stitch-matrix interaction. Stitching can cause significant damage in composite adherents such as delamination and can influence the mechanical performance of the structure due to the passing through viscous pre-preg layers [8], Figure I.34. Moreover, stitching threads can cause other defects such as more stitches result in more holes, hence increasing the stress concentration and stitches can also increase the material's porosity by introducing microbubbles due to the chemical reaction [102], Figure I.35- I.36.



(a) Top view



(b) Front view

Figure I.34: Damaged stitched specimen for out-of-plane tests [113]

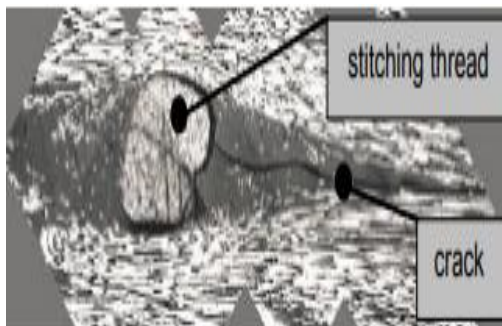


Figure I.35: Crack owing to the stitching thread

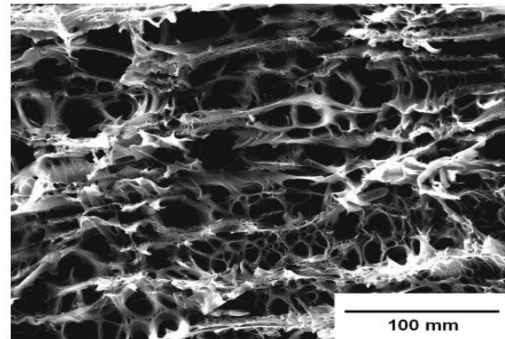


Figure I.36: Porous microstructure of EMAA stitch

Stitching can also cause a significant loss of bending strength if the bond thickness of SLJ is increased after a certain value due to the broken stitched yarns and reinforcement fibers during the loading stage before achieving the peak load. Moreover, stitching can result in large notches that can be partially filled with resin in the skin layer; the increase of the layup thickness may the stitching to occur in large notches which can be partly filled with resin in the skin layer [166]. Variation of bending stress for stitching showed that the bending strength was decreased because stitching could cause the formation of a concave notch. This decrease in bending strength was due to the presence of a large number of layers however, the bonded lap joint without stitching showed an improvement in bending strength by increasing the thickness of the joint [135], Figure I.37.

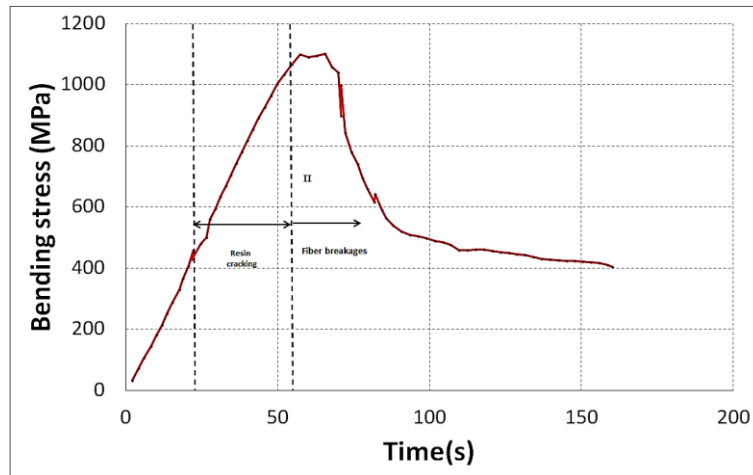


Figure I.37: Influence of stitching on the bending stress-time curve for shifted BLJ samples [98]

I.8.3 Adding inter-adherent glass fibers

Aktas and Polat [8] introduced a novel technique in which glass fibers can be reinforced into adhesively-bonded joints to improve their mechanical performance. In this method, the inter-adherent glass fibers pass through the composite adherent as a pin so this method is specifically applicable to improve the adhesively joint performance of composite /composite. This method is easier in fabrication as compared to other previously mentioned processes and is more effective under high failure loads. The inter-adherent glass fibers enhancement method works more effectively on increasing the joint tensile strength and is faster hence more convenient for most applications.

Beymergil *et al.* [8] applied four glass fiber pins at each edge of the overlap zone and showed that strength and failure limit was increased by 80% and 60% respectively, Figure I.38- I.39. They confirmed that this method is better than Z-pining and stitching because both Z-pining and stitching methods improved the joint performance only by 25% and 40% respectively. In addition, Aktas and Polat [114] stated in their study that the static strength of single-lap joints was increased significantly by incorporating the inter-adherent fibers on the adhesively-bonded joint.

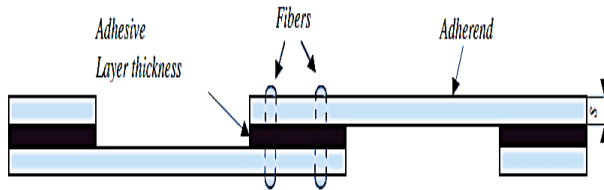


Figure I.38: Sample of the joint with fiber [8]

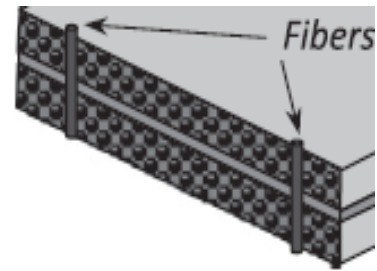
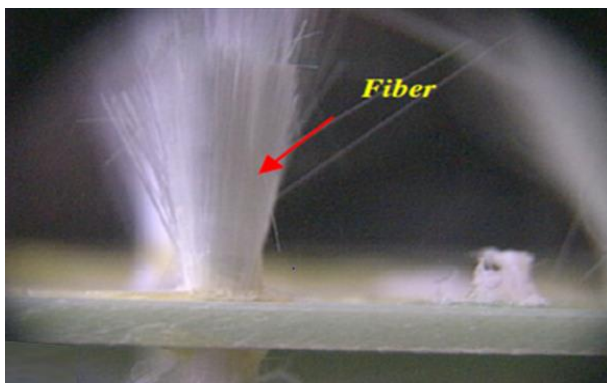
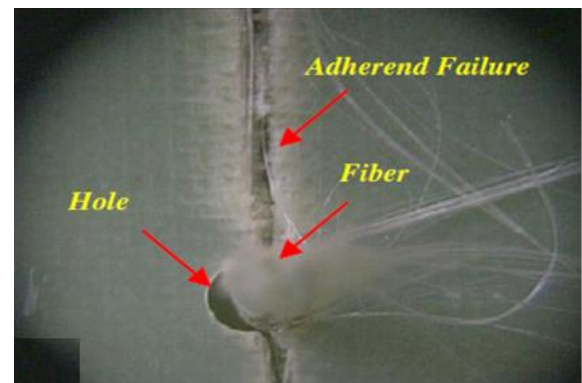


Figure I.39: Incorporation of fiber [8]

However, even this method has the well-known problem of creating stress concentration regions near the line of holes. Also, they increase the brittleness of the bond and make the failure a sudden catastrophic failure with little bursting sound. This phenomenon will fail in adhesive first and then transfer the entire load to the adherend making it critical for them. The inter-adherent fiber would then start lifting out of the adherent [8], Figure I.40.



(a) Lifting out failure



(b) Adherent failure

Figure I.40: Type of failure with including glass fiber [8]

I.9 Adhesive enhancement

In addition to the surface treatment and modifying the entire bonded structure, it is also possible to modify the morphology of the polyepoxide resin to strengthen its resistance to external stress. The proposed amendments as a whole concern the incorporation of nanoparticles to increase the overall strength and durability of the material. The incorporation of nanoparticles in the

resin consists in constructing a nanocomposite structure which is to be studied to improve its mechanical properties

I.9.1 The principle of nanocomposite

Nanocomposites are composites with nanoscale morphologies such as nanoparticles (nanotubes, graphene...), or lamellar nanostructures in one phase. They have multiphase, and multiphase materials should have at least one phase with diameters in the 10-100 nm range.

Nanocomposites have developed as viable options to overcome the limitations of various engineering materials nowadays. The dispersed matrix and dispersion phase components in nanocomposites can be categorized [115].

It is now possible to generate numerous fascinating new materials with unusual properties using creative synthetic approaches thanks to this fast-expanding discipline. The properties of the so-called founds were determined not only by their originals' properties but also by their interfacial and morphological traits. Of course, we can't ignore the fact that the newly formed property of a material is occasionally unknown to the parent constituent materials [116]. As a result, the concept behind nanocomposite is to develop and produce new materials with remarkable flexibility and improvements in their physical qualities by using building blocks with dimensions in the nanoscale range.

Nanocomposite materials, which are made by combining two or more different building constituents into one material, have unique features that are attributed to their small size, vast surface area, and, of course, the interfacial contact between the phases. Nanocomposites are solid mixtures of a bulk matrix and nano dimensional phase(s) with different properties due to structural and chemical differences [117].

I.9.1.1 Matrix

Polyepoxide resins were introduced in the late 1930s. Commonly used due to their high mechanical strength compared to other adhesives structural, their low shrinkage after crosslinking, their good adhesion on many types of substrates, as well as their good chemical and thermal resistance. These adhesives consist of two main compounds: an epoxy prepolymer and a hardener [15]. The choice of hardener influences the type of chemical bond obtained, the degree of crosslinking, the reaction rate, the degree of exotherm and the glass transition temperature of the resulting network. There are several types of reactions. Most of the crosslinking agents used are of the amine or anhydride type. For adhesives, the reaction with the amine hardeners (termination in $-NH_2$) is preferred. In general, epoxy amines have a higher adhesion than epoxy anhydrides, the latter being essentially used for their electrical insulation property. The choice of hardener is made according to the conditions of use and the desired properties.

I.9.1.2 Nanodimensional phase

Since the discovery, nanotechnology has revolutionized the field of research and now a day these nanofillers are being continuously utilized to improve the mechanical performance of structural materials at different domains such as improving the performance and overcoming the limitations of adhesively-bonded joints [118]. They improve the tensile strength and fracture toughness of bonded joints, without imparting the phenomenon of embrittlement because they form micro or nano scale bond-lines [27].

In general, nano-additives that ameliorate the mechanical properties of adhesive consist of graphite, diamond, fullerene, carbon black (CB), metallic particles and carbon nanotubes (CNT) which are classed as stable allotropic forms of carbon. In addition, it was found that functionalizing the carbon nano materials can further modify a large number of

physicochemical properties, such as conductivity, filler transfer/separation, filler transport, magnetism, fluorescence, dispersibility and morphology, Figure I.41.

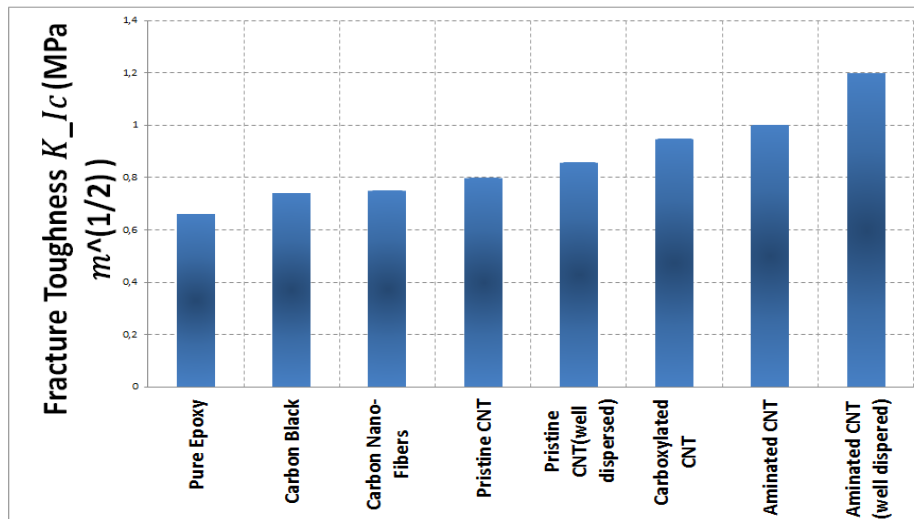


Figure I.41: Fracture toughness values for a variety of nanofillers

Furthermore, their properties depend on other parameters such as the dispersion state of the nanofillers in the adhesive, added weight percentage, the interface between the adhesive and the intrinsic parameters of fillers (shape, length, density, and morphology) [27]. During the dispersion CNTs in adhesive, an important phenomenon to prevent is the appearance of agglomerates which is caused by non-uniform dispersion of reinforcement in the adhesive. Moreover, it was also reported in several investigations that intrinsic strength and shape (aspect ratio) of nano-fillers play a vital role in the strengthening of the interfacial bond between the fillers and the matrix. This can lead to enhancement of mechanical performance of matrix material for example CNT, GNP and CNH have different shapes and affect the properties of matrix differently from each other [13].

I.9.1.3 Carbon Black (CB)

The carbon black (CB) is a powder consisting of nano spherical shape particles created by carbon atoms with a more or less graphitic organization and with sizes of a few tens of nanometers of 30nm [119], Figure I.42. To be more precise, carbon atoms are linked together

by covalent bonds and organized in clusters to form complex three-dimensional entities and then these entities are linked together on a scale of hundred nanometers to form aggregates. These aggregates are then assembled into bigger clusters by attractive Van der Waals forces and form agglomerates of several hundred microns, Figure I.43. CB plays an important role not only in improving the mechanical performance but also in improving the electrical conductivity of polymers by improving the flow of electrical charge through the material [120], [121].

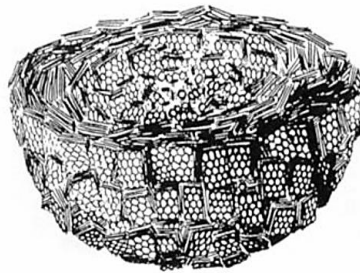


Figure I.42: Carbon Black particle (CB) [122]

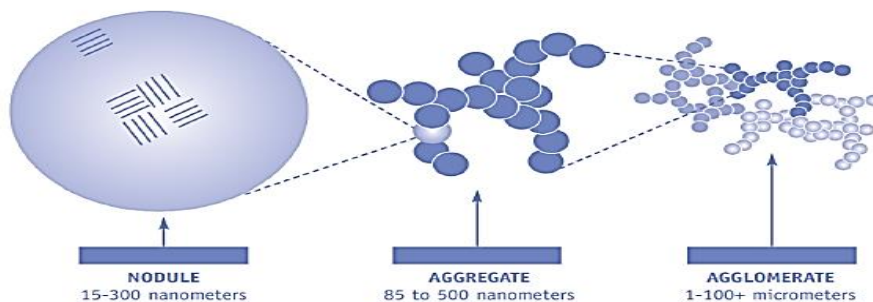


Figure I.43: Carbon Black structures [122]

I.9.1.4 Metallic powder

The metal powders such as silver, nickel, copper, aluminum have densities ranging from 0.6 to 2.2. They have a low form factor (geometry) and therefore require high weight concentrations to obtain a conductive network. However, these metallic powders have very high electrical and thermal conductivities for example, the electrical conductivity of this type of material is in the order of 10^7 S/m. At the same time, metal charges have a high coefficient of thermal expansion and can be easily oxidized due to their very high surface energy. That is why these fillers perform badly in an oxidizing environment.

I.9.1.5 Graphene Nanoplatelets (GNPs)

The GNPs are well-known for their electrical behavior, thermal performance, mechanical reinforcement, and gas barrier layers however, GNPs properties can be affected by their manufacturing methods, Figure I.44. They are also known as graphene nano-platelets (GNPs), graphene, and graphene oxide [27]. Graphene has several functionalities with polymers, ceramics and metal as a replacement in structural reinforcements (Carbon/glass fiber replacement), in high-temperature performance, flexible strain sensing and total barrier coating (anticorrosion paint) due to their electrical conductivity, damage tolerance (fatigue, toughness, and wear resistance), high aspect ratio (length to thickness ratio), a unique graphitized planar structure and low manufacturing cost. That is why currently, polymer composites are preferred with GNP-reinforcement. Moreover, in a polymer matrix, these nanofillers show the formation of larger contact areas thus leading to a higher load transfer and mechanical properties. Tarfaoui et al. mentioned in their work that including the low percentage weight of GNPs was classified as part of a strategy to improve the mechanical properties of the nanocomposites [123].

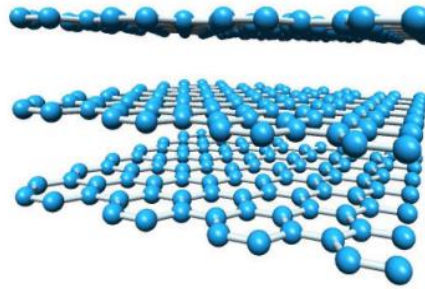


Figure I.44: Multilayer Graphene

I.9.1.6 Graphite

Graphite structure consists of stacked graphene planes separated by a distance of 3.3 Angstroms. A graphene plane consists of carbon atoms with a 1.4 Å interatomic distance and these carbon atoms are organized in a hexagon. These planes can slide relative to each other due to weak Van der Waals links present between the layers.

I.9.1.7 Diamond

Diamond is a three-dimensional allotropic form of carbon. Diamond further has several crystalline forms and cubic diamond with a mesh size of 0.35 \AA and an interatomic distance of 0.15 \AA is the most common one. Hexagonal diamond is also known as “lonsdaleite” is another example that is a metastable crystalline structure.

I.9.1.8 Fullerene

Fullerenes are pure carbon molecules consisting of 60 carbon atoms that are arranged in a balloon-shaped cage and were discovered in 1996. The First fullerene discovered was “Buckyball”, Figure I.45. The creation of fullerenes began in 1990 and was the third allotropic form of carbon after graphite and diamond. C₆₀ are solid molecules and good acceptors of electrons, redox reactions and good ability to trap its extraction solvents, hydrocarbons and gases like oxygen from the air. Different chemical groups or species can be attached to their surface which can modify their physicochemical characteristics. In addition, it can also behave like a catalyst in different chemical reactions. There are other types of fullerenes depending on the number of carbon atoms such as C₇₀, C₇₆, C₇₈ and C₈₄.

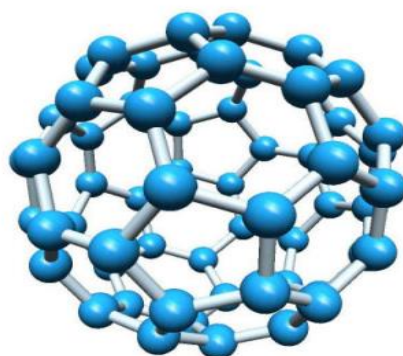
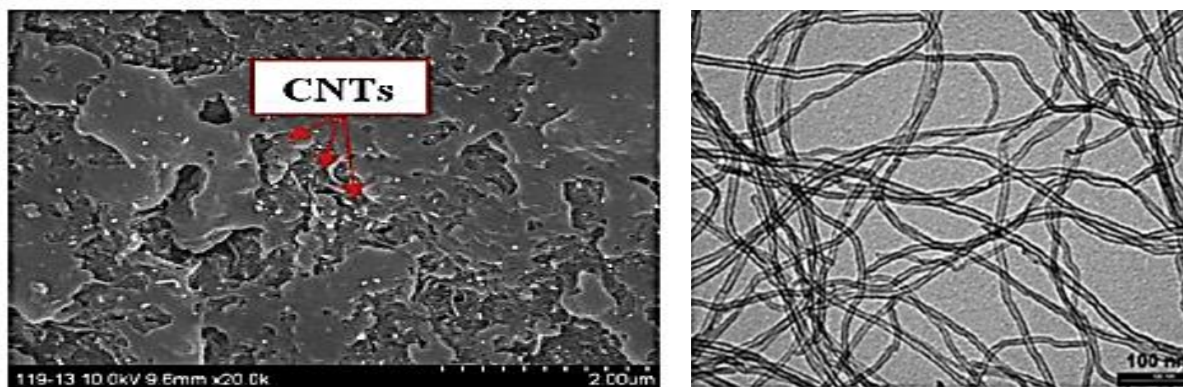


Figure I.45: Buckyball

I.9.1.9 Carbone nanotubes (CNTs)

Carbon nanotubes were first discovered by Sumio Iijima in 1991 [124]. The structure of CNTs is cylindrical and is formed by rolling graphene layers. The CNTs can be monolayer (single-wall) or multilayer (multiwall) depending on the number of graphene layers used in fabricating

them. CNTs are used intensively as a reinforcement in next-generation materials due to their good specific strength, specific modulus, thermal conductivities, electrical conductivities and reinforcement abilities [119][125], Figure I.46. The CNTs had been investigated to enhance the mechanical, electrical, and thermal properties of polymer composites in numerous studies and many researchers found that adding CNTs to epoxy adhesive improve even with a low concentration [10], [12], [126]–[128]. CNTs can form two types of bonds when dispersed in the matrix material i.e., covalent attachment and non-covalent attachment. A non-covalent attachment [129] makes the nanotube's surface more compatible with the polymer matrix due to absorption of an organic molecule but their interactions are poor and are presented by Van der Waals interaction or hydrophobic interactions. The non-covalent bond contributes more to stabilizing the electrical properties, however; they show a reduction in the mechanical properties. In contrast, a covalent attachment certainly plays an important role in enhancing the interfacial interaction between the polymer and CNTs [130] while, it can create a risk of losing some electrical properties of the CNTs as is mentioned in the work of El Moumen *et al.* [128] [131].



(a) SEM morphology of CNTs randomly distributed

(b) TEM morphology of CNTs into Epoxy

Figure I.46: Morphology of random distribution of nanotubes with epoxy matrix [128]

CNTs can be aligned or randomly arranged in the poly and their orientation can show different mechanical properties, for example, the aligned CNTs act as reinforcing fibers and show a

significant increase in their mechanical strength [132]. However, randomly oriented CNTs show a slight improvement in the mechanical properties due to their poor dispersion which can result in agglomeration thus, decreasing the interfacial bonding strength between them and matrix [133], Table I.1.

Table I.1: Mechanical properties of CNT in a different orientation

	Aligned oriented nanotubes	Randomly oriented nanotubes
Young's modulus	Varied from 80 GPa	Do not exceed 6 GPa
Tensile strength	Varied from 3600 MPa	Do not exceed 100 MPa

In addition to mechanical properties, CNTs also influence the electrical behavior of the epoxy but it depends on the parameters such as the temperature of measurement, the concentration of CNTs and morphology of CNTs, the presence of carbonaceous impurities or residual catalytic particles, the presence of defects on the surface of the nanotubes, their cluster aggregation state, and CNT-CNT and CNT-matrix interactions [134].

Moreover, in respect of thermal properties, the addition of CNTs in matrix material increases the glass transition temperature, thermal conductivity, thermal diffusivity and thermal diffusion coefficients and these properties are influenced by their purity, dispersion and orientation (alignment) in the matrix [135].

Adding CNT thus contributes to reducing damage area in composite samples as is demonstrated by Benyahia *et al.* [136]. El Moumen *et al.* [131], [137] proved in their numerical model that adding a low percentage of CNTs enhances the fracture interfacial rigidity and can block the progress of micro-cracks.

I.9.1.10 Single-walled nano-tube (SWCNT)

A single-walled carbon nanotube (SWCNT) is composed of a single layer of graphene rolled up on it forming a cylinder, Figure I.47. This graphene layer is characterized by several hanging

bonds with high surface energy [138]. To eliminate these hanging bonds, the total energy of the carbon atoms is reduced, which contribute to increasing the deformation energy and as a result a formation of a tubular structure [138]. A graphene layer can be rolled in either direction to form two kinds of edges of CNTs called "zigzag" and "armchair", Figure I.48. SWCNTs have a classical diameter of 2 nm and a length of 30–50 nm [139].

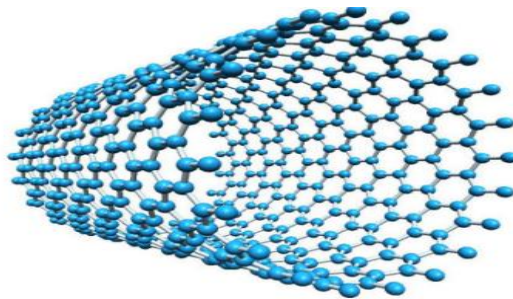


Figure I.47: Single-walled nano-tubes (CNT)

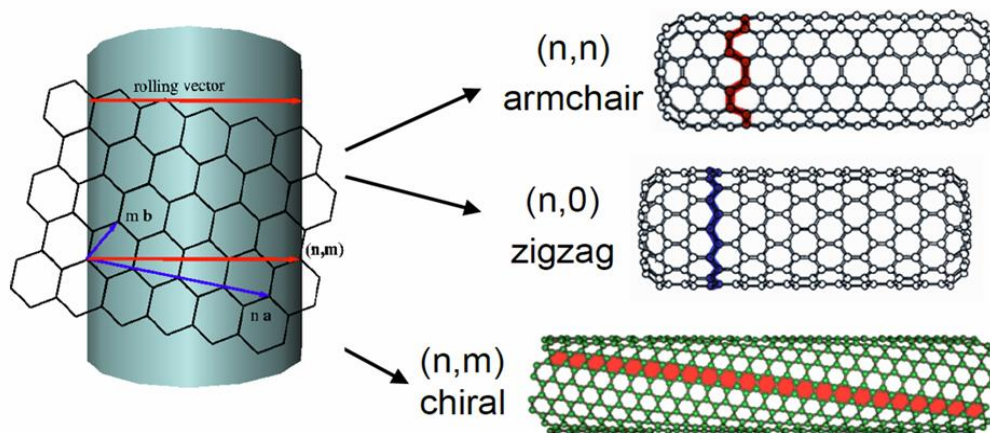


Figure I.48: Kind types of Single-walled Carbon [122]

I.9.1.11 Multiplied walled nanotubes (MWCNTs)

Multi-walled carbon nanotubes (MWCNTs) are created with several concentric tubes with different chirality, Figure I.49. The distance that separates two consecutive layers in MWCNTs is to the order of 0.34 nm. The diameter and length of the MWCNTs can range from 5 to 50 nm and from 10 nm to several hundred micrometers, respectively.

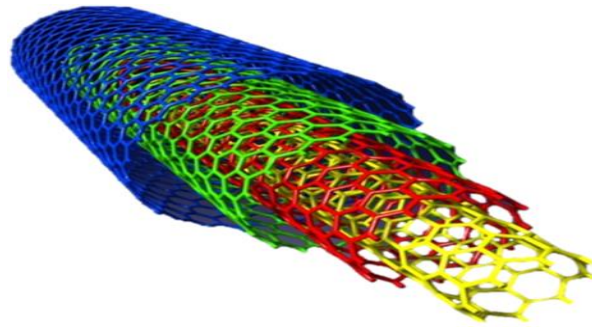


Figure I.49: multi-walled carbon nanotubes (MWCNTs)

Table 2 gives a comparison between the SWCNT and MWCNT properties.

Table I.2: Carbon nanotube proprieties

Proprieties	SWCNT	MWCNT
Density (g/cm ³)	0.8	0.8
Young's modulus (TPa)	1.3±0.3	1.28±0.6
Electrical conductivity (S/m)	5.10 ³ -5. 10 ³	10 ³ à 10 ⁵
Specific surface (m ² /g))	1200	300

I.9.2 Influences of Nanofillers on adhesive performances

I.9.2.1 Metallic Nanoparticles

Dudkin *et al.* [140] clarified that the interaction makes it within active surface groups of the oxide nanoparticles and functional groups of the epoxy matrix make the reinforcement g-Al₂O₃ result in a strength increase. However, they indicate that even though the inclusion of filler particles can enhance the mechanical properties, it still generates other factors that cannot be examined in isolation using commercial adhesive systems [141]. Zhai *et al.* [142] showed in their study that integrating 2% nano- Al₂O₃ improved the strength of adhesive by 5 times in comparison to adhesive without reinforcement. They also demonstrated in their study that their type of nanofillers and roughness of counter faces contributed to enhancing the strength of the epoxy adhesive.

Moreover, many researchers studied the effects of adding metallic macro-fiber-reinforcement in adhesively-bonded joints and showed that this-reinforcement method ameliorated the

mechanical properties of the adhesive. Adding metal fiber-reinforcement presented a significant increase in the mechanical performance due to their different direction such as longitudinal and transverse directions in the adhesive fillet and adhesive layer [209]. You *et al.* [10] examined the influence of circular and triangular metal fibers when inserted into the fillet of adhesively-bonded single lap joint. Their results showed that the circular metal fibers were more effective and increased the bond strength up to 45%. Khoramishad and Razavi [10] indicated that including aluminum fiber a-reinforcement into the adhesive layer of a single lap decreased the shear and peel stresses and ensured better stress distribution thus making the bond joint more resistant.

I.9.2.2 Carbon nanotubes (CNT)

Many researchers studied the effects of CNTs a-reinforcement in the adhesively-bonded joints. Kim *et al.* [143] found in their study that CNTs were a very efficient reinforcement material that can affect the bond and the joint strength positively. Srivastava [144] studied that adding 3% CNTs a-reinforcement in adhesive, showed a significant increase in the properties of single-lap joints formed between carbon/carbon composites and carbon/carbon-silicon carbide composite materials. This investigation demonstrated that the CNTs, a-reinforcement, ameliorated the toughness and strength of the epoxy resin, leading to the increase of resistance of adhesively-bonded joint against the shear and the crack deformation, Figure I.50.

Yu *et al.* [144] showed in their study the effect of adding CNTs in epoxy adhesive joints by applying the Boeing Wedge test under water at 60°C. They indicated that 5wt.% CNT improved the strength and durability of the joint. In addition, they showed in their results that even with 1wt% CNTs, the fracture toughness was enhanced up to $7.4 \cdot 10^6 \text{ J m}^2$ in comparison to neat epoxy joint i.e., 1983 J m^2 . Park *et al.* [145] studied that including 1.5 wt% carbon black (CB) in the adhesive, improved the performance of the joint by 22%. Garrett *et al.* [146] studied the effect of adding CNTs in the adhesive on Mode II steel composites rupture strength and

composite-composite bonding applications. It was found that including 1-5% MWCNTs into the adhesive contribute to improving the shear strength by about 46% [147]. Kang *et al.* [148] investigated the influence of including 2wt.% CNTs in the adhesive on both static and dynamic strengths of composite-aluminum single-lap joints. They examined the fatigue strength and found that 2wt.% CNTs made the joint 13% tougher.

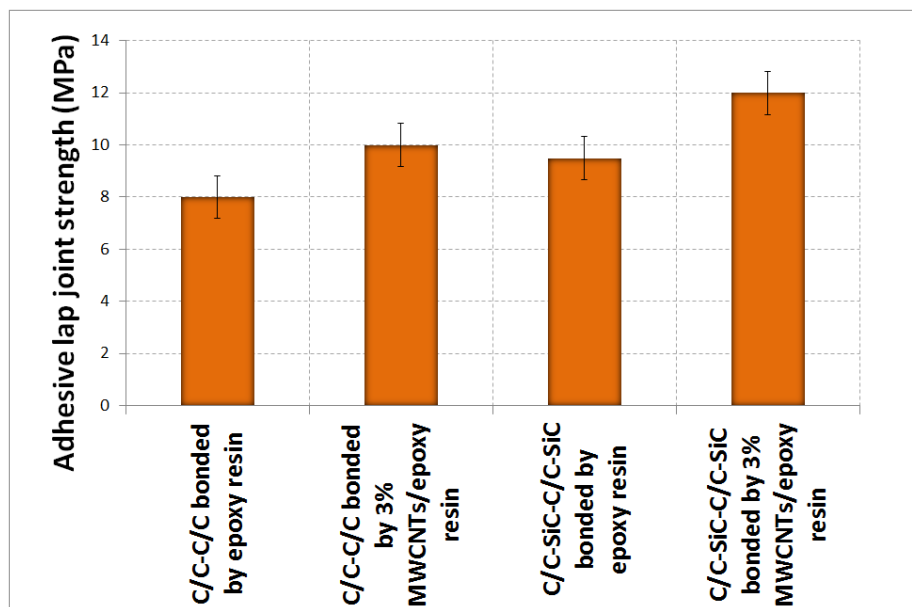


Figure I.50: Influence of adding 3% of Carbon Nanotube (CNT) on the adhesive strength [144]

Soltannia *et al.* [149] examined the influence of adding graphene and CNT-reinforcements to the adhesive single-lap joint between composites. The results showed that graphene and CNTs improved the fracture strength of the joint by 15% and 40% respectively. Wernik and Mrguid added CNTs with Polyvinylpyrrolidone (PVP) which were used to stabilize CNTs in an aqueous environment and studied their influence on adhesive, Figure I.51. Adhesive bond presented excellent enhancement in its tensile strength about 90%, while there was only a 54% improvement by adding just CNTs. Moreover, the DLS tests showed an increase of just 25% in shear bond strength by adding CNT & PVP while there was no evident transition by adding just

CNTs. Similarly, the DCB tests show that adding CNT & PVP lead to an increase of about 36% in the critical strain energy release rate in comparison with the pure epoxy, Figure I.52.

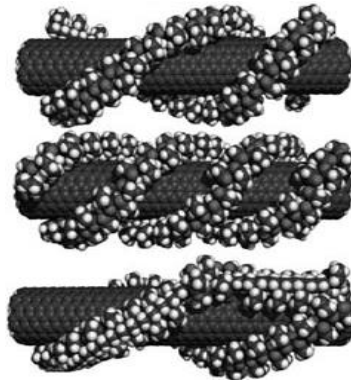


Figure I.51: CNT+PVP

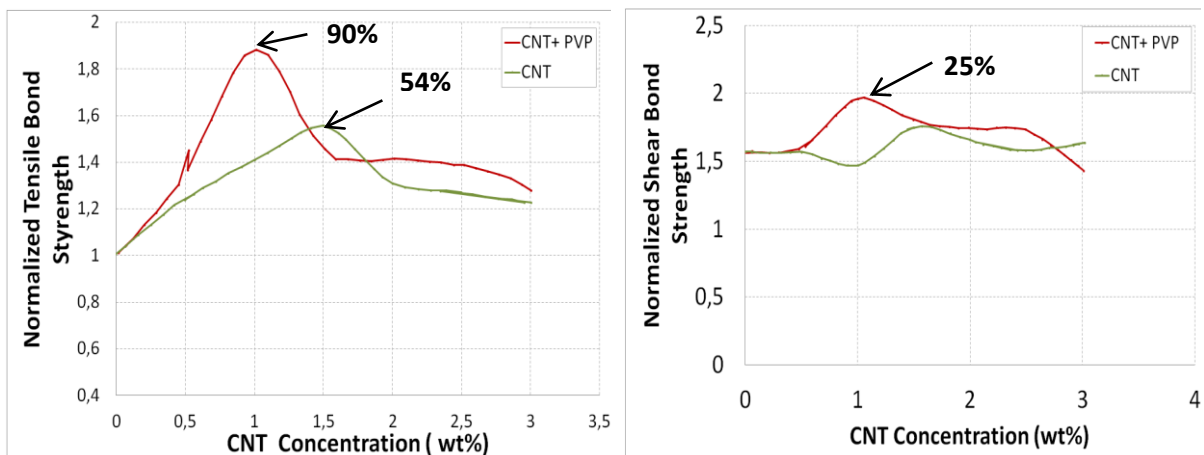


Figure I.52: Mechanical properties of the epoxy adhesive reinforced with the CNT & PVP

Sydlik *et al.* [82] showed that reinforcing epoxy adhesive with functionalized CNT increased the strength by about 36% and 27% compared to neat epoxy and unfunctionalized MWCNT adding to the epoxy respectively. Ruchi *et al.* [150] indicated that incorporating 1wt.% CNT to epoxy adhesive increased the shear strength by 48%. They also showed that adding CNTs increased the shear strength of adhesive by approximately 52%. Yu [146] indicated that adding MWCNTs in the epoxy-resin leads to good fracture toughness and fatigue strength, Figure I.53, I.54. The SEM micrographs verified that nanomaterials gave a different aspect to the fracture surfaces due to their distinct mechanisms of energy dissipation. Zielecki *et al.* [151]

investigated the influence of incorporating MWCNT reinforcements in the adhesive on the fatigue strength and peel-load of the adhesive joint. They stated that the fatigue behavior was improved even by adding 0.5 wt% MWCNT to the adhesive [152]. Similarly, another study [140] stated that adding 1wt% MWCNTs contributed to enhancing the fatigue properties of peel-loaded epoxy-based adhesive joints, Figure I.55.

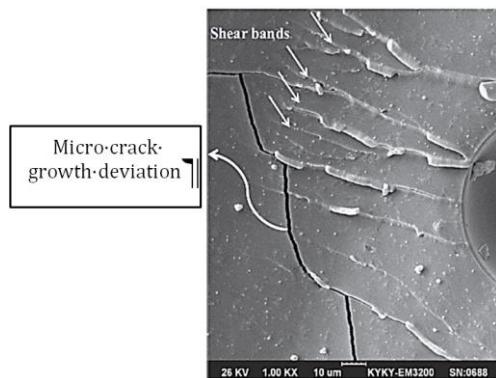


Figure I.53: Deviation of a micro crack in the reinforced adhesive layer with MWCNTs [14]

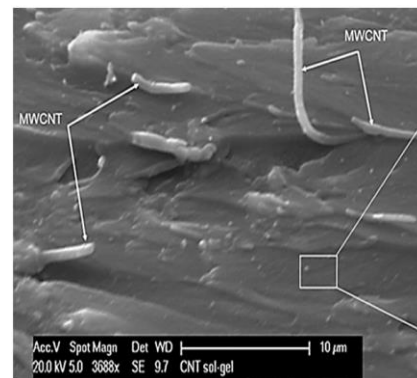


Figure I.54: Distribution of MWCNT on the fracture surface [27]

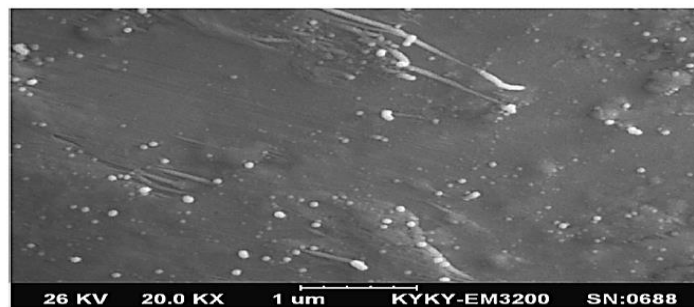


Figure I.55: SEM image of the distribution of multi-walled carbon nanotubes in the epoxy adhesive

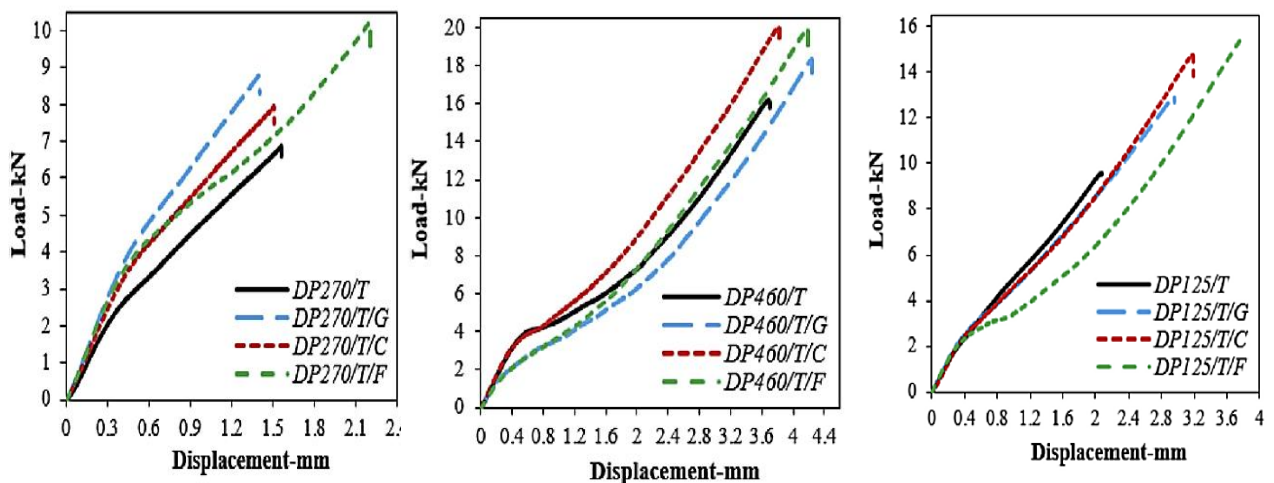
Liu *et al.* [153] indicated in their study that including 2wt% of MWCNTs in a nylon-6 matrix increase the tensile modulus and the yield strength by about 214% and 162% respectively. They indicated that these significant enhancements in the rigidity and strength were due to the uniform dispersion of the CNTs and the excellent interfacial adhesion between the nanotubes and the matrix. Gojny *et al.* [154] examined the mechanical properties of an epoxy reinforced

with both non-functionalized and amino-functionalized CNTs. They proved that the amino-functionalized CNTs provided better results as compared to the non-functionalized CNTs given the good dispersion and interfacial adhesion between the CNTs and epoxy. The results indicated that 0.5 wt% concentrations of the amino-functionalized MWCNTs produced the best increase in the tensile modulus and strength with 14.5% and 8.4%, respectively. Also, they indicated that 1wt% of functionalized MWCNTs improved the fracture toughness by about 26% as compared to the neat epoxy. May *et al.* [155] stated that adding 0.07 wt% MWCNT in epoxy adhesive increased the shear strength by about 13%. Sancaktar *et al.* [156] demonstrated that adding CNTs into the adhesive improved the load-carrying capacity of the joint.

I.9.2.3 Graphene and Fullerene

Many researchers have studied the effects of adding graphene and fullerene in adhesively-bonded joints. For example, inserting 1% and 2% Graphene-COOH into the rigid adhesively-bonded joint resulted in an increase of 109% and 276% in fracture strength, respectively. At the same time,, adding Fullerene into a rigid adhesive didn't show any sufficient effect on the fracture strength of the bond [27]. However, fullerene nanofillers increased the fracture strength of ductile adhesives by about 40% and 65% in the single-lap joints. The maximum value of fracture strength was achieved by adding just 1% of fullerene a-reinforcement [168]. Some studies have also found that 1% of Graphene-COOH reinforced joints presented 15%, 1% of CNT-COOH reinforced joints presented 19% and 1%. Fullerene reinforced joints presented a 28% increase in the bond strength [27]. Guadagno *et al.* inserted 1 wt% GNP in epoxy adhesive and showed that the bond strength was increased however, increasing the weight percentage of GNP up to 4wt% made a significant reduction in the joint strength [157]. Neto *et al.* [158] demonstrated that adding 1wt % and 2wt% graphene in epoxy resin increased the maximum strength by 21% and 57% respectively. In a study conducted by Akpinar *et al.*[159], the addition of 1wt% graphene-COOH, carbon nanotube-COOH, and fullerene C60 into a different kind of

adhesive (rigid, tough and flexible) with single-lap composite joint geometry manufactured by using CFR composite, were analyzed. The results showed that the addition of 1wt% graphene (DP270/T/G), carbon nanotube-COOH (DP270/T/C), fullerene (DP270/T/F) to the rigid adhesive indicated an increase of tensile strength of approximately 28%, 15% and 49% respectively, Figure I.56a. However, in the tough adhesive, it demonstrated an improvement in the tensile damage load of the joint about 13.6% for the addition of 1% of graphene, and 23.8% for 1% carbon nanotube-COOH (DP460/T/C) and 1% fullerene (DP460/T/F) respectively, Figure I.56b. At the same time, incorporating nanofillers to the flexible adhesive DP125 enhanced the tensile damage load of joints by 34% with (DP125/T/G), 53% with (DP125/T/C), 60% with (DP125/T/F) but the significant increase in the average damage load of the joint was secured with the inclusion of the fullerene, Figure I.56c.



(a) Rigid adhesive DP270

(b) Tough adhesive DP460

(c) Flexible adhesive DP125

Figure I.56: Influence of adding 1% Carbon Nanotube, Graphene, and Fullerene onto a different type of adhesive

Recently, some researchers [160], [161] have found that including different graphene fillers such as unreformed GNP, oxidized and amine-functionalized GNP increased the elastic modulus of the epoxy matrix. In addition, excellent properties have been found with low graphene concentration (<3%). Salom *et al.*[162] carried out a similar study by using three

different types of graphene to reinforce the epoxy adhesive: two un-functionalized graphene powders (GNP_{neat} and GNP_{M25}) with different lateral sizes and amine-functionalized graphene (NGP_{NH_2}) with the same size as GNP_{neat} . In their results, they asserted that Young's modulus in reinforced epoxy with GNP was higher than the neat epoxy and it raised by increasing the content of NGP. They established that the tensile strength of the epoxy/GNP nanocomposites was less as compared to the neat epoxy thermoset, however, epoxy with low GNP_{NH_2} content (2-4%) showed almost the same strength as pure epoxy thermoset. In addition, they also confirmed that the epoxy/GNP nanocomposites were brittle in behavior when compared with the pure epoxy and GNP_{NH_2} nanocomposites. Moreover, epoxy/graphene adhesives had less lap shear strength compared to the pure epoxy adhesive due to their weak tensile strength and toughness, for example, the lap shear strength was higher for 1% GNPs nanocomposites in comparison to 6% GNPs, Figure I.57. Shioya *et al.*[163] studied the dispersion of graphene oxide nanoribbons GONR with CNTs in the adhesive with the same percentage and showed that GONR increases the fracture toughness further than the dispersion of CNTs, Figure I.57.

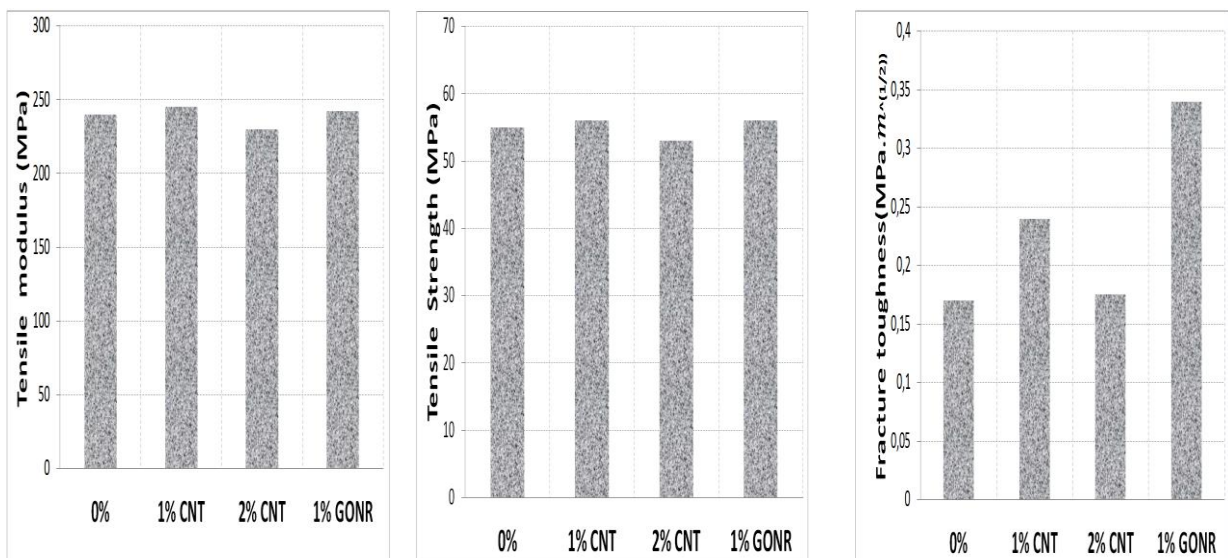


Figure I.57: Influence of CNT and GONR on the adhesive performances

Moreover, it has also been demonstrated that by adding 0.5 to 1 wt.% of GNP individually, the bonded joint strength was reduced, while CNTs with the same percentage increased it. Adding 1 wt.% CNT, 0.5 wt.% GNP and 0.5 wt.% CNH in the adhesive showed an improvement in the bond strength by 53%, 49% and 46% respectively [119], Figure I.58.

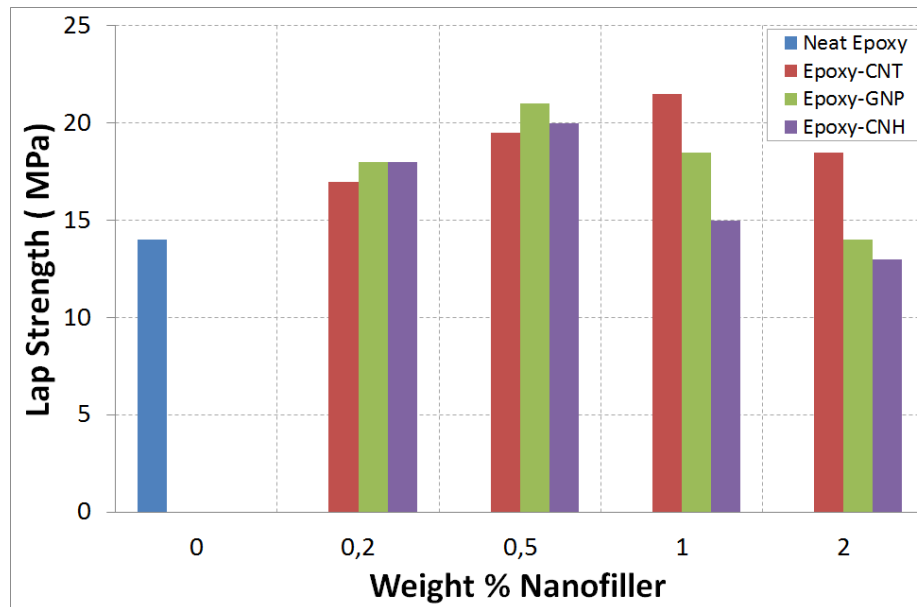


Figure I.58: Influence of different percentages of the nanofillers in the epoxy adhesive on the lap shear strengths

I.9.3 Effects of the excess amount of nanofillers on adhesives

It is a well-known fact that an excess of anything may result in the reduction of properties of the material. The same applied to nanofillers: if certain threshold value is exceeded, the excess nanofillers can result in a phenomenon known as agglomeration, which can give rise to the local stress concentration regions in the adhesive layer. It can therefore cause premature damage and a decrease in the shear strength and toughness of the adhesively-bonded joint [14], Figure I.59. Jojibabu *et al.* [119] investigated the effect of different percentages of nanofillers on the strength of bonded joints and showed in their results that CNT was distributed homogeneously until 1 wt% without any visible agglomerates. But, with the 2 wt% samples, the agglomeration

was initiated in the adhesive and was visible. While GNP and CNH presented a homogeneous distribution till 0.5wt%, and further addition, caused the formation of agglomerates, Figures 60-61-62. El Moumen and Tarfaoui [128] proved that including 4% of CNTs reduced the dynamic properties due to different factors, one of which was the agglomeration phenomenon. An advanced electron microscopy method showed that with a CNT concentration of 1wt% the results present a relatively uniform and homogeneous dispersion, yet the concentrations of 2 and 3wt% showed the presence of significant agglomerates. Hence, it led to the mechanical degradation of the adhesive, Figure I.63-I.64. In this case area, Tarfaoui *et al.* [164] have proven that the degradation of the mechanical proprieties can be clarified by the influence of CNTs distributions and the existence of an upper limit that appears to be from 2% and above, and the significant agglomeration will be from 4%.

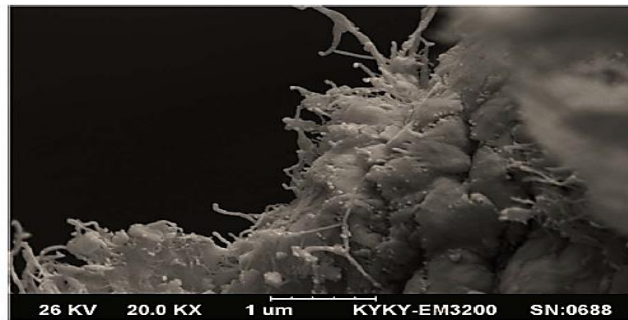


Figure I.59: Agglomerated at the level of an adhesive layer with 0.8 wt% of MWCNTs [14]

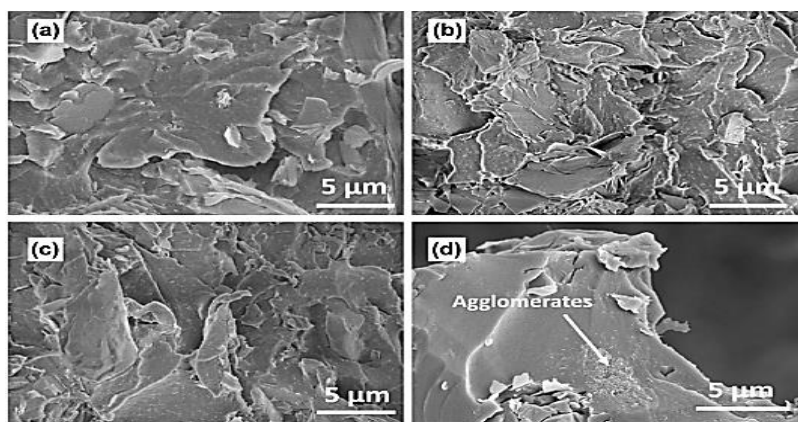


Figure I.60: The progress of the fracture surface with different percentages of CNT in Epoxy showed by SEM image ((a) 0.2% CNT, (b) 0.5% CNT, (c) 1 % CNT and (d) 2% CNT) [13]

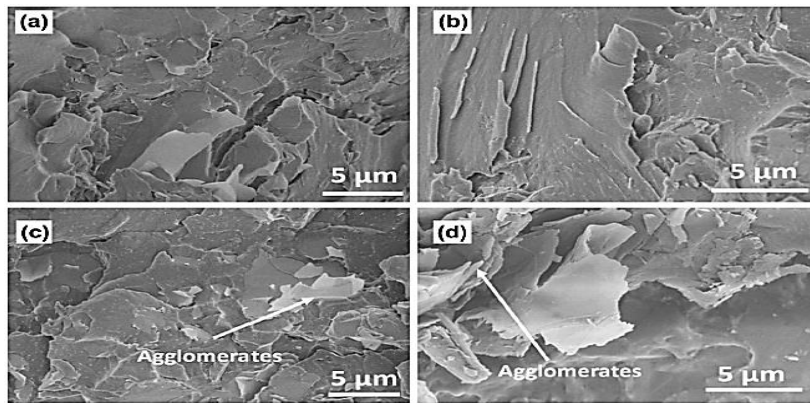


Figure I.61: The progress of the fracture surface with different percentages of CNT in Epoxy showed by SEM image ((a) 0.2%NGP, (b) 0.5%NGP, (c) 1% GNP and (d) 2%NGP) [13]

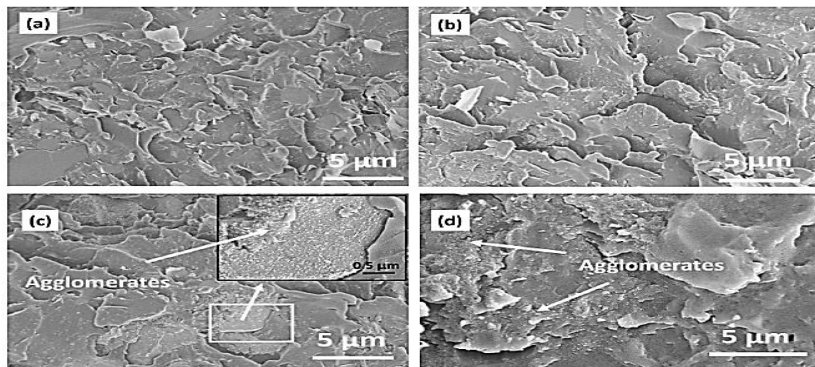


Figure I.62: The progress of the fracture surface with different percentages of CNT in Epoxy showed by SEM image((a) 0.2% CNH, (b) 0.5% CNH, (c) 1% CNH and (d) 2% CNH) [13]

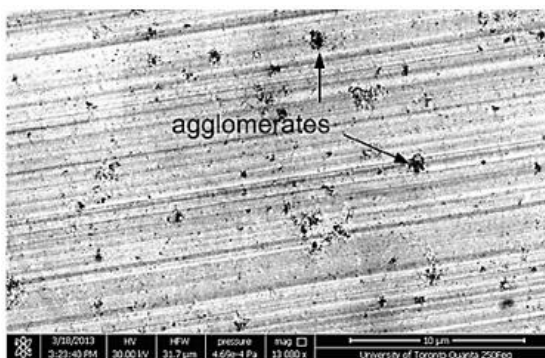


Figure I.63: STEM micrographs of adhesive reinforced with 2wt.% CNT & PVP

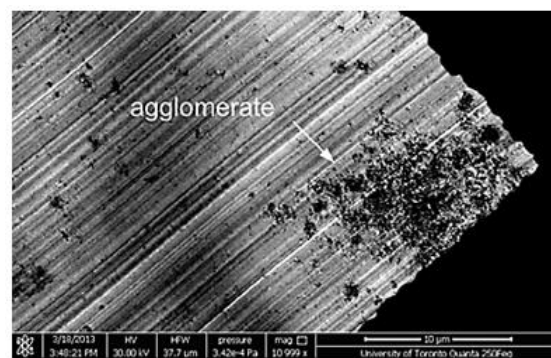


Figure I.64: STEM micrographs of adhesive reinforced with 3wt.% CNT & PVP

I.10 Conclusion

Nowadays, assemblies form all structures, instead of a whole single configuration. It is therefore essential to increase the reliability of a joint or assembly used in the structure to improve its overall quality, performance and service life. For this reason, continuous research and advancement have been ongoing to study and modify the behavior of all joints by not only using varied materials in a structure, but also by selecting a good and improved bonding method. This paper presents a concise and brief overview regarding the development and advancement of bonding methods from traditional processes such as mechanical fastening and welding to advanced bonded joints. The way in which adhesively-bonded joints overcome the limitations such as constraints singularities around the holes, the creation of localized heat region in the vicinity of the welded zone, galvanic corrosion and the different damage modes such as matrix cracks, delamination, and rupture of fibers especially in composite structures of traditional methods are all topics which have been subject to detailed discussion. In addition, hybrid joints consisting of both mechanical fastening and adhesive bonding were also discussed as a potential solution to obtain better and reliable structures due to their good strength, flexibility, tolerance of damage and resistance to fatigue. Each bonding technique had its pros and cons and specific application but, the chief advancement started with the development of adhesively-bonded joints. This was the reason the main objective of this review paper was focused on adhesively-bonded joints, type of adhesives, factors affecting their performance and different processes such as z-pinning, stitching, insertion of inter-adherent fibers used to further improve their mechanical performance. Nonetheless, the performance of adhesively-bonded joints was revolutionized by the development of nanofillers because they enhanced the performance of adhesive bonds without compromising structural integrity. Nanofillers such as CNTs, graphene, fullerene, etc., had their properties and influence on the performance of the bonded joint thus, contributed to improving the adhesive performance in their respective

manner. After the detailed discussion, it was found that the CNTs were the best amongst all to improve the performance of the adhesively-bonded joint but even these nanofillers showed a limitation due to the agglomeration phenomenon. This agglomeration gave rise to the local stress concentration regions in the adhesive layer and could hence decrease the shear strength and toughness of the adhesively-bonded joint and cause premature damage. The integration of nanofillers in adhesive bonds is a critical process that is still preliminary in investigation and requires detailed research. Several techniques had been put forward, but they did not guarantee the good dispersion necessary to improve properties, especially on an industrial scale. So, there remains a lack of studies on the good insertion and required weight percentage for the respective nanofillers and detailed investigations regarding the improvement of bonded joints are required.

Chapter II:

Methodology

II. Methodology

Summary

II. Methodology	88
II.1 Introduction	89
II.2 Resin	89
II.3 Nanoparticles	91
II.3.1 Carbon nanotubes (CNTs).....	91
II.3.2 Graphene	92
II.3.3 Carbon Black.....	95
II.3.3.1 Particle Size	96
II.3.3.2 Structure	97
II.3.3.3 Surface Chemistry	98
II.3.3.4 Aggregate Size	98
II.3.3.5 Aggregate Shape.....	99
II.4 Dispersion and implementation of nanofiller-doped adhesive resin	99
II.4.1 Graphene and Carbon Black dispersion	100
II.4.2 CNT dispersion with planetary agitators.....	102
II.5 Homogeneity optimization via DIGIMAT	104
II.5.1 Clustering	104
II.5.2 Cluster size distribution.....	105
II.6 Microstructural study.....	106
II.6.1 Differential Scanning Calorimetry (DSC).....	106
II.6.2 Micro-indentation.....	108
II.7 Mechanical Characterization of Nanocomposites	111
II.7.1 Static tests: Mechanical test bench – INSTRON	111
II.7.2 Compression Test.....	115
II.8 Study of the dynamic behavior of nanocomposites.....	117
II.9 Conclusion.....	125

II.1 Introduction

This chapter presents (i) the basic components (adhesive resin, nanoparticles) which were initially used to prepare reinforced adhesive nanocomposites and the selection criteria, (ii) the manner of nanofiller distribution such as for graphene platelets, carbon nanotubes, carbon black, (iii) methods of nanocomposite implementation and (iv) methods for the physico-chemical characterization and structural analysis of the reinforced nanocomposite, as well as the experimental conditions for each technique. (v) Methods for quasi-static characterization of unreinforced reinforced adhesive nanocomposite materials. (vi) Dynamic characterization techniques for unreinforced and reinforced adhesive nanocomposite.

II.2 Resin

The adhesive epoxy resin used to prepare the nanocomposite in this work is the diglycidyl ether of bisphenol A: DGEBA, available from MOMENTIVE. DGEBA is an epoxy amine resin, a thermosetting resin, which is produced by the addition polymerization reaction between epoxy monomers (with epoxy terminal groups or ethylene oxide) and amine hardeners or reticulation agents. It is produced through the alkaline condensation reaction of epichlorohydrin (chloro-1-epoxy-2.3-propane) and bisphenol A (diphenylpropane), which is based on the overall reaction presented in Figure II.1.

The value of the polymerization index is based on the ratio of epichlorohydrin to bisphenol A. Depending on its value, the prepolymer molecule DGEBA is more or less long and its viscosity changes. Therefore, at room temperature, the prepolymer is liquid for $0 < n < 1$, highly viscous for $1 < n < 1.5$, and solid for $n > 1.5$ [165]. The molecular structure of the prepolymer DGEBA contributes to its good chemical resistance and mechanical properties Figure II.2, the aromatic core brings heat resistance, corrosion resistance and rigidity. Adhesion is the hydrolysis of hydroxyl functional groups and ether bridges [166], [167].

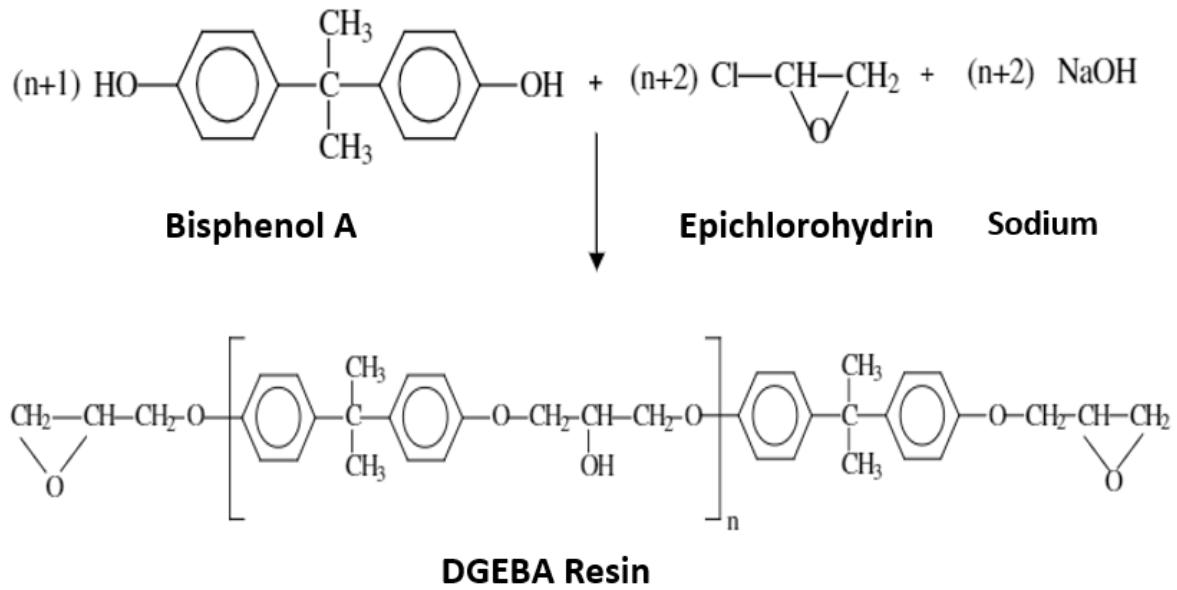


Figure II.1: Reaction of epichlorohydrin (chloro-1-epoxy-2.3-propane) and bisphenol A (diphyllopropane)

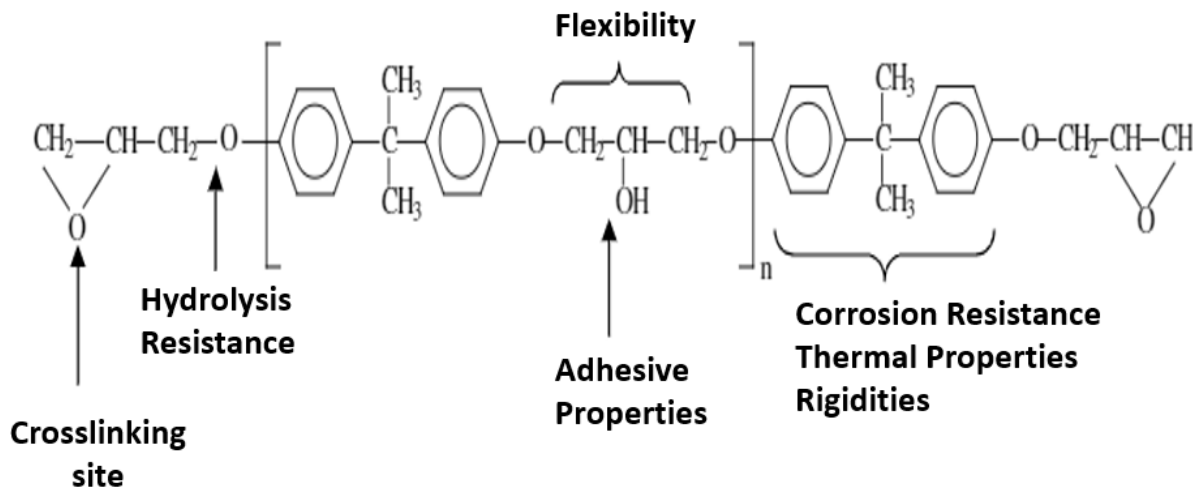


Figure II.2: Relationship structure properties

Therefore, the prepolymer has two types of reaction sites: ethylene oxide clusters and hydroxyl functional groups. The two main types of organic compounds (hardeners) that can open the ethylene oxide cycle are labile hydrogen amino products and diacid anhydrides, which lead to polycondensation and chain polymerization reactions, respectively. In this study, we have

chosen to limit our scope to Huntsman's Jeffamine D230, which is an aliphatic diamine type amino hardener. The advantages of this type of curing agent are low cost, low viscosity, easy mixing, ability to react at room temperature, and responsiveness. At the same time, in regard to potential disadvantages, these compounds are highly volatile [168], are relatively toxic, and have a short shelf life. Momentive DGEBA dispersions have been mixed with a stoichiometric amount of Huntsman Jeffamine D-230 (32 g D-230 for every 100 g DGEBA (EPON 828)).

II.3 Nanoparticles

The mechanical properties and fracture toughness properties among several nanofillers are consolidated in this chapter to support the improvement of nanocomposite adhesive in this evolving field. The method of focus is founded on the arrangement of carbon nanotubes in adhesive resin, graphene, and carbon black as nanofillers.

II.3.1 Carbon nanotubes (CNTs)

Carbon nanotubes were discovered in 1991 as a tubular carbon structure with as many as 10 graphite shells, and the distance between adjacent shells is 0.34nm, which is the so-called multi-walled carbon nanotube (MWCNT) [169]. Later, Iijima and Ichihashi [170] and Bethune et al. [171] synthesized single-walled carbon nanotubes (SWCNT). Structurally, a carbon nanotube can be seen as a seamless, rolled graphene sheet. Graphene sheets are composed of carbon atoms arranged in a hexagonal lattice. Multi-walled carbon nanotubes are composed of multiple graphene sheets, which are arranged concentrically around a core with an outer diameter ranging from 5 nm to hundreds of nanometers. The single-walled carbon nanotube has only one graphene sheet, and its typical diameter is in the range of 1-2nm [172]. The illustrations of SWCNT and MWCNT are shown in Figure II.3 (a) and (b), respectively.

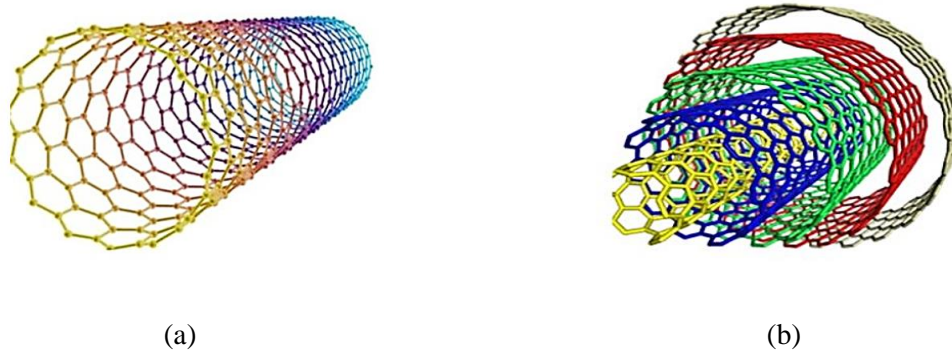


Figure II.3: (a) Single-walled carbon nanotube and (b) multi-walled carbon nanotube

The carbon-carbon (C-C) sp^2 bonding makes the graphite bond very strong in the in-plane direction, giving the carbon nanotubes high rigidity, and the axial strength is 100 times higher than steel. Experimental and theoretical studies have thoroughly explored the elastic, inelastic, buckling, yielding, and fracture behaviors of SWCNTs and MWCNTs [173]–[182]. Young's modulus of CNT is in the range of 103 GPa, the tensile strength is approximately 50 GPa, the compressive strength is in the range of 100 GPa, and the CNT is easily bent and restored to its original shape after deformation.

II.3.2 Graphene

Graphene is an atomically thick two-dimensional sheet of sp^2 carbon atoms arranged in a hexagonal lattice Figure II.4 (a) [183]. Graphite is a naturally-occurring, abundant material, and it is thought to be composed of graphene sheets arranged on top of each other [184]. The attempt to study graphene can be traced back to Brodie's work in 1859 [185]. With the development of Novoselov and Geim in 2004, the study of single-layer graphene became possible where they used the "Sellotape method" to extract from graphite Figure 4 (b) [186], [187].

Due to the unique properties of graphene, the research field surrounding graphene has developed rapidly around the world. Between 2005 and 2014, the number of research publications including "graphene" in the title has exceeded 66,600 (By ISI-Web Search Science, November 4, 2014). Graphene has many exclusive properties, which has stimulated such high

research interest by its mechanical, electrical, thermal, and gas barrier properties. It has been established that Young's modulus of graphene is 0.5-1 TPa [188], [189], and the ultimate strength is 130 GPa [189].



Figure II.4: (a) The structure of graphene (b) Large pieces placed on SiO₂ wafer prepared by "Sellotape method"

According to reports, it has a high conductivity of up to 6000 S/cm and thermal conductivity of 4840-5300 W/(mK), which is higher than the informed value of carbon nanotubes [190]. In addition, the theoretically high surface area of 2630 m²/g and gas impermeability have opened graphene to be widely used in various fields [191].

The preparation method for graphene is currently the subject of in-depth study. There are two main strategies: top-down and bottom-up. In the top-down method, the graphene sheet is peeled from the graphite. A micromechanical cutting technique called the "*Sellotape method*" stimulated the initial interest in graphene research. Although the number is limited, it is still the most reliable method for producing high-quality graphene sheets found so far [186].

Chemical exfoliation and ultrasonic treatment are also extensively used, and the graphene dispersion can be stabilized by specific surfactants [192], [193], and ionic liquids [194]. Oxidation of graphite [195] is also an appropriate method for this process. Another method is

to heat graphite oxide and inert gas at 1000°C in a single step to yield thermally reduced graphene oxide. Furthermore, surface science has delivered a new strategy for growing graphene using the "bottom-up" method. Chemical vapor deposition (CVD) on metal substrates [196], [197], and epitaxial growth on SiC [198], [199] can produce large-scale graphene sheets in small quantities. Most of these technologies produce several layers of graphene (2 to 5 layers) with a thickness of about 0.7 to 1.7 nm, rather than a single layer of graphene with a thickness of 0.34 nm.

As the graphene results reported the Young modulus between 0.5 - 1 TPa and an ultimate force of 130 GPA, it is believed that graphene is a good candidate for mechanical reinforcement of the polymer adhesive matrix-based nanocomposites. With a view to this, a major research project was carried out, in which graphene has been added to various polymers to create nanocomposites, with a variant success level [200] [201]. There is a summary of the mechanical features of nanocomposite polymers. Interestingly, in addition to the mechanical properties of the graph, there are two additional rigid devices for graphene and graphene derivative nanoparticles to stiffen any polymer matrices.

With hydrogen bonding, graphene oxide (GO), Figure II.5(a) varies typically with polar polymers to offer a higher glass transition temperature, which causes higher mechanical reinforcements due to the variation of the viscoelasticity of the polymer matrix. Rather than extraordinary strengthening by graphene [202]. For semi-crystalline polymers [203], graphene can improve the degree of crystallinity as a nucleating agent, thereby strengthening the polymer matrix by increasing crystallinity. In addition to changing rigidity, the tensile strength and extension to breaking the polymer graphene nanocomposites are also asserted. With a good distribution, the tensile strength with the addition of graphene [203], reduces a breaking extension, resulting in increased growth [203].

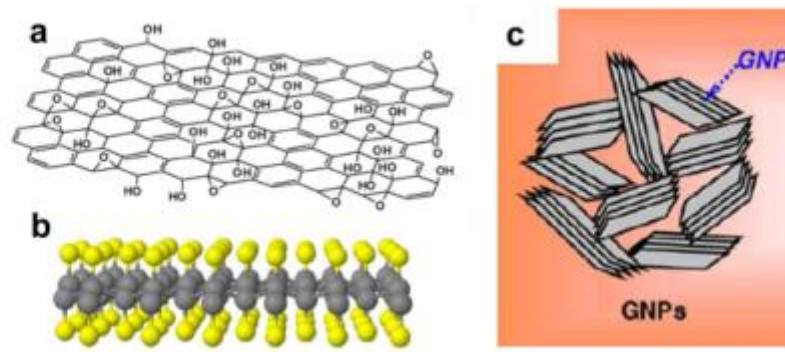


Figure II.5: Graphene derived nanoparticles: (a) Graphene oxide (GO), (b) Fluorographene, (c) Graphene Nanoplatelets (GNP)

II.3.3 Carbon Black

Carbon Black is essential carbon within the frame of extremely fine particles with a somewhat amorphous atomic structure. It is classified as an aggregated conventional molecule with nanoscopic measurement (1-100nm) and high electrical conductivity but no perspective proportion. Carbon Black is among the nanoscale particles produced in commercial amounts (tons). Depending on the strategy of production, normal essential molecule breadths in a sample of commercially-produced Carbon Blacks range from 10-500 nm, whereas normal essential particles have breadths which range from 100-800 nm. Carbon Black was one of the long-established nanotechnology applications and nanomaterial utilized to adjust the mechanical, electrical, and other physical properties of polymers[204], [205]

The Carbon Black's complex structure detected during an electronic microscope shows that they have typically merged spherical particles as shown in Figure II.6. The spherical particles are of different sizes. The particles associated with a chain are referred to as a "structure". Several practical sets, such as the carboxylic or hydroxyl group are on the CB surface [206]. The name "the surface chemical" is designated based on the composition or quantity. The size and structure of the particle in the chemistry of the surface are simple Carbon Black properties.

These properties are the main parameters of Carbon Black and have a great influence on the particle properties, such as dispersability and blackness capacity when mixed with toner, paint, or resins [207], [208]. Therefore, Carbon Black can be generally defined as an aggregate of extremely fine particles of possession of the quasi-formless molecular structure without shape. The largest areas of differences between a furnace black and thermal black are the size of the particle and the structural formula. Furthermore, Carbon Blacks are consigned and categorized with a number of the grade identified on the surface area and its structural capacities [207], [209], [210] [211]

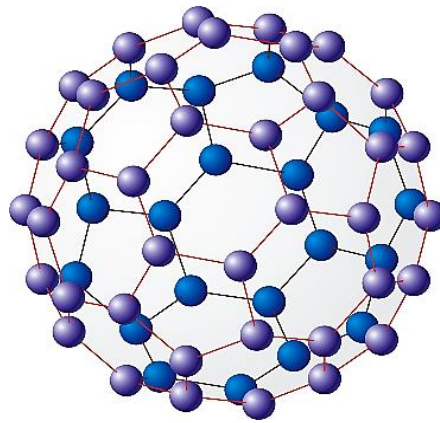


Figure II.6: Spherical CB Structure

II.3.3.1 Particle Size

The size of the CB particles, in particular the diameter of the particles when there is a spherical form, as shown in Figure II.7, is considered to be an essential feature that greatly affects the dispersability and blackness when mixed with resin. Generally, the minimum size particle becomes the most significant Carbon Black darkness. However, it appears to be complex owed to growth in coagulation force. The first extensive measurements were captured by Ladd et. al. [212] for commercial-grade Carbon Blacks. They were measured manually with appropriate micrographs. In general, based on high-regularity discharge, the dispersions used in these early

studies have spread to the thin plastic membranes of formal CB, polyvinyl or nitrocellulose [213].



Figure II.7: Carbon Black Particle Dimension Comparison

II.3.3.2 Structure

Like the particle size, the size of the structure also affects the dispensability capacity and blackness of Carbon Black, as shown in Figure II.8. Usually, the size increase of the structure increases the dispensing capacity, although it simultaneously lowers the darkness. CB with a larger structure or construction demonstrates excellent conductivity [213].

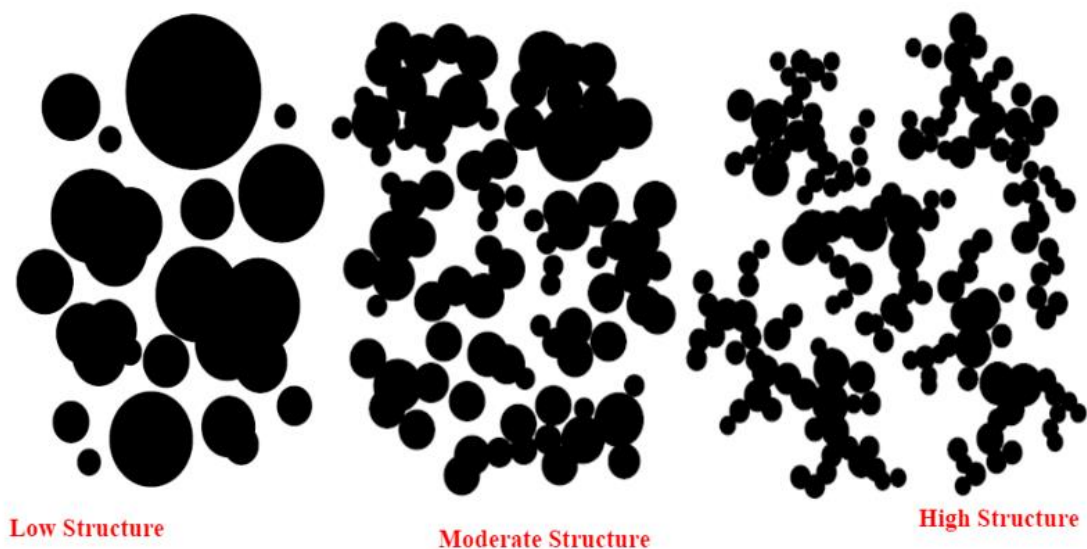


Figure II.8: Carbon Black Structure

II.3.3.3 Surface Chemistry

Numerous practical groups are available on the CB surface. The affinity of CB with paints or inks changes, dependent on the type and quantity of practical groups. In large quantities and when it is administered by oxidation therapy, low surface area/low surface/high-structure; high surface area/high structure; high surface area/low structure form Figure II.9. The surface area of particles plays a significant role in the production and classification of CB degrees.

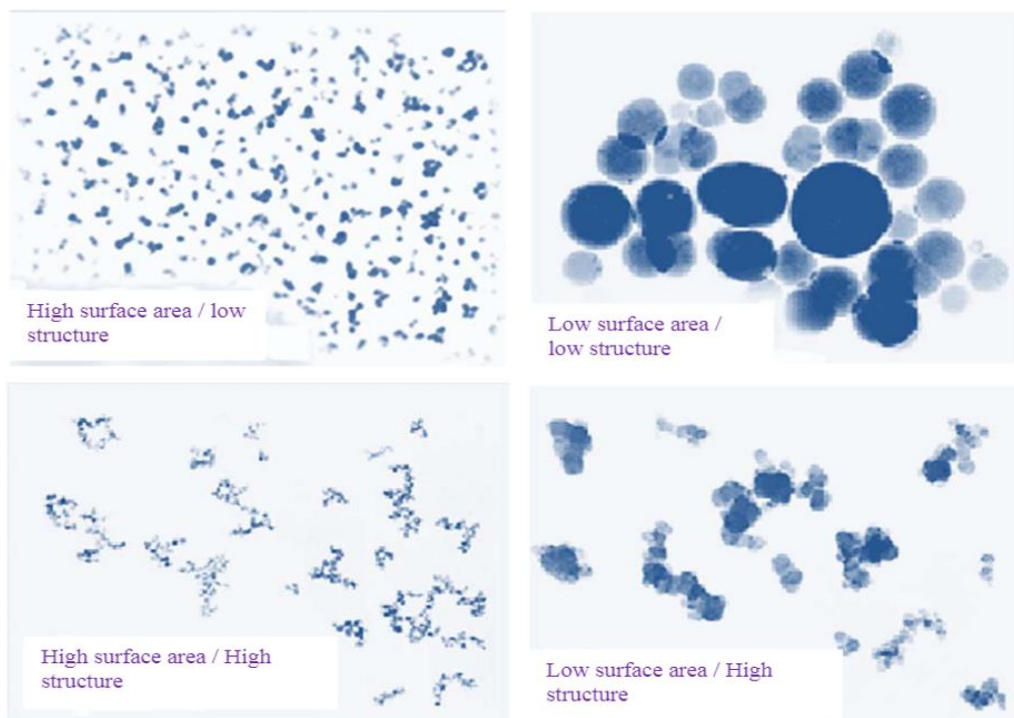


Figure II.9: surface area Comparison of diverse particles structures [50]

II.3.3.4 Aggregate Size

Aggregates represent CB's actual primary priorities. However, unlike a particle size that mechanical treatment does not affect, the additional size depends on the system. High loading in polymer systems causes significant aggregate degradation with dry space.

II.3.3.5 Aggregate Shape

The CB aggregates differ in the shape of specific spherical particles established in the thermal certification bodies on the grouped and rubber additional types, which are common in all other grades (77). These more complex forms generate internal VIPs in a given bulk sample of Carbon Black that is much larger than those found in a simple batch of spheres. The absorption capacity of carbon black for liquids is linked to aggregates (i.e., many open aggregates).

II.4 Dispersion and implementation of nanofiller-doped adhesive resin

The main challenge in developing nano-reinforced adhesive nanocomposites is the dispersion of the load in the adhesive resin matrix. Subsequently, the mass fraction of various nanoparticles applied for treating adhesive behavior was 1wt.% to 5wt.%. Before we compare the effects of various nanoparticles on the system, it is interesting to understand their dispersion in the adhesive resin. The dispersion of nanoparticles plays a vital role in obtaining good performance [214].

At the same time, the uniform dispersion of nanoparticles aims to produce a large interface area. Therefore, when the particle size reaches the nanometer level, in addition to the particle/matrix interaction, the particle interaction must also be taken into consideration. These interactions can, in some cases, lead to improved mechanical properties [215]–[219], thermal properties [220]–[223], electrical properties [224]–[228], or even the generation of new properties [227]–[230]

The optimum performance of reinforced adhesive nanocomposites can be achieved through the proper dispersion of nanofillers in the adhesive resin. Many researchers have studied the method of dispersing different nanomaterials into an adhesive matrix, as seen in references [231]–[233]. Furthermore, when a uniform dispersion is obtained, the nanocomposite material performance is significantly improved due to the load's transfer via the nanofillers. Also, the higher aspect

ratio, alignment, and positive stress transfer contribute to the higher performance of the adhesive resin [234].

Furthermore, the curing behavior of adhesive resin is fundamentally impacted by the addition of nanofillers. The incorporation of nanofillers into adhesive resin matrix systems usually leads to increased viscosity and the shear-thinning behavior of the latter [234]. In our case, the RESCOLL company we cooperated with used two different mechanical methods to disperse the nanomaterials in the adhesive resin, depending on the nanoparticles type contained.

II.4.1 Graphene and Carbon Black dispersion

This part is based on combining two dispersion methods, such as the traditional planetary agitator method and the three roll mill agitator method. This step remains very fragile and a satisfactory dispersion cannot be obtained, whereas dispersion is one of the key conditions for understanding the performance of the final structure material. The better the dispersion, the more uniform the product will be. The ARV-930 planetary agitator is an excellent model with a large capacity of up to 1L and can achieve sub-micron degassing. It provides a vacuum technology in the cup holder, which can radically reduce the decompression time.

The Three Roll Mill is equipped with rolls that rotate in opposite directions at different speeds and strengths. Due to the shear force generated, the nanofillers are uniformly dispersed in the adhesive resin matrix. The principle of this agitator is shown in Figure II.9. In our case, the distance between the rollers adjusted within the range of 5m in the order of micrometers. When passing between the rollers, the load is brought into the vortex, and then the agglomerates contained in the resin are subjected to an extremely high shear force so that it can be reduced to a very fine size, corresponding to the distance between the rollers.

Figure 10 presents the manufacturing process of the nanocomposite loaded into this part, which includes all the suspension processes for weighing the graphene and Carbon Black components and are of good quality, as shown in Table II.1.

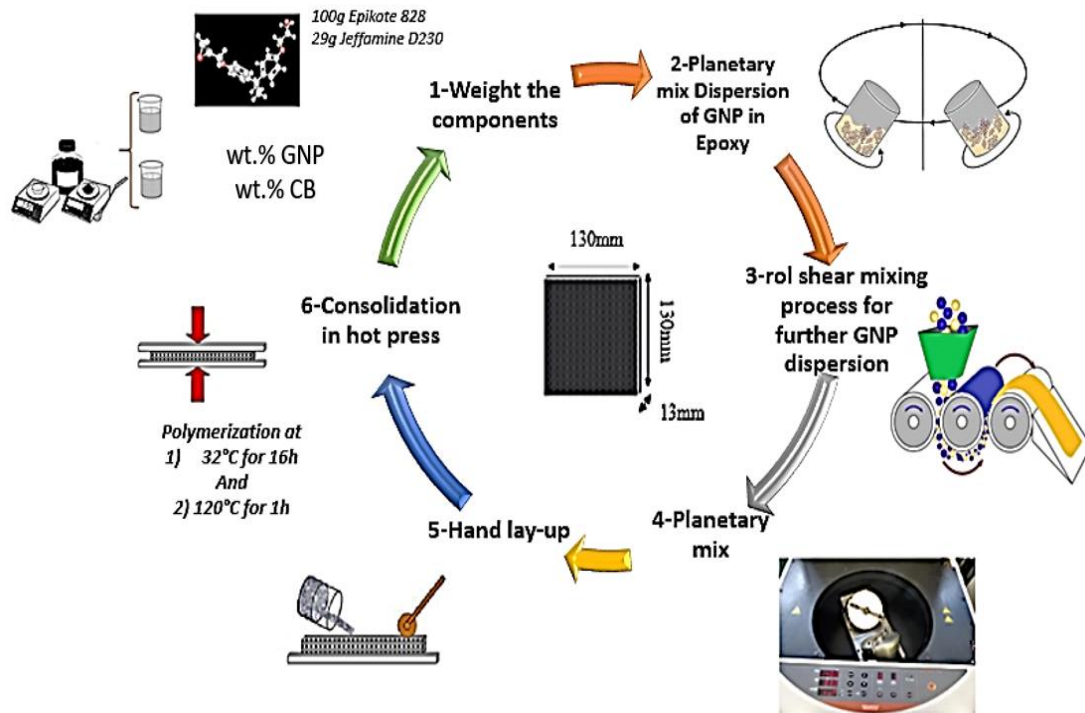


Figure II.10: Manufacturing CBs-GNP-reinforced DGEBA epoxy nanocomposite

The mass fraction is fixed at 1wt.%, 2wt.%, and 5wt.%. Then after completing the mixing process under a partial vacuum of 60 to 1000 rpm, the planetary agitator ARV-930 is used for the first mixing of 60 s to 1400 rpm. Then the product is injected into the three roll mill at a speed of 100tr/min. Subsequently, the same procedure is repeated with the planetary agitator ARV-930 to continue stirring.

Manual lay-up and compression hot-pressing techniques are used to prepare the final reinforced nanocomposite material sample. Finally, the sample was pre-cured at 32°C for 16 hours, and then at 120°C for 1 hour. The thickness of each sample plate is 13mm and then manufactured to obtain a cubic sample of 13×13×13mm.

II.4.2 CNT dispersion with planetary agitators

On the contrary, the research conducted by Fu et al. [235] is inconsistent with previous statements. They disagree about using Three-Roll-Mill calendaring technology to distribute carbon nanotubes. Where this method was applied to prepare CNT-based adhesive epoxy nanocomposites. After processing the reinforced nanocomposite structure, the original length of the CNT is reduced, which ultimately affects the mechanical properties, causing poor performance. Retaining the residual CNTs length is essential to achieve optimal mechanical properties.

Since the minimum gap between the rollers is about 1-5 μm , which can be further explained, the gap is almost equal to the length of the CNTs, which is much larger than the diameter of each CNT [236]. Suarez et al. [237] concluded that the design of this technology should take into account any surface functionalization to be applied. This is due to the ineffective dispersion due to higher agglomerates in the presence of surface functionalization.

To make the CNTs bundles fall off, high shear stress is very critical, so that the nanofillers are uniformly dispersed in the adhesive resin matrix [214]. In that case, we only use a planetary agitator to limit the dispersion of CNTs as shown in Figure II.11. In the planetary agitator, a high-shear mixing process is used to disperse CNTs in the adhesive resin [238]. Table II.1 present the exact weight of CNTs included for each mass fraction into the DGEBA adhesive resin. According to reports, this process can achieve good CNT dispersion and confinement because clusters may be generated [219], [239], [240]. The fabrication of the reinforced adhesive nanocomposite first includes dispersing CNTs in an adhesive polymer and then mixing them at a speed of 1400 rpm for 60 seconds using the planetary agitator method.

Manual lay-up and compression hot-pressing techniques are used to prepare the final reinforced nanocomposite material sample. Finally, the sample was pre-cured at 32°C for 16 hours, and

then at 120°C for 1 hour. The thickness of each sample plate is 13mm and then manufactured to obtain a cubic sample of 13 x 13 x 13 mm.

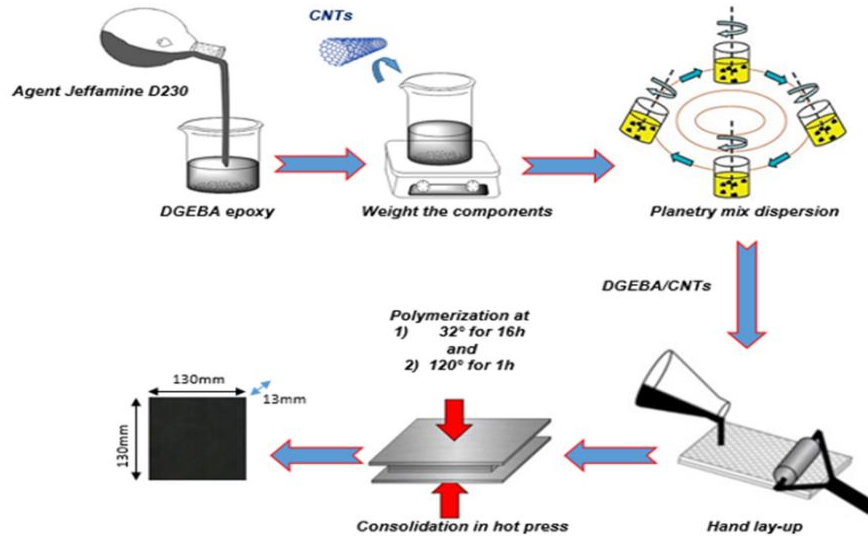


Figure II.11: Manufacturing CNT-reinforced DGEBA epoxy nanocomposite

Table II.1: The different composition ratios of CB-GNP-CNT reinforced DGEBA epoxy nanocomposites

Epoxy		Reinforcement: nanofillers			Agent	Polymerization cycle	
g	g	% Weight		g			
100	DGEBA	-	-	-	32	Jeffamine D230	16h à 23°C + 1h at 120°C
100	DGEBA	1,6	1,2	CBs	32	Jeffamine D230	16h à 23°C + 1h at 120°C
100	DGEBA	3,2	2,4	CBs	32	Jeffamine D230	16h à 23°C + 1h at 120°C
100	DGEBA	8	5,7	CBs	32	Jeffamine D230	16h à 23°C + 1h at 120°C
100	DGEBA	1.6	1.2	GNPs	32	Jeffamine D230	16h à 23°C + 1h at 120°C
100	DGEBA	3.2	2.4	GNPs	32	Jeffamine D230	16h à 23°C + 1h at 120°C
100	DGEBA	8	5.7	GNPs	32	Jeffamine D230	16h à 23°C + 1h at 120°C
75	DGEBA	25	1	CNTs	32	Jeffamine D230	16h à 23°C + 1h at 120°C
50	DGEBA	50	2	CNTs	32	Jeffamine D230	16h à 23°C + 1h at 120°C
0	DGEBA	100	5	CNTs	32	Jeffamine D230	16h à 23°C + 1h at 120°C

II.5 Homogeneity optimization via DIGIMAT

The purpose of this section is to better understand the dispersion phenomenon of nanoparticles in adhesive resin, which varies depending on different factors such as shape, size type, aspect ratio, and so on. We suggest using the discrete homogeneous technology based on nanocomposite material RVE modeling to establish the equivalent continuum model of nanoparticles, as described above. The model was performed using DIGIMAT-FE software for the different types of nanoparticles and diverse mass fractions to visualize how nanoparticles are deposited on the adhesive resin to form the entire network, as shown in Figure II.12.

Digimat-FE is used to generate very realistic RVE microstructure geometry. Digimat-FE is a micromechanical material modeling software that uses a direct, realistic finite element (FE) representation of the representative volume element (RVE) of the composite microstructure.

The main advantages of Digimat-FE:

1. The possibility of generating highly complex RVEs containing elliptical and/ or non-elliptical inclusions (such as semi-crystalline microstructure morphology).
2. The consideration of geometric effects, such as inclusion clustering and percolation.
3. In addition to calculating the macro-response of the composite material, the actual distribution of the local field must also be calculated on the micro-scale).

The following are the functions that Digimat-FE must provide in nanocomposite material modeling:

II.5.1 Clustering

Digimat-FE provides many options and parameters to use in designing the selected microstructure. One option is to force the inclusions to be clustered. The user can specify the required number of clusters and the degree of clustering. For example, the user can choose

to have 2 clusters in the RVE, and the generator will then randomly place the inclusions to have a higher probability of finding an inclusion close to one of the cluster centers.

II.5.2 Cluster size distribution

The size distribution can be specified in the stage pane of Digimat-FE: the size of the inclusions can be a constant value or a random value between the minimum and maximum values, which in turn affect the particle-matrix interface and particle-particle interaction. If it is a coating, the RVE geometry generator will generate the microstructure geometry, including the coating (if any), and adhere to the mass or volume fraction of the phase as much as possible. In addition, Digimat-FE can generate coatings of geometric shapes containing impurities or impurities that intersect to a specified degree. This can enhance the modelling of interfaces and interactions [241].

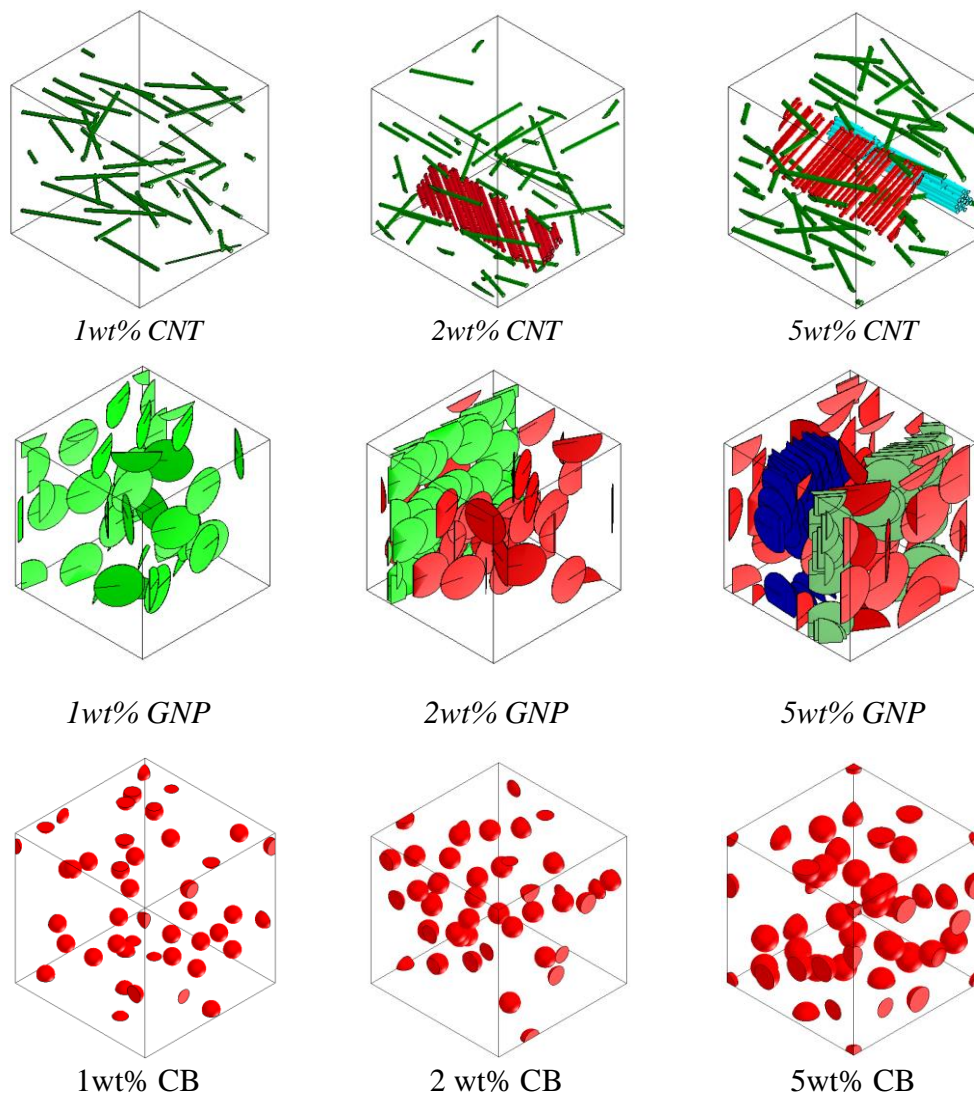


Figure II.12: Simulation of dispersion modes of CB-GNP-CNT nanofillers in DGEBA Adhesive using DIGIMAT

Figure II.12 presents the different nanoparticles distribution into the DGEBA matrix. The type of distribution changes according to the type of nanoparticles (CBs, GNPs, CNTs) and the mass fraction percentage. Digimat contributes to creating some kind of agglomeration that depends on the form of the nanoparticle as mentioned in Tarfaoui work [164], [242]–[244].

II.6 Microstructural study

II.6.1 Differential Scanning Calorimetry (DSC)

The addition of carbon nanoparticles to adhesive resins affects density, which affects polymer chain mobility, free volume, energy system, and the interaction between polymer chains. In addition, it causes a change in the glass transition. Differential Scanning Calorimetry (DSC) characterization will allow us to highlight the crystal structure changes of adhesive resins based on the patterns of different mass fractions of nanoparticles, Figure II.13. We used Differential Scanning Calorimetry (DSC) technology to physically and chemically characterize the reinforced adhesive nanocomposite formulation and adhesive epoxy network [245].

Differential calorimetric analysis can be used to determine (depending on the temperature) the state change caused by the physical transformation of the structure (glass transition temperature, melting, crystallization) or chemical action (polymerization, oxidation, degradation). The measurement was recorded on a NETZSCH DSC 204. The equipment includes a mechanical gas compression cooling system that controls the cooling of the furnace atmosphere, as shown in Figure II.13. Figure II.14 shows the different steps of DSC sample preparation. In this study, the researchers focused on the effect of T_g glass transition temperature, T_c crystallization, and melting T_f on the X_c crystallization rate of our system.

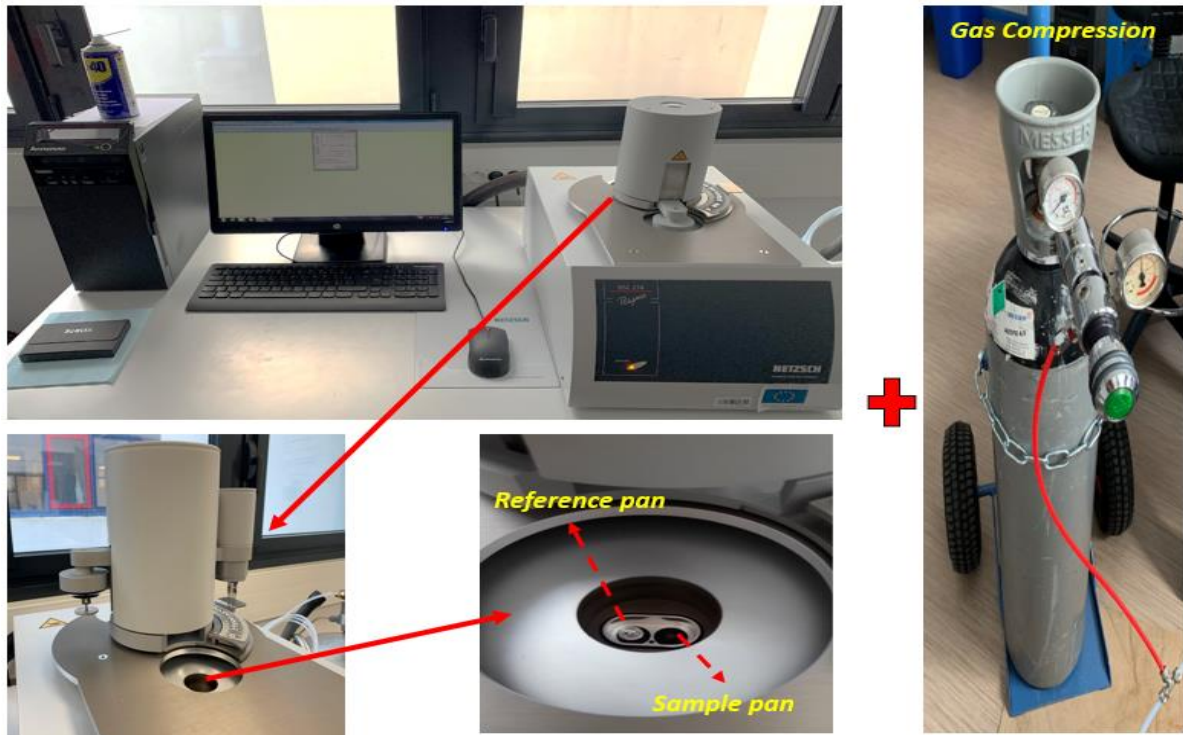


Figure II.13: DSC machine



Figure II.14: DSC sample preparation steps

The X_c criticality of the polymer matrix is calculated by integrating the melting peak to obtain the melting enthalpy ΔH_f . The calculation formula is as follows: ΔH_{cf} represents cold crystallization. The melting enthalpy (ΔH_∞) of the fully crystalline polymer is 93.1J/g. In the presence of nano-charges, the polymer enthalpy ($\Delta H_{\text{polymère}}$) will be recalculated according to the following expression eq (1):

$$\Delta H_{\text{polymère}} = \frac{\Delta H_{NC}}{M_p} \quad 1$$

This is with ΔH_{NC} as the enthalpy of nanocomposite structure and M_p as the mass fraction of the polymer.

The analysis is carried out in two cycles (a rise, and a drop in temperature): the first cycle eliminates the thermal history of the sample, and the second cycle allows for the thermal transition of the contact material. The curve corresponds only to the second cycle (i.e. the second climb) [246].

II.6.2 Micro-indentation

Local tests were conducted to determine the local mechanical properties of the reinforced nanoparticles adhesive as a function of the charges. Micro-indentation testing has long been used to extract certain mechanical properties of materials, such as elasticity, plasticity, viscosity, and damage, Figure II.15.

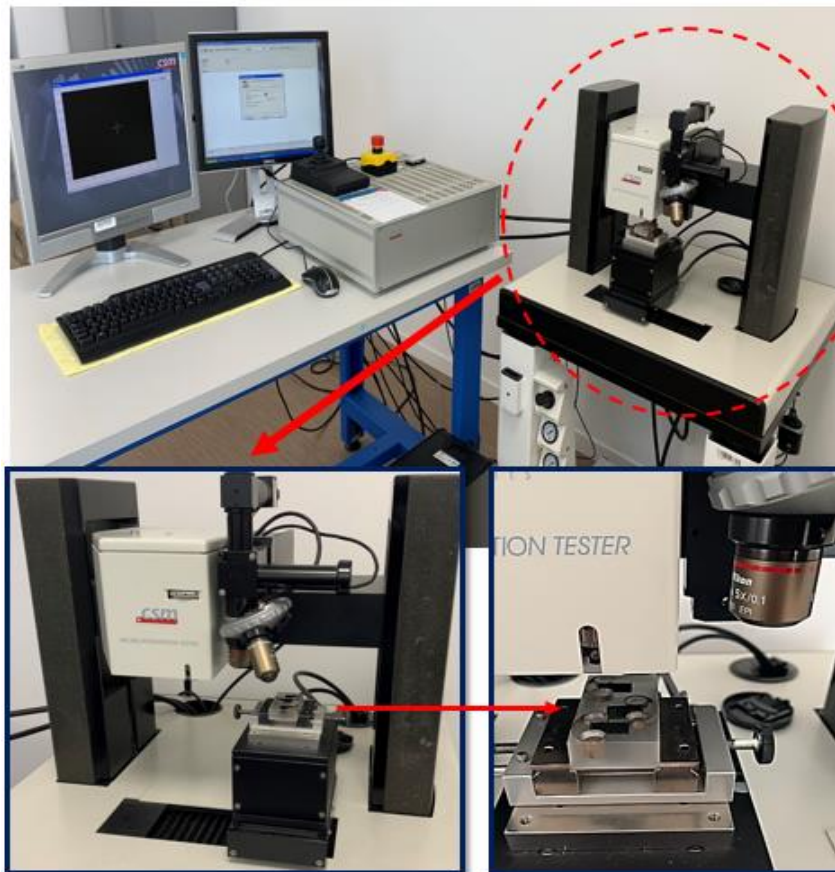


Figure II.15: Micro-indentation machine

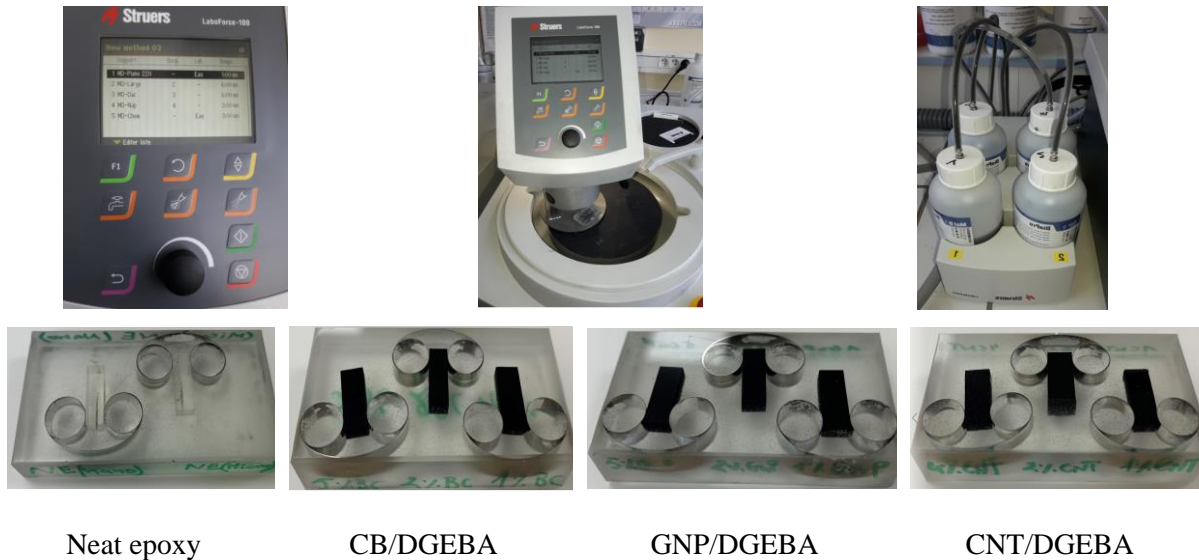
Traditional indentation techniques are based on the measurement of electrical resistance relative to the penetration of a diamond indenter. The general hardness tester in the material has tested

the spectral imprint, and the size of the imprint is related to the hardness value by measuring the diagonal of the imprint or estimate the diameter of the diagonal of the imprint (Vickers hardness). Before starting the micro-indentation test, such important surface preparation of the specimen has to be done as shown in Figure II.16.

Conventional mechanics is different from the viewpoint of the load range. Unlike ductile materials that can be tested under high loads (macro-hardness), fragile materials may experience microcracks that exceed the load threshold. In these cases (fragile materials), a sharp indenter (Vickers, Knoop, Berkovich) must be used obtain prints and it must be limited to small charges (micro-hardness or nano-hardness) to avoid cracks.

The instrument indentation technology makes it possible to create the force penetration curve of the indentation test. The curve consists of two different parts: the load curve corresponding to the penetration of the indenter and the discharge curve corresponding to the withdrawal of the indenter, Figure II.17. On this curve, you can determine the different amplitudes related to indenter depression, h_t as the maximum penetration force of the indenter, h_f : as the plastic shaping depth and the imprint: plastic depth under load (obtained by drawing the intersection point), and maximum penetration (the distance between the tangent of the flow curve at a point and the abscissa axis) [247].

The indentation curve provides information about the elasticity and plasticity of the material [248]. During the discharge, two phenomena can be observed. In the beginning, all solids have undergone elastic recovery. According to the elastoplastic properties of the material, part of the indented solid may be plasticized again during discharge[249], [250]. However, the discharge curve mainly provides information about the elasticity of the material. Instrument indentation technology is not only a method to determine the hardness and elastic modulus of materials but is also a method allowing for the study of the changes of H and E with various loads, temperatures and times, as well as other parameters.



Neat epoxy

CB/DGEBA

GNP/DGEBA

CNT/DGEBA

Figure II.16: Steps of surface sample preparation

In our work, a CSM microhardness tester using a Vickers diamond indenter was used, and its nominal angle was set at 136° . For the test, the micro-indentation parameters used are approach speeds of 50 mm/min, contact load 20 mN, load rate of 2000 mN/min, unload rate of 2000 mN/min, maximum load of 1000 mN, and 20 s pause. Besides, the micro-indentation test can be carried out in four steps: (1) Vickers indenter indentation of the surface; (2) loading stage to the maximum level, the maximum load used is 1000 mN, (3) maintaining the load. It is completed to avoid the influence of creep on the unloading characteristics and (4) in the final unloading stage [123].

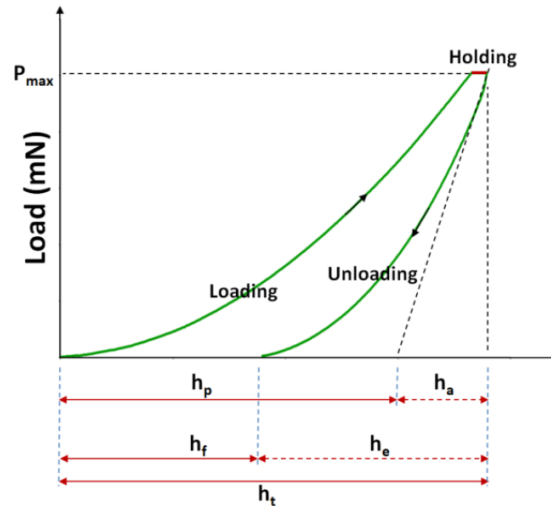


Figure II.17: Indentation depths expression

h_t is the whole depth below a load of P_t ,

h_e is the elastic rebound depth for the unloading duration,

h_f is the depth of the residual impression,

h_a is the surface displacement at the perimeter,

h_p is the depth of the contact indentation.

II.7 Mechanical Characterization of Nanocomposites

II.7.1 Static tests: Mechanical test bench – INSTRON

The quasi-static tests were carried out on an INSTRON type 5585H universal traction machine with a 10kN force cell and an INSTRON AVE 2663-821 model video extensometer.

A computer runs the test through the Bluehill modular software. According to the charging process, the tensile or compressive force is applied to the sample until it breaks at a constant speed. The machine allows for large cross-sectional positions, so it is possible to apply a maximum of more than 1000% deformation to the test, if necessary (in our case, the deformation will not reach these levels). The force measurement is attributed to a load cell with a capacitance of 1KN. The latter is very suitable for our test, to the extent that it is not necessary

to apply a lot of force to deform the polymer. The machine is driven within a specific range of deformation speeds, and the explored speed ranges from 10^{-4} s^{-1} to 10^{-1} s^{-1} so that the load can be regarded as quasi-static. All tests are performed at ambient temperature and are repeated three to five times on different tests of the same shade to ensure that the results obtained are repeatable. Carrying out tests to characterize the mechanical properties of the material and the measurement of the magnitude (stress and deformation) will not cause any particular issues.

Among all mechanical tests, the tensile test is certainly the most basic, as shown in Figure II.18. It is used to determine the main mechanical properties, such as elastic modulus, Poisson coefficient, elastic limit, fracture resistance, elongation at break, and shrinkage coefficient. In research, it can be used to characterize new materials, and in industry, it can be used for regular inspections to monitor the quality of alloys, polymers, ceramics, and composite materials [245]. These tensile tests consist of subjecting a dumbbell-shaped specimen to continuous deformation at a constant speed (2mm/min.) and recording the resulting stress.

The tensile test applies a tensile (pulling) force to the material and measures the response of the sample to the stress. In this way, the tensile test can determine the strength of the material and the extent to which it can be stretched. We can learn a lot about substances from the tensile test. By measuring the material as it is pulled, we can obtain a complete profile of its tensile properties. When plotted on a graph, this data produces a stress vs. strain curve that shows how the material structure responds to the applied force. The breaking point is of great interest, but other important properties include elastic modulus, yield strength, and strain.

One of the most important properties of the material structure that we can determine is its ultimate tensile strength (UTS). This is the maximum stress that the specimen can withstand during the test. UTS may or may not be equal to the fracture strength of the specimen, depending on whether the material structure is brittle, rigid, or both. Sometimes, certain material may be

malleable when tested in a laboratory, but when it is put into use and exposed to extremely low temperatures, it may turn into brittleness.

For the mechanical behavior of most materials, the initial part of the test will show a linear relationship between the applied force or load and the elongation. In this linear region, the straight line obeys the relationship defined as "Hooke's Law", in which the ratio of stress to strain is a constant or $\frac{\sigma}{\epsilon} = E$. E is the slope of a straight line proportional to stress (σ) and strain (ϵ) in this region and is called "modulus of elasticity" or "Young's modulus".

The modulus of elasticity is a measure of the rigidity of a material and is only applicable to the initial linear region of the curve. In this linear region, the tensile load can be removed from the sample, and the material will return to the same state as before the load was applied. When the curve is no longer linear and deviates from the linear relationship, Hooke's law no longer applies, and some permanent deformation will occur in the sample. This is called the "elasticity or proportional limit". From this point on, in the tensile test, the material will react plastically to any further increase in load or stress. If the load is removed, it will not return to its original, stress-free state.



Figure II.18: Tensile test with INSTRON machine

The "yield strength" of a material is defined as the stress exerted on the material that begins to undergo plastic deformation. For some materials (e.g., metal and plastic), deviations from the linear elastic region cannot be easily identified. Therefore, the offset method can be used to determine the yield strength of the material. We will also be able to find the amount of stretch or elongation experienced by the sample in the tensile test. This can be expressed as an absolute measure of length change, or as a relative measure called "strain". Strain itself can be expressed in two different ways, namely "engineered strain" and "true strain". The engineered strain may be the simplest and most common expression method of strain used. It is the ratio of the length change to the original length $= \frac{L-L_0}{L_0} = \frac{\Delta L}{L_0}$. The true strain is similar but based on the instantaneous length of the sample during the test, $\varepsilon = \ln\left(\frac{L_i}{L_0}\right)$ where L_i is the instantaneous length and L_0 is the initial length.

II.7.2 Compression Test

The quasi-static compression tests were carried out on the same machine as for the tensile tests as shown in Figure II.19. The machine is equipped with a force cell with a capacity of 100kN and specific compression jaws consisting of two Marval steel plates with a 2GPa elastic limit. The compression test samples are cubes measuring 13x13x13mm.

Compression testing is used to determine the performance of the material under the applied crushing load, usually by applying compression pressure to the sample (usually a rectangular parallelepiped or cylindrical geometry, in our case it is a cube) using an INSTRON machine. During the test, various properties of the material will be calculated and drawn as stress vs. strain curve to determine such qualities as the elastic limit, proportional limit, yield point, yield strength, and compressive strength of certain materials.

Compression testing allows manufacturers to evaluate the integrity and safety of materials, components, and products at multiple stages of the manufacturing process. Potential applications may range from the strength testing of car windshields to durability testing for concrete beams used in buildings. Materials that exhibit high tensile strength tend to (but not systematically) exhibit low compressive strength. Similarly, materials with high compressive strength tend to exhibit lower tensile strength. Therefore, compression testing is usually used for brittle materials such as concrete, metals, plastics, ceramics, composites, and corrugated materials (such as cardboard). These materials are usually selected and used for their load-bearing capacity, in which case their integrity under compressive forces is critical.

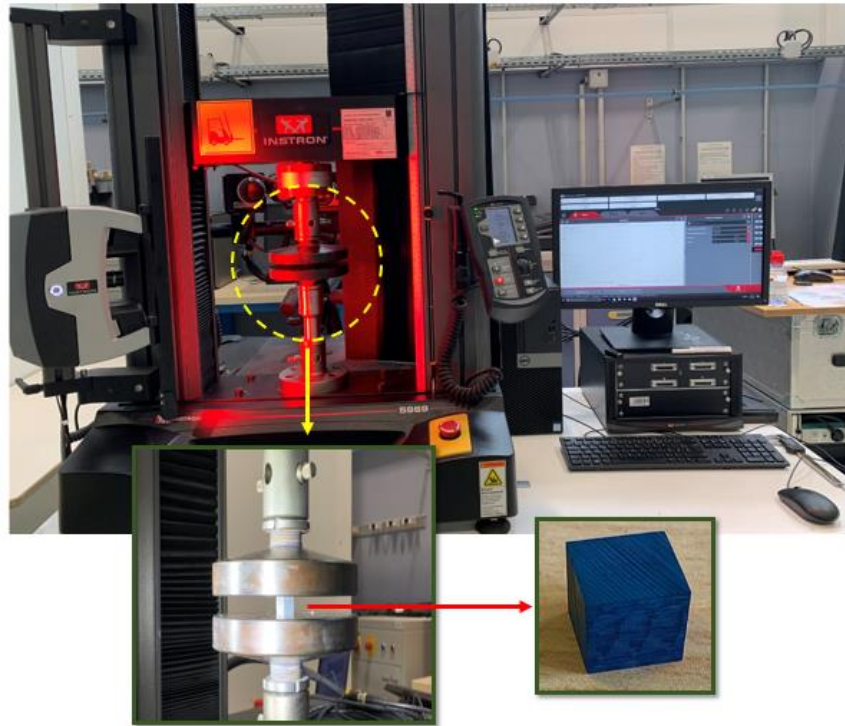


Figure II.19: Compression test under INSTRON machine

Unlike the tensile test, which tends to be used to determine the tensile properties of a particular material, the compression test is usually performed on the finished product. Common items such as tennis balls, golf balls, water bottles, protective covers, plastic pipes, and furniture are examples of products that need to be evaluated for their compressive strength. For example, an engineer may want to save plastic by making thinner-walled water bottles, but these water bottles must still be strong enough to fit in a pallet and be stacked together for transportation. Compression testing can help engineers fine-tune the balance between product strength and material savings.

The final compressive strength of a material is the value of the compressive stress reached when the material fails. When brittle materials reach their ultimate compressive strength, they will be crushed, and the load will drop sharply. Materials with higher ductility (most plastics) will not break but continue to deform until no more load is applied to the sample, and no more load is applied between the two pressure plates. In these cases, the compressive strength can be

reported as a specific deformation, such as 1%, 5%, or 10% of the original height of the specimen.

II.8 Study of the dynamic behavior of nanocomposites

The dynamic compression tests use the same sample geometry as the compression test. When determining the size of the sample, the constraints related to the dynamic test should be considered. The Split Hopkinson Pressure Bar (SHPB) technology is widely used to study the dynamic behavior of materials subjected to loads at high deformation speeds where different types of stress (traction, compression, or torsion) can be envisaged as shown in Figure II.20. This section will review the "Split Hopkinson Pressure Bar" assembly technique introduced by Kolsky in 1949 [251], which was used in this research work for dynamic compression testing.



Figure II.20: Split HOPKINSON bar apparatus

The principal strong point of the Hopkinson bar is known and has been the subject of many publications [252][253][106], [128], [136], [254]–[256]. The basic point is inserting the sample to be analyzed between two identical bar where the bar should have a high elastic limit

compared to the samples of the materials. The first and second bar are named "incident bar" and "transmitted bar" respectively. The free end of the entry bar receives the longitudinal impact of the cylindrical projectile, Figure II.21.

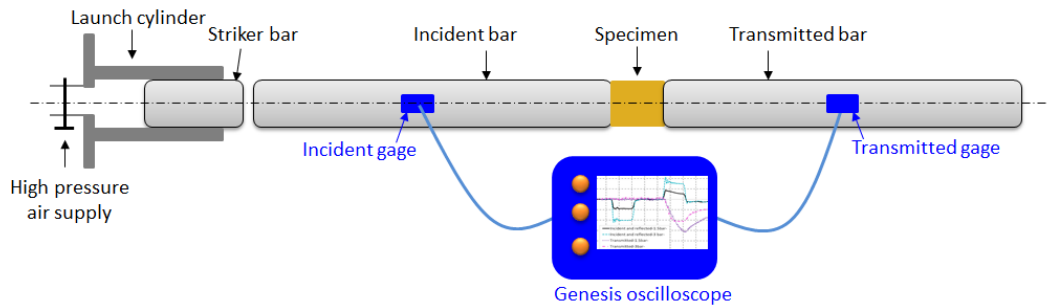


Figure II.21: Schematic description of the Hopkinson bar device

The elastic wave produced by the impact of the projectile is propagated from the incident bar to the sample. Upon reaching the contact surface of the incident bar/ sample (interface 1), part of this wave propagates in the sample and the other part is reflected. The transmitted wave passes through the sample and reaches the surface of the sample/transmitted bar (interface 2).

A portion of this wave is reflected and then passes through the sample again, in the opposite direction. Therefore, this wave propagation makes it possible to generate the dynamic stresses of the test sample. Figure 21 shows the Hopkinson Bar device used in this work. The rod is made of high mechanical-strength steel with a high elastic limit (1GPa) and high hardness properties. The impactor is usually made of the same material as the feed and discharge bar, and also has the same cross-section. It really should be mentioned that the elastic limit and hardness of the strip's material are considerably greater than the elastic limit and hardness of the test material.

The wave propagation is shown in the Lagrangian diagram of Figure II.22, where time $t=0s$ corresponds to the instant of the impact of the projectile. The deformation meter is bonded onto the two steel bars for measurement:

- The incident wave is generated by the force of the projectile hitting the incident bar.
- Waves are reflected at the interface of the incoming bar sample.
- The waveform is transferred to the transmitted bar on the sample transmitted bar interface.

The positioning of the gauge should ensure that the incident and the reflected wave will not diverge, so that the measurement can be performed separately, as shown in Figure 22.

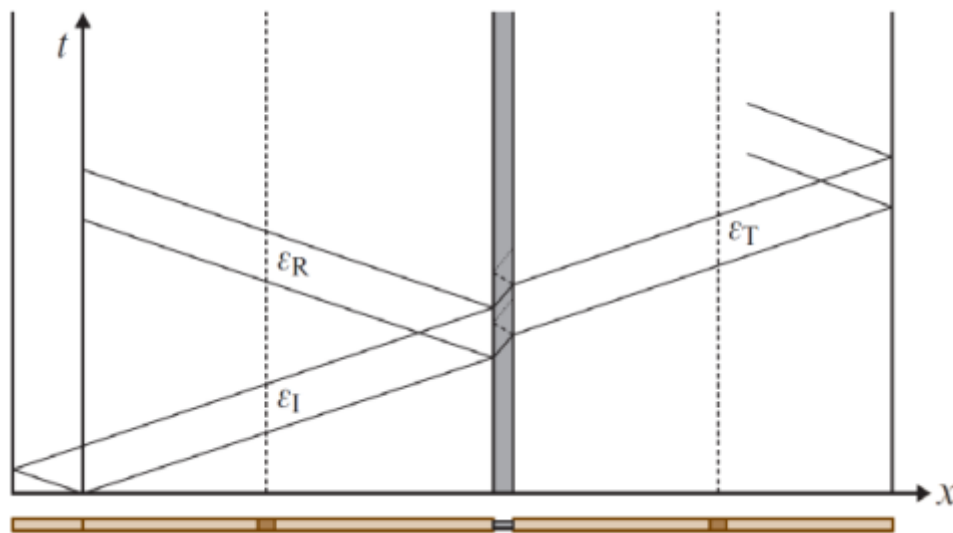


Figure II.22: Principle of wave propagation, Lagrange diagram (the length of the sample is exaggerated to show the reverberation of the waves in the sample)

The projectile fired at the initial velocity V_0 strikes the incident bar and produces an incident elastic wave that propagates in the bar at a velocity of C_0 :

$$C_0 = \sqrt{\frac{E}{\rho}} \quad (2)$$

Where E and ρ respectively represent the Young modulus and the density of the material constituting the bar.

Thus, the intensity of the incident stress is defined by:

$$\sigma_I = \frac{1}{2} \rho C_0 V_0 \quad (3)$$

When the incident wave reaches a geometric discontinuity in the interface strip sample, part of the wave is reflected ε_R , and the other part is transmitted, ε_T . The characteristic equations related to the one-dimensional expansion of elastic waves in the bar allow us to express particle speed in two interfaces:

$$\begin{aligned} v_e(t) &= C_0(\varepsilon_I(t) - \varepsilon_R(t)) \\ v_s(t) &= C_0 \varepsilon_T(t) \end{aligned} \quad (4)$$

The average axial deformation speed in the sample is as follows:

$$\dot{\varepsilon}_n = \frac{v_e(t) - v_s(t)}{l_0} = \frac{C_0}{l_0} (\varepsilon_I - \varepsilon_R - \varepsilon_T) \quad (5)$$

Whereby l_0 represents the initial length of the sample. Having identified the deformation of the steel bar, we can calculate the pressure of the steel bar and calculate the normal force of the two interfaces of sample/bar from there:

$$\begin{aligned} F_I(t) &= A_0 E [\varepsilon_I(t) + \varepsilon_R(t)] \\ F_T(t) &= A_0 E \varepsilon_T(t) \end{aligned} \quad (6)$$

The nominal average axial stress in the sample is expressed as:

$$\sigma(t) = \frac{F_I(t) - F_T(t)}{2A_s} \quad (7)$$

$$\sigma(t) = \frac{A_0 E [\varepsilon_I(t) + \varepsilon_R(t) + \varepsilon_T(t)]}{2A_s}$$

Among them, A_0 is the bar cross-section, and A_s is the sample cross-section.

It is interesting to look at the propagation of the wave in the sample in detail. When the incident wave reaches the sample, it generates a compression wave, which will then propagate through the sample and reach the sample/output bar interface. In the design, the sample impedance is smaller than the impedance of the steel bar. The wave reflected at the sample/outlet steel bar interface is still a load wave, which leads to higher compressive stress. Then, the wave reaches the incoming steel bar/sample interface, again generating higher impedance, and it is reflected as a load wave again, which leads to a further increase in compressive stress.

This process continues until the stress inside the sample reaches a value, which is high enough to produce inelastic deformation, which subsequently leads to limited plastic flow of the sample under a compressive load. Once the plastic flow of the material starts, as the amplitude of the wave edge at the back is small, the continued propagation of the wave in the sample can be discounted. Therefore, after a while, the stress field in the sample becomes uniform: the stress is considered to be balanced. If the boundary conditions are frictionless, the stress in the sample is also uniaxial.

Once the equilibrium condition is reached ($F_I = F_T$), equation 6 is simplified to:

$$\varepsilon_I(t) + \varepsilon_R(t) = \varepsilon_T(t) \tag{8}$$

In other words, let us suppose:

- The stress and deformation in the sample are uniform.
- The stress in the sample is uniaxial.

- The elastic wave propagation is one-dimensional (1D), and it is not dispersed in the strip.
- The nominal deformation speed, nominal deformation and nominal stress (all average values in the sample) can be estimated:

$$\begin{aligned}\dot{\varepsilon}_n(t) &= -\frac{2C_0}{l_0} \varepsilon_R(t) \\ \varepsilon_n(t) &= \int_0^t \dot{\varepsilon}_n(\tau) d\tau \\ \sigma_n(t) &= \frac{EA_0}{A_s} \varepsilon_T(t)\end{aligned}\tag{9}$$

The true deformation and deformation rate in the sample are as follows:

$$\begin{aligned}\varepsilon(t) &= -\ln[1 - \varepsilon_n(t)] \\ \dot{\varepsilon}(t) &= \frac{\dot{\varepsilon}_n(t)}{1 - \varepsilon_n(t)}\end{aligned}\tag{10}$$

Assuming that plasticity is not compressible, the true stress in the sample is provided by:

$$\sigma(t) = \sigma_n(t)[1 - \varepsilon_n(t)]\tag{11}$$

Some basic condition requirements need to be met in order to certify that the response given by the Hopkinson Bar experiment is indeed the compositional material behavior under testing conditions.

- **Homogeneity of the mechanical field**

Equation 9 [257], which gives the average stress-deformation relationship only makes sense when the stress and deformation fields in the sample are approximately uniform [258], [259]. This assumption of homogeneity is difficult to obtain strictly. There is a time to transfer the load through the sample. Therefore, depending on whether this time is negligible compared to the test duration, this assumption is more or less valid. This assumption still applies to many

metal materials that use short sample lengths [257], but this is not the case for fragile materials (such as concrete, rock), and the opposite method should be used [260]. There is no need to assume the same quality. For these materials, short samples that are representative (ratio effect) cannot be used.

- **The friction effect**

The friction at the bar/sample interface will cause changes in the uniaxial stress state and could lead to inaccurate results [261]. Several authors who have studied this topic [251], [253], [257], [262] have demonstrated that the geometric shape of the sample, that is, the ratio of $\frac{l_0}{d_0}$ (where d_0 represents the initial diameter of the sample), determines the friction effect the importance of test results. In order to reduce the influence of this issue, it is recommended to lubricate the interface strip/sample and fix the report $\frac{l_0}{d_0}$ between 0.5 and 1 [263]. However, it is necessary to apply the method of correcting the effect of friction provided by Klepaczko-Malinowski, which is described in the part of almost static compression (the model is effective in terms of both dynamic and static properties).

- **The effect of inertia**

The stresses related to the axial and radial inertia must be low compared to the flow stress of the material being measured. During SHPB testing, the stress wave generated in the test bar at a high deformation rate can cause inertial effects, which affect the measured characteristics (stress and deformation in the sample). The impact of inertia on obvious stress depends on the density of the material and the sample size. To correct this effect, the model proposed by Klepaczko-Malinowski can be applied. The full expression of the model includes the friction effect, as shown below:

$$\sigma_{material} = \sigma_{measurement} - \Delta\sigma_{friction} - \Delta\sigma_{inertia}$$

$$\sigma_{material} = \sigma_{measurement} \left(1 - \frac{\mu d_0}{3 l_0}\right) - \frac{1}{12} \rho d_0^2 \left(\frac{l_0^2}{d_0^2} - \frac{3}{16}\right) (\dot{\varepsilon}^2 + \ddot{\varepsilon}) + \frac{3}{64} \rho d_0^2 \ddot{\varepsilon} \quad (12)$$

μ is the coefficient of friction.

Since the test is carried out at an almost constant deformation speed, the acceleration can be regarded as zero ($\ddot{\varepsilon} \rightarrow 0$). In this case, the effect of inertia can be minimized [263]. For example, under the conditions of ($\ddot{\varepsilon} = 0$) and $\frac{l_0}{d_0} = 0.5$, the stress increase caused by the inertial effect is less than 0.3 MPa for a deformation rate of 104 s^{-1} [263].

- **The punching effect**

Safa and Gary [264] analyzed the recently observed effect called punching. This phenomenon causes errors in the estimation of the macroscopic longitudinal deformation imposed on the sample. As shown in Figure II.23, during the dynamic loading process, the steel bar undergoes elastic deformation, which causes local displacement $U_p(r, t)$. It is therefore necessary to include this additional displacement in the definition of the actual length change of the sample. However, it is impossible to accurately measure the displacement with a known experimental measuring device. Safa and Gary proposed a new formula to account for the change in actual sample length during the loading process, in order to illustrate the punching effect:

$$l(t) = l_0 - |\delta_{SHPB}(t)| - 2U_p(r = 0, t) \quad (13)$$

Where $\delta_{SHPB}(t)$ is the relative displacement of the end of the steel bar, and U_p is the displacement of the bar with the punching effect.

Jankowiak et al. [263] show that for very rigid steel bar with elastic limits that are strictly greater than the limit of the tested sample material, the punching effect on deformation wave measurement is very small. In fact, for the elastic limit steel of 300 MPa, the maximum

displacement due to the punching action is estimated to be $18 \mu\text{m}$. For a sample with an initial length of 4mm , the error of deformation measurement is 0.007 [263]. Therefore, we have discounted this influence in this study.

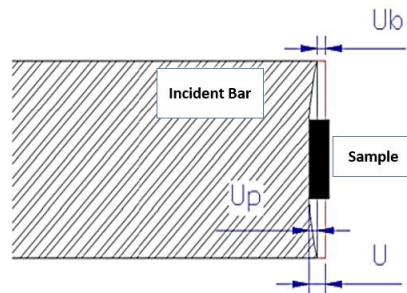


Figure II.23: Schematic description of the punching effect during dynamic compression using Hopkinson bar

To complete the SHPB skin test in this study, we used the MAPLE software algorithm using Fast Fourier Transformation to obtain the dynamic parameters: stress vs. strain, strain rate vs. time, incident and transmitted load and velocity vs. time at the interfaces of incident bar/specimen and transmitted bar/specimen.

II.9 Conclusion

Studies on the effect of the nanofillers on the properties of adhesive nanocomposites require good choices of the adhesive resin, the appropriate nanofillers, the method of implementation, and fine-tuned characterization of the microstructure. In this chapter, we have described the main characteristics of the materials used basically, on the one hand, for the preparation of the different mass fractions of the different nanofillers applied and, on the other hand, for the preparation of the reinforced adhesive nanocomposite samples.

Additionally, good nanofiller distribution contributes to good mechanical performance improvement of the adhesive nanocomposite structure. For this reason, highly efficient manufacturing methods have a very important role. This chapter presents the techniques used

for integrating carbon nanotube, graphene platelets, and carbon black. Moreover, the techniques and conditions for the use of unreinforced and reinforced nanocomposite samples are also described in detail.

According to scientific research and on a microscopic scale, direct observations have shown that a good choice for the implementation method has made it possible to distribute the nanoparticles well in the adhesive resin but has not been sufficient to avoid aggregation of high mass fraction of nanoparticles, which increases the reduction of the bonds between the nanoparticles and the adhesive. Subsequently, it leads to a reduction in chain mobility. The properties of the polymers being intrinsically linked to the mobility of the chains could cause a modification of the properties of the adhesive resin.

In the following chapters, we will look at the effect of nanoparticles on physico-chemical and mechanical properties, to then attempt to link the identified parameters with the measured properties.

Chapter II:

Physico-chemical properties

III. Physico-chemical properties

Summary

III. Physico-chemical properties	128
III.1 Introduction	129
III.2 Thermal properties.....	129
III.3 Mechanical properties at a local scale	132
III.3.1 CNTs/ DGEBA epoxy nanocomposite	136
III.3.2 GNPs/DGEBA epoxy nanocomposite	141
III.3.3 CBs/DGEBA epoxy nanocomposite	145
III.3.4 Comparative analysis with different nanoparticles (CNTs/ GNPs /CBs) reinforced DGEBA adhesive	151
III.4 Conclusion.....	155

III.1 Introduction

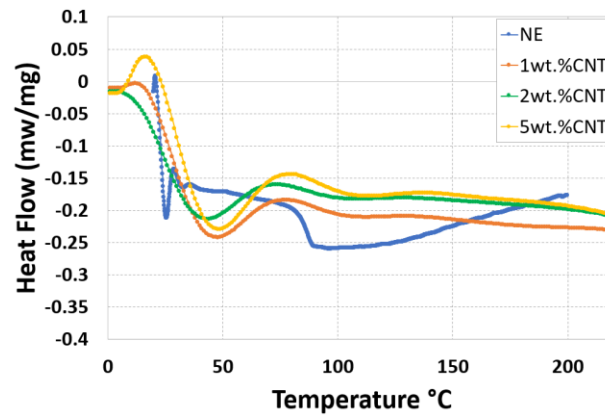
Thermal analysis and micromechanical study are test methods widely used in physico-chemical analysis laboratories for quality control purposes. This section is interested in the distribution manner of the carbon nanoparticle-reinforced DGEBA adhesive resin nanocomposite structure. To evaluate this distribution manner, we combined two experimental techniques: DSC and micro-indentation. The first technique allows for the determination of the glass transition temperature of various-reinforced adhesives, and the second technique allows for the determination of the local mechanical properties using micro-indentation (elastic modulus, hardness, etc.), specifically viscoelastic behavior at different points.

III.2 Thermal properties

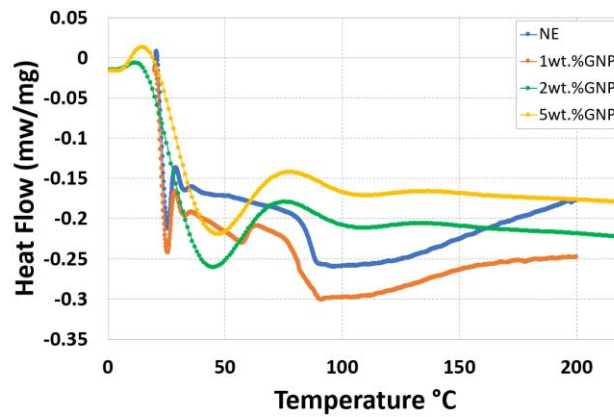
DSC was used to study the thermal properties of the original and enhanced coating samples, such as the glass transition temperature (T_g), as is revealed in Figure III.1. The glass transition temperature (T_g) is commonly used to evaluate the interaction between fillers and polymer adhesive [265][266]. From the results shown in Table III.1, it can be seen that the T_g of neat DGEBA adhesive and reinforced DGEBA adhesive nanocomposites increase with the addition of nanoparticles. Nanoparticles positively affect thermal properties, more specifically on the crystallization rate of nanocomposite adhesive. It was found from the DSC tests that the 3 types of nanofillers tended to increase these parameters. The addition of CNTs showed the most significant improvement of thermal properties in DGEBA adhesive nanocomposites [164], [254], [267], [268]. The increase in T_g is accredited to the strong interaction between CNTs and the DGEBA adhesive resin, resulting in the restricted mobility of adhesive chains.

As stated in Table 1, 1wt.% CNTs exhibit a higher T_g value than neat adhesive. Therefore, 1wt.% CNTs, nanoparticles form an influence zone around their surface, identified as interphase, which restricts the mobility of the resin matrix in this phase. This limited (restricts)

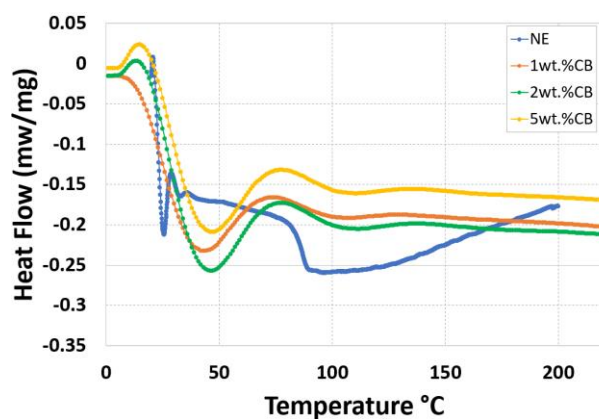
mobility can lead to a higher glass transition temperature, mainly because the nanoparticles have a larger surface area.



(a)



(b)



(c)

Figure III.1: Glass transition temperature for reinforced DGEBA epoxy nanocomposite (a)

CNTS (b) GNPS S (c) CB

However, compared with 1wt.% CNTs, the decrease in T_g values at 2wt.% and 5wt.% CNTs may be due to their agglomeration, which leads to a disturbance in adhesive polymer heat flow. Due to the agglomeration of fillers, adding 5wt.% CNTs reduces the crosslink density of the adhesive resin matrix [269]. Aggregate development also creates free volume at the interface, increasing the segment's fluidity [270].

In addition, changes in thermal stability are related to the strong interfacial bonding effects of nanoparticles, including covalent bonding and higher cross-linking systems [271].

In the other hand, adding GNPs to DGEBA adhesive nanocomposite will cause a slight decrease of 1wt.% GNPs, which may be due to the restriction of polymer mobility (fluidity). In addition, the reduction in T_g may be caused by the decrease in crosslink density. However, the effective increase of 2wt.% and 5wt.% GNPs in glass transition temperature indicates a robust interfacial adhesion between the matrix and the graphene sheet at high mass fractions, with the highest improvement at 5wt.% GNPs.

On the other side, adding CBs in DGEBA adhesive nanocomposite showed a slight increment with a low mass fraction of 1wt.%. However, it presents an increase in T_g with 2wt.% and 5wt.%. The slight increment could be due to the free volume percentage at the interface, which influences the flexibility of the segments and couldn't add such significant improvement. Besides, the improvement that appeared with Carbon Black at high mass fraction may be due to the efficient interface created around the surface of the nanoparticles, which contributes to limits the mobility of the adhesive. This delimited mobility would be able to contribute towards higher glass transition temperatures, particularly given that nanoparticles possess large surface areas, whereby 5wt.% CBs shows the highest T_g.

In this part, built up 1wt.% CNT-reinforced DGEBA adhesive nanocomposite structure present the most appropriate Tg contrasted to graphene GNPs and Carbon Black CBs to enhance the glass transition temperature.

Table III.1: Different thermal parameters of reinforced DGEBA nanocomposite sample

			Tg	Cp
NE	0wt.%	AVERAGE	87.84	0.32
		St Dv	0.16	0.15
CNTs	1wt.%	AVERAGE	152.19	0.42
		St Dv	6.43	0.06
	2wt.%	AVERAGE	115.13	0.65
		St Dv	5.00	0.19
	5wt.%	AVERAGE	110	0.84
		St Dv	6.30	0.04
GNPs	1wt.%	AVERAGE	78.74	0.56
		St Dv	4.30	0.12
	2wt.%	AVERAGE	92.21	0.36
		St Dv	0.30	0.06
	5wt.%	AVERAGE	93.247	0.21
		St Dv	0.04	0.11
CBs	1wt.%	AVERAGE	88.44	0.48
		St Dv	0.31	0.17
	2wt.%	AVERAGE	91.66	0.53
		St Dv	0.01	0.07
	5wt.%	AVERAGE	95.10	0.36
		St Dv	0.1	0.13

III.3 Mechanical properties on a local scale

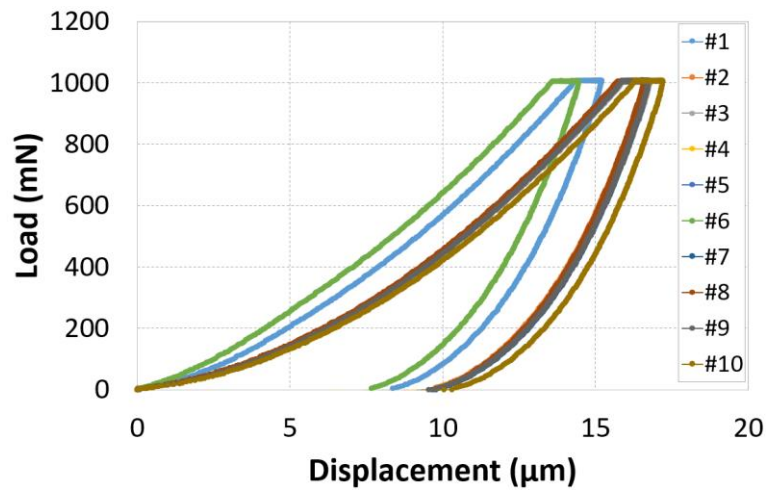
Not having extraordinary methods and analyzing nanoparticle dispersion in DGEBA adhesive nanocomposite, micro-indentation has shown up as an original and modern procedure for this consideration. In fact, with the diverse estimations on reinforced DGEBA adhesive nanocomposite with distinctive nanoparticles, we propose to assess the dispersion manner of

the carbon nanotubes, graphene, Carbon Black through the values of the elastic module, the durability and the resistance measured on the sample surface. To assess the nanoparticle distribution pathway, it is essential to form indents on a polished surface of each reinforced and unreinforced DGEBA adhesive sample. Micro-indentation could be a method that is profoundly sensitive to the surface condition of the sample. All estimations in this area have subsequently been made on mirror-polished surfaces ($R_a = 0.2 \mu\text{m}$). All tests are conducted at room temperature.

Before launching the test campaign, it is critical to have a dependable and repeatable test method for both the force applied and the load/unload cycle time. The CSM micro-indenter utilized allowed a force of up to 1000 mN to be applied. Figures III.2-III.5 show the different micro-indentation estimations made within the test samples. As it is illustrated, the penetration depth increments with force applied, which makes sense. Subsequently, it is fundamental to choose which force to apply to the test [272][131].

At any rate, it is noted that this depth evolution is homogeneous in any case of the nature of the nanocomposite (CNTs-GNPs-CBs)/DGEBA analyzed as it is in Figure III.3-III.5. The results do not display a completely uniform homogenate of nanoparticles on the adhesive network as it appears that there are various measures, and not all of the curves are reproducible [256], [272]. We will base our interpretation within the following scenario, with the measurements that align with the comparative curves.

It should be noted that adhesive resin is a viscoelastic material with deformation behavior that is dependent on time. A diverse rate of deformation will cause a distinction in adhesive properties as well as in it-reinforced nanocomposites.



(a) Test repeatability



(b) Micro indentation residual impressions

Figure III.2: Micro-indentation tests on neat DGEBA adhesive sample

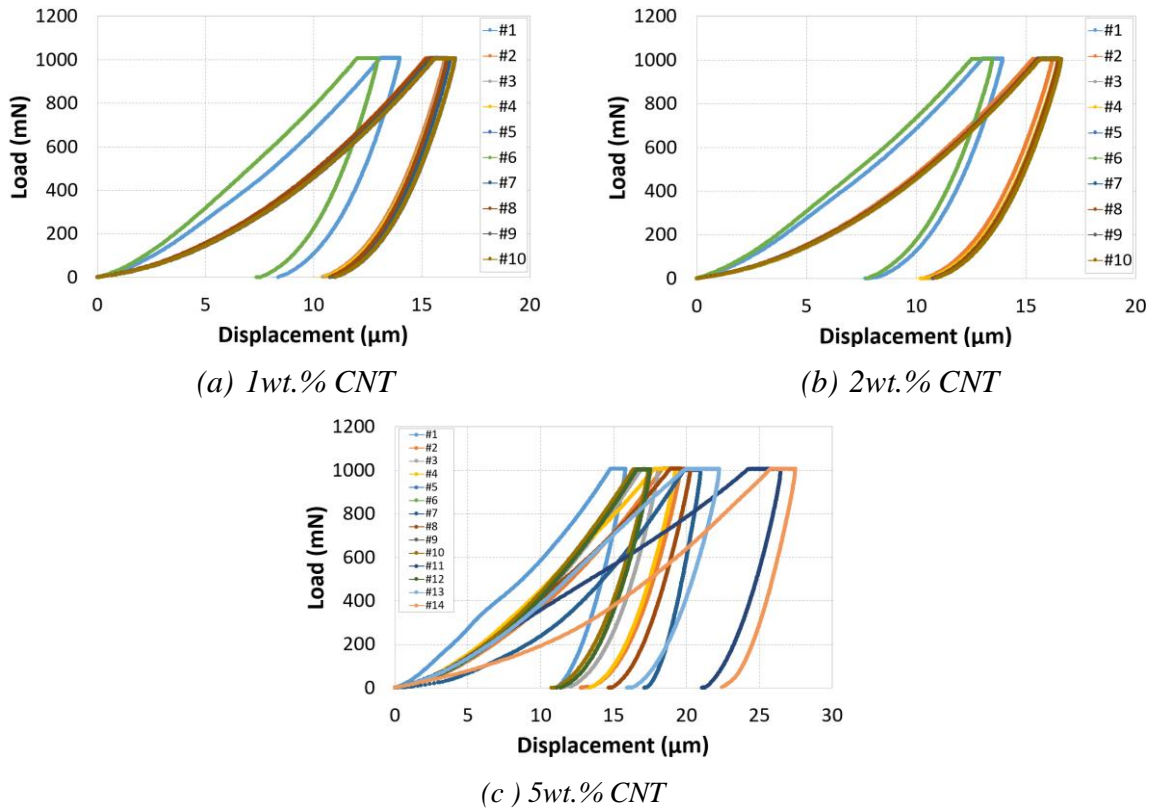


Figure III.3: Repeatability of the load-displacement response of micro-indentation test on CNT-reinforced DGEBA adhesive nanocomposite sample

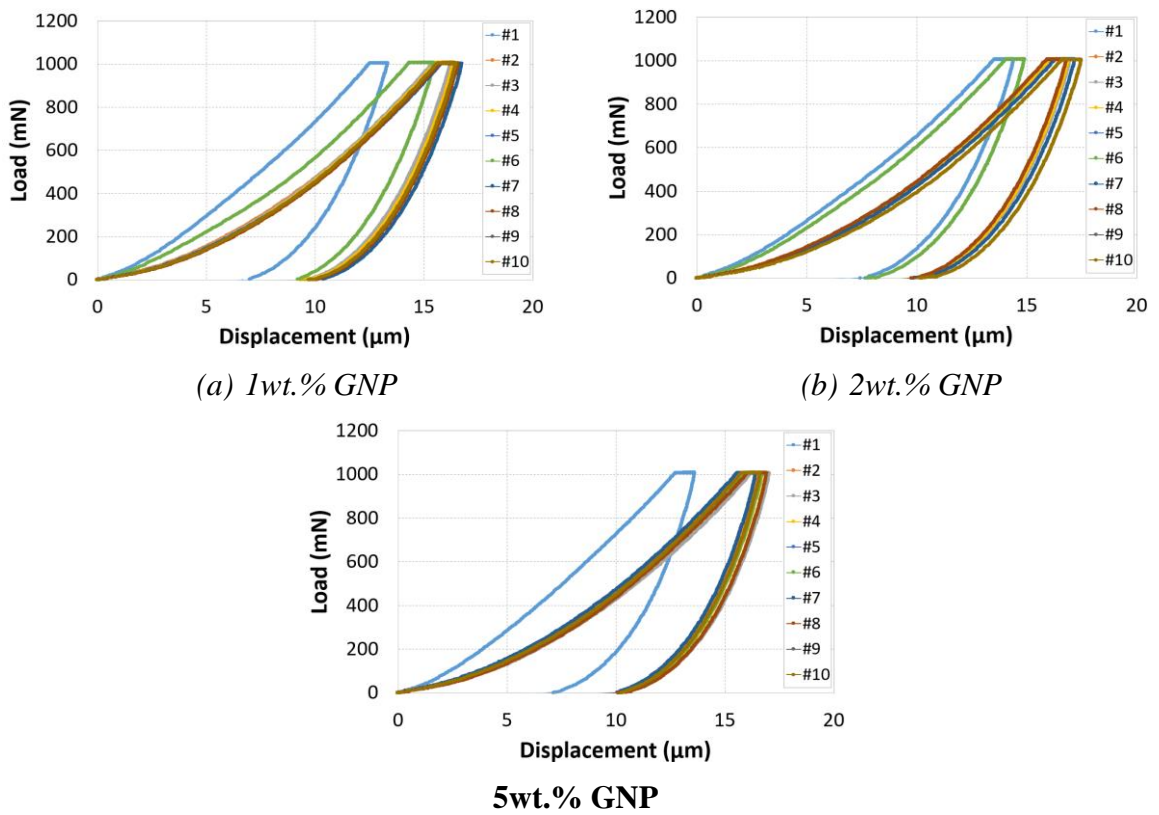


Figure III.4: Repeatability of the load-displacement response of micro-indentation test on GNP-reinforced DGEBA adhesive nanocomposite sample

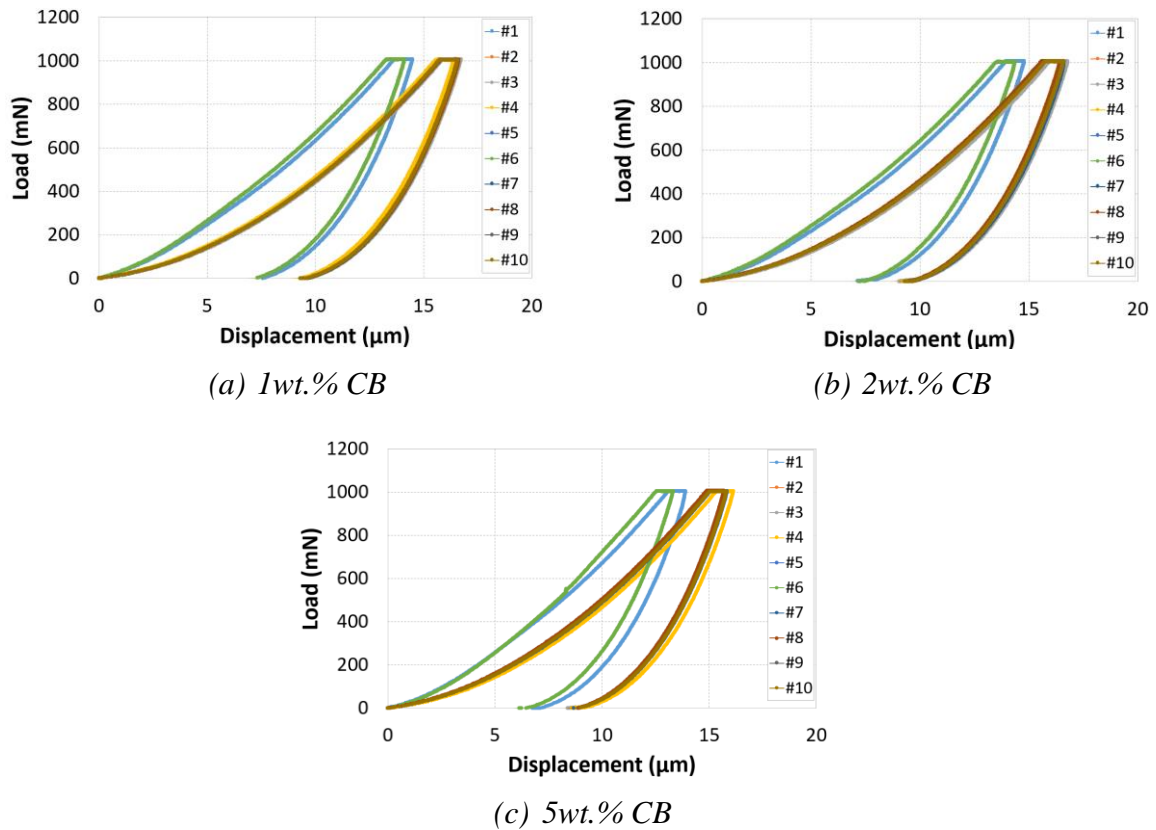


Figure III.5: Repeatability of the load-displacement response of micro-indentation test on CB-reinforced DGEBA adhesive nanocomposite sample

III.3.1 CNTs/ DGEBA epoxy nanocomposite

Figure III.6 shows load-displacement curves where no discontinuities or steps were found on the loading curves, demonstrating that no cracks were shaped during indentation [273], [274]. Since no steps or cutoffs were detected on the loading curves, it shows no crack arrangement throughout indentation. The load-displacement curves for CNTs/DGEBA adhesive nanocomposite tests show more extensive slopes of dP/dh within the unloading step and lower values of h_{max} compared with neat DGEBA adhesive nanocomposite tests, reflecting the critical upgrade impact of carbon nanotube on micro-mechanical properties of nanocomposites. The indentation depths at the peak load extend from $15\mu\text{m}$ to $16\mu\text{m}$, as it is specified in Table III.2. As the mass fraction of carbon nanotubes gradually increases, lesser indentation depth and higher unloading slopes are observed. The 1wt.%, 2wt.%, and 5wt.% CNT tests display comparable indentation depths, then distinctive unloading inclines. Besides, the increment

within the penetration depth Δh among the load holding step is due to the viscous effect [275] [276].

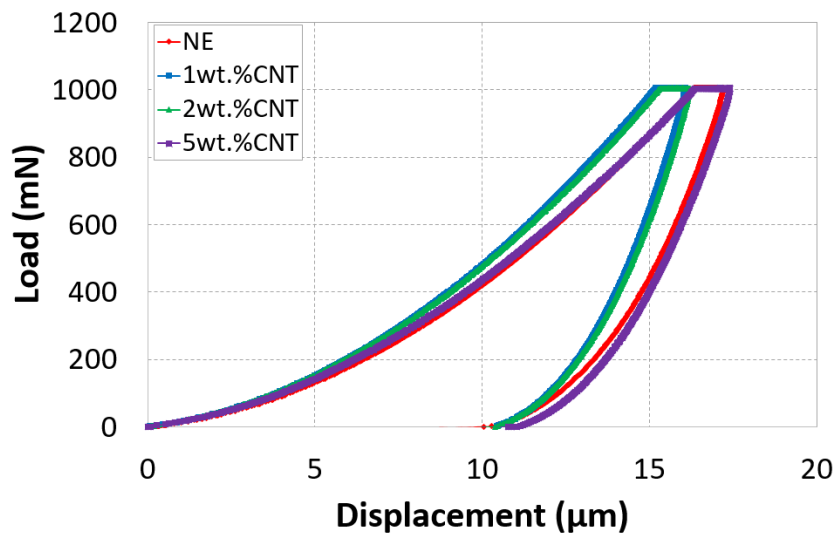


Figure III.6: Influence of CNTs nanofillers on the mechanical performance of the DGEBA adhesive

The CNT-reinforced specimens display advanced hardness and elastic modulus than the neat DGEBA adhesive specimen, as is mentioned in Figure III.7 (a-b). The modulus value increased owing to the high modulus value of carbon nanotube CNTs ($E=500\text{GPa}$). The value of the hardness increased given the decrease of indentation surface area. Both hardness and elastic modulus increased in correlation with the growing mass fraction of nanotubes, showing the reinforcing benefits with nanotubes. Compared with the pure DGEBA adhesive nanocomposite structure, including CNTs significantly reduces the polymer matrix's chain mobility, which improves the structural performance[164], [243].

The integration of the CNTs improved the mechanical properties in reports of hardness and elastic modulus. These CNTs have strong interfacial attachment with the matrix, improving the crosslinking density of the cured adhesive. Besides this, they decrease the segmental chain arrangements, subsequently avoiding adhesive disaggregation through the curing process.

Correspondingly, an increase in creep resistance and a reduction in creep deformation of the nanocomposite are detected in all nanocomposite coatings, as is clear in Figure III.7(d). This may be due to drop-in chain mobility of adhesive by CNTs, performing as sites, blocking the movement of the adhesive chain when subjected to an exterior indentation force. Consequently, they limit the viscous flow of the amorphous adhesive. Also, a great load transfer between the adhesive resin matrix and the filler may allow rise to great creep resistance of the nanocomposite as a whole [277]. The characteristic properties of the incorporated CNTs, such as high aspect ratio and the large interfacial zone, contribute meaningfully to improving the interface adhesion amongst the CNTs and the adhesive matrix, in this way coming about in high values of creep resistance [278].

Table III.2: Micromechanical properties of CNT/DGEBA nanocomposite sample

		0wt.%	1wt.%	2wt.%	5wt.%
E(GPa)	Average	4.24	5.19	4.9	4
	St. dev.	0.28	0.53	0.47	0.59
Hv(Vickers)	Average	32.86	34.84	33.66	24.42
	St. dev.	4.33	6.94	6.5	5.76
S(mN/μm)	Average	285.38	339.25	332.22	312.69
	St. dev.	2.75	4.34	4.72	13.15
D(μm)	Average	16.77	15.6	15.94	18.67
	St. dev.	0.19	1.2	1.19	1.82

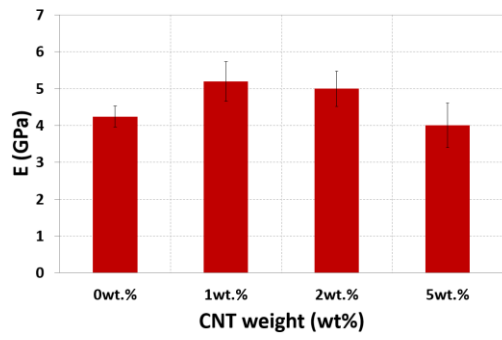
However, in Figure III.7a and Table III.2, it is renowned that the 5wt.% CNTs test displays a slight increment in elastic modulus compared to the neat adhesive and does not indicate any significant increase in hardness compared to the CNT-reinforced DGEBA adhesive nanocomposite sample and neat adhesive. These results can be clarified by the fact that, given

the high surface area of carbon nanotubes, when the concentration of nanotubes within the composite is expanded, there is less accessible polymer for intercalating into the bundles. As a result, the interactions between the nanotubes are higher, giving rise to the formation of aggregates capable of the measured mechanical properties below their theoretically anticipated potential [279] [280][281]. Besides, less accessible polymer interpolating into the bundles might weaken the adhesive and nanotube bonding [282].

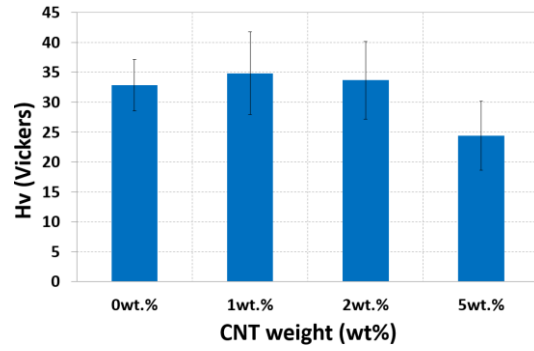
The slope presented in the second part of load-displacement curves represents the rigidity under unloading [283]. The more extreme the slope of the curve shows a more rigid construction. Interlaminar and intralaminar adhesive properties show a critical role within the character of the curve, and subsequently, a steeper slope moreover demonstrates a much better interfacial interaction.

Figure III.7(c) shows that the highest rigidity is gotten for 1 wt.% CNTs addition. Thus, it can be established that the finest interlayer and intralaminar adhesion is obtained for this composition. It is also apparent from Figure III.7(c) that inflexibility essentially decreased in correlation with the increment of nanoparticles amount as it is with 5wt.% CNT.

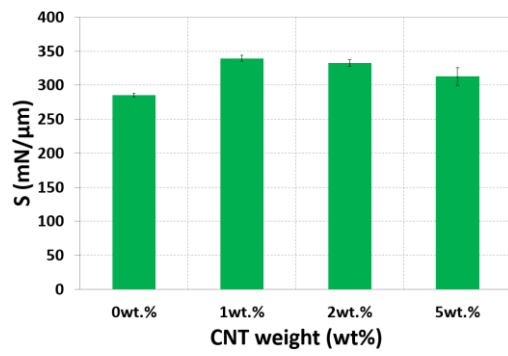
Furthermore, the energy absorption amount increases with the raised velocity. Figure III.7e shows the absorbed energies for the different mass weights of CNT substance. In contrast, the amount of energy absorption is connected explicitly to damage development. It is seen that the least energy absorption is gotten for 1 wt.% CNT substance. This circumstance refers to minimal damage shaping specimens with 1 wt.% CNT substance as proved by the indenter print in Figure III.8. The absorbed energy changes, obtained via the distinctive wt.%, are similar in Figure III.7e. In Figure III.7e, it is evident that the absorbed energy increase with increased CNTs compared to neat adhesive, at that point, it tends to be as stable as the nanoparticles. However, the elastic energy decreases slightly with CNT increases [284].



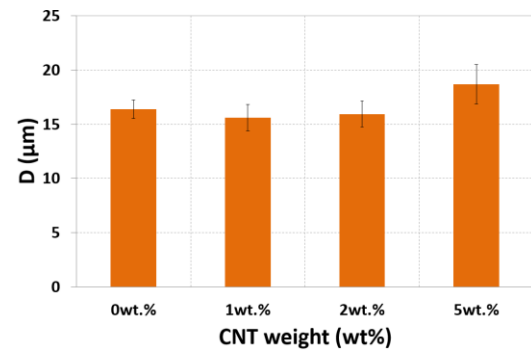
(a) Young's Modulus (MPa)



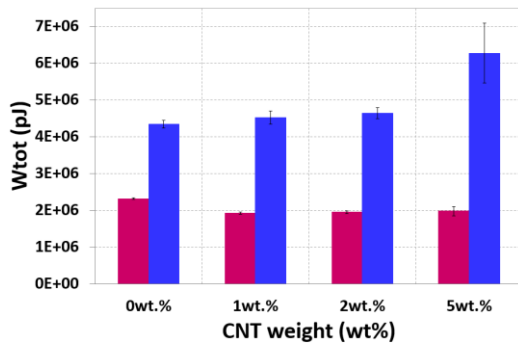
(b) Hardness (Vickers)



(c) Stiffness (N/μm)



(d) Indenter depth (mm)



(e) Energy (pJ)

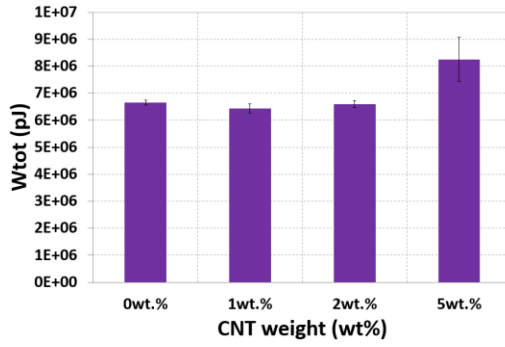


Figure III.7: Variation of micromechanical properties of CNTs/DGEBA nanocomposite

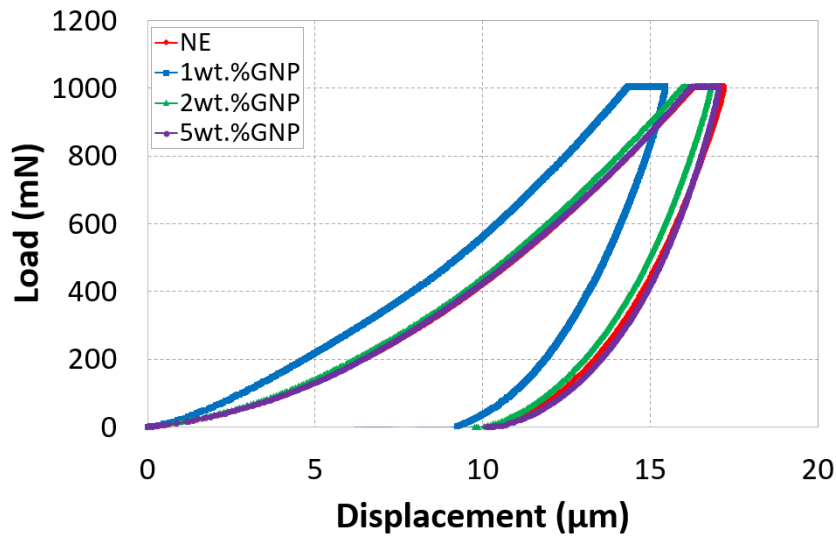


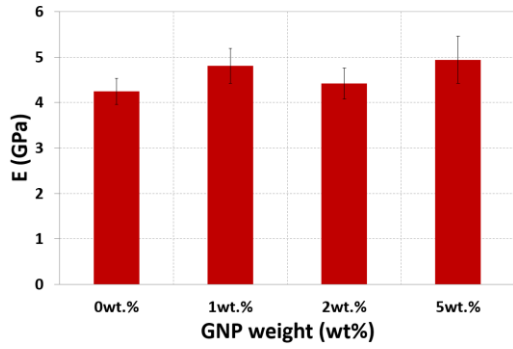
Figure III.9: Influence of GNPS S nanofillers on the mechanical performance of the DGEBA adhesive

Additionally, a reduction in creep resistance of the reinforced adhesive nanocomposite structure appears in the displacement vs mass fraction curve. The indenter displacement decreases with including graphene nanoplatelets where 1wt.% GNPs show less displacement compared to 2wt.% , 5wt.% GNPs and the neat DGEBA adhesive. The reason can be the fall in chain mobility of adhesive resin by GNPs, performing as sites, obstructive the movement of the adhesive chain when subjected to an external indentation force; thus, they limit the viscous flow of the amorphous adhesive. The inherent properties of the joined GNPs , such as the high angle ratio and the large interfacial area, contribute meaningfully to improving the interface adhesion amongst the GNPs and the adhesive resin [256], thus causing high values of creep resistance, Table III.3. In addition, the increase within the indenter displacement with 2wt.% and 5wt.% GNPs might be clarified by the question of agglomeration creation, contributing to degradation of the nanocomposite structure, Figure III.10(d).

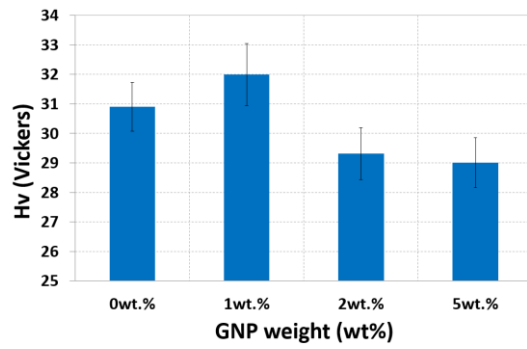
Table III.3: Micromechanical properties of GNPS S /DGEBA nanocomposite sample

		0wt.%	1wt.%	2wt.%	5wt.%
E(GPa)	Average	4.24	4.81	4.42	4.94
	St. dev.	0.28	0.38	0.34	0.52
Hv(Vickers)	Average	32.86	32.00	29.32	29.01
	St. dev.	4.33	1.05	0.88	0.84
S(mN/μm)	Average	285.38	307.71	303.21	338.11
	St. dev.	2.75	1.95	1.09	1.96
D(μm)	Average	16.77	15.58	16.54	16.83
	St. dev.	0.19	1.00	1.01	0.22

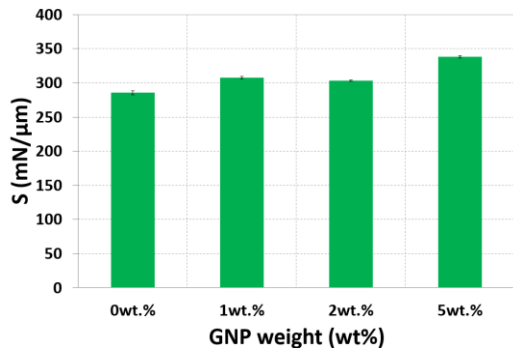
In contrast to the neat adhesive, the rigidity in Figure III.9 under the unloading section of the load-displacement curve, there is an evident progression with increasing graphene GNPs mass fraction, whereas with 5wt.% GNPs it demonstrates the maximum rigidity, as evidenced by Figure III.10(c). These GNPs have good interfacial adherence to the adhesive, increasing the cured epoxy's cross-linking density. Furthermore, when GNPs are used as nanofillers in the adhesive resin, there is a minor increase in plastic energy in Figure III.10(e), where the material becomes slightly stiff, as is proved by the indenter print in Figure III.11. Figure III.10(e) shows that adding GNPs does not result in a stable improvement as the mass fraction increases. In contrast, the amount of absorbed energy is proportional to the quantity of damage caused. The minimal absorbed energy is attained with 1wt.% GNPs, Figure III.10(e).



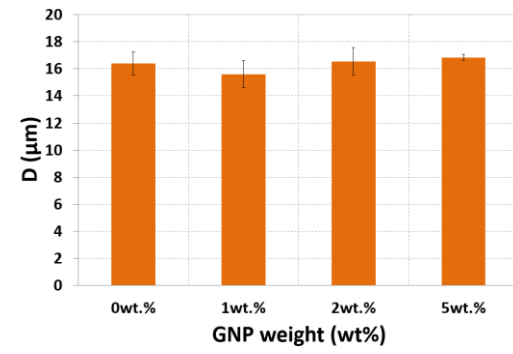
(a) Young's Modulus (MPa)



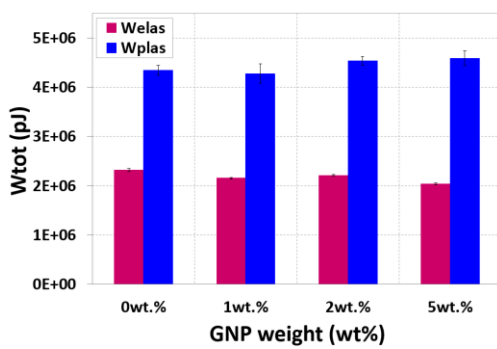
(b) Hardness (Vickers)



(c) Stiffness (N/μm)



(d) Indenter depth (mm)



(e) Energy (pJ)

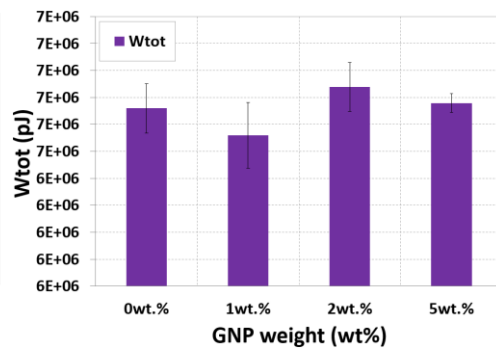


Figure III.10: Variation of micromechanical properties of GNPs /DGEBA nanocomposite

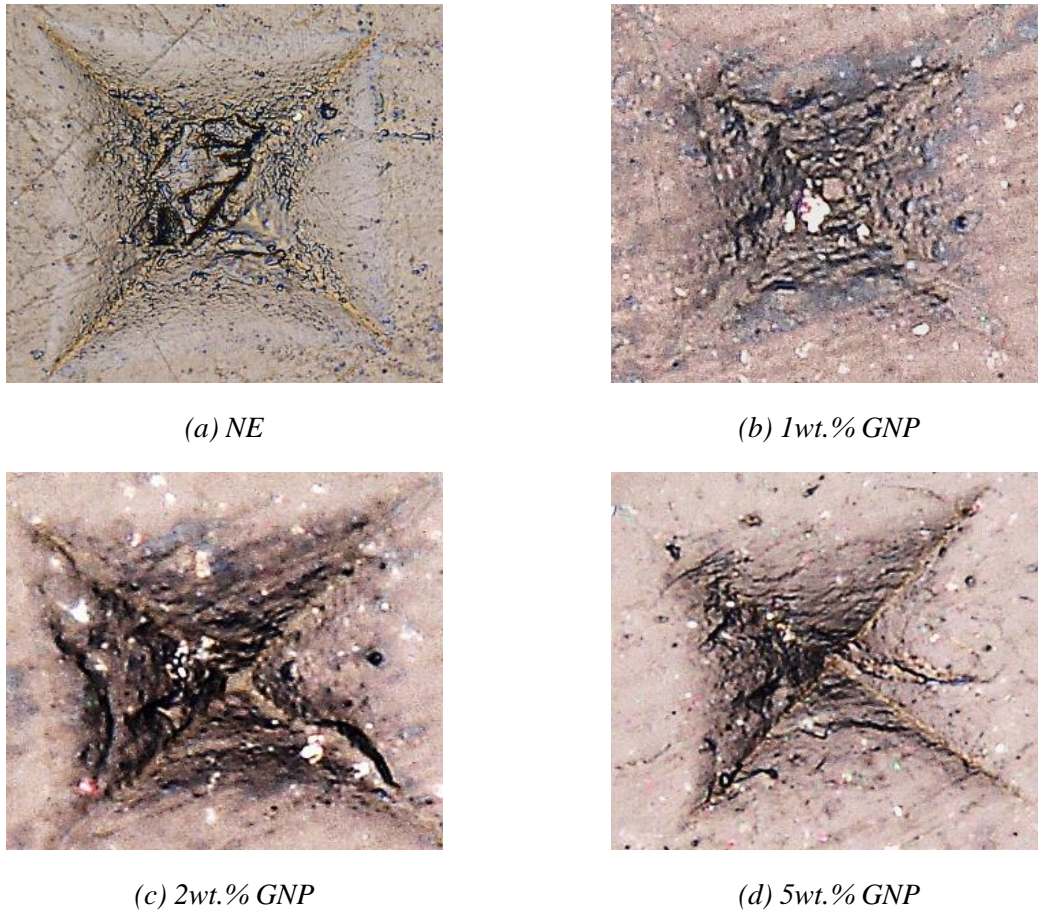


Figure III.11: Print Indentations of Vickers microhardness for GNP/DGEBA nanocomposite

III.3.3 CBs/DGEBA epoxy nanocomposite

The results of the micro-indentation tests revealed that adding CBs to the DGEBA adhesive nanocomposite had a significant effect, as shown in Figure III.12. The addition of CBs to the DGEBA adhesive nanocomposite increased Young's modulus, as seen in table III.4 and Figure III.13(a). The strength bonding between the CBs nanoparticles and the adhesive resin may account for this rise.

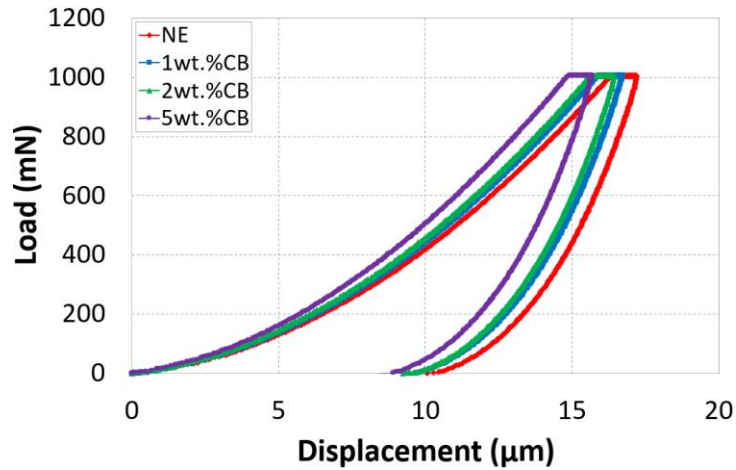


Figure III.12: Influence of CBs nanofillers on the mechanical performance of the DGEBA adhesive

Table III.4: Micromechanical properties of CB/DGEBA nanocomposite sample

		0wt.%	1wt.%	2wt.%	5wt.%
E(GPa)	Average	4.24	4.76	4.74	5.28
	St. dev.	0.28	0.36	0.29	0.65
Hv(Vickers)	Average	32.86	34.64	33.56	36.56
	St. dev.	4.33	5.24	4.63	5.48
S(mN/μm)	Average	285.38	284.87	288.53	295.13
	St. dev.	2.75	2.05	2.77	4.50
D(μm)	Average	16.77	16.04	16.21	15.07
	St. dev.	0.19	0.97	0.88	1.44

These results are related to the hardness value results, as shown in Figure III.13(b) and Table III.4. The microhardness of CBs-reinforced DGEBA adhesive nanocomposites rises in direct proportion to the number of CBs in the adhesive resin matrix. Whereas, with the highly reinforced samples (5wt.% CBs), the highest hardness is found. This value has increased due to the resistance of relatively hard CBs nanoparticles to plastic deformation.

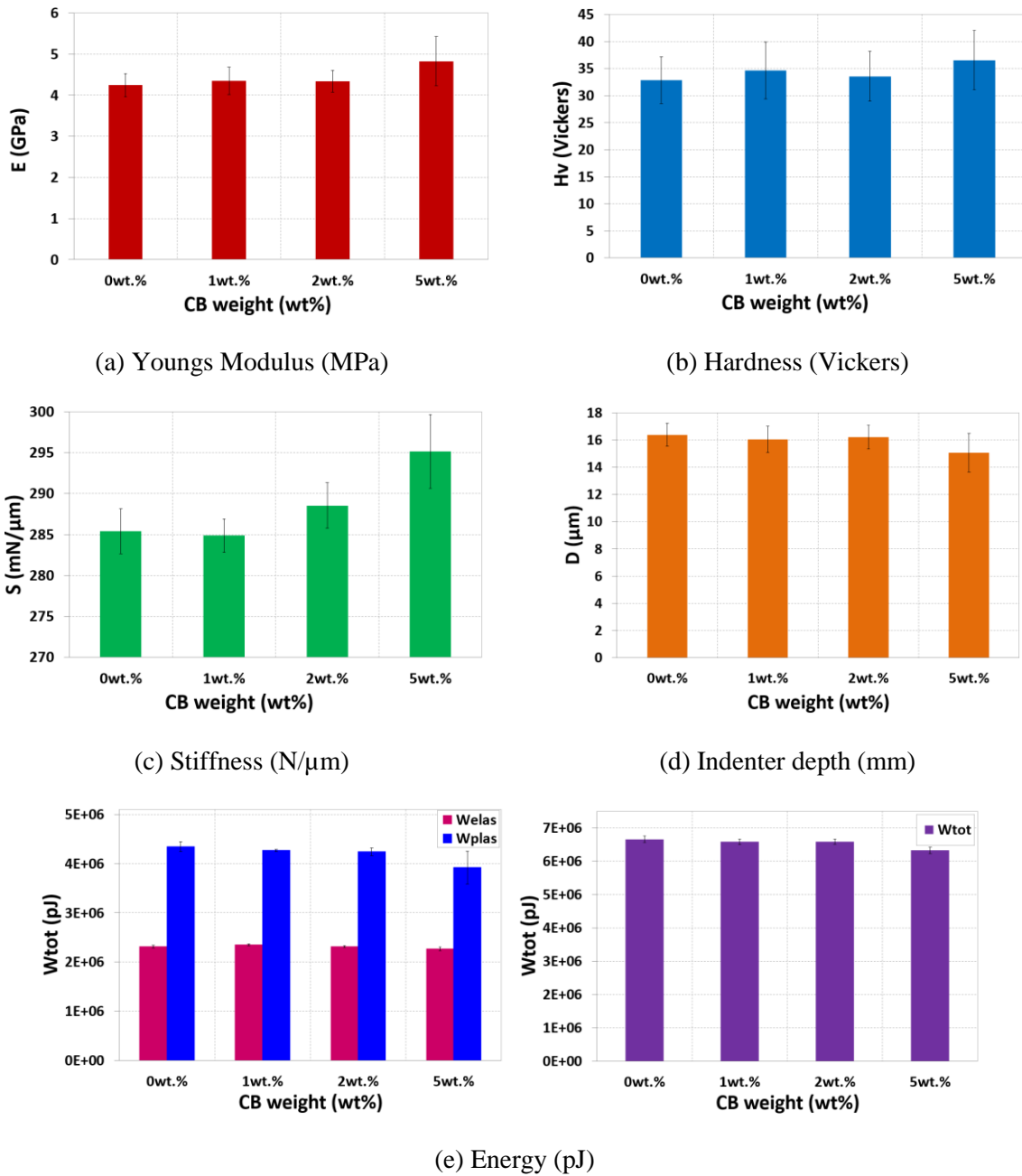


Figure III.13: Variation of micromechanical properties of CB/DGEBA nanocomposite

This improvement is attributable to Carbon Black's high aspect ratio and intrinsic mechanical performance compared to the adhesive matrix and the superior dispersion and interfacial bonding with the adhesive resin.

Furthermore, the addition of carbon black CBs to the DGEBA adhesive resin enhances the slope of the unloading curve, hence improving the material's rigidity, as it is in Figure III.12. As seen in Table III.5, highly concentrated samples with CBs attain higher rigidity, Figure III.13(c). This improvement could be attributed to a higher particle concentration, which raises the bonding strength.

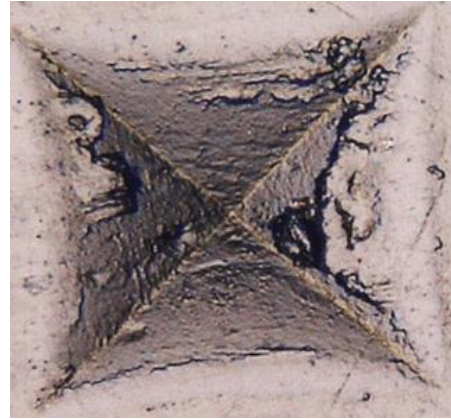
Similarly, Figure III.13(d) shows that as the carbon black mass fraction increases, the indenter displacement decreases, with 5wt.% CB-reinforced DGEBA adhesive nanocomposite indicating less plasticity behavior as it is presented in Figure III.14. Plastic energy reduction confirms the reduction in plastic deformation, Figure III.13(e).

Furthermore, when CBs were introduced to the DGEBA adhesive resin matrix as nanofillers, the material became stiffer, with increased elastic characteristics and decreased plasticity (fluidity). The amount of energy absorbed is proportional to the quantity of damage created. For all impact velocities, the minor energy absorption is obtained with a 5wt.% CBs concentration. This condition relates to the fact that little damage has formed within specimens containing 5wt.% CBs.

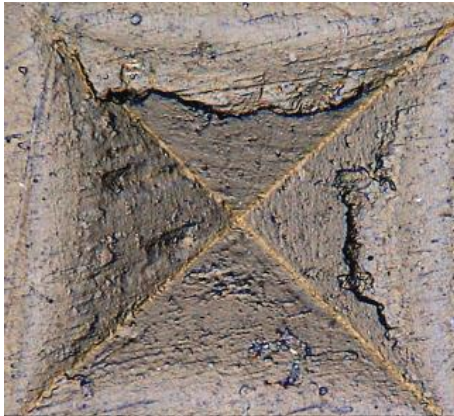
Table III.5 gives a synthesis of the results of the micro indentation tests carried out on a pure adhesive DGEBA and reinforced with different types of nanofillers (CNT, GNPs, and CB) for different mass fractions (1wt.%, 2wt.%, and 5wt.%).



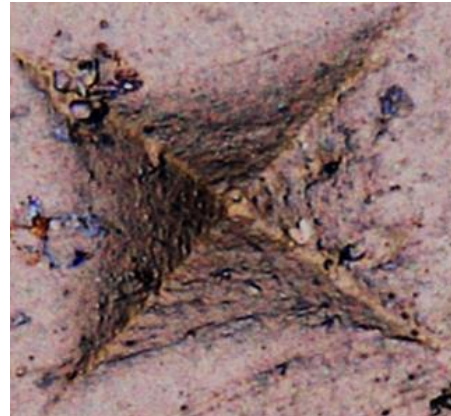
(a) NE



(b) 1wt.% CB



(c) 2wt.% CB



(d) 5wt.% CB

Figure III.14: Print Indentations of Vickers microhardness for CBs/DGEBA nanocomposite

Table III.5: Different micromechanical properties of reinforced DGEBA nanocomposite sample

			NE	CNT	GNPs	CB	
E(GPa)	0wt.%	Average	4.24	-	-	-	
		St dev	0.28	-	-	-	
	1wt.%	Average	-	5.19	4.80	4.34	
		St dev	-	0.53	0.37	0.32	
	2wt.%	Average	-	4.9	4.41	4.33	
		St dev	-	0.47	0.341	0.26	
	5wt.%	Average	-	4	4.93	4.82	
		St dev	-	0.59	0.51	0.59	
	Hv(Vickers)	0wt.%	Average	32.86	-	-	-
			St dev	4.33	-	-	-
1wt.%		Average	-	34.84	31.99	34.63	
		St dev	-	6.94	1.05	5.24	
2wt.%		Average	-	33.66	29.31	33.55	
		St dev	-	6.50	0.87	4.62	
5wt.%		Average	-	24.42	29	39.84	
		St dev	-	5.76	0.84	9.40	
S(mN/μm)		0wt.%	Average	285.38	-	-	-
			St dev	2.75	-	-	-
	1wt.%	Average	-	339.25	307.70	284.86	
		St dev	-	4.34	1.95	2.04	
	2wt.%	Average	-	332.22	303.20	288.52	
		St dev	-	4.72	1.08	2.77	
	5wt.%	Average	-	312.69	338.1138	295.13	
		St dev	-	13.15	1.96216081	4.50	
	D(μm)	0wt.%	Average	16.77	-	-	-
			St dev	0.19	-	-	-
1wt.%		Average	-	15.60	15.57	16.03	
		St dev	-	1.20	1	0.96	
2wt.%		Average	-	15.94	16.01	16.21	
		St dev	-	1.19	1.23	0.87	
5wt.%		Average	-	18.67	16.67	15.07	
		St dev	-	1.82	0.094	1.43	

III.3.4 Comparative analysis with different nanoparticles (CNTs/ GNPs /CBs) reinforced DGEBA adhesive

The degree of nanofiller dispersion, their alignment inside the adhesive resin, and the interfacial adhesion degree, which is critical for creating a reinforced composite, are all directly related to improved mechanical performance in adhesive polymer nanocomposites. Because these fractures depend on the nanoparticle type, it is critical to match the DGEBA adhesive with the appropriate nanoparticle. There is a difference in the findings between the different types of nanoparticles under different mass fractions, as shown in Figure III.15. The latter requires that the polymer adhesive's connection with the nanofillers is strong enough to enable load transmission to the nanoparticles, rather than developing two sliding surfaces [285].

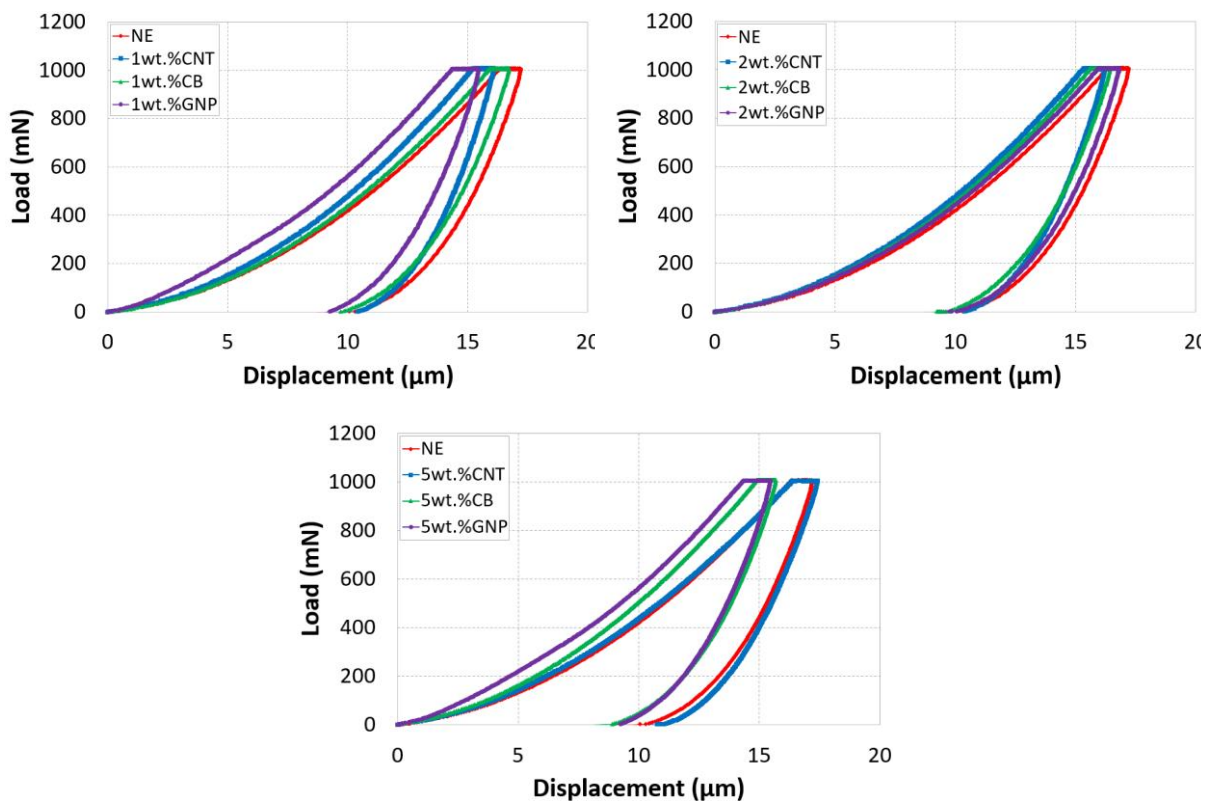


Figure III.15: Comparison of the load-displacement curve for reinforced DGEBA with nanofillers (CNT, GNP, CB) under different mass fraction

The rise was gradual up to a 1wt.% filler loading for both Young's modulus and filler loading, with the samples containing CNTs that showing the best results, Figure III.16. GNPs also had a greater elastic modulus than the neat adhesive. At the same time, CBs were only moderately improved compared to CNTs, given the dimensional scale dissimilarity of the domain for the two particles and due to their diverse shapes [286]–[289]. In general, raising the aspect ratio of the nanofillers increases the composite's elastic modulus [290].

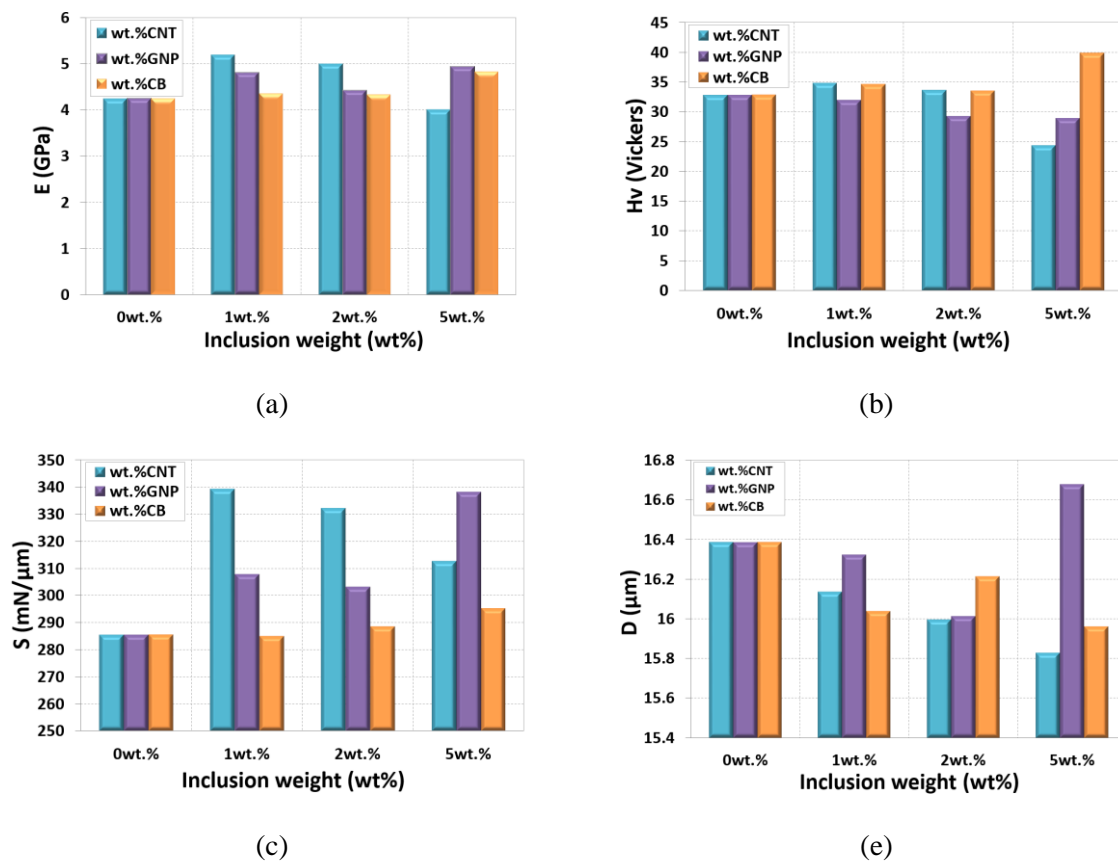


Figure III.16: Comparison of the different micromechanical properties for reinforced DGEBA with nanofillers (CNT, GNP, CB) under a different mass fraction

As previously stated by Pradhan et al. [291], the influence of the nanofiller's dimensionality (0D, 1D, 2D, and 3D), has a significant touch on tensile characteristics. They evaluated the reinforcing capacity of fillers with varied dimensionalities as follows: 0D > 1D filler > 2D filler > 3D filler. This is consistent with the improved results observed with CNTs, which have a

single dimension, compared to GNPs. Rigid nanofillers, as expected, increase nanocomposite rigidity, as seen by a steady increase in the adhesive nanocomposite elastic modulus. Figure III.15 and Figure III.16(a) show that CNTs outperform GNPs and CBs in terms of rigidity, where 1wt.% CNTs occupying the appropriate mass fraction with high rigidity values.

When comparing the hardness data, Figure III.16(b), it is evident that graphene causes fragility in the matching nanocomposite as well as a significant reduction in the reinforced adhesive nanocomposite hardness. The lack of a mechanical interlocking influence and the introduction of weaknesses into the polymer adhesive can be attributed to unfortunate dispersion of GNPs and weak interfacial adhesion with the resin matrix, which results in the non-appearance of a mechanical interlocking influence. This in turn leads to defects into the DGEBA adhesive that has an undesirable effect on the bulk mechanical properties. For CNTs, the increase was progressive up to a 1wt.% than a drop starts from 2wt.%. The usual effect of CBs is a small to moderate increase in hardness at low mass fractions, which disappears at higher mass fractions (5wt. % CBs).

The indentation depth of 1wt.% CNT-reinforced DGEBA adhesive nanocomposite samples was significantly lower than that of neat DGEBA adhesive, Figure III.16(e). The proportion of mass fraction affected the reduced indentation depth for the reinforced nanoparticles DGEBA adhesive nanocomposite. In comparison to CBs and GNPs, CNTs display the least amount of indentation. As a result, carbon nanotube additions can significantly improve the polymer nanocomposite's indentation resistance. As shown in Table III.6, the surface area of the Vickers indentation imprint varies from nanoparticle to nanoparticle and also depends on the mass fraction. It is evident that when comparing 1wt.% CNT-reinforced DGEBA adhesive nanocomposite to 2wt.% CNTs and 5wt.% CNTs, as well as GNPs and CBs, 1wt.% CNT-reinforced DGEBA adhesive nanocomposite has the least surface area.

Furthermore, when 1D nanoparticles [292], such as CNTs, are utilized as reinforcement for adhesive resin-dominated nanocomposites, essential increases in resistance have been observed. This is due to the extremely large contact area of 1D nanoparticles and the bridging mechanism, which prevents crack propagation and contributes to higher structural durability. At the same time, 0D fillers, such as the CBs used in this study, show improvement that is more minor, as compared to that of CNTs at low mass fractions but a significant decrease in indentation depth at high mass fractions, such as 5wt.%. This is not the case with 2D fillers like GNPs, which show decreased indentation depth at low mass fractions relative to neat DGEBA adhesive and a considerable increase at high mass fractions like 5wt.% GNPs. Owing to the high nanocomposite viscosity, a reduced filler dispersion degree, and increased risk of creating void weaknesses, the magnitude of development in mechanical characteristics may be inappropriate or even detrimental at more significant filler loadings [293]. This degradation with 2D nanoparticles may be caused by poor dispersion, resulting in a folded down and buckled morphology in the filler, contributing to the classification of graphene as one of the worst nanoparticles for use with DGEBA adhesive resin. Aside from the minor gain in mechanical performance that GNPs provide over CNTs, the orientation of the sheets formed by injection molding is most likely to blame. The optimal elastic modulus of the GNPs sheet is around 1 TPa, making it one of the most robust materials ever recorded, although it is not compatible with all adhesives. Due to the creation of a 2D-dimensional network, such conditions cause structural changes in the nanocomposite.

Table III.6: Indenter surface area of different reinforced DGEBA nanocomposite under a different mass fraction

		Indenter surface area	
NE	<i>0wt.%</i>	<i>Average</i>	30.55
		<i>ST.Dev</i>	0.29
CNTs	<i>1wt.% CNT</i>	<i>Average</i>	28.87
		<i>ST.Dev</i>	0.16
	<i>2wt.% CNT</i>	<i>Average</i>	29.81
		<i>ST.Dev</i>	0.16
<i>5wt.% CNT</i>	<i>Average</i>	41.15	
	<i>ST.Dev</i>	0.29	
GNPs	<i>1wt.% GNPS S</i>	<i>Average</i>	31.37
		<i>ST.Dev</i>	1.29
	<i>2wt.% GNPS S</i>	<i>Average</i>	34.25
		<i>ST.Dev</i>	2.00
	<i>5wt.% GNPS S</i>	<i>Average</i>	34.63
		<i>ST.Dev</i>	1.12
CBs	<i>1wt.% CB</i>	<i>Average</i>	29.02
		<i>ST.Dev</i>	0.19
	<i>2wt.% CB</i>	<i>Average</i>	29.92
		<i>ST.Dev</i>	0.31
	<i>5wt.% CB</i>	<i>Average</i>	25.19
		<i>ST.Dev</i>	0.07

III.4 Conclusion

For this chapter, the mechanical characterization of reinforced and unreinforced DGEBA adhesive resin was performed. Micro-indentation tests showed the differences in behavior depending on the type of nanoparticles and the mass fraction.

First, a comparative study of the glass transition temperature between the different nanoparticles' structures was carried out. The DSC study revealed a significant change in the glass transition temperature (T_g) between the different implementing nanoparticles. In this part, nanocomposites with 1wt.% CNT-reinforced DGEBA adhesive shows the highest T_g compared to GNPs and CBs.

Second, this chapter presents the analyses carried out on the different nanocomposites (DGEBA reinforced with (CNTs, GNPs, CBs)) to evaluate the different combinations' influence on the local mechanical properties of adhesive resin nanocomposites. The study of the dispersion manner of nanoparticles as carbon nanotube, graphene, carbon black in the DGEBA adhesive by micro indentation is presented. The elastic modulus, hardness, rigidity, and other mechanical properties of reinforced specimens showed a substantial rise with 1 wt.% CNTs, whereas there was a substantial difference with 1wt.% GNPs, but it was still less than 1wt.% CNTs. This revealed a variety of mechanical properties of which 1wt.% CNT-reinforcements DGEBA nanocomposite present the most preferential structure.

In summary, this study has found an improvement in the adhesive resin's thermal and local mechanical properties through the simple addition of the nanocharges under different mass fractions. Additionally, a lot of research has proven that the dispersion of the nanocharges is good at the core of the sample and remains less at the surface. Thus, local mechanical tests using micro indentation cannot reach the core of the sample, which is why it cannot be as functional to select the most appropriate nanoparticles as to extract the efficacious-reinforced adhesive nanocomposite. Also, this effect of the nanocharges of CNTs, GNPs, CBs on DGEBA adhesive is optimal up to a critical point, beyond which the dispersion is poorer, but the hardness increases.

Correspondingly identifying the progression of thermal and local mechanical properties is insufficient to diagnose the efficient adhesive structure and identify the most appropriate type of nanoparticles.

In the next chapter, we will examine the influence of nanoparticles under different mass fractions on quasi-static properties, and we will attempt to establish a link between the parameters identified and the physico-chemical properties measured during DSC and micro-indentation testing.

Chapter IV:

Quasi-static properties

IV. Quasi-static properties

Summary

IV. Quasi-static properties.....	159
IV.1 Introduction	160
IV.2 Tensile Test.....	160
IV.2.1 CNT-reinforced DGEBA adhesive nanocomposite	162
IV.2.2 GNP-reinforced DGEBA adhesive nanocomposite	165
IV.2.3 CB reinforced DGEBA adhesive nanocomposite	167
IV.2.4 Comparison analysis	169
IV.3 Compression test.....	172
IV.3.1 CNT reinforced DGEBA epoxy nanocomposite.....	174
IV.3.2 GNP reinforced DGEBA epoxy nanocomposite.....	178
IV.3.3 CB reinforced DGEBA epoxy nanocomposite	182
IV.3.4 Comparative analysis	185
IV.4 Conclusion.....	188

IV.1 Introduction

This chapter covers the investigational discoveries that focused on the impact of various nanoparticles on adhesive nanocomposites. Given that working on a nanoscale remains complex, specific methods use macroscopic characterizations to assess the quality of the interfaces within a nanocomposite. Therefore, produced adhesive nanocomposites, including varying quantities of CNTs, CBs, and GNPs, were examined under compressive and tensile loading regimes. The findings reveal that adding nanoparticles to adhesive has a significant impact on its behavior. For each case, at least three specimens were tested. Indeed, the quality of the interfaces between reinforcement and adhesive matrix determines the mechanical properties of composite materials, whether reinforced by micronic or nanometric fibers [294].

The mechanical characteristics of carbon nanoparticle-charged nanocomposites can only be improved by using an optimal mass fraction of nanoparticle/matrix interfaces to scatter the nanofillers appropriately. The type of nanoparticle utilized in the matrix has an impact on these criteria. However, if dispersion is poor, these properties may be lower than the polymer alone [295].

IV.2 Tensile Test

A unidirectional tensile test was used to study the tensile strength and tensile modulus of neat DGEBA adhesives (Figure IV.1) and reinforced DGEBA adhesive nanocomposites. In addition, tensile testing was used to assess the effect of nano-reinforcement on the mechanical characteristics of DGEBA adhesive nanocomposites reinforced with carbon nanotubes, Carbon Black, and graphene.

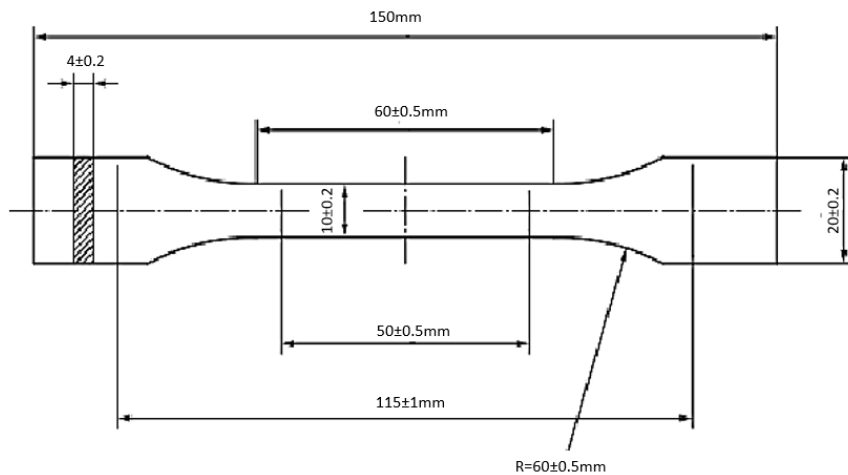
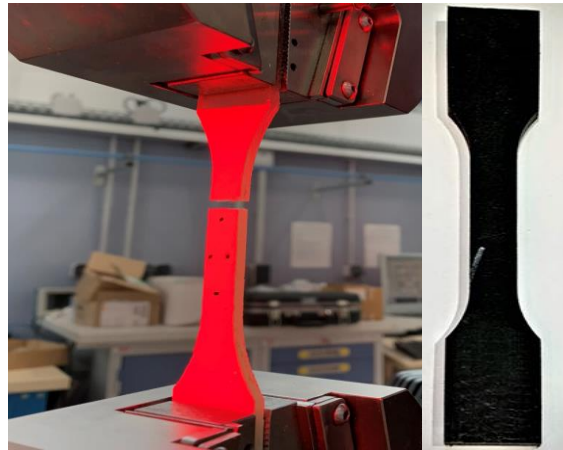


Figure IV.1: Dumbbell sample of neat DGEBA epoxy nanocomposite under tensile test

Before starting an experimental study for a quasi-static case, it is crucial to replicate the test. With this goal in mind, at least three tests need to be performed under the same velocity for each mass fraction to analyze the test reproducibility. As shown in Figure IV.2 , it should be noted that the tests are repeatable for the neat DGEBA adhesive, and each test controls a fact.

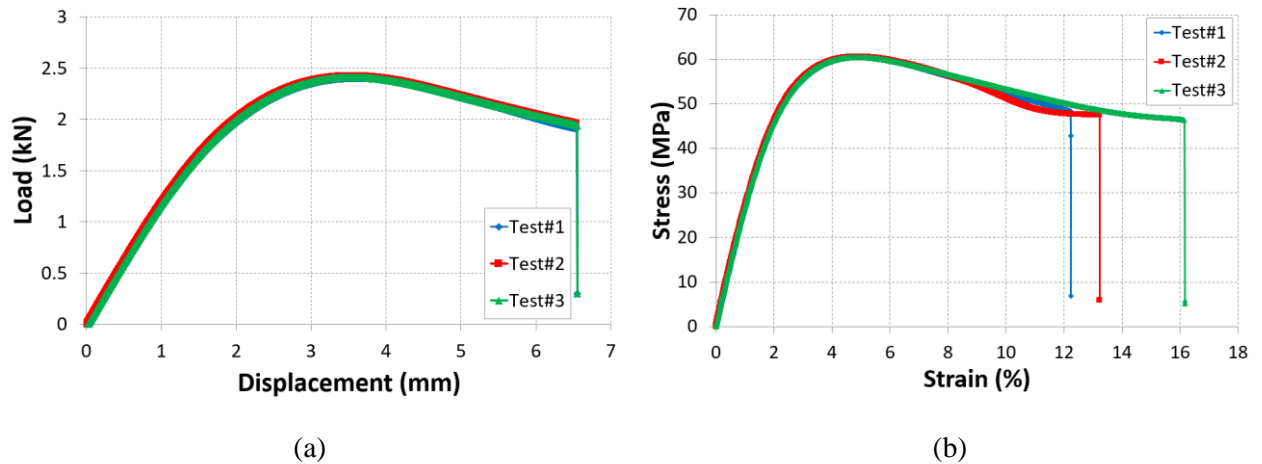


Figure IV.2: Test reproducibility of (a) the neat adhesive and (b) 1wt.% CB/DGEBA under tensile test

The neat and reinforced DGEBA adhesive nanocomposite tensile stress-strain curves are shown in Figure IV.3, IV.4, IV.5. The strain–stress curves of a representative nanocomposite structure at various levels of nanoparticle concentrations are illustrated, with the tensile modulus and strength calculated from these curves. Three samples of each type of adhesive nanocomposites are tested under the same conditions.

IV.2.1 CNT-reinforced DGEBA adhesive nanocomposite

The tensile strength and modulus obtained are not linear with the wt.% nanofillers, which could be attributed to the nanofillers' unstable orientation and agglomeration during charging on adhesive nanocomposites, Figure IV.3. Furthermore, as some research [296] has shown, CNTs improve internal strength by increasing crack propagation resistance via the bridging effect [297]. The tubular form of CNT also reveals that the nanocomposite is difficult to break and therefore has a high tensile strength [298].

The tensile modulus of the 1wt.% and 2wt.% CNT-filled epoxy nanocomposite is shown in Table IV.1 to be significantly higher than that of the neat DGEBA adhesive nanocomposite. In addition to this, the tensile strength of the 1wt.% CNTs demonstrates favorable effects on the reinforcement of DGEBA adhesive nanocomposites. Tensile strength increases when the CNT

loading is increased up to 1wt.% and decreases when the loading is continually increased to 2wt.% and 5wt.%. The negative effect of CNTs at 5wt.% concentrations was clarified by a heterogeneous dispersion above this critical filler content, a decline in ductility with increasing load, and a higher number of voids obtained during processing, which in turn leads to the formation of microcracks. These results were supported by certain research, such as that of Song et al. [299], who discovered that tensile strength was higher in the case of well-distributed CNTs, and that tensile strength dropped with the number of poorly scattered CNTs, as agglomerates operated as the initiator of cracks [300].

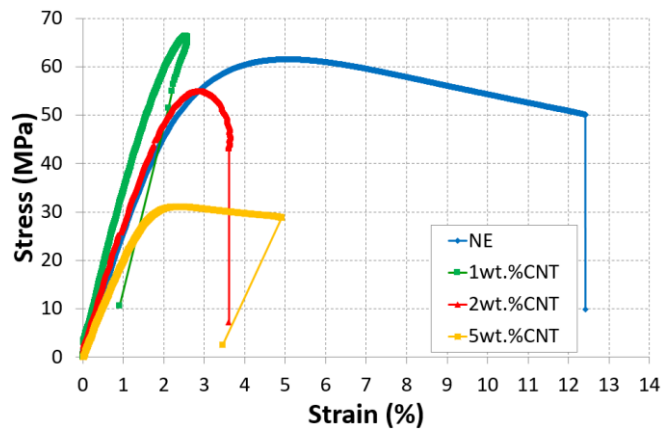


Figure IV.3: Stress-strain curves of carbon nanotube-reinforced composite under different wt.% for uniaxial tensile tests

Table IV.1: Evolution of the CNTs/adhesive nanocomposites mechanical properties

	E (GPa)	Coef Poisson	U max (mm)	F max (kN)	S max (MPa)	LE_Longi max (%)	LE_Trans max (%)
NE	24.82±1.17	0.40±0.01	6.88±0.5	2.41±2.4	61.59±0.11	12.41±0.001	-5.18±0.8
1wt.% CNT	36.08±5	0.45±0.12	2.80±0.7	2.59±0.02	66.32±0.9	2.60±0.16	-1.05±0.06
2wt.% CNT	29.62±2.8	0.35±0.14	3.14±0.22	2.18±0.06	54.95±0.5	4±0.7	-1.05±0.004
5wt.% CNT	21.26±0.8	0.23±0.02	2.94±0.02	1.22±0.02	30.69±0.78	4.95±0.07	-1.15±0.086

At low mass fractions, the effect size of the CNTs may cause smooth dispersion in the wet form and avoid agglomeration, as well as an attractive interfacial force between the components, resulting in improved strength of the nanocomposites. In comparison to changes in particle concentration, particle dispersion may be more meaningful. The observed values of tensile strength and tensile modulus for neat DGEBA adhesive resin and CNT-reinforced adhesive nanocomposites are obtained in the following order, according to the analysis results of Figure IV.3: neat DGEBA adhesive < 5wt.% CNTs/DGEBA < 2wt.% CNTs/DGEBA < 1wt.% CNTs/DGEBA. This order could be explained by the dispersion level at each mass fraction of CNTs, particularly 1wt.% CNTs beating 2wt.% CNTs and 5wt.% CNTs. As a result, particle dispersion significantly influenced the nanocomposite properties in the presence of a modest number of additives. The content component, on the other hand, was still a significant factor. The particle content was favorably connected with nanocomposite performance, according to tensile modulus and tensile strength data. The good dispersion could be one of the elements that leads to a more extensive contact area and more significant interaction between the CNTs and the adhesive matrix, as well as improved load transmission. As a result, the addition of a low mass fraction of CNTs is projected to improve the mechanical properties of the nanocomposites considerably.

In addition, the inclusion of 1wt.% and 2wt.% CNTs in the adhesive matrix cause brittle failure in specimen necking, but the addition of 5wt.% CNTs cause a ductile fracture in the nanocomposite structure. Thus, brittle materials are complicated and can't be hammered or stretched like ductile materials; therefore, they break instead. The primary distinction between ductile structures, such as neat DGEBA adhesive and 5wt.% CNTs/ DGEBA, and brittle structures, such as 1wt.% CNTs/ DGEBA and 2wt.% CNTs/ DGEBA is that ductile substances can be drawn out into thin wires, whereas brittle substances are hard but easily breakable. Thus,

there is also the problem at the process level that contributes to degrading the performance of the material at such a level of a mass fraction.

IV.2.2 GNP-reinforced DGEBA adhesive nanocomposite

The stress-strain curves for neat adhesive and GNPs/DGEBA adhesive nanocomposites are shown in Figure IV.4. As the filler concentration increases, the initial modulus is almost constant (very small improvement), as illustrated in Table IV.2.

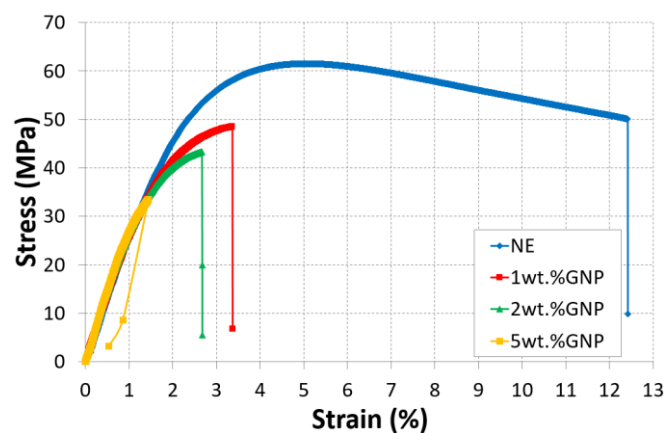


Figure IV.4: Stress-strain curves of Graphene reinforced adhesive nanocomposite under different wt.% for uniaxial tensile tests

Graphene nanoplatelets (GNPs) have been nominated as one of the most robust materials based on various studies [256], [272], [301]. In a platelet shape, graphene layers are layered together. GNPs have an ultrahigh aspect ratio (600–10000), which improves the contact area with the resin matrix and maximizes stress transmission from the polymer to the nanofillers [302].

However, the degree of compatibility between graphene nanoparticles and adhesive resin matrix influences the interaction. GNPs dispersion in the polymer adhesive matrix is especially difficult due to high Van der Waals forces and strong π - π contacts between platelets, which cause them to re-agglomerate even after dispersion [302] [303] [304].

According to the findings, tensile modulus and tensile strength are initially increased with the addition of GNPs in various increments. The main effect of each component on the tensile modulus is depicted in Table IV.2. GNPs raised the tensile modulus continuously. The enhancing impact of 1wt.% GNPs was optimum indicating a high tensile modulus. Improved tensile modulus of adhesive nanocomposite requires higher modulus, condition of dispersion, and aspect ratio of nanoparticles. Corcione et al. [305] found that adhesive resin reinforced with GNPs at 1, 2, and 5wt.% had a greater tensile modulus than neat adhesive. The appropriate dispersion of nanoparticles improves the tensile modulus of nanocomposite materials. The influence of graphene dispersion on the mechanical characteristics of graphene-reinforced adhesive nanocomposites was examined by Tang et al. [289]. High dispersion was found to cause higher strength and modulus than weak dispersion.

Table IV.2: Evolution of the GNPs/adhesive nanocomposites mechanical properties

	E (GPa)	Coef Poisson	U max (mm)	F max (kN)	S max (MPa)	LE_Longi max (%)	LE_Trans max (%)
NE	24.82±1.17	0.40±0.01	6.88±0.5	2.41±2.4	61.59±0.11	12.41±0.001	-5.18±0.8
1wt.% GNP	27.95±0.5	0.17±0.09	2.53±0.11	1.96±0.04	49.26±1.66	3.306±0.28	-0.99±0.06
2wt.% GNP	29.6±0.5	0.12±0.008	1.96±0.06	1.72±0.01	43.349±0.26	2.65±0.02	-0.79±0.07
5wt.% GNP	36.46±1.8	0.23±0.05	1.09±0.03	1.24±0.1	32.51±1.43	1.36±0.11	-0.39±0.001

Furthermore, as seen in Figure IV.4, adding GNPs reduces tensile strength, with the highest loss occurring in the 5wt.% GNPs. The reduction could be due to a weak interface between the graphene and adhesive resin matrix, which causes particle deboning. Additionally, the agglomeration of GNPs that occurs as the mass fraction increases produces stress concentration and influences tensile strength, which is why at 5wt.% GNPs, the tensile strength shows a

significant drop. Even though these GNPs/DGEBA nanocomposites grew stronger, the polymer resin matrix broke down before attaining their maximum yield strengths. This resulted in a reduction in plastic deformation capacity and energy absorbance, as well as a reduction in toughness. Some researchers have also reported decreased adhesives' tensile strength after adding GNPs [306] [307]. These tensile strength decreases with the addition of GNPs, indicating that there is no apparent interaction between GNPs and DGEBA. The enhancing impact of 1wt.% GNPs was optimal, as indicated in Figure 4, indicating high tensile strength.

Besides, Figure IV.4 shows the behavior of the elongation at break as a function of each variable. The elongation at break is sensitive to nanoparticle content. In comparison to neat DGEBA adhesive, the presence of GNPs in the adhesive matrix reduced the elongation at break, causing the GNP-reinforced DGEBA adhesive to become brittle.

When comparing neat adhesive to reinforced adhesive with a high number of GNPs, the elongation at break dropped dramatically. Adding a high mass fraction of GNPs to the system decrease rigidity and makes the adhesive more brittle, resulting in decreased elongation at break [308]. Zaman et al. [309] also showed a reduction in elongation at the break due to the inclusion of GNPs.

IV.2.3 CB reinforced DGEBA adhesive nanocomposite

The main effect of carbon black on tensile modulus and tensile strength is depicted in Figure IV.5. CBs nanofillers enhanced the tensile modulus continually up to 2wt.% CB confirmed by reference [310], as shown in Table IV.3.

Figure 5 shows the tensile strength of carbon black reinforced adhesive with various mass fractions. The relationship between the tensile modulus and the mass fraction of the carbon black reinforced adhesive resin matrix at various loading levels is shown in Table IV.3.

As the carbon black concentration rises, the small size of carbon black causes agglomeration, making it harder to disperse along adhesive, resulting in a poor interface between the microspherical and the adhesive resin matrix, lowering the tensile strength. Due to agglomeration in adhesive, the tensile modulus reaches a maximum value at 2wt.% and subsequently decreases as the weight fraction of carbon black increases to 5wt.% CB, resulting in a weak interface between particle and epoxy matrix.

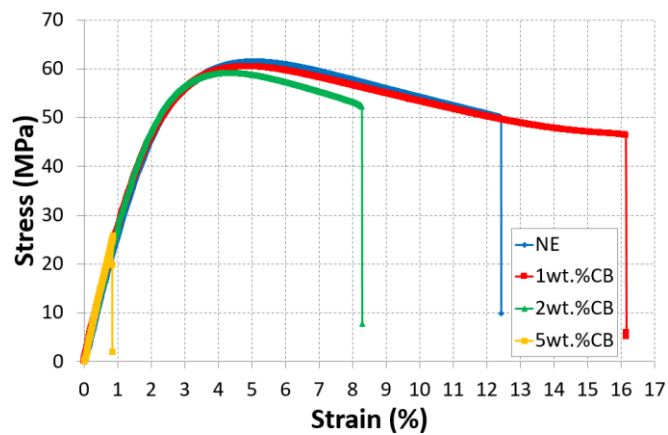


Figure IV.5: Stress-strain curves of carbon black reinforced adhesive nanocomposite under different wt.% for uniaxial tensile tests

Table IV.3: Evolution of the CBs/adhesive nanocomposites mechanical properties

	E (GPa)	Coef Poisson	U max (mm)	F max (kN)	S max (MPa)	LE_Longi max (%)	LE_Trans max (%)
NE	24.82±1.17	0.40±0.01	6.88±0.5	2.41±2.4	61.59±0.11	12.41±0.001	-5.18±0.8
1wt.% CB	28.23±0.72	0.24±0.02	6.66±0.04	2.41±0.009	60.46±0.07	12.73±0.69	-4.56±0.64
2wt.% CB	29.7±1.9	0.23±0.08	4.46±0.14	2.35±0.01	58.92±0.51	7.61±0.94	-3.03±0.004
5wt.% CB	27.76±2.38	0.33±0.1	0.75±0.08	1.01±0.1	25.64±2.38	0.92±0.09	-0.32±0.07

As seen in Figure IV.5, adding CBs reduces tensile strength, with the most considerable reduction occurring in the 5wt.% of CBs. The reduction could be due to a weak contact between the carbon black and adhesive matrix, which causes particle debonding.

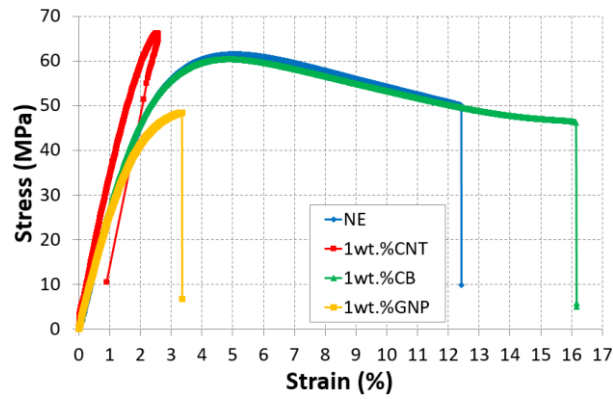
The association between the mass fraction of carbon black added to adhesive [21] and the elongation percentages obtained at a breakpoint is shown in Figure IV.5. Up to a filler content of 2wt.%, the elongation percentage at break does not reduce much but then drops sharply when the mass fraction of carbon black increases to 5wt.%. Compared to the elongation at break of neat adhesive, the results revealed that the most significant elongation percentage was a break. This is because nanoparticles cause deformation processes that contain matrix deformation and that nanoparticles do not increase the brittleness of the polymer matrix but rather maintain its ductility. The results are consistent with those of other studies [311], [312].

IV.2.4 Comparison analysis

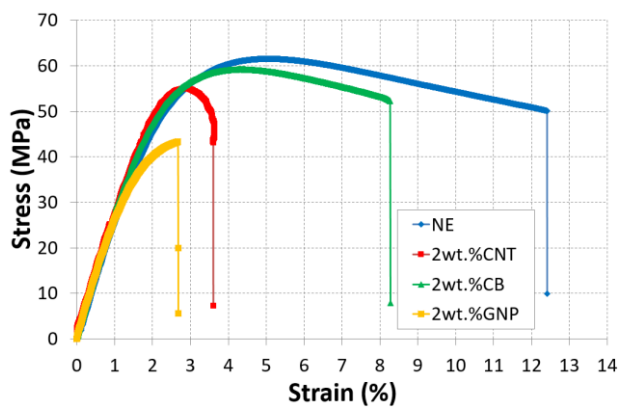
To produce and select high mechanical performance adhesives, graphene nanoplatelets, carbon nanotubes, and carbon black were selected to be nominated a-reinforcement.

The GNPs, CNTs, and CBs nanofillers impact DGEBA adhesive performance, as shown in Figures IV.6 and IV.7. At a low mass fraction of 1wt.% and 2wt.%, the most considerable improvement in tensile modulus was achieved by incorporating CNTs, followed by CBs then GNPs. Furthermore, CBs show the highest toughness and plasticity with the highest strength. Additionally, GNP-reinforced adhesive shows lower plasticity with lower strength compared to CNTs and CBs. However, as the filler loading was increased, the tensile modulus decreased sharply. As a result, CNTs exhibit a significant decline at high mass fractions and 5wt.% CBs provide the most sufficient reinforcement for better tensile modulus accompanied with plasticity degradation compared to CNTs and GNPs.

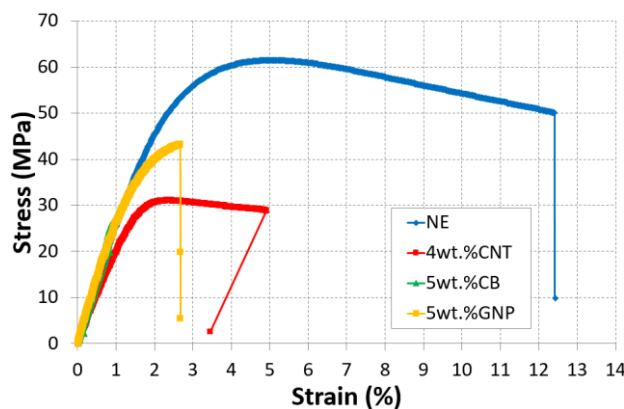
At the same time, compared to CNTs and GNPs, CBs exhibits high toughness and moderately high tensile modulus at low mass fractions of 1wt.%. Thus, in such a situation, 1wt.% CNT is chosen as the best option for improving the adhesive DGEBA tensile elasticity and strength.



(a)



(b)



(c)

Figure IV.6: Stress-strain comparison curves of different categories of reinforced adhesive nanocomposite under different wt.% for uniaxial tensile tests

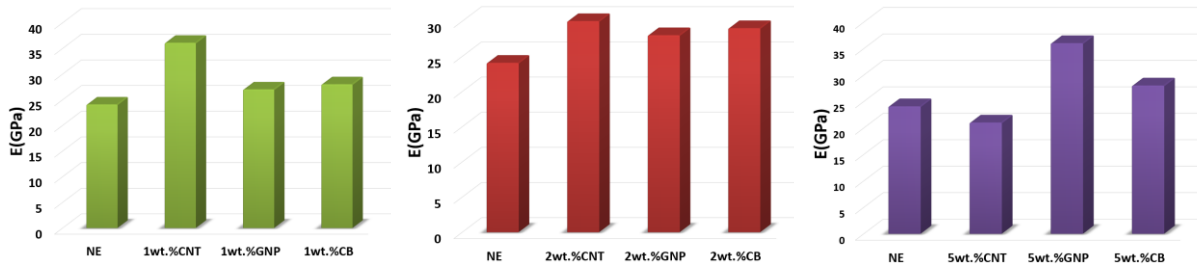


Figure IV.7: Diagram of Young modulus progress of different categories of reinforced adhesive under uniaxial tensile tests

As previously stated by Pradhan et al. [291], the impact of the nanofiller's dimensionality (0D, 1D, 2D, and 3D), and the aspect ratio, affect significantly the tensile characteristics. They evaluated the reinforcing capacity of fillers with varied dimensionalities as follows: 0D filler > 1D filler > 2D filler > 3D filler. This is consistent with the improved results observed with CNTs, which have a single dimension, compared to GNPs, which have two dimensions, and CBs, which have 0 dimensions, Figure IV.8. The quasi-static experimental results obtained in this paper are in agreement with the work of Pradhan et al. [291].

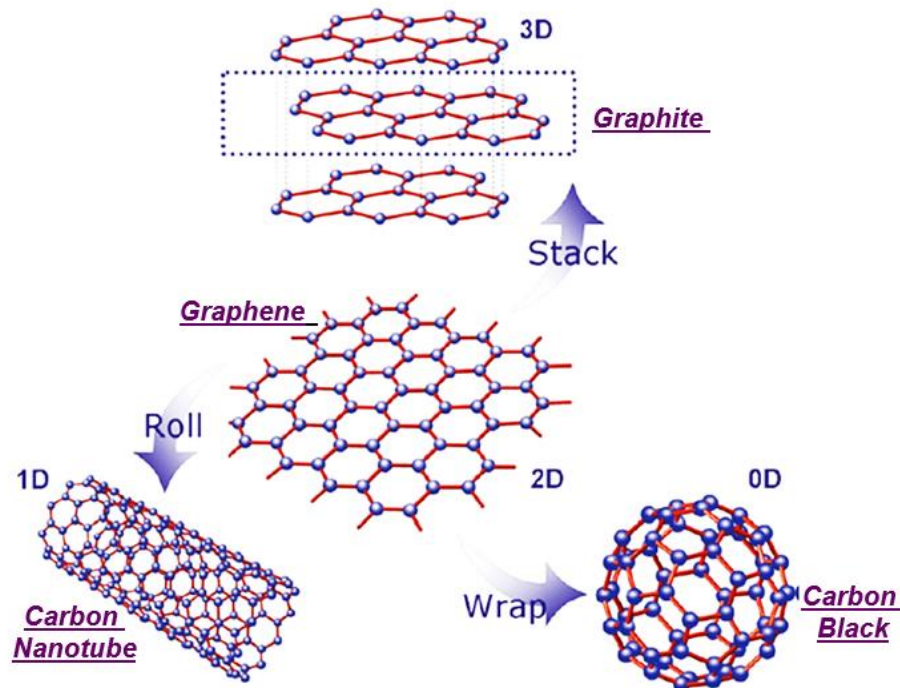


Figure IV.8: Carbon black, Carbon nanotube, Graphene, 0D, 1D, and 2D materials

IV.3 Compression test

Figure IV.9 shows typical stress-strain curves of cubic specimens loaded in static uniaxial compression. Before rupture, all specimens exhibit elastic (region A) and plastic (area B) behavior, as seen by the stress-strain curve [313]. The stress rises linearly in proportion to the strain at first until it approaches an elastic limit (point C). As the load exceeds the proportional limit, the strain increases more rapidly with each increase in stress until it hits yield stress (point D), at which the material deforms without an increase in applied force. After yielding, the shortening increases as the applied load decreases, a process known as plastic strain softening (area E), until the curve reaches a plateau (shortening with no significant increase in compressive stress; (region F). The cross-sectional area of the material increases when it undergoes considerable softening stress, resulting in enhanced resistance to further deformation. As a result, after region F, continued shortening necessitates an increase in compressive load (known as the plastic hardening mechanism) until it achieves maximum load (region G), at which point the material ruptures (known as ultimate stress, point H).

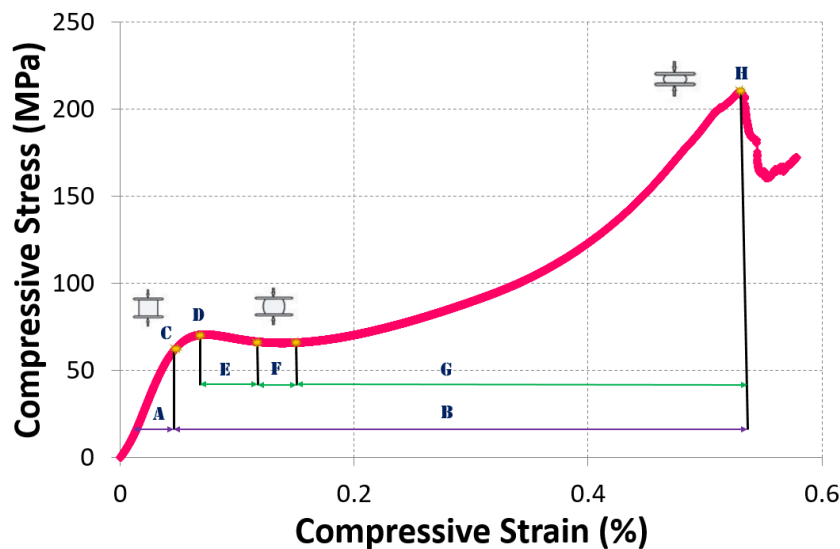


Figure IV.9: Stress-strain curves of neat DGEBA epoxy nanocomposite for uniaxial compressive

Before starting an experimental study for a quasi-static case, it is indispensable to ensure that the test can be replicated. With this goal in mind, at least three tests need to be performed under the same velocity for each mass fraction to analyze the test reproducibility. As shown in Figure IV.10, the tests are repeatable for the neat DGEBA adhesive, and each test checks a fact.

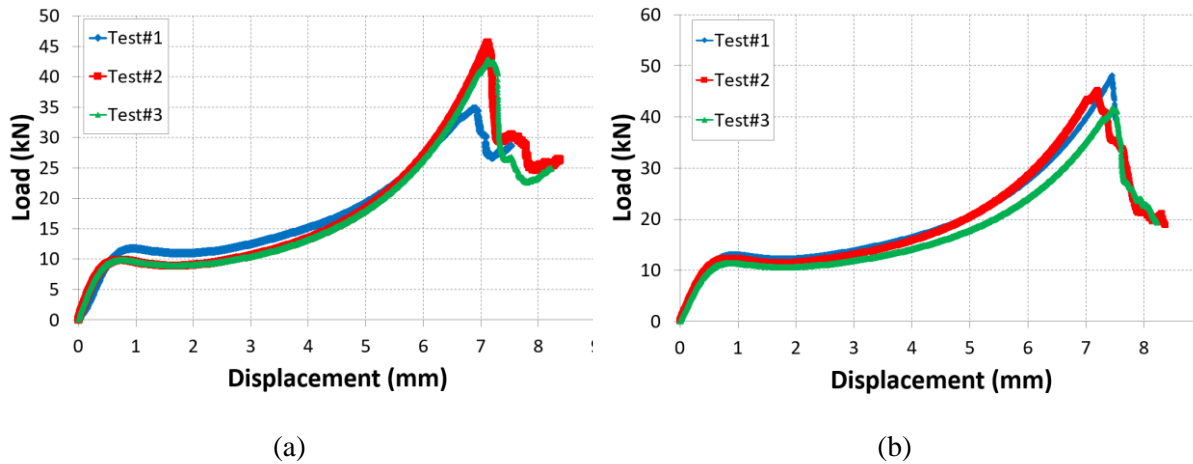


Figure IV.10: Test reproducibility of (a) the neat adhesive and (b) 1wt.% CBs/DGEBA adhesive under compressive test

When comparing compressive yield strength to tensile strength for the corresponding modified adhesive systems, it is clear that compressive yield strength is substantially higher than the tensile strength, although compressive modulus is lower. Fracture failure in tensile specimens could be the cause. In addition, bubbles and aggregations will cause stress concentration in adhesive matrix resins.

To determine the morphology of the neat DGEBA adhesive samples, Figure IV.11 shows the higher magnified SEM images with neat DGEBA adhesive, and ribbons and river lines were presented. However, with surface photographic images in Figure IV.12 of neat DGEBA adhesive after compression, it is clear the degradation of the behavioral state where it presents the failures and sample crack.

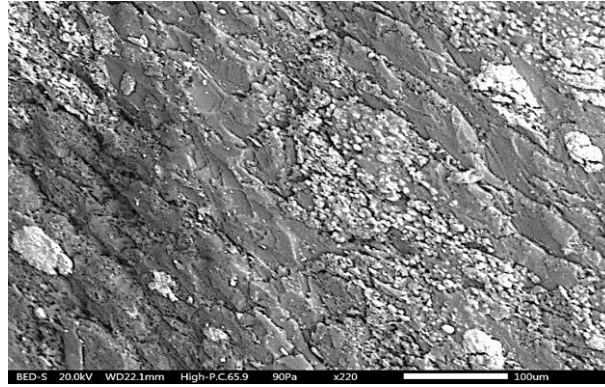


Figure IV.11: SEM images of neat DGEBA epoxy nanocomposite



Figure IV.12: Surface Photographic images of neat DGEBA epoxy nanocomposite after compression

IV.3.1 CNT reinforced DGEBA epoxy nanocomposite

The influence of carbon nanotubes on the compressive stress-strain behavior of DGEBA adhesive is shown in Figure IV.13. By increasing the filler content in the adhesive nanocomposite, the compressive modulus was investigated. The CNTs increased the adhesive's compressive modulus, as seen by a steeper slope in the elastic area of the stress-strain curve. The compressive modulus of a composite was shown to increase as the filler content was increased, Table IV.4. The reinforcing impact of the carbon nanoparticles and nanoparticle-adhesive interaction forces in nanocomposite leads to increased compressive modulus with carbon nanotube mass fraction.

Moreover, there was a notable effect on the compressive yield strength and failure strain. The addition of the rigid carbon nanotube boosts the compressive yield strength of the matrix at low mass fractions, as can be seen from the compressive characteristics of the DGEBA adhesive. However, at 5wt.% CNTs, there was also a decrease in compressive strength. This demonstrates that under compression at large mass fractions, the intercalated structure of CNTs causes high-localized stresses in the matrix. Thus, the capacity to transfer load and plastic deformation is limited by poor nanoparticle-matrix contact. Furthermore, the drop in compressive stress at 5wt.% could be attributed to increased aggregation, which could in turn cause nanocomposites to break prematurely.

Figure IV.13 demonstrates that Carbon nanotubes affect ductility and allowed for increased plastic hardening behavior when the adhesive was yielded. Whereas at 5wt.% CNTs, the mechanical behavior is essentially plastic; the elastic phase is significantly reduced. This behavior shows that rigid nanoparticles introduce additional energy absorption mechanisms during the applied loading. As a result, deformation resistance is enhanced, resulting in higher compressive stress and plastic hardening. Consequently, the addition of CNTs improved the material's compressive strain behavior; nonetheless, even under severe strain, the CNT-reinforced nanocomposite material did not attain fracture or maximum fracture strength until the maximum load was reached. The increase in the area under the stress-strain curve suggests that the nano-reinforced adhesive network has improved fracture toughness.

Figure IV.14 depicts the structural behavior of carbon nanotube reinforced DGEBA adhesive nanocomposite after compression with different mass fractions. It demonstrates the difference in fracture intensity at various mass fractions; 5wt.% CNTs exhibit the most significant structural damage when compared to 1wt.% CNTs. As displayed in Figure IV.14, the crack severity increases as the mass fraction increases, becoming extremely serious.

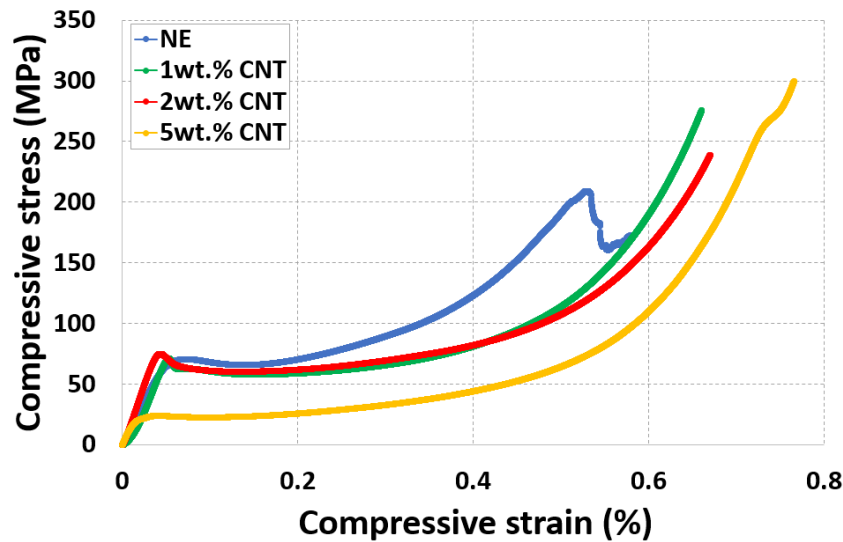


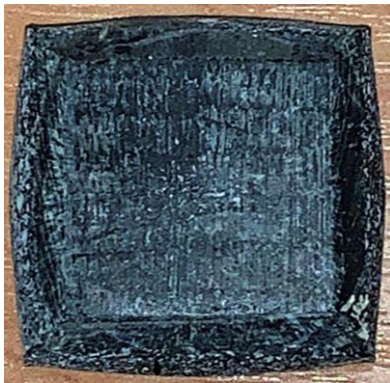
Figure IV.13: Stress-strain curves of carbon nanotube-reinforced composite under different wt.% for uniaxial compressive tests

Table IV.4: Evolution of the CNTs/ Adhesive nanocomposites mechanical properties

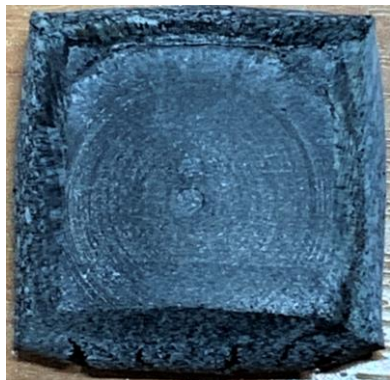
	Young Modulus (GPa)	LE_Longi max (%)	Elastic limit C (MPa)	Yield stress D (MPa)	H (MPa)
NE	1017±20	0.57±0.03	56.36±0.5	70±1	209.18±1.2
1 wt.% CNT	591±50	0.66±0.03	62.18±0.1	71.32±0.3	-
2 wt.% CNT	1455±100	0.65±0.03	65.10±2	75.077±0.5	-
5 wt.% CNT	1630±125	0.68±0.04	13.80±0.6	23.02±1	-

To determine the morphology of the created nanocomposite samples, Figure IV.15 show the difference in higher magnified SEM images. In pure adhesive, there are only ribbons and river lines, shown in Figure IV.11. However, for the nanocomposite-reinforced with carbon nanotubes, Figure IV.15, numerous fractured areas show severe roughness, and this behavior was observed irrespective of the CNT concentration. Thus, through increasing CNT mass fraction, the structure morphology changes with the increase of voids and such

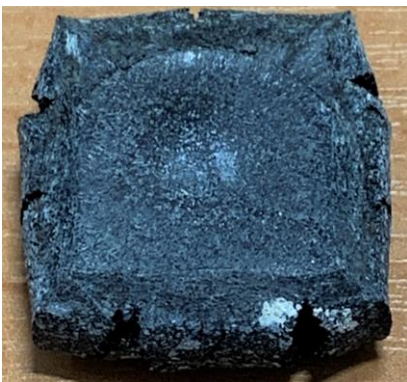
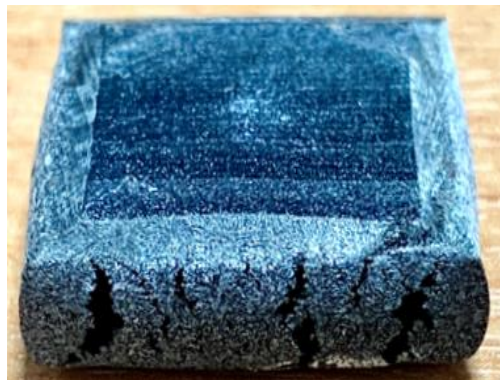
agglomerations, which is evident in Figure IV.15c and IV.15d that with 5wt.% CNTs a lot of porosity presented owing to the nanocomposite structure. The morphology of fractured surfaces of the nanocomposites implies that carbon nanotubes effectively obstructed fast crack growth and increased the fracture toughness compared to neat DGEBA adhesive. The fracture energy was dependent on the creation of a new fracture surface, as shown by the formation of the severely distorted surface.



1wt.% CNT/DGEBA



2wt.% CNT/DGEBA



5wt.% CNT/DGEBA



Figure IV.14: Surface Photographic images of CNTs/DGEBA epoxy nanocomposite with different wt.% after compression

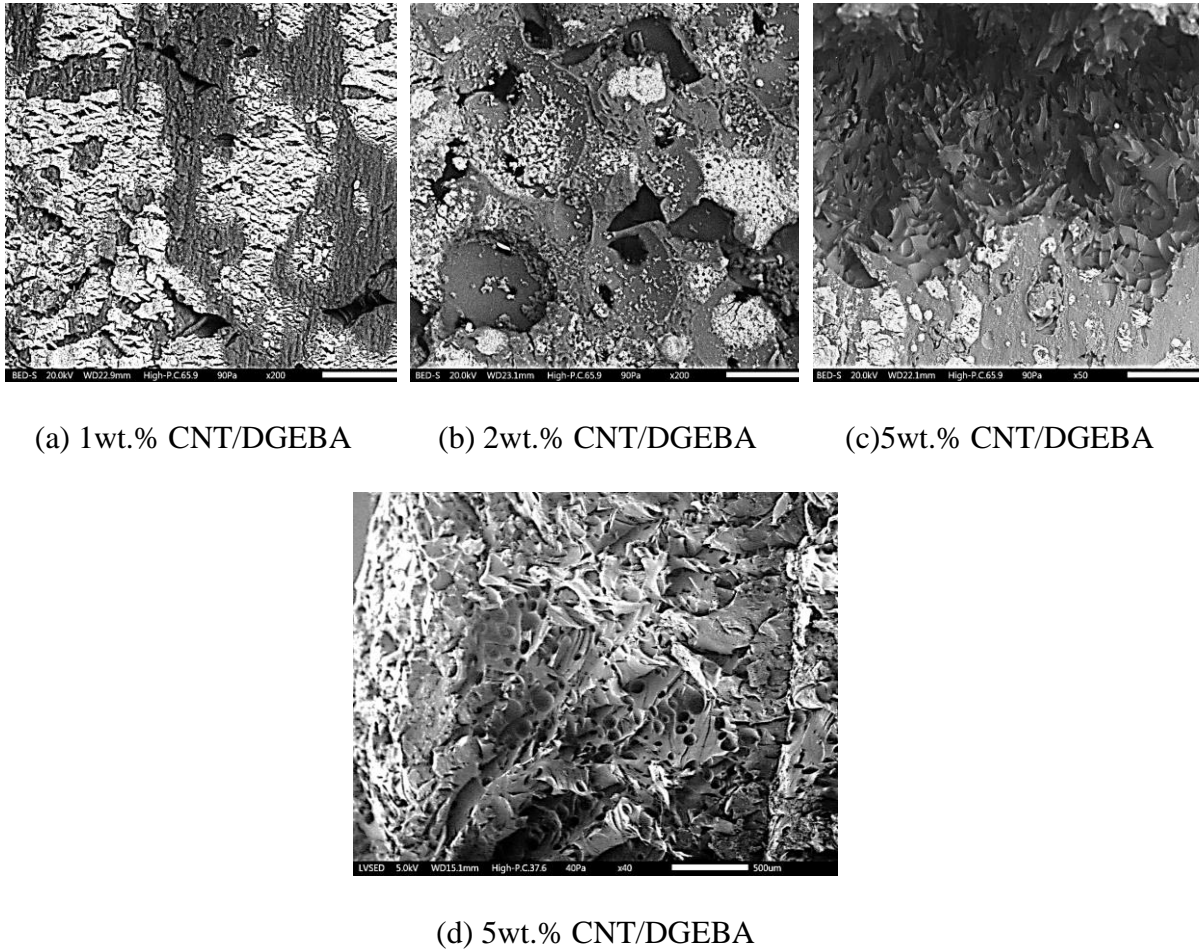


Figure IV.15: SEM images of CNTs/DGEBA adhesive nanocomposite

IV.3.2 GNP reinforced DGEBA epoxy nanocomposite

The effect of Graphene in DGEBA adhesive on compressive Stress-Strain behavior is seen in Figure IV.16. By increasing the graphene nanoplatelet content in the composite, the compressive modulus was investigated. In Table IV.5, the GNPs increased the adhesive's compressive modulus, as evidenced by a steeper slope in the elastic area of the stress-strain curve up to 2wt.%, compared to a drop at a high mass fraction of 5wt.% GNPs. Although compressive modulus degrades at high mass fractions, even with degradation, GNP-reinforced

DGEBA adhesive nanocomposite still has a high compressive modulus compared to neat DGEBA adhesive.

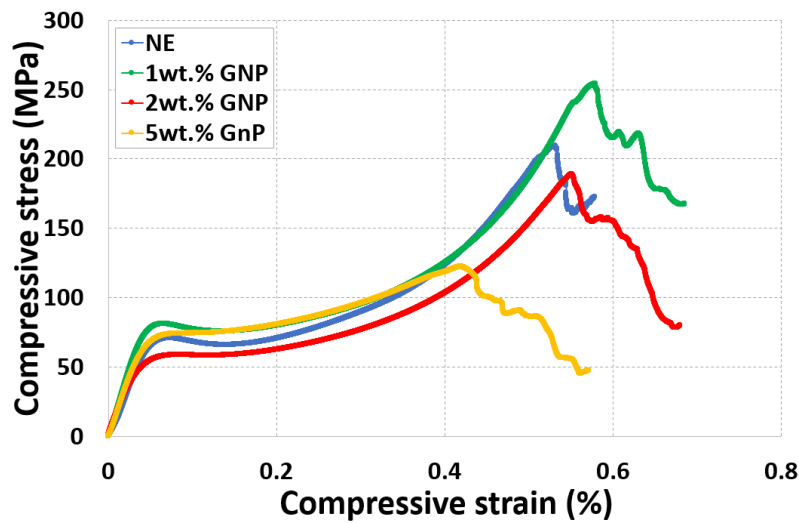


Figure IV.16: Stress-strain curves of Graphene reinforced composite under different wt.% for uniaxial compressive tests

Furthermore, there was a positive influence on compressive yield strength and failure strain. Compared to neat DGEBA adhesive, using graphene boosts the compressive yield strength of the matrix at low mass fractions up to 1wt.% GNPs, accompanied by the maximum failure strain. However, when the mass fraction is increased up to 5wt.% GNP, the failure strain decreases dramatically when compared to neat DGEBA adhesive. Figure IV.16 shows the intense degradation of the reinforced nanocomposite structure with 5wt.% GNPs. The 1wt.% GNPs enhancement effect was excellent, demonstrating the robust compressive behavior of reinforced DGEBA adhesive nanocomposite.

Figure IV.17 shows the structural response of graphene reinforced DGEBA adhesive nanocomposite after compression at different mass fractions. It emphasizes a significant degree of structure degradation where even with low mass fraction, the GNPs/DGEBA present severe crack. The severity of the crack grows as the mass fraction increases, as shown in Figure IV.18. With 5wt.% GNPs having the most damaged structure when compared to 1wt.% GNPs.

Table IV.5: Evolution of the GNPs/ Adhesive nanocomposites mechanical properties

	Young Modulus (GPa)	LE_Longi max (%)	elastic limit C (MPa)	yield stress D (MPa)	H (MPa)
NE	1017±20	0.57±0.03	56.36±0.5	70±1	209.18±1.2
1 wt.% GNP	1446±130	0.66±0.01	66.19±0.2	80.153±0.5	254.09±2
2 wt.% GNP	1759±48	0.65±0.02	49.39±1.2	57.79±2	188.47±0.5
5 wt.% GNP	1470±10	0.58±0.01	63.78±0.2	73.23±0.4	122.27±2



1wt.% GNP/DGEBA



2wt.% GNP/DGEBA



5wt.% GNP/DGEBA

Figure IV.17: Surface photographs of GNP/DGEBA epoxy nanocomposite with different wt.% after compression

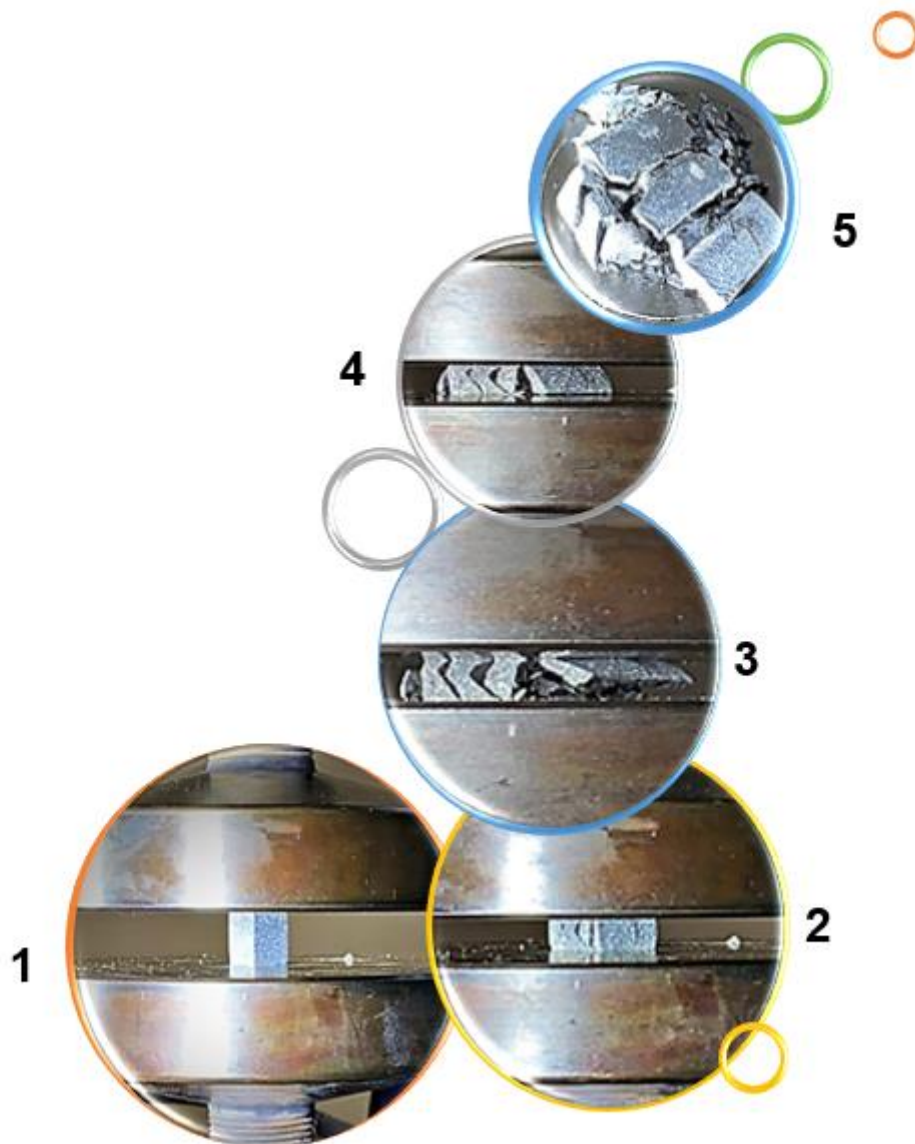


Figure IV.18: Photographs of GNP reinforced DGEBA adhesive nanocomposite samples (5wt.% GNP loading) before and after the compressive tests

IV.3.3 CB reinforced DGEBA epoxy nanocomposite

Figure IV.19 depicts the influence of Carbon Black on the compressive stress of a DGEBA adhesive resin at various loading levels. The compressive modulus of CBs increased with increasing mass fraction, as demonstrated by a steeper slope in the elastic area of the stress-strain curve, Table IV.6. The maximum value of compression strength was found with 1wt.%

CBs and 2wt.% CBs, which appear to be almost identical to the compression strength of neat DGEBA adhesive.

This can be attributed to nanoparticles' reinforcing abilities and highly-attached filler. Furthermore, when the filler content exceeds 5wt.%, the compression strength of the nanocomposite steadily decreases. This suggests that, with increased filler quantities, there was a decreased degree of nanoparticle-polymer interaction [314]. This conclusion is consistent with Lin's study [315].

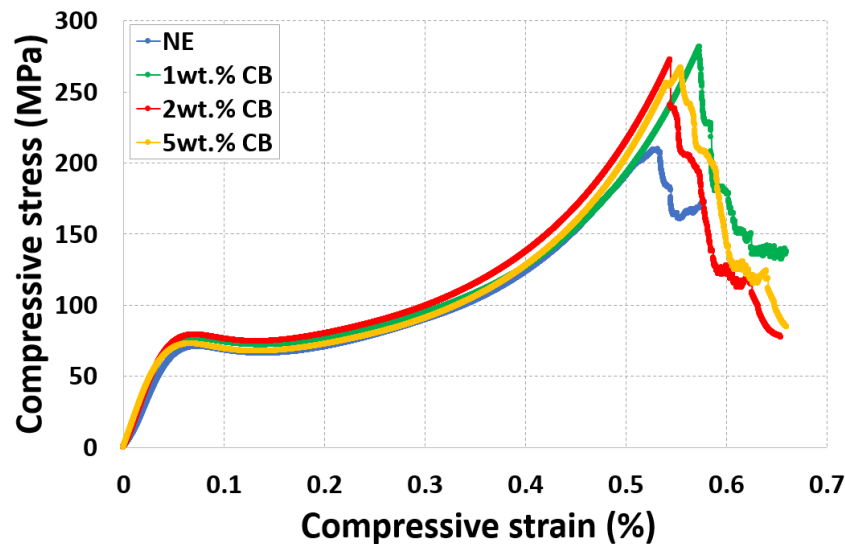


Figure IV.19: Stress-strain curves of Carbon Black-reinforced adhesive nanocomposite under different wt.% for uniaxial compressive tests

Aside from the CBs, the nanofiller increased ductility and enabled more plastic hardening behavior once the adhesive yielded. Compared to neat adhesive, high strain failure increases when CBs is added, with 1wt.% showing the highest values. This response shows that the stiff CB nanoparticles introduce additional energy-absorption mechanisms under the applied loading. As a result, deformation resistance is enhanced, resulting in higher compressive stress and plastic hardening. The increased area under the stress-strain curve implies that the nano-reinforced adhesive network has improved fracture toughness [313].

To determine the morphology of the created nanocomposite samples, Figure IV.20 shows the Surface photographs of CB/DGEBA adhesive nanocomposite with different wt.% after compression. Nanocomposite-reinforced with carbon black shows drastic fracture and this behavior was observed irrespective of the CBs concentration. Thus, with increasing CBs mass fraction, the structure morphology changes with the increase of voids and CBs agglomeration, where it is clear in Figure IV.21 that with 5wt.% CBs a change in the viscosity was observed, owing to the nanocomposite structure. The morphology of fracture surfaces of the nanocomposites implies that the Carbon Black effectively obstructed fast yet slight growth, as compared to the neat adhesive.

Table IV.6: Evolution of the CBs/Adhesive nanocomposite mechanical properties

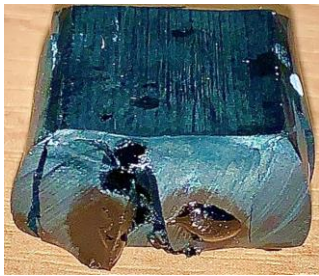
	Young Modulus (GPa)	LE_Longi max (%)	Elastic limit C (MPa)	Yield stress D (MPa)	H (MPa)
NE	1017±20	0.57±0.03	56.36±0.5	70±1	209.18±1.2
1 wt.% CB	1731±30	0.66±0.01	59.97±0.01	76.21±0.05	281.17±0.5
2 wt.% CB	1979±	0.65±0.03	63.80±0.01	78.54±0.5	272.11±0.5
5 wt.% CB	1946±30	0.66±0.06	53.39±0.02	72.70±0.5	266.48±0.6



(a) 1wt.% CB/DGEBA



(b) 2wt.% CB/DGEBA



(c) 5wt.% CB/DGEBA

Figure IV.20: Surface photographs of CB/DGEBA adhesive nanocomposite with different wt.% after compression

IV.3.4 Comparative analysis

In terms of choosing the appropriate nanoparticles that may increase compressive mechanical behavior, graphene platelets, carbon nanotubes, and Carbon Black were selected and filled with adhesive resins.

Changing nanoparticle categories has a clear impact on mechanical behavior progression, as shown in Figures IV.21 and IV.22. Thus, incorporating Carbon Black CBs at a low mass fraction and high mass fraction improves compressive modulus. However, it results in the highest strain failure with high toughness at a low mass fraction, and at a high mass fraction, it faces a degradation in toughness.

At the same time, CBs/DGEBA shows an intensity fracture accompanied with poor plasticity that could play a dangerous factor, as shown in Figure IV.22, which degrades the huge structure in several areas. Then, in the second position, Figure IV.21 and IV.23 confirm that CNTs demonstrate significant plastic behavior and a high compressive resistance, as well as moderately affected damages when compared to GNPs and CBs. Thus, DGEBA adhesive reinforced with CNTs shows an almost smooth edge after compressive loading, confirming its high plasticity. However, adhesive reinforced with GNPs and CBs showed severe edge explosion, which confirms that they have less plasticity. Figure IV.23 confirms the significant toughness with the undefined area under the curve.

In such instances, 1wt.% CBs is chosen as a good option for improving adhesive DGEBA elastic performance, followed by 1wt.% CNTs that enhance the DGEBA strength and plasticity.

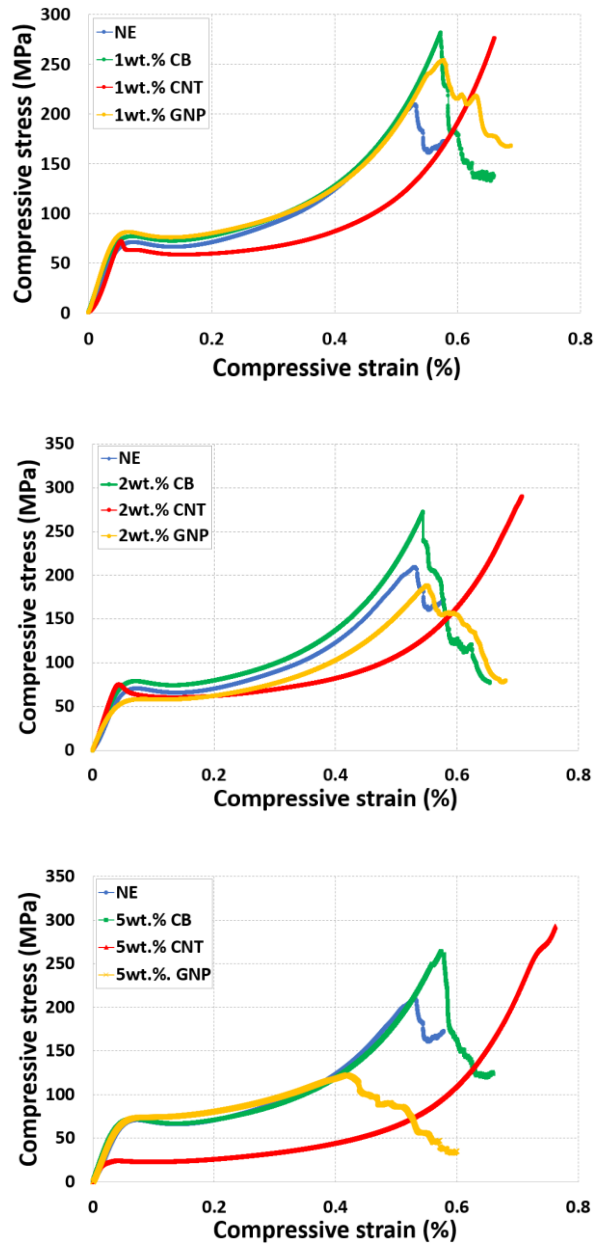


Figure IV.21: Stress-strain comparison curves of different categories of reinforced adhesive nanocomposite under different wt.% for uniaxial compressive tests

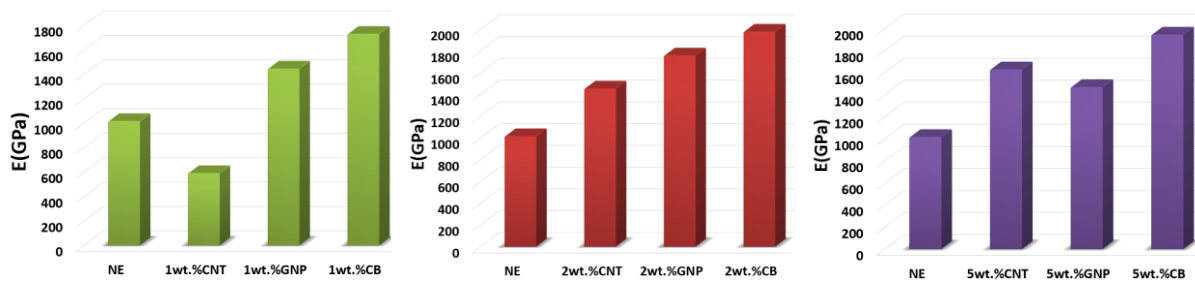


Figure IV.22: Diagram of Young modulus progress of different categories of reinforced adhesive under uniaxial compressive tests

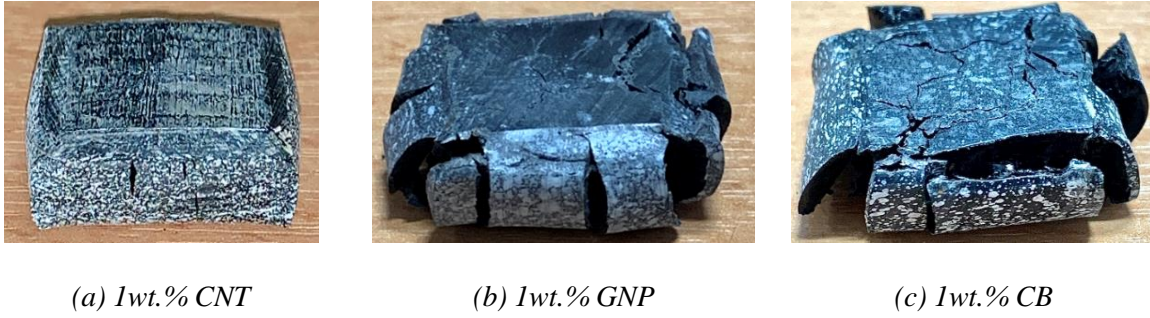


Figure IV.23: Deformation and failure progress of different 1wt.% (CNT/GNP/CB) reinforced adhesive under compressive test

IV.4 Conclusion

Under tensile and compressive loading conditions, the influence of several categories of nanoparticle-reinforced adhesive nanocomposites with different contents was examined. The neat DGEBA adhesive and CNT/CB/GNP-reinforced DGEBA nanocomposite displayed tensile yield strength, tensile modulus, compressive tensile, compressive strain failure, and compressive yield strength. For low mass fractions, this behavior yields positive outcomes. Given the strong interfacial contacts, these results showed the presence of a good stress transfer to the polymer-nanoparticle interface. The appropriate transfer is also determined by the type of nanoparticles, their shape, and their dispersion level. However, at high mass fractions, the formation of clusters resulted in stress concentration, which degraded the mechanical behavior of the nanocomposite.

Furthermore, when compared to GNPs and CBs under tensile circumstances, it was revealed that 1wt.% CNT is the best-suited nanoparticle for enhancing DGEBA. Furthermore, 1wt.% CBs were found to be compatible nanoparticles with DGEBA adhesive under compressive test. However, this does not negate the fact that the efficient role that 1% CNT takes where it improved the mechanical structure of DGEBA adhesive, resulting in higher toughness-reinforced nanocomposite structure and higher plasticity compared to neat adhesive.

The quasi-static results showed different behavior changes between neat DGEBA adhesives and reinforced adhesives, whereby each nanoparticle has its own influence on the mechanical behavior. The diversity of the responses obtained justifies the relevance of the study on reinforced adhesives in quasi-static conditions. A comparison of the results of the dynamic testing was then carried out using the Split Hopkinson Pressure Bar (SHPB). The objective is to verify whether these tests allow for the identification of a similar mechanical behavior progression for the reinforced adhesive studied with the different type of nanoparticles.

Chapter V:

Dynamic behavior of adhesive doped

with nanofillers

V. Dynamic behavior of adhesive doped with nanofillers

Summary

V. Dynamic behavior of adhesive doped with nanofillers.....	191
V.1 Introduction	192
V.2 Overview	192
V.3 Influence of nanofillers CNTs, CBs, GNPs on the dynamic velocity of nanocomposites based DGEBA adhesive	195
V.4 Effects of CNTs, GNPs, CBs on DGEBA adhesive Nanocomposites' Dynamic Behavior.....	198
V.4.1 Strain rate sensitivity	199
V.4.2 Stress-strain Behavior	204
V.4.3 Comparison analysis	212
V.5 Conclusion.....	227

V.1 Introduction

Even DGEBA adhesives have good dynamic strength due to their unique internal structure; they are now being improved through the addition of nanoparticles to enlarge their dynamic applications. Carbon Black (CB), carbon nanotubes (CNT), and graphene nanoplatelets (GNP) are integrated into DGEBA adhesive nanocomposites.

This chapter aims to investigate the effect of different percentages of CNTs, GNPs, and CBs in the DGEBA adhesive on its dynamic performance and energy absorption. An experimental study was carried out to study this behavior of the nanocomposite adhesives based on CNTs/DGEBA, GNPs/DGEBA, CBs/DGEBA under dynamic load, using the SHPB device. Samples were taken with mass fractions of 1wt.% and 2wt.%, and 5wt.% and the sample with neat DGEBA adhesive was considered to be a benchmark. Furthermore, these dynamic compression tests were performed at three different impact pressures, namely 1.5, 2 and 4 bar, in order to study the mechanical behavior progress and the energy absorption capacity evolution of these nanocomposites in greater detail.

V.2 Overview

The findings of dynamic loading testing and mechanical behavior modeling of the several materials tested CNTs/DGEBA, GNPs/DGEBA, CBs/DGEBA adhesive nanocomposite are presented in this chapter. A wide variety of impact pressure is used for each nanocomposite (1bar, 2bar, 4bar). The bar theory was confirmed by the dimensions of the samples, which were 13×13×13mm. Figure V.1 confirms that these dimensions are within the standard range, with a smooth and stable progression of strain rate vs strain curve.

The effect of the impact pressure, as well as the effects of nanofiller types and mass fraction on the mechanical behavior and the damaged kinetics of the reinforced nanocomposite

structure, are of particular interest to us, and are mentioned in several research studies [243], [267][244], [254], [301], [316], [317].

The results of the dynamic response of adhesive nanocomposites doped with different types of nanofillers will be presented in the first part of this chapter, followed by an analysis of the damage mechanisms of the tested specimens (post-impact) by optical microscopy using the SEM. The results will be analyzed in the second phase for a comparative examination of the various materials.

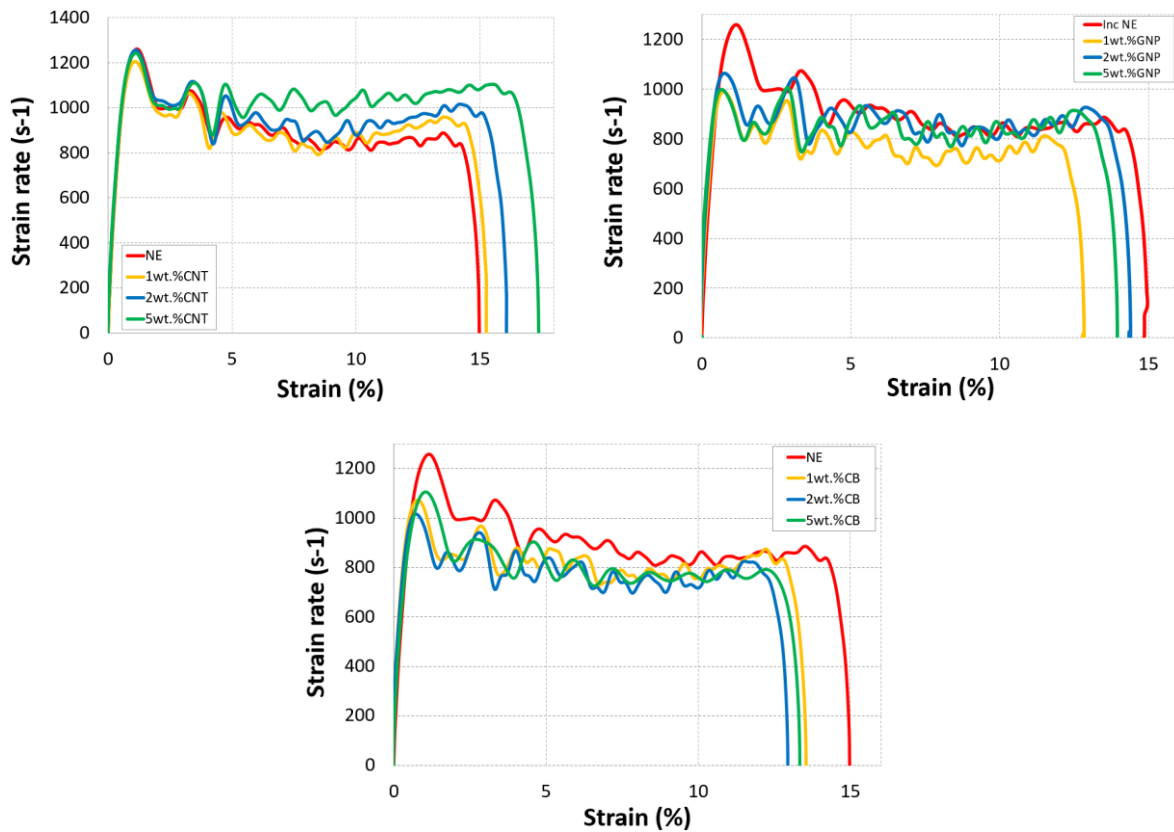


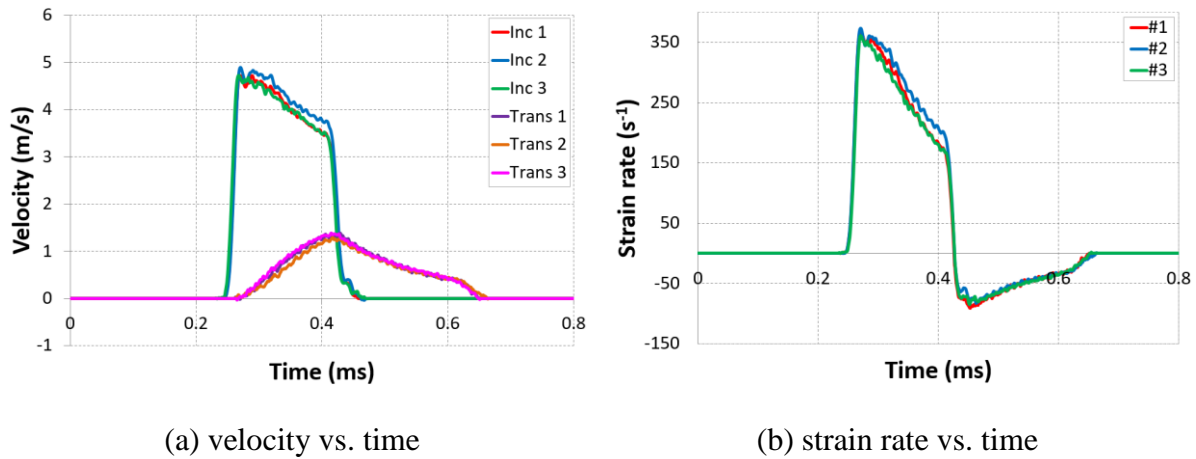
Figure V.1: Strain Rate vs. Strain of CNTs/DGEBA, GNPs/DGEBA, CBs/DGEBA under 4 bar impact pressure

In this context, we investigated the effect of nanofillers carbon nanotubes (CNTs), graphene nanoplatelets (GNPs) and Carbon Black (CBs) on the dynamic behavior of a DGEBA adhesive nanocomposite structure. The Hopkinson Bar device was used in a dynamic compression test

program. The experiments were conducted on nanocomposite specimens with various mass fractions, including 0 wt.% (neat adhesive) as a reference, 1wt.%, 2wt.%, and 5wt.%

It has been demonstrated that the dynamic behavior is sensitive to the impact pressure (strain rate). The findings of these studies also allowed us to gain a better understanding of the impact of nanofillers on the material's microstructure, dynamic behavior, and damage kinetics. The mechanical behavior of the samples improved with each mass fraction of each carbon nanofiller, demonstrating an increase in mechanical properties, dynamic characteristics, and rupture resistance due to increased rigidity of the adhesive, as well as an improvement in the interfacial bond between the adhesive matrix and the nanofillers.

Each test was carried out three times to ensure that the results were consistent. Before going into the various test campaign findings, we must ensure that the bar theory is verified in line with our scenario. We constantly check the various validation assumptions by comparing the forces applied on the incident bar-sample bar and sample-bar interfaces conveyed. As a result, it is critical to guarantee that the tests are repeatable. To determine the dispersion, a minimum of three tests were conducted for each impact pressure. The typical temporal fluctuations of the incident and transmitted velocity signals as a function of loading time are shown in Figure V.2. The equilibrium hypotheses are reasonably respected since the computed forces at the incoming and outgoing interfaces evolve mainly in the same way and have the same amplitude (bearing), implying that the sample is close to equilibrium during loading for various damage tests. However, there is a slight variation between an incident and transmitted forces for each impact pressure. This can be attributed not only to the sample's self-installation between the bar but also to the parallelism of the facets of the samples in contact with the bar, which is not 100% guaranteed, as the previous study demonstrated [54], [255], [318].



(a) velocity vs. time

(b) strain rate vs. time

Figure V.2: Test reproducibility under 1.5bar, Neat adhesive

V.3 Influence of nanofillers CNTs, CBs, GNPs on the dynamic velocity of nanocomposites based DGEBA adhesive

Similar to neat adhesive samples, nanocomposite-reinforced with CNTs, CBs, and GNPs under varied mass fractions were inspected during dynamic compression tests at three impact pressures of 1.5 bar, 2 bar, and 4 bar. CNTs, CBs, and GNPs insertion into DGEBA affected its dynamic features, as seen in Figures V.3-V.4-V.5. The velocity vs. time curve revealed that as the impact pressure grew, so did the peak velocities. With the modification to the proportion of nanofillers, no substantial improvement in velocities was observed at 1.5 and 2 bar, and no second peak was observed. At 4 bar, the velocity behavior increases quickly when the mass fraction of CNTs, CBs, and GNPs increases [39]. The presence of damage within the samples was confirmed by a small but visible second peak in the results at 4 bar, and the apparent beginning of the second peak became more dominant with high mass fractions of CNTs, CBs, and GNPs, which is accurate with the following works [255], [301], [318]–[320]. The appearance of a second peak on the $\dot{\epsilon}=f(t)$ curve, according to Tarfaoui's research [128], [268], [321], can be used to pinpoint the site of macroscopic damage. A decrease in stress is associated with the creation of this peak. In much of their research, Tarfaoui et al. [54], [137], [316], [318] explained how the presence of a second peak in the reflected wave indicates the presence of

macroscopic and microscopic damage in composite materials. The first thing that can be noticed is that the material is more durable. Damage occurs only under high impact pressure, which is reasonable when there is a second peak in the signal, showing the accumulation of failure modes in the sample. The damage also becomes more visible as the impact pressure increases. At the same time, low impact pressure causes merely residual "elastic-visco-plastic" deformation in the adhesive.

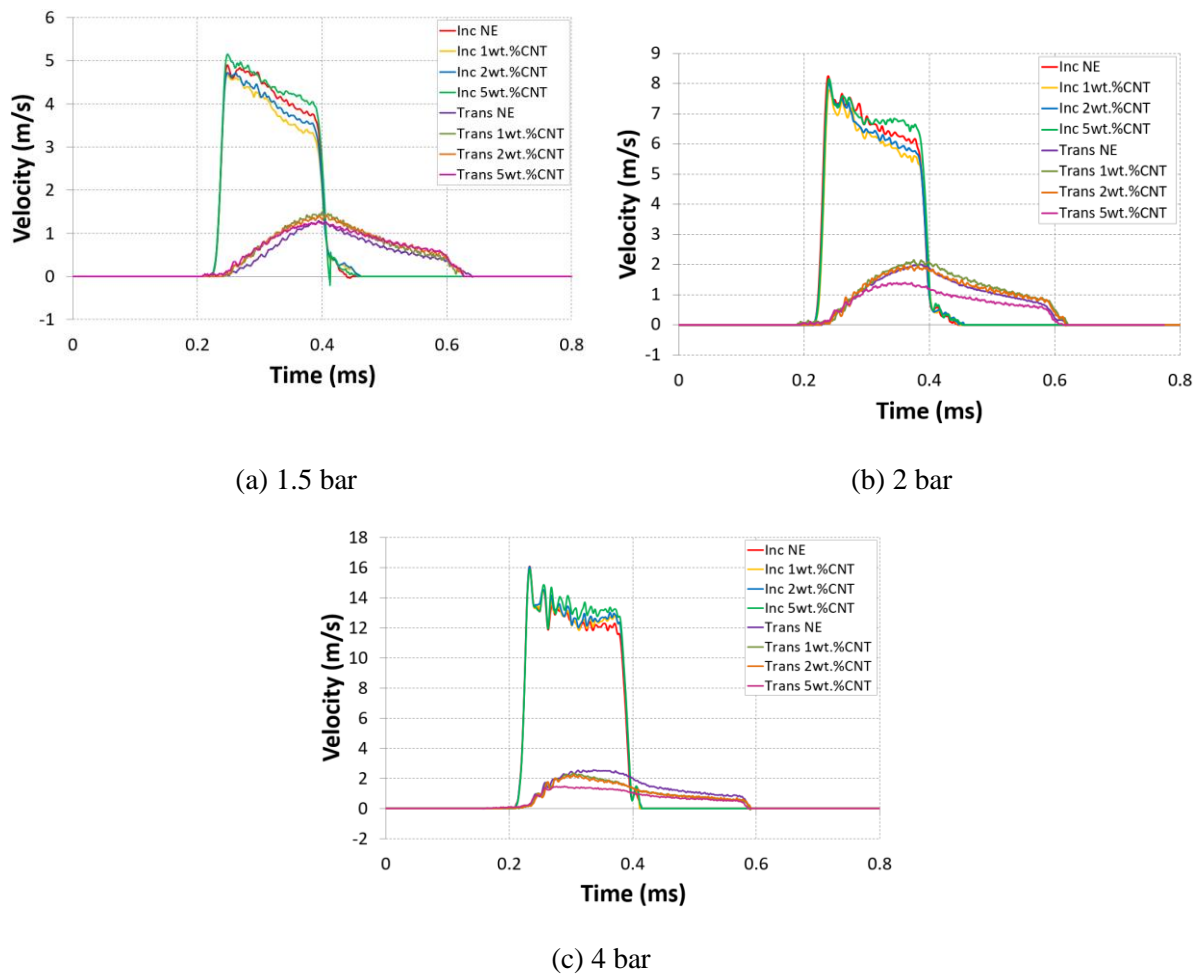
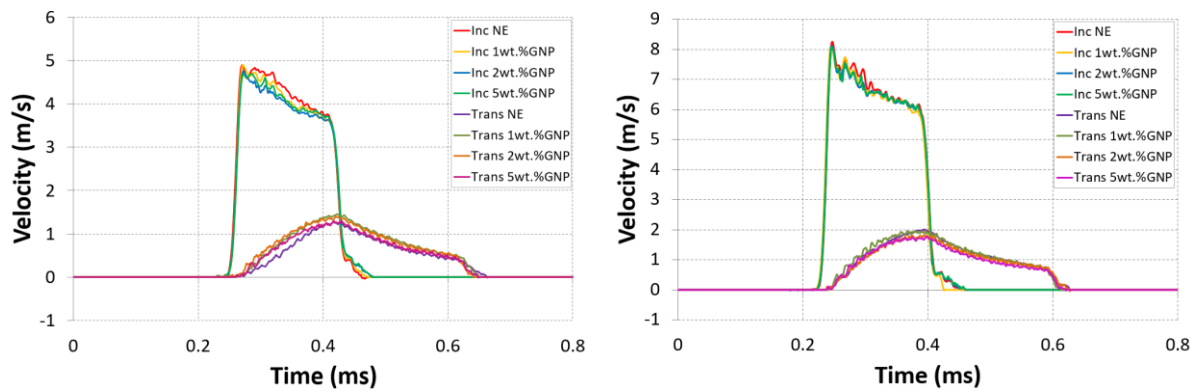


Figure V.3: The Velocity –time curves of CNT-reinforced DGEBA epoxy nanocomposite for different impact pressure

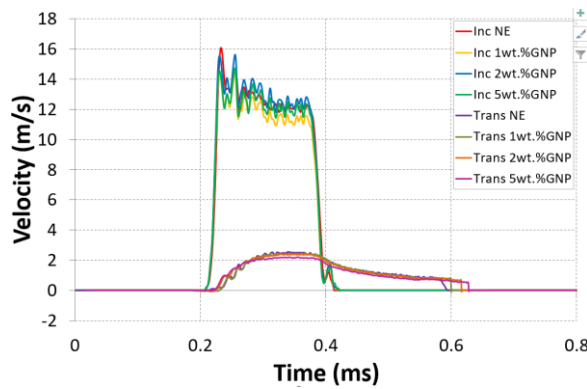
The mass fraction of nanofillers introduced to the DGEBA adhesive, as well as their random distribution, have a significant impact on the nature of damage. This data, shown in Figure V.3-V.4-V.5 at 2 bar, do not demonstrate a particularly significant emergence of the second peak,

but this level already shows that the specimen is not free of micro-damage (plasticity, microcracks). It exhibits significant residual plastic deformation due to adhesive behavior, which can be particularly severe when the impact pressure surpasses 4 bar and entails the catastrophic failure of reinforced adhesive nanocomposites. More failure modes are implicated as the impact pressure increases, from adhesive cracking to final fracture.



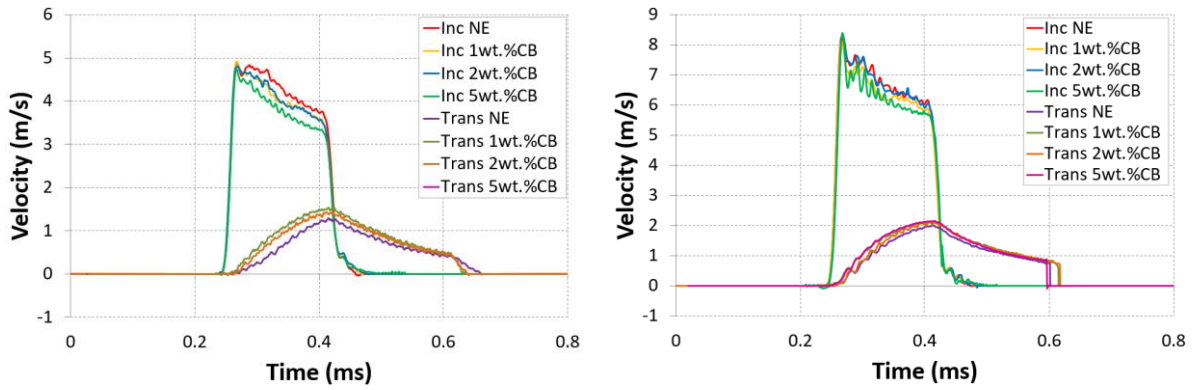
(a) 1.5 bar

(b) 2 bar



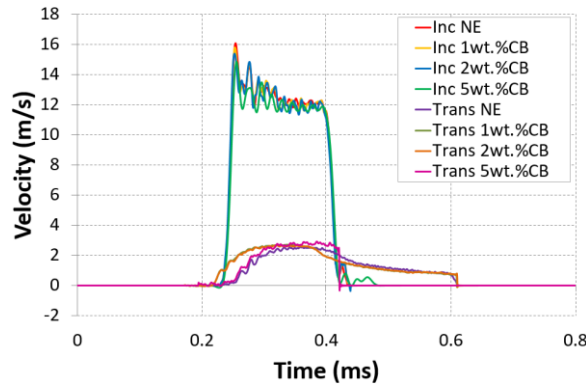
(c) 4 bar

Figure V.4: The Velocity –time curves of GNP-reinforced DGEBA epoxy nanocomposite for different impact pressure



(a) 1.5 bar

(b) 2 bar



(c) 4 bar

Figure V.5: The Velocity–time curves of CB-reinforced DGEBA epoxy nanocomposite for different impact pressure

V.4 Effects of CNTs, GNPs, CBs on DGEBA adhesive Nanocomposites': Dynamic Behavior

A dynamic compression test was performed on nanocomposite samples containing 0, 1, 2, and 5wt.% CNTs, GNPs, and CBs at three distinct impact pressures, namely 1.5, 2, and 4 bar. In addition, the dynamic behavior of these reinforced nanocomposites was explored in depth using the experimental results. These findings revealed that variations in impact pressure had a substantial impact on the dynamic characteristics of CNTs/GNPs/CBs-reinforced DGEBA adhesive nanocomposite.

V.4.1 Strain rate sensitivity

These results reveal that variations in impact pressure had a meaningful effect on the dynamic characteristics of CNTs/GNPs/CBs-reinforced adhesive nanocomposite. The strain rate increases quickly, then reduce and finally tends to diminish. The strain rate drops to negative values, which correspond to the sample's elastic return after impact, confirming the spring-back phenomenon.

Figures V.6, V.7 and V.8 depicted a comparison of the strain rate vs. time curve in dynamic compression studies with various impact pressures. The enhancement efficiency is substantially higher at lower impact pressures, while it gradually diminishes at higher impact pressures [322]. This is because raising the impact pressure reduces the plastic deformability of the polymer adhesive matrix, which hinders the interactions between the polymer and the nanofillers, which are critical for nanofiller reinforcement [323]. However, in reference [324]–[329], the impact pressure effect on enhancement efficiency is quite complicated; in some cases, it increases with impact pressure [325][330], while in other cases, it declines with impact pressure [324]–[329], as improvement reliability is reliant on not only the particle type or size but also the adhesive matrix properties.

In comparison to neat DGEBA adhesive, the strain rate for 1wt. % and 2wt. % CNTs decreases gradually at low impact pressures of 1 and 2 bar, as shown in Figure V.6, however, at 5wt.% CNTs, the strain rate exceeds the reference neat DGEBA adhesive strain rate. This could be due to a change in a structure where agglomeration is present. Similarly, adding GNPs to DGEBA adhesive nanocomposite shows a steady drop in strain rate development at low impact pressure, but at a large mass fraction of 5wt.%, the strain rate aspires to exceed neat adhesive, which explains the structural poverty. Adding CBs, on the other hand, tends to decrease the

strain rate of reinforced DGEBA adhesive nanocomposite dramatically in different levels of mass fraction.

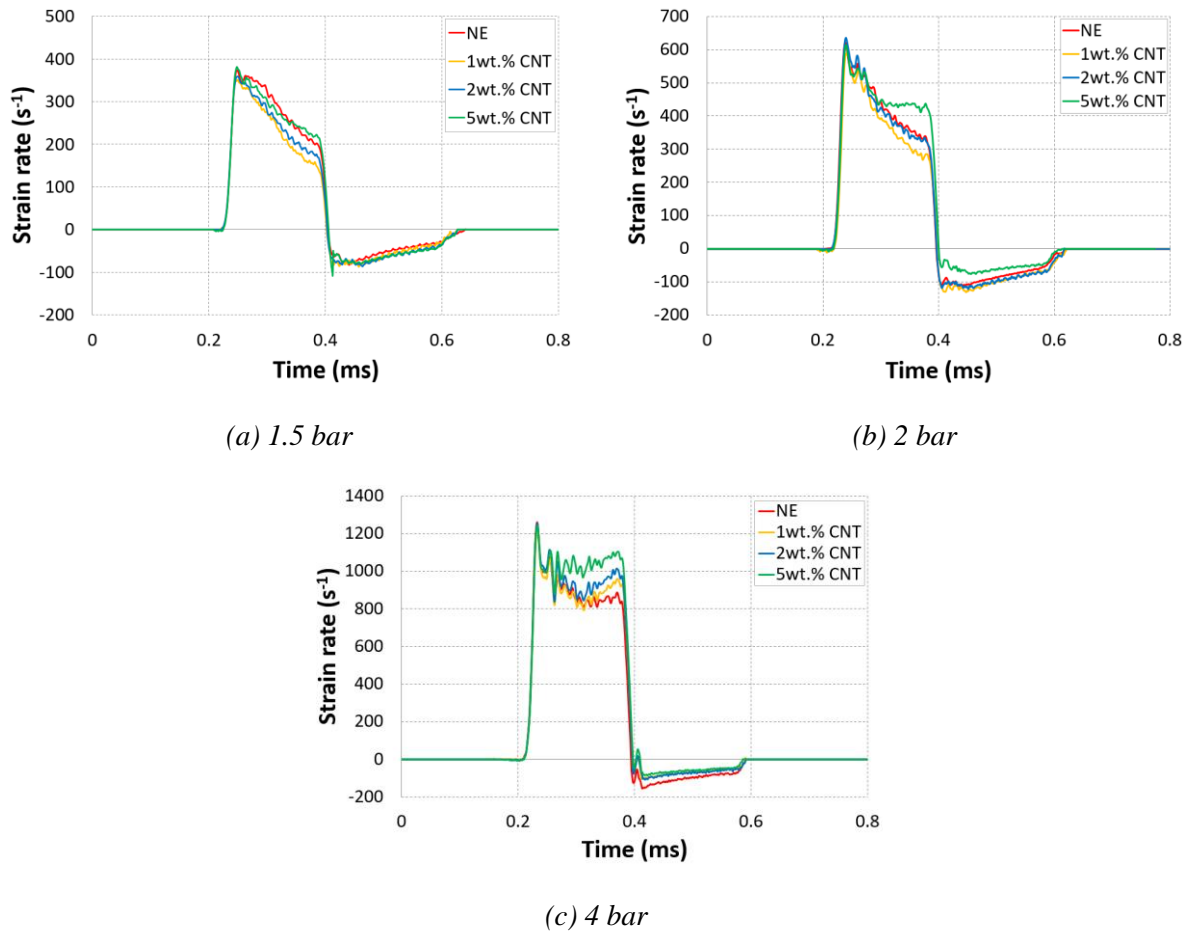


Figure V.6: The Strain rate–time curves of CNT-reinforced DGEBA epoxy nanocomposite for different impact pressure

Unreinforced and reinforced DGEBA adhesive nanocomposite samples with CNTs and GNPs show an onset second peak at high impact pressure 4 bar, which is the key feature of these curves. The second peak marks the start of macroscopic and microscopic damage. When macroscopic damage occurred, the existence of the second peak in the case of polyester material corresponded perfectly with the decline in stress in the sample. The studies demonstrated that the strain rate behavior was sensitive to the high impact pressure applied by the SHPB striker bar, mainly when the mass fraction was large. 2wt.% and 5wt.% CNTs showed a higher second peak, as compared to 1wt.% CNTs and neat DGEBA adhesive.

Similarly, to 2wt.% and 5wt.% GNPs showed a higher second peak compared to 1wt.% GNPs and neat DGEBA adhesive, which explain that higher mass fraction increased the viscosity of the matrix and made a non-uniformed distribution. The formation of cracks was the result of damage and the energy-absorbing mechanism of neat adhesive resins under high impact pressure loading. The appearance of the phenomena of agglomeration and the rise in damage and energy-absorbing mechanisms with nanofiller dispersion into resins was due to nanofiller debonding and the appearance of the agglomeration phenomenon [25]. At the same time, adding CBs, on the other hand, attempts to maintain the strengthened DGEBA adhesive nanocomposite structure even under high impact pressure. The strain rate vs. time of CBs/DGEBA at 4 bar shows an improvement with rising mass fraction, which is linked with a negligible second peak, indicating that deterioration is imminent but still has a vital behavior compared to the neat DGEBA adhesive nanocomposite.

Furthermore, as shown in Figures V.6(c), V.7(c) and V.8(c), the maximum strain rate can explain the influence of impact pressure, providing a foundation for modeling the dynamic behavior of nanocomposites under dynamic loadings for optimal design purposes. This involves calculating the average of all findings for each impact pressure using the error sensitivity curve. The change of impact pressure confirms the change of strain rate, and the reliability of curve fitting is almost at 99 %. The reinforced adhesive nanocomposite strain rate becomes more noticeable as the impact pressure increases, as shown in Figure V.9. The addition of CNTs, GNPs, and CBs, on the other hand, lowered the evolution of strain rate by up to 1wt.%, and the curve fitting accuracy was 99%.

The dynamic compressive strength generally increases as the strain rate decreases unless the damage propagates slowly at lower impact pressure and uses the most applied energy. However, macro-damage occurs at much higher impact pressures because the adhesive polymer chains do not have enough time to respond to the immediate strain, resulting in reduced polymer

mobility [42]. The strain rate appears to decrease in all samples, whereas the strain energy at fracture appears to be remain, more or less, steady. The viscoelastic nature of the DGEBA adhesive resin appears to play a role in dynamic compressive strength growth [184], [331]. Furthermore, a high mass fraction of reinforcement with CNTs and GNPs affects the structure's viscosity and creates weak interaction bonding with the adhesive, which can lead to degradation of the adhesive's mechanical properties. In contrast to reinforcement CBs at high mass fractions, improve the adhesive nanocomposite specimens [205], [332]. In this case, the optimal alternative for increasing the CNTs/DGEBA and GNPs/DGEBA nanocomposite strain rate performance is 1wt.% CNTs and GNPs. At the same time, the ideal mass fraction for enhancing the CBs/DGEBA nanocomposite is 5wt.% CBs.

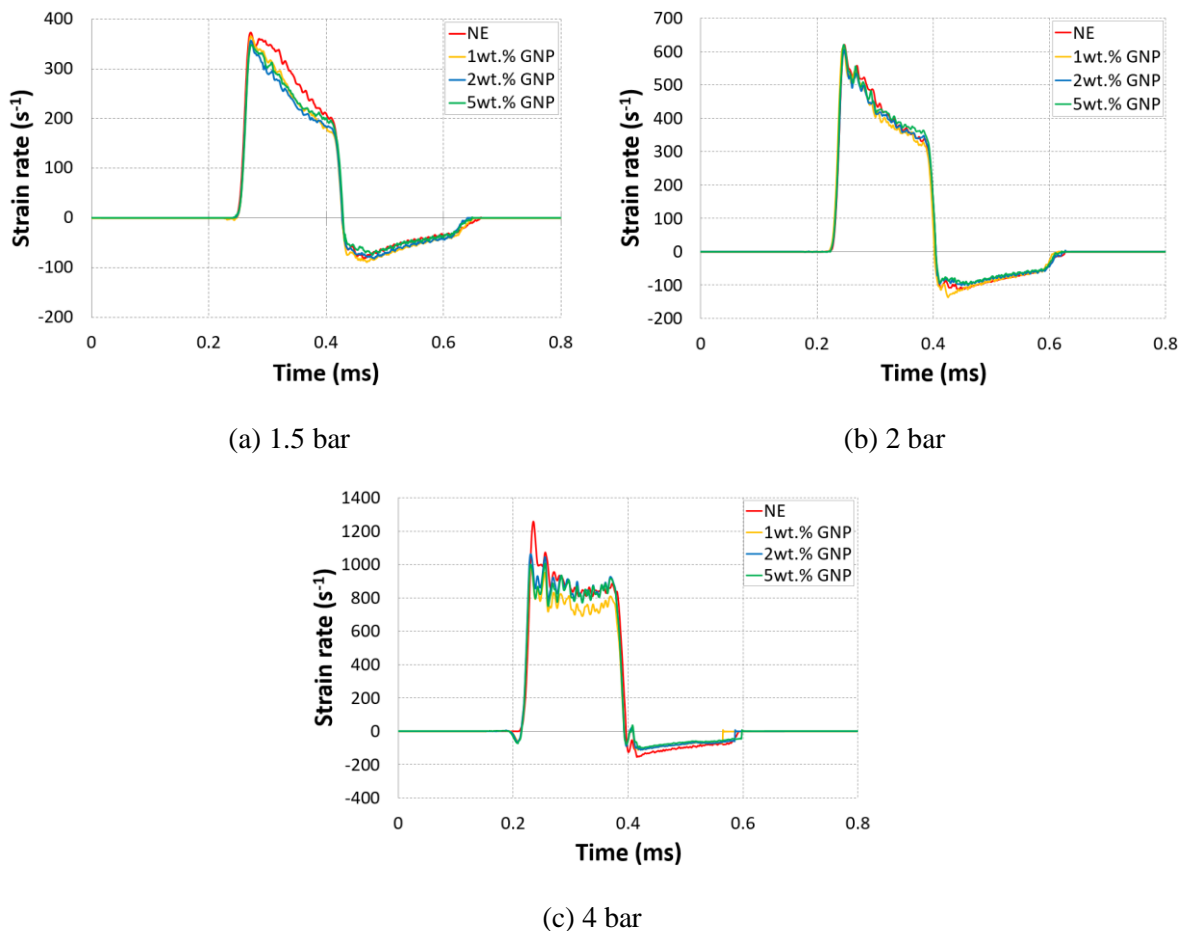


Figure V.7: The Strain rate–time curves of GNP-reinforced DGEBA epoxy nanocomposite for different impact pressure

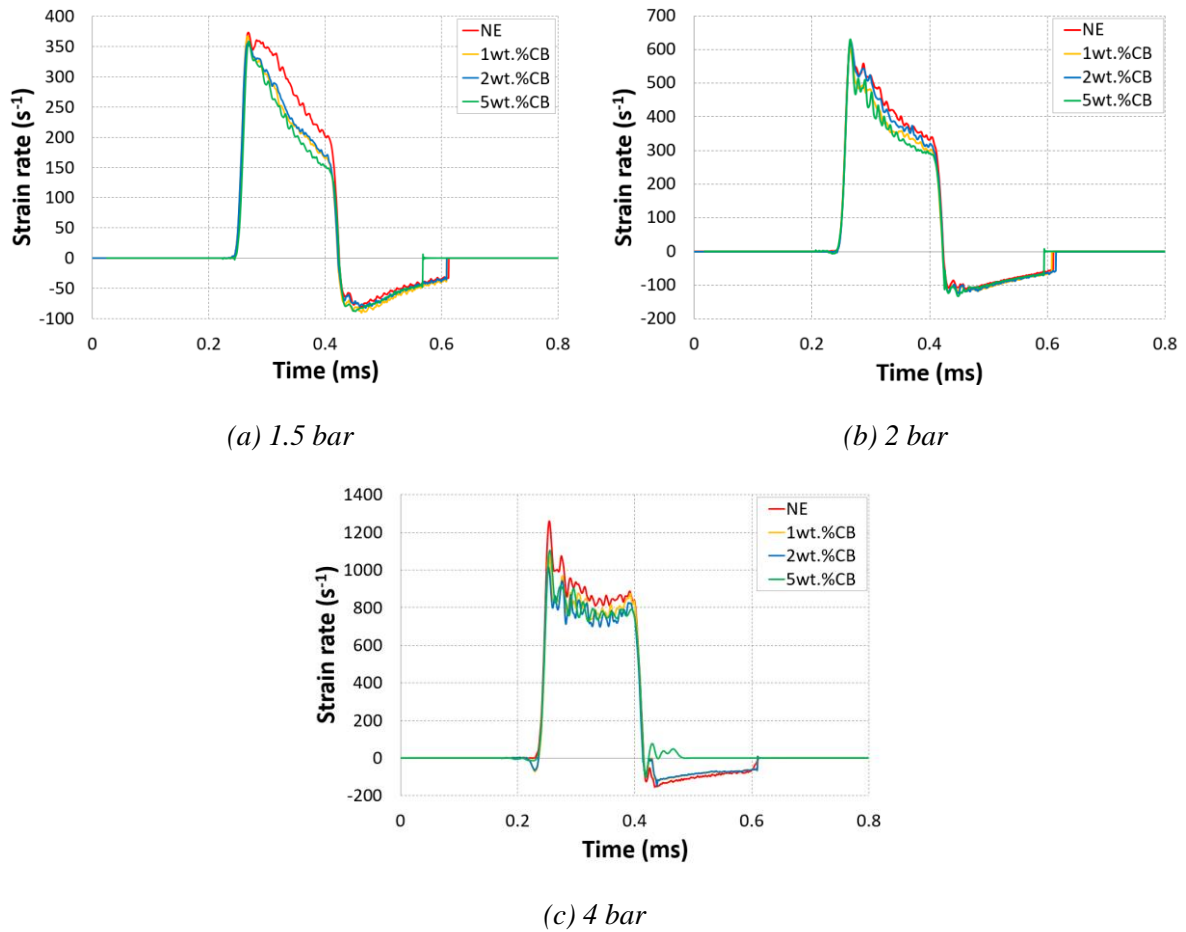


Figure V.8: The Strain rate–time curves of CB-reinforced DGEBA epoxy nanocomposite for different impact pressure

$$\varepsilon(\text{NE}) = -71.094x^2 + 745.39x - 584.83$$

$$\varepsilon(1\text{wt.\% CNT}) = -65.759x^2 + 703.1x - 555.4$$

$$\varepsilon(1\text{wt.\% GNP}) = -93.025x^2 + 794.15x -$$

$$\varepsilon(1\text{wt.\% CB}) = -93.025x^2 + 794.15x -$$

$$614.68$$

$$614.68$$

$$\varepsilon(2\text{wt.\% CNT}) = -96.517x^2 + 889.34x -$$

$$\varepsilon(2\text{wt.\% GNP}) = -136.3x^2 + 1014.4x -$$

$$\varepsilon(2\text{wt.\% CB}) = -136.3x^2 + 1014.4x -$$

$$757.87$$

$$859.75$$

$$859.75$$

$$\varepsilon(5\text{wt.\% CNT}) = -61.043x^2 + 679.09x -$$

$$\varepsilon(5\text{wt.\% GNP}) = -122.55x^2 + 972.57x -$$

$$\varepsilon(5\text{wt.\% CB}) = -122.55x^2 + 972.57x -$$

$$499.9$$

$$824.23$$

$$824.23$$

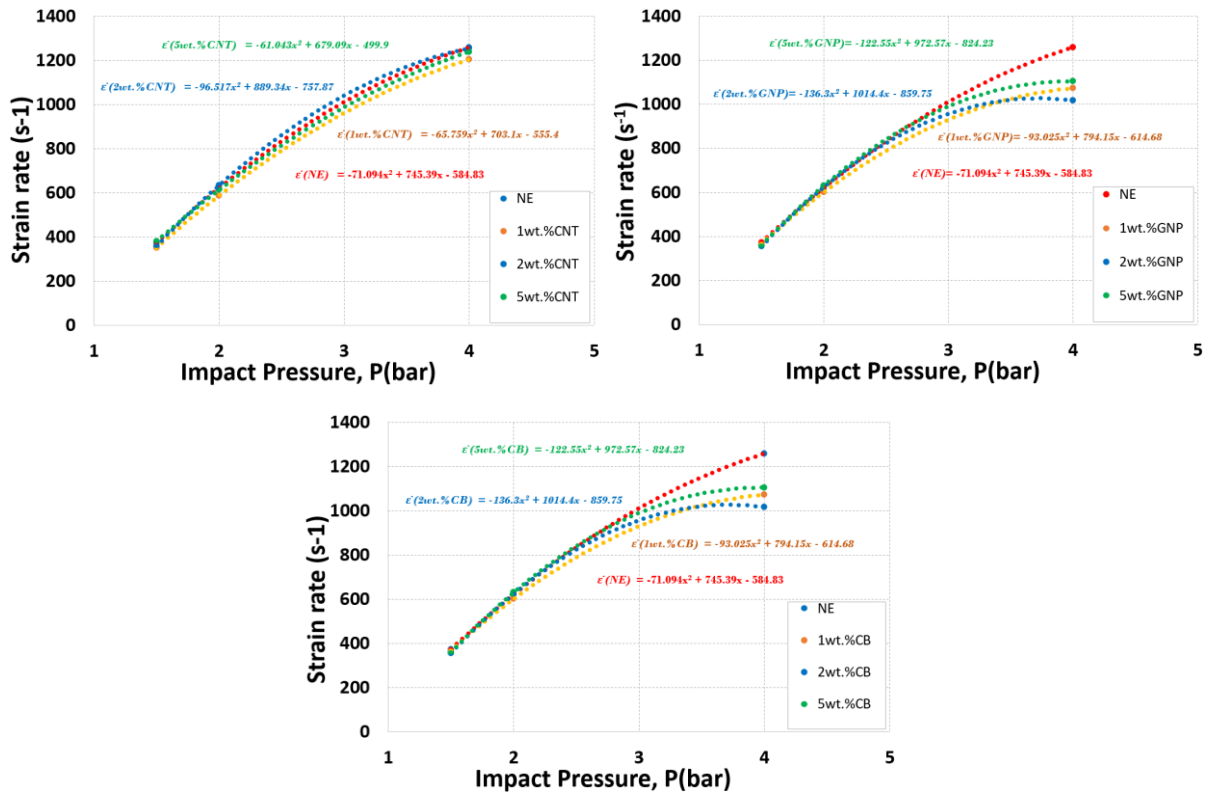


Figure V.9: Strain rate vs Pressure for CNTs/DGEBA, GNPs/DGEBA, CBs/DGEBA

V.4.2 Stress-strain behavior

The dynamic compressive curve for different reinforced DGEBA adhesive nanocomposites can be roughly divided into four parts, as shown in Figure V.10-V.11-V.12:

(1) the initial elastic deformation area, where stress increases approximately linearly with compressive strain, (2) the non-linear zone, where stress increases non-linearly with strain and plasticity is moderate, (3) the plastic plateau, which is critical at high mass fractions, where stress is nearly constant with strain (note that the plastic plateau does not exist at low impact pressure). Remarkable plasticity occurs at that point, and a micro-crack could occur. (4) stress decreases due to the end of the dynamic compression test. An elastoviscoplastic is defined as the mechanical behavior of various structures at different levels. The final stress value gets higher as the impact pressure increases, which can be explained by the damage propagating at a slower rate at lower impact pressures, allowing the applied energy to be used more efficiently.

At the same time,, the impact pressure effect can be linked to the polymer chains' molecular mobility [333]. As shown in Figure V.10-V.11-V.12, increasing the impact of pressure loading affects the structure's behavior. In furthermore to the time-dependent nature of accumulated damage, the viscoelastic character of the polymer DGEBA adhesive matrix itself is responsible for the rise in the final strength of the samples evaluated in the transverse direction at high impact pressure [334].

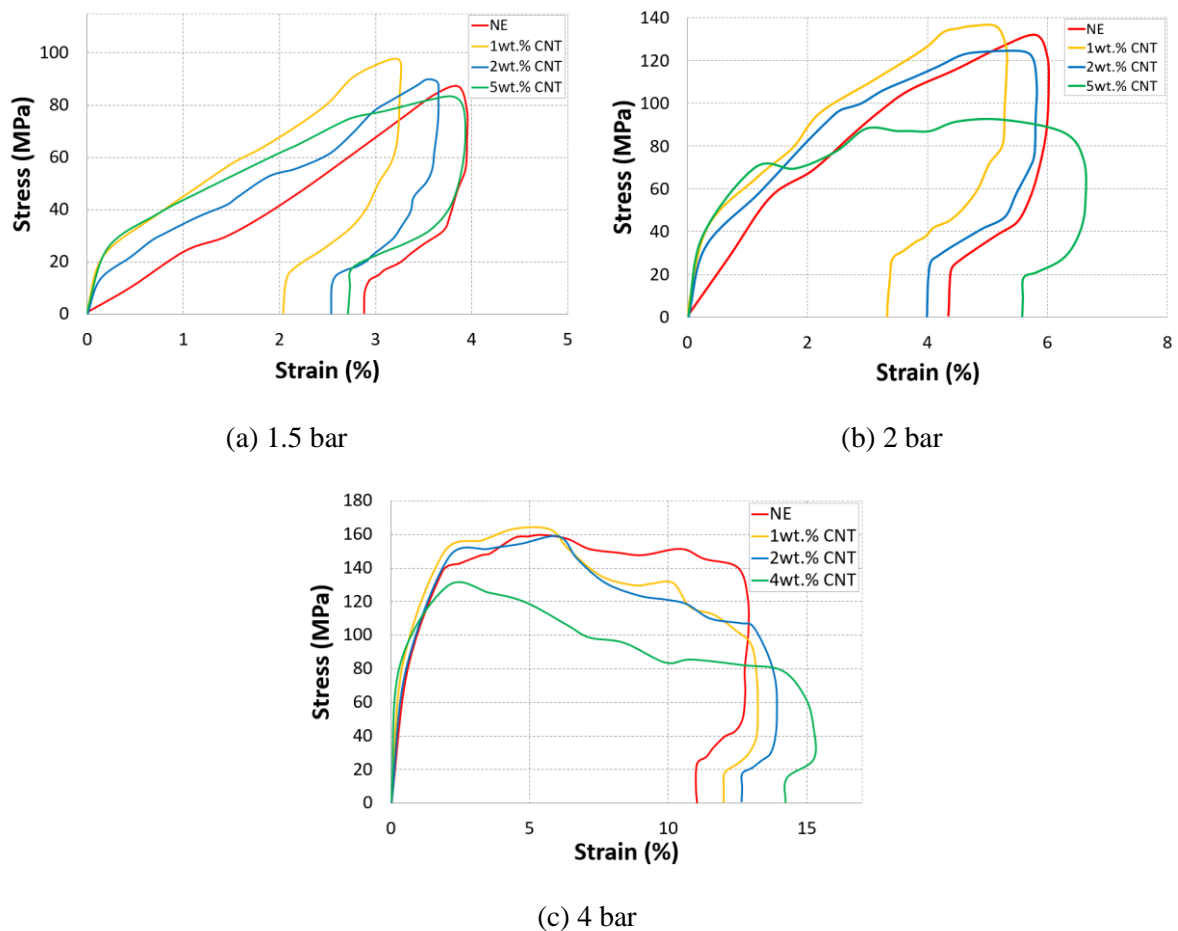


Figure V.10: Stress-strain curves of the CNT-reinforced DGEBA epoxy nanocomposite for different impact pressure

The evolution of the maximum stress is predominantly focused on the impact pressure, as shown in Figures V.10-V.11-V.12, and the curve fit precision is 99%. The results in Figure V.10(a)- V.11(a)- V.12(a) show that maximum strength develops as impact pressure increases

and that the maximum increase in strength of samples with 1% CNTs, GNPs, and CBs increases as dynamic impact pressure increases. As a result, adding CNTs, GNPs, CBs to the adhesive nanocomposite sample at 1 wt.% mass fraction enhances the specimens' maximum strength and the dependence of these dynamic features under dynamic compression allowing for design optimization. This strength increase has been proved also by Figure V.13.

The molecular mobility of the chains is restricted under high impact pressure [335]. On the time scale of high impact pressure tests, there is no time for polymer chain rearrangement. Hence a greater quantity of energy is absorbed in this condition because the primary process of amorphous polymer yielding is the transition of macromolecule segments from one equilibrium position to another [336], a more enormous impact pressure results in higher molecular resistance to jumps and, as a result, higher yield stress.

The evolution of dynamic Young's modulus (E_{dyn}) for different impact pressures with various mass fractions is shown in Figures V.9(b)- V.10(b)- V.11(b). At low mass fraction, 1wt. % CNTs shows high E_{dyn} for CNTs/DGEBA nanocomposite at low impact pressure, while high mass fraction 5wt.% classed with high E_{dyn} at high impact pressure. Figure V.14 presents high-speed photographs of the dynamic compression experiment of the CNT-reinforced DGEBA adhesive sample under the three different mass fractions at 4 bar. Thus, it presents the difference in mechanical behavior evolution of the different mass fractions during dynamic compression. Contrarily to GNPs/DGEBA that show at 1.5 bar and 4 bar, 5wt.% presents the important E_{dyn} ; however, at 2 bar, 2wt.% presents the highest E_{dyn} . This development shows that increasing the mass fraction of graphene in a GNPs/DGEBA adhesive nanocomposite improves its elasticity.

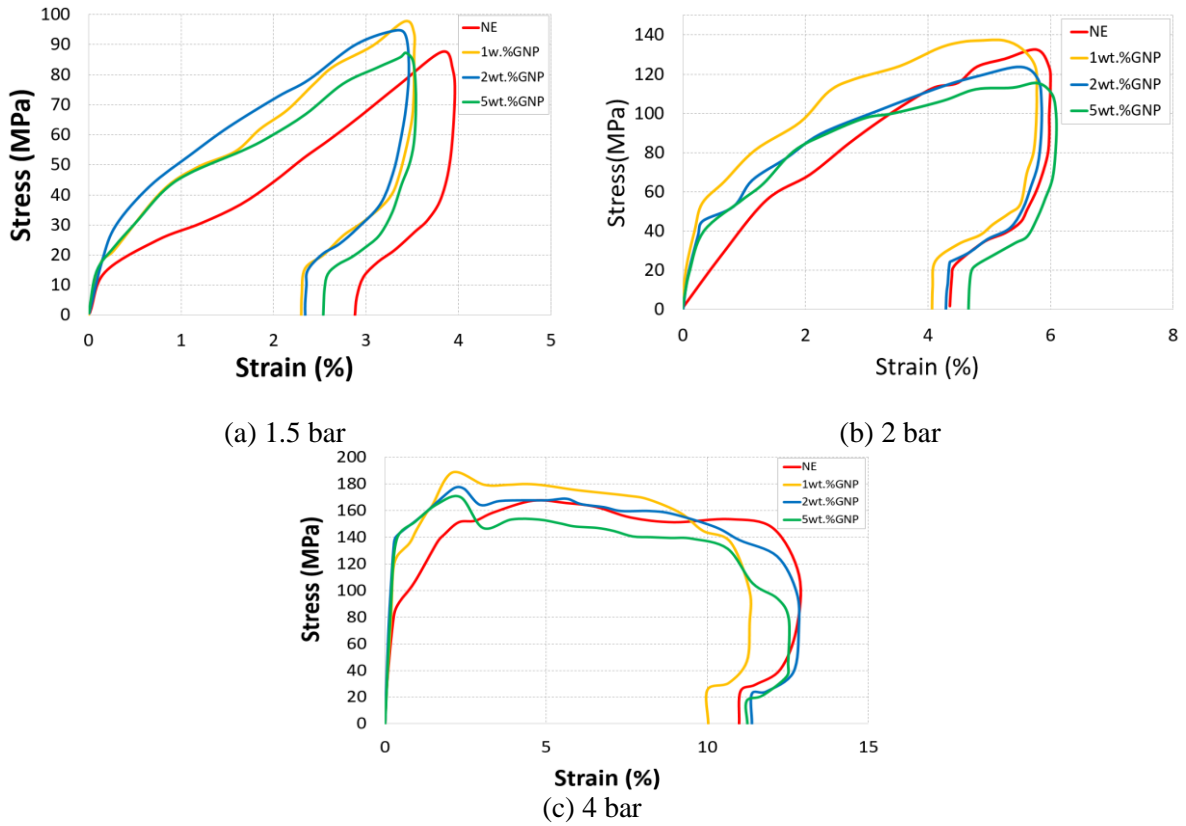


Figure V.11: Stress-strain curves of the GNP-reinforced DGEBA epoxy nanocomposite for different impact

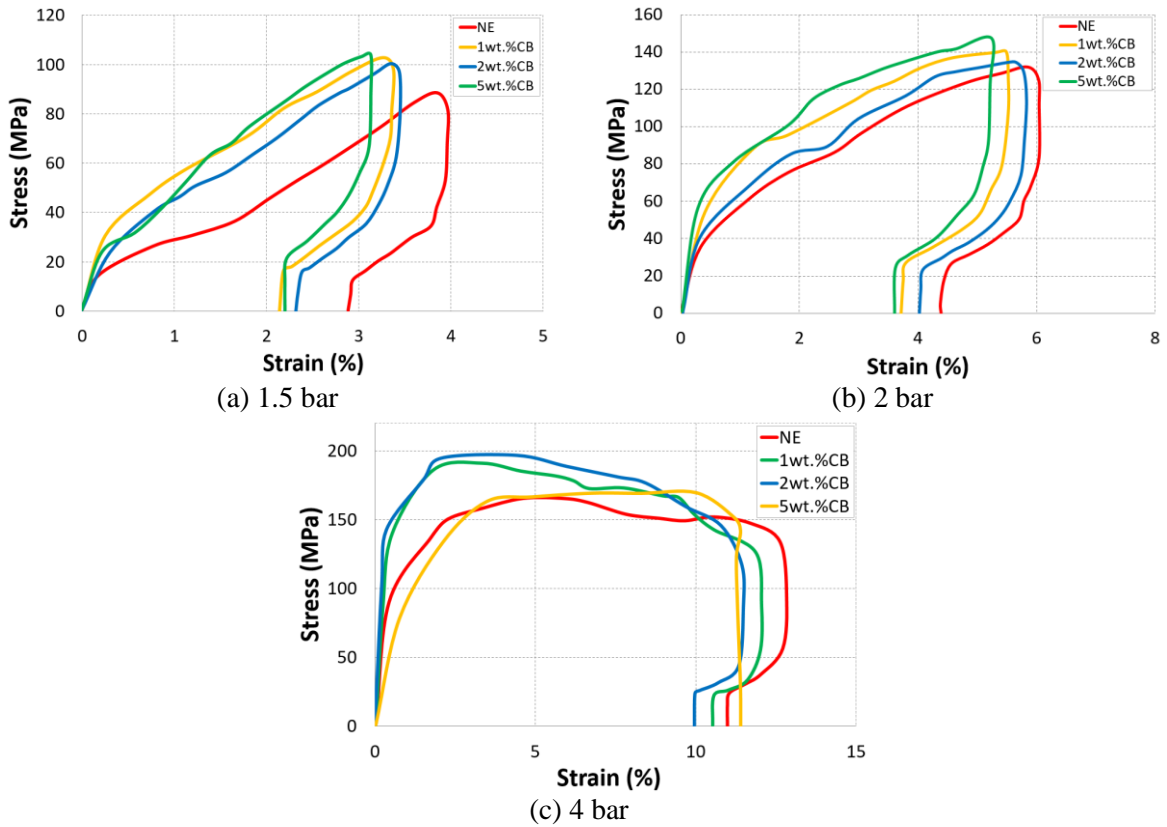


Figure V.12: Stress-strain curves of the CB-reinforced DGEBA epoxy nanocomposite for different impact pressure

Figure V.15 shows the difference in mechanical behavior evolution of the different GNPs mass fractions during dynamic compression.

At the same time, CBs/DGEBA demonstrate that at 1.5 and 4 bar, 2wt. % shows the highest E_{dyn} , while at 2 bar, 5wt.% shows the highest E_{dyn} . This demonstrates that the behavior trend does not increase in positive correlation with the mass fraction of CBs because the interaction with the matrices does not match the mass fraction level. Figure V.16 shows the difference in mechanical behavior evolution of the different CBs mass fractions during dynamic compression.

Many additional variations appeared in the non-linear regime at a high-impact pressure of 4 bar for the various CNTs/DGEBA, GNPs/DGEBA, and CBs/DGEBA structures, followed by a progressive decline in stress until the end of the dynamic compression test. As established in the study conducted by Arruda et al. [337], this behavior was attributable to thermal softening in the polymeric material as the impact pressure was raised under the impact. The matrix plasticity and failure modes in the polymeric material under impact could cause this thermal softening, as shown in Figures V.10(a)- V.11(a)- V.12(a). These discoveries supported the theory that the internal heat generated upon impact in unreinforced and reinforced nanocomposite materials [7] was solely due to the polymeric matrix's viscoplastic behavior and failure process. This fundamental understanding of the dynamic behavior of the polymer will be taken into account in regard to the strain rate when developing a rate-dependent-dynamic model of polymeric matrix composites under impact with this new insight [255].

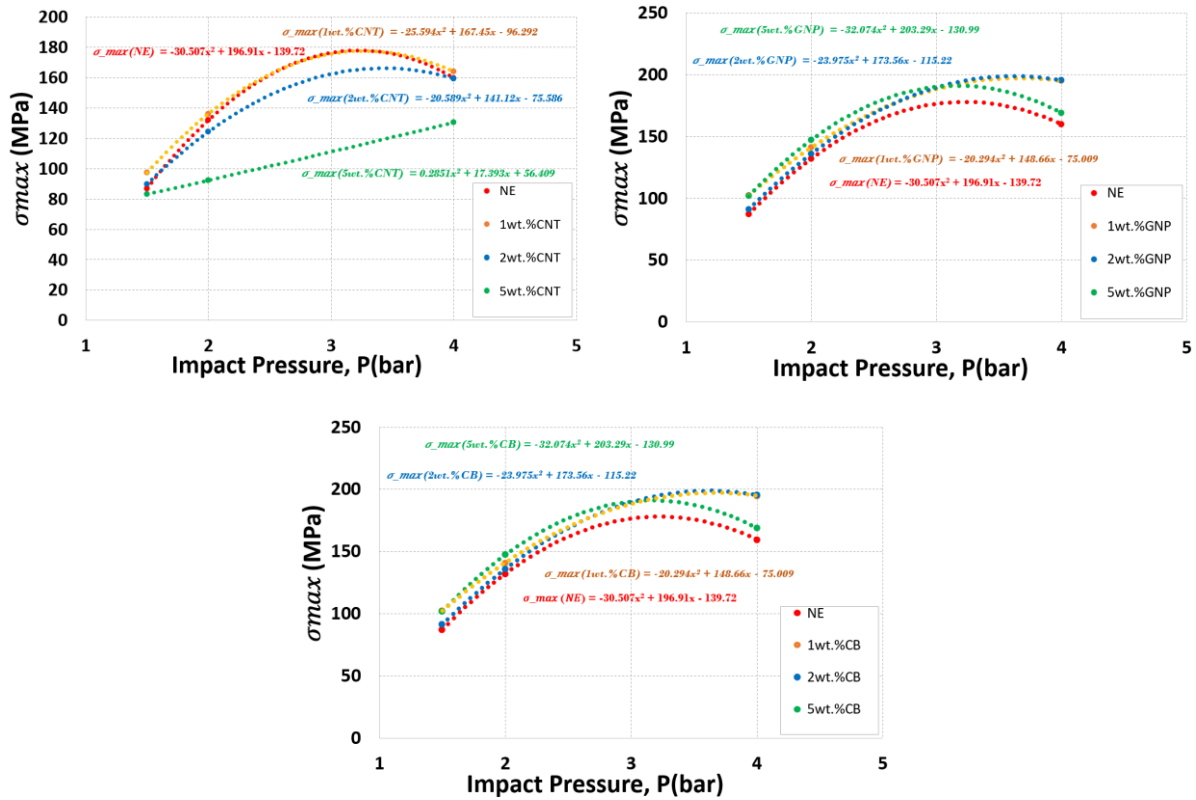


Figure V.13: Max Stress vs Pressure for CNTs/DGEBA ; GNPs/DGEBA; CBs/DGEBA

$$\sigma_{max}(NE) = -30.507x^2 + 196.91x - 139.72$$

$\sigma_{max}(1wt.\%CNT) = -25.594x^2 + 167.45x - 96.292$	$\sigma_{max}(1wt.\%GNP) = -20.294x^2 + 148.66x - 75.009$	$\sigma_{max}(1wt.\%CB) = -20.294x^2 + 148.66x - 75.009$
$\sigma_{max}(2wt.\%CNT) = -20.589x^2 + 141.12x - 75.586$	$\sigma_{max}(2wt.\%GNP) = -23.975x^2 + 173.56x - 115.22$	$\sigma_{max}(2wt.\%CB) = -23.975x^2 + 173.56x - 115.22$
$\sigma_{max}(5wt.\%CNT) = 0.2851x^2 + 17.393x + 56.409$	$\sigma_{max}(5wt.\%GNP) = -32.074x^2 + 203.29x - 130.99$	$\sigma_{max}(5wt.\%CB) = -32.074x^2 + 203.29x - 130.99$

Various parameters such as interfacial adhesion, adhesive material strength, and particle diffusion in the matrix affect the strength of nanocomposites, which could justify the up and down behavior progression. One of the most important things to consider is the dispersion of nanofillers (CNTs, GNPs, CBs) in the DGEBA adhesive matrix. At high mass fractions, the agglomeration of nanofillers in adhesive causes local stress concentration and reduces nanofiller-matrix adherence.

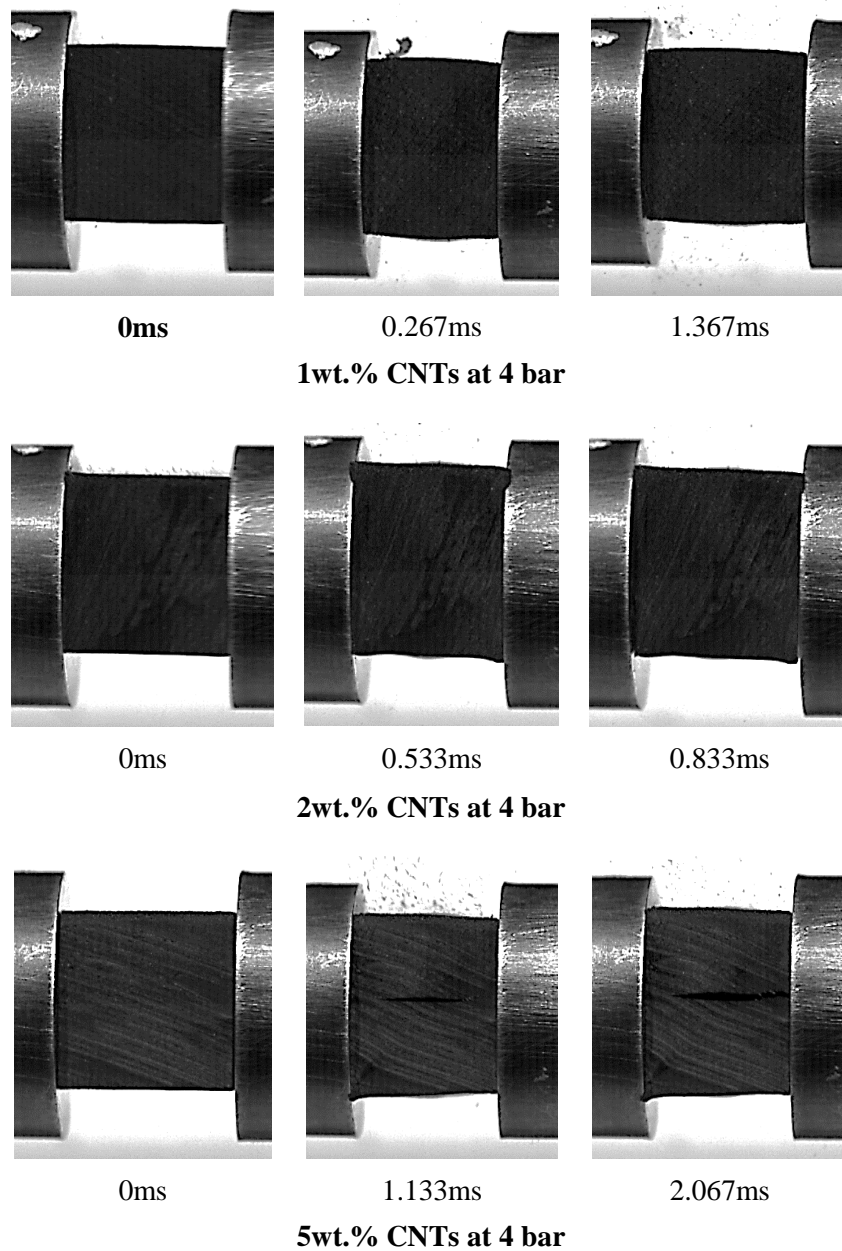


Figure V.14: High-speed photographs of dynamic compression experiment of the CNT-reinforced DGEBA adhesive sample under 4bar impact pressure

As shown in Figure V.14, a decline in toughness has been observed at 5wt.% CNTs, 5wt.% GNPs, and 5wt.% CBs, especially with high impact pressure, which may be attributed to reduced load transmission efficiency at the interface induced by stress accumulation around the clusters. It is challenging to make nanocomposites without agglomeration using typical solution mechanical mixing techniques. As a result, the increase in strength of nanocomposite over neat DGEBA adhesive is not significant, Figure V.13.

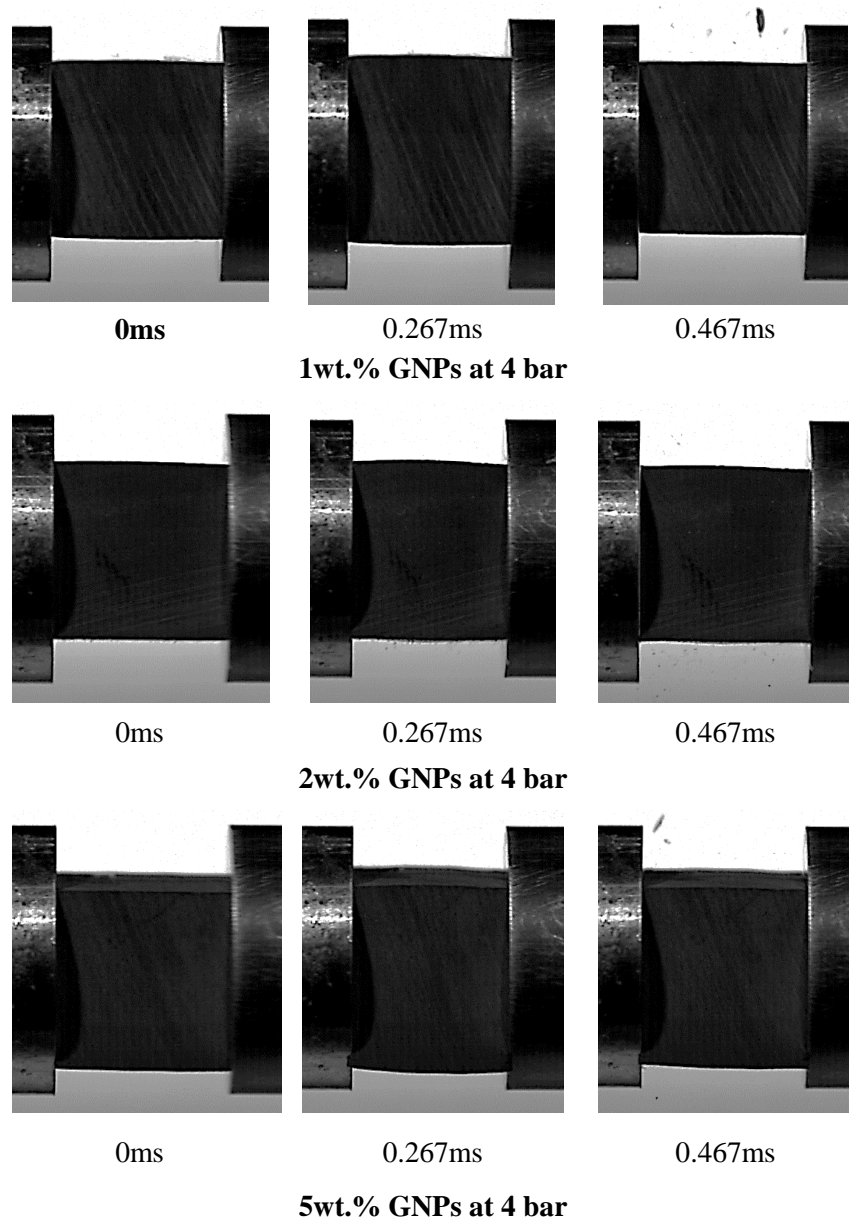


Figure V.15: High-speed photographs of dynamic compression experiment of the GNP-reinforced DGEBA adhesive sample under 4bar impact pressure

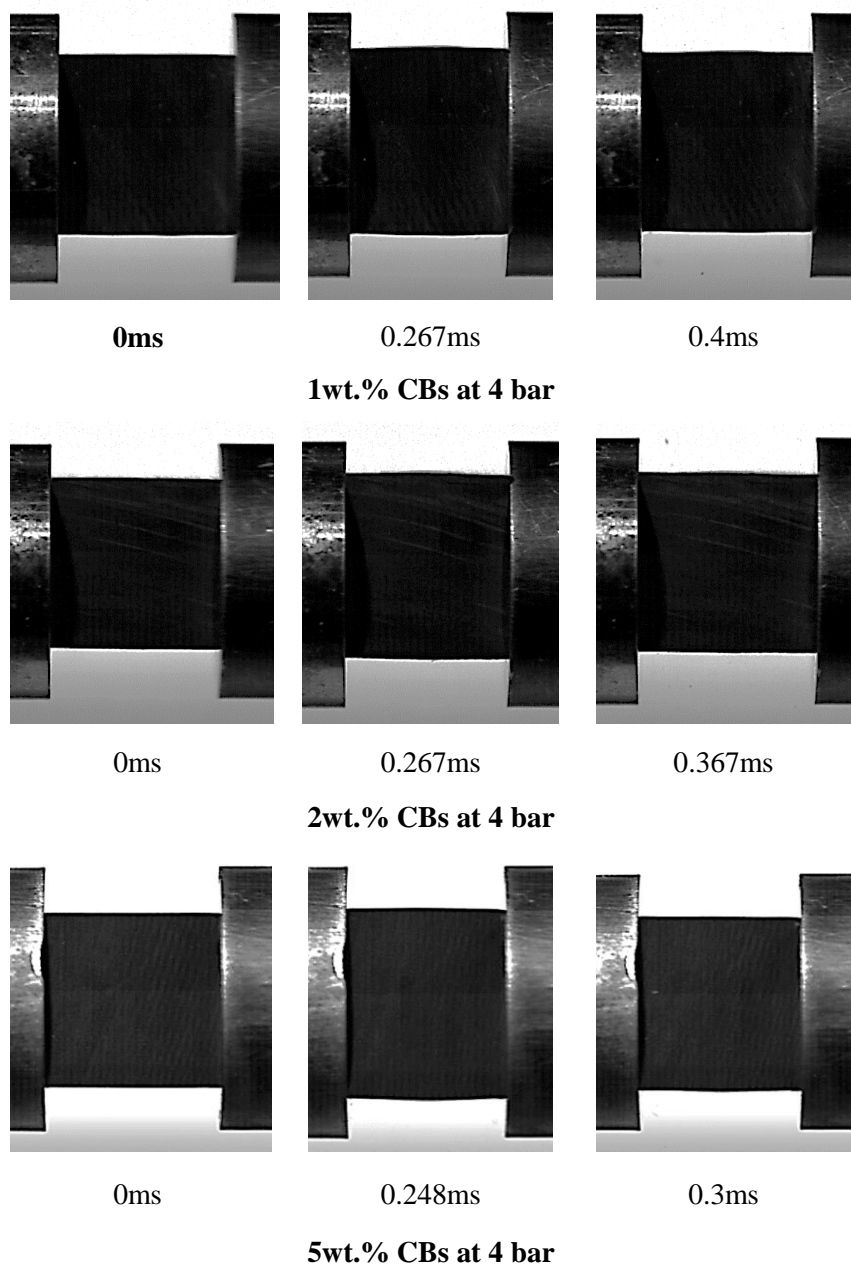


Figure V.16: High-speed photographs of dynamic compression experiment of the CB-reinforced DGEBA adhesive sample under 4bar impact pressure

V.4.3 Comparison analysis

Basing on neat DGEBA adhesive as a reference, Table V.1 , Graphene nanoplatelets, carbon nanotubes, and Carbon Black were suggested as suitable nanofillers for improving the dynamic mechanical performance of the DGEBA adhesive nanocomposite Table V.1. As shown in the preceding section, changing nanofiller categories impacts mechanical behavior advancement,

confirming that each kind of nanoparticle has its improvement and influence. Figures V.18-V.24 compare the structural progress with different nanofillers under different impact pressures and compares the dynamic compressive behavior as stress vs. strain and strain rate vs. time curves for different reinforcements in DGEBA adhesive resin. Selecting the optimum nanofillers required careful consideration, as shown in the Figures below.

Table V.2: Dynamic mechanical properties of neat DGEBA adhesive under different impact pressures

		Impact Pressure (bar)		
		1.5	2	4
NEAT Adhesive	Strain rate	373.29	621.57	1259.22
	Edyn	21.123	39.925	136.47
	Smax	87.01	132.08	159.82
	LE for Smax	3.87	5.80	5.45
	LE for S=0	2.88	4.34	11.03

Using neat DGEBA adhesive as a reference, which has the lowest dynamic mechanical behavior, CNTs outperforms CBs and GNP-reinforced DGEBA adhesive nanocomposite has the less strain rate at low-mass fractions of 1wt.% (Figure V.14-V.16). However, CNTs degrade and become weaker than CBs/DGEBA and GNPs/DGEBA when subjected to high impact pressures with high mass fractions. The loss of CNTs/DGEBA performance is caused by agglomerated nanofillers, which act as stress raisers and crack initiation sites, causing early failure and lowering matrix and interfacial characteristics. As a result, SEM images of CNTs nanofiller-added samples revealed weak nanocomposite bonding, and these samples deformed more due to their flexible shape, as seen in Figure V.17.

Table V.3: Dynamic mechanical properties of reinforced DGEBA adhesive under different impact pressures

		Impact Pressure (bar)								
		1.5			2			4		
		Weight percentage (wt.%)								
		1	2	5	1	2	5	1	2	5
CNTs/DGEBA Adhesive	Strain rate	351.29	358.98	381.40	587.77	634.74	614.12	1204.85	1255.22	1239.78
	Edyn	122.13	103.72	114.22	121.46	121.46	157.9	201.59	155.17	275.2
	Smax	97.29	89.77	83.14	136.23	124.30	92.34	163.51	158.68	129.07
	LE for Smax	3.15	3.53	3.81	4.77	5.57	4.51	4.47	6.07	2.02
	LE for S=0	2.04	2.54	2.71	3.33	3.99	5.58	12.00	12.66	14.24
GNPs/DGEBA Adhesive	Strain rate	98.12	96.20	88.25	610.50	605.65	620.42	988.86	1064.44	1005.82
	Edyn	73.416	115.96	116.44	115.59	130.74	98.064	334.95	365.03	451.81
	Smax	95.07	89.78	87.36	132.45	122.01	116.26	177.37	184.27	173.04
	LE for Smax	3.31	3.01	3.42	4.86	5.28	5.77	5.00	2.38	2.23
	LE for S=0	2.26	2.28	2.53	3.86	4.32	4.69	9.99	11.39	11.24
CBs/DGEBA Adhesive	Strain rate	367.24	355.21	358.89	601.52	623.89	630.71	1073.52	1017.14	1105.24
	Edyn	108.4	140.37	103.06	156.13	132.53	202.21	322.07	466.19	101.37
	Smax	102.32	91.18	101.78	141.13	136.00	147.29	194.92	195.43	168.98
	LE for Smax	3.18	2.75	3.02	5.43	5.63	5.21	3.27	2.10	8.34
	LE for S=0	2.15	1.76	2.19	3.70	4.05	3.62	10.46	9.85	11.41

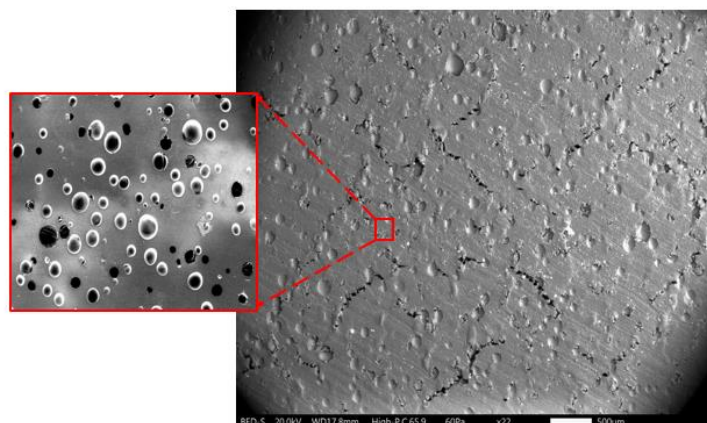
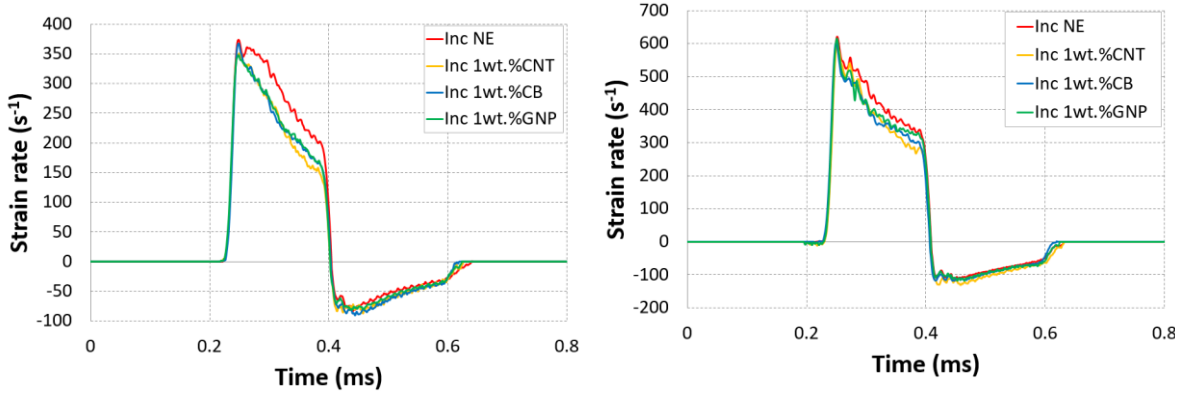


Figure V.17: Microscopic observation of a specimen for 4wt.% CNT reinforced DGEBA epoxy nanocomposite

When compared to CNTs/DGEBA and GNPs/DGEBA at high mass fractions such as 5wt.%, CBs/DGEBA is the most stable structure under diverse impact pressures. Figures V.18-V.24.

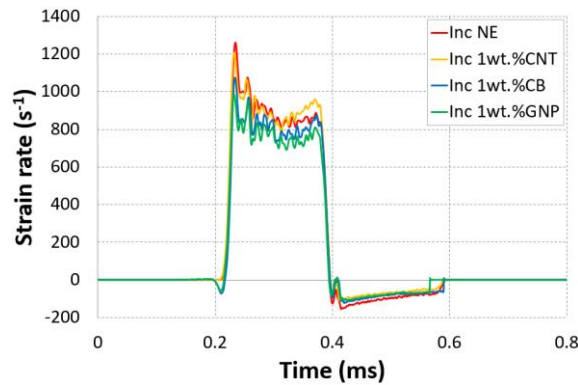
At the same time, when the stress vs. strain curves of CNTs/DGEBA, GNPs/DGEBA, and CBs/DGEBA at a low mass fraction were compared, the results showed that reinforced DGEBA adhesive nanocomposite had the same aspect behavior as a neat adhesive (unreinforced DGEBA), but with a different gradient, Figure 21. CNTs/DGEBA, GNPs/DGEBA, and CBs/DGEBA exhibit elasto-viscoplastic behavior for varied mass fractions at 1.5 and 2 bar, Figure V.22 and V.23. However, they imply a transition to plastic behavior with significant toughness at a high mass fraction under high impact pressure. Nonetheless, at 4bar, 5wt.% CBs and GNPs aspires to deliver better behavior than neat DGEBA adhesive consistently, yet CNTs failed to develop and showed a strength loss, which could be due to agglomeration take-up, Figure V.24. This is explained by the growing impact pressure, which causes the sample's temperature to rise during loading [54], [255], [318], [338]. Polymer chain mobility becomes more accessible as temperature rises, reducing effective stress transfer between the nanofiller and adhesive matrix of nanocomposite samples. As a result, as the temperature rises, the rigidity of the viscoelastic samples decreases, causing the elasticity curve to fall. The shape of the

nanofillers influenced this evolution and how they interacted with the adhesive matrix, the temperature rises, polymer chain mobility in nanofiller-reinforced samples that become comparably easier, and they lose rigidity at a faster rate. Compared to CNTs and GNPs, which have 1D and 2D structures, CB-added samples demonstrated superior mechanical stability due to their 0D structure.



(a) 1.5 bar

(b) 2 bar



(c) 4 bar

Figure V.18: Strain rate-time curves of CNTs/DGEBA, GNPs/DGEBA, CBs/DGEBA nanocomposite, 1wt.%

Furthermore, with the addition of CNTs, GNPs, or CBs, albeit at various increments, Young's modulus and dynamic compressive strength initially show progression. CBs had a more substantial reinforcing effect than CNTs and GNPs at varied impact pressures, as shown in

Figures V.22, V.23, V.24. Toughness and ductility follow similar patterns. Compared to the neat DGEBA adhesive, both GNPs and CBs increase the strength and adhesive toughness at all fractions, whereas CNTs tend to become more plastic at high mass fractions and lower the strength behavior.

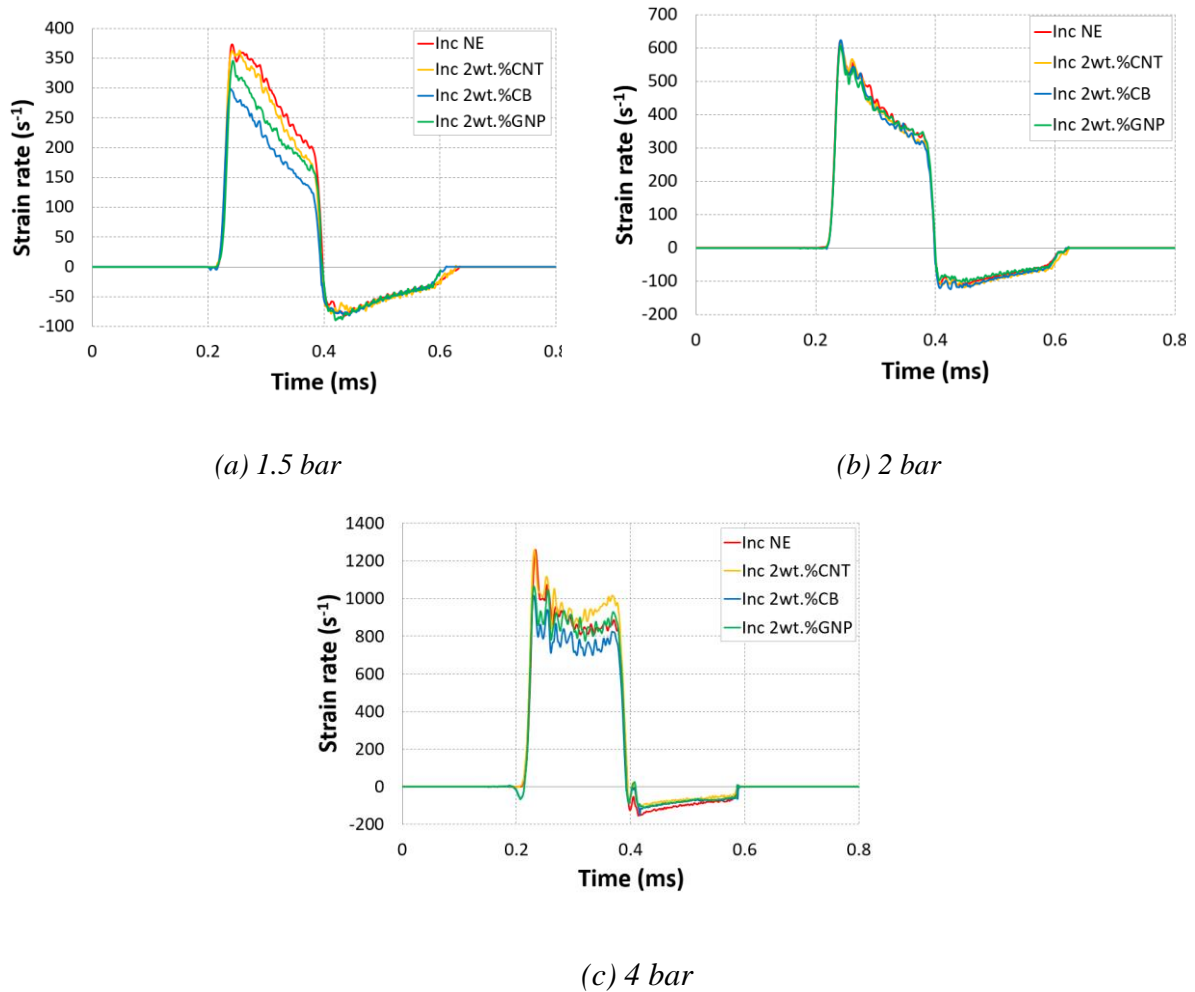
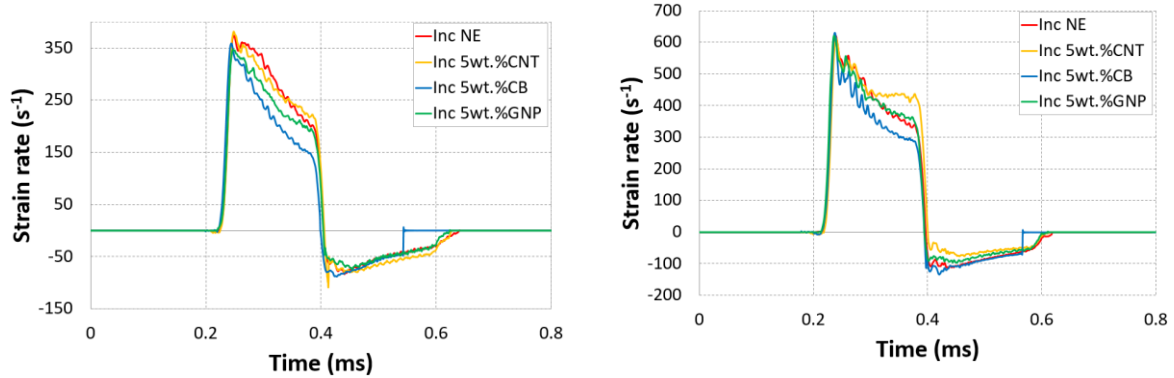


Figure V.19: Strain rate-time curves of CNTs/DGEBA, GNPs/DGEBA, CBs/DGEBA nanocomposite, 2wt.%

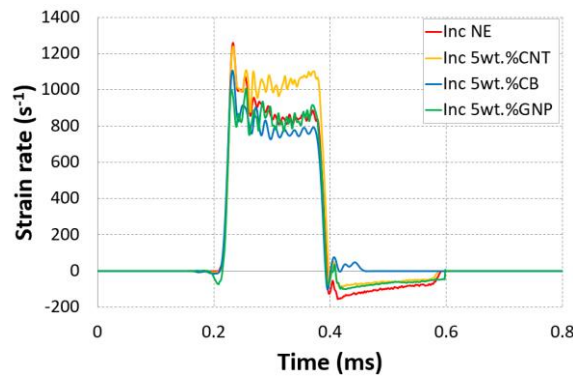
These results show a specific filler concentration beyond which the nanocomposite adhesives' Young's modulus, dynamic compressive modulus, and compressive strength begin to deteriorate. Moreover, according to the results, the crucial fraction varies depending on the

nanofiller's geometrical structure (plate-like structure, tube-like structure, and spherical structure).



(a) 1.5 bar

(b) 2 bar



(c) 4 bar

Figure V.20: Strain rate-time curves of CNTs/DGEBA, GNPs/DGEBA, CBs/DGEBA nanocomposite, 5wt.%

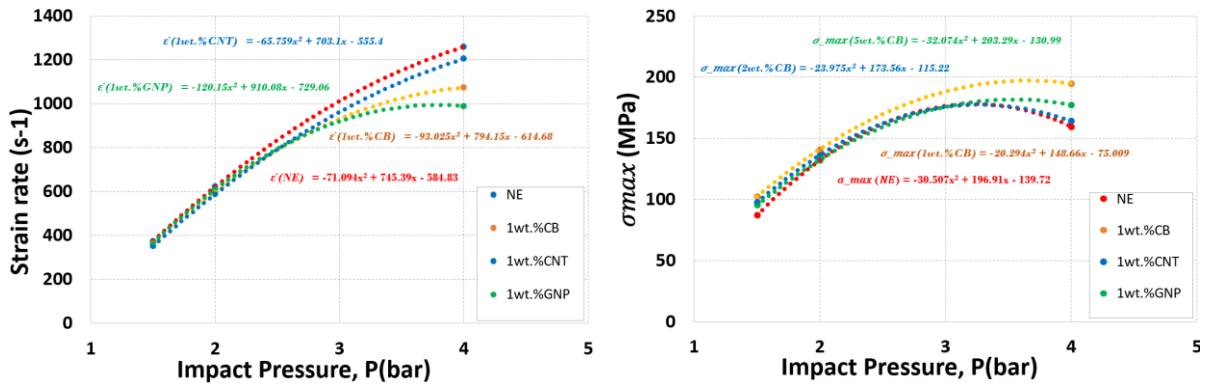
Mechanical reinforcement depends on two fundamental factors: (i) the uniform dispersion of the reinforcing phase; and (ii) the interfacial bonding strength between the host adhesive matrix and the reinforcing phase. CNTs, GNPs, and CBs can disperse uniformly in adhesive resin at low fractions but with various reflective properties. Compared to the tube-like form of CNTs, the plate-like structure gives GNPs an advantage in terms of robust interfacial bonding with adhesive matrix in the face of dynamic compressive load. However, compared to

GNPs/DGEBA and CNTs/DGEBA, CBs have a tremendous advantage due to their 0D structure, which tends to become more resistant and displays stronger interfacial bonding with DGEBA adhesive matrix.

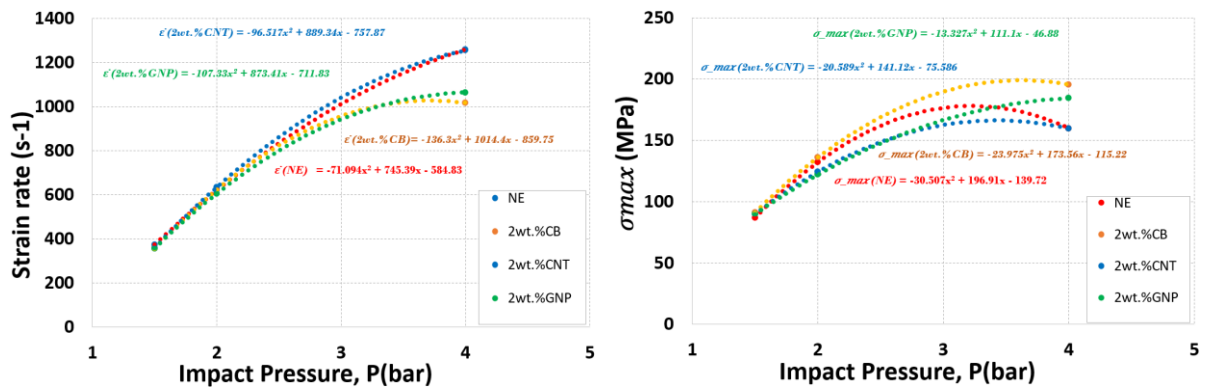
GNPs stack on top of each other, producing clusters, and CNTs clump together at large fractions. The difference in geometrical structure between the two carbon nanofillers causes different responses in adhesive resin nanocomposites.

Despite CBs having a less uniform dispersion, they play a more prominent role in reinforcement than GNPs and CNTs. Several studies have also proved that at high mass fractions of CBs, agglomeration forms with a size of 1-100nm, which somewhat reduces the dynamic compressive strength and elongation at the breaking point by increasing the filler concentration.

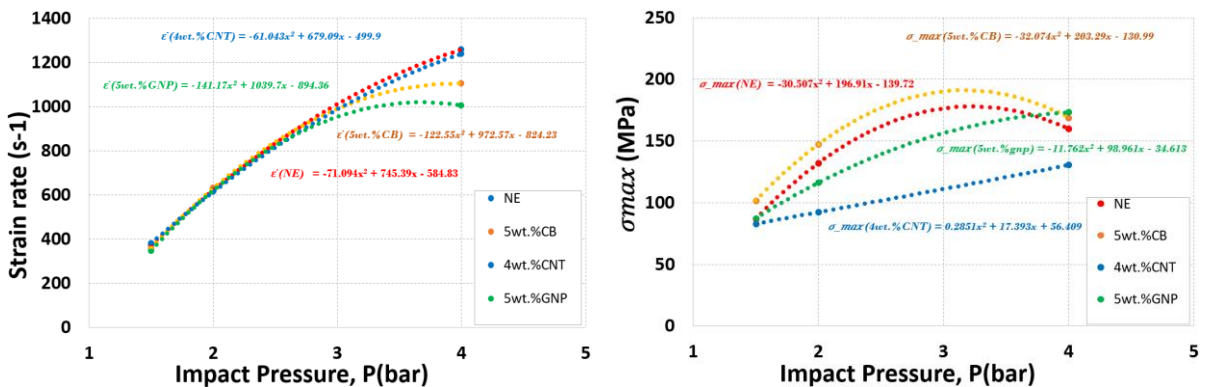
The CBs nanofillers act as nucleating agents, but they also produce a dramatic reduction in chain mobility, as seen in nature's shift of behavior, resulting in the production of considerably smaller and less organized crystallites. The progress percentages of the different reinforced nanocomposites with varying impact pressures are listed in tables V.1-V.3. As it is cited in these tables, the 2wt.% CBs/DGEBA epoxy nanocomposite has the most improved specimen, making it the best nanofiller for improving the dynamic mechanical behavior of DGEBA adhesive. The mechanical behavior under low mass fraction progresses in the following order: CBs/DGEBA, CNTs/DGEBA, then GNPs/DGEBA. At the same time, the CBs maintain the same classification for high impact pressure, with GNPs/DGEBA occupying the second position. The CNTs/DGEBA occupy the position of the weakened structure.



(a) 1 wt.%

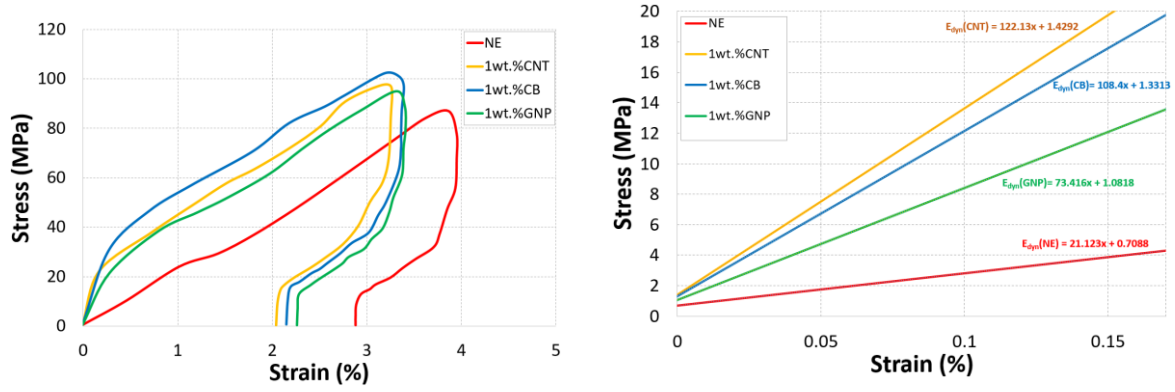


(b) 2 wt.%

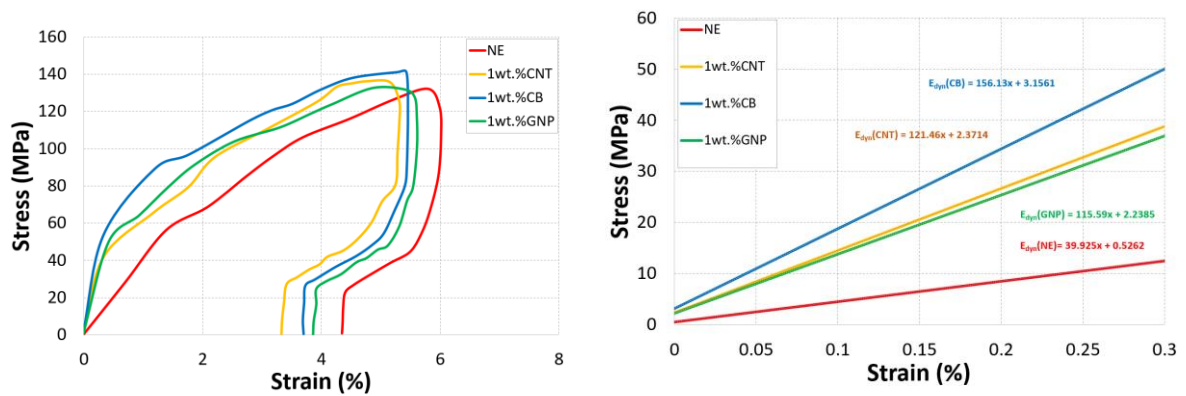


(c) 5 wt.%

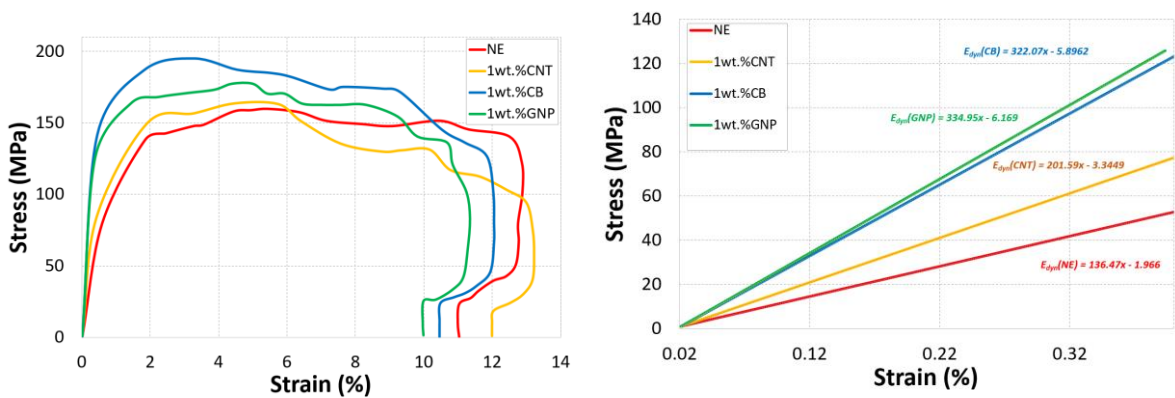
Figure V.21: Strain rate and Max Stress vs Impact Pressure for neat adhesive and adhesive doped with nanofillers



(a) 1.5 bar

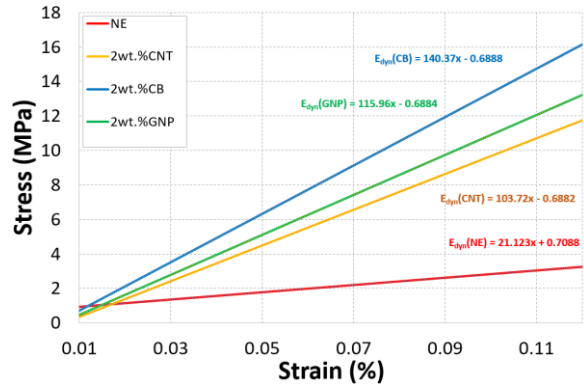
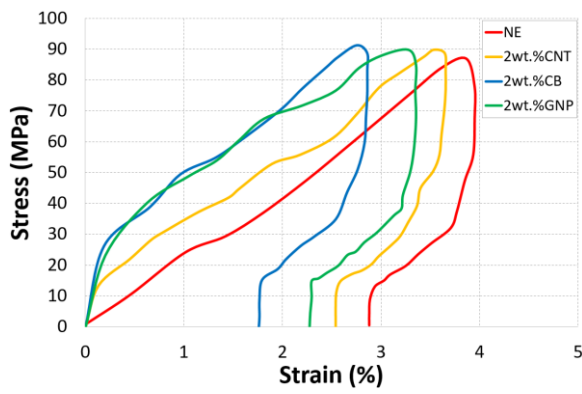


(b) 2 bar

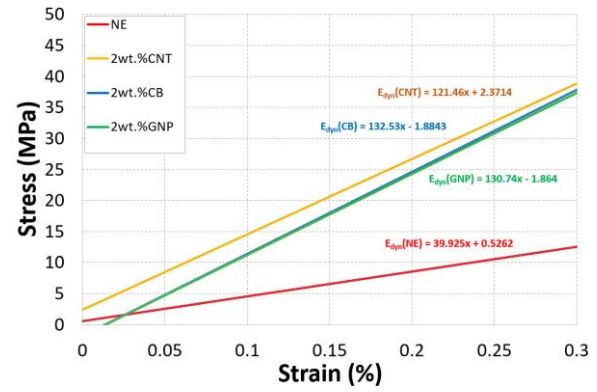
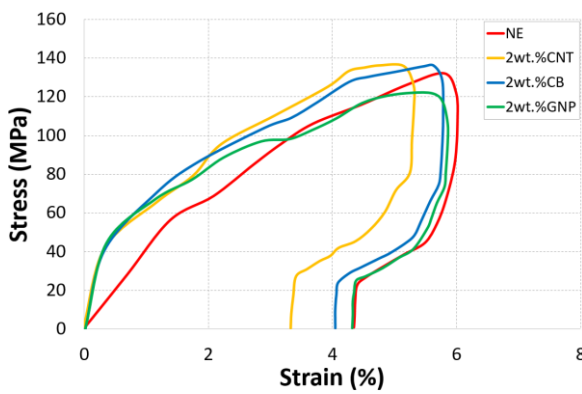


(c) 4 bar

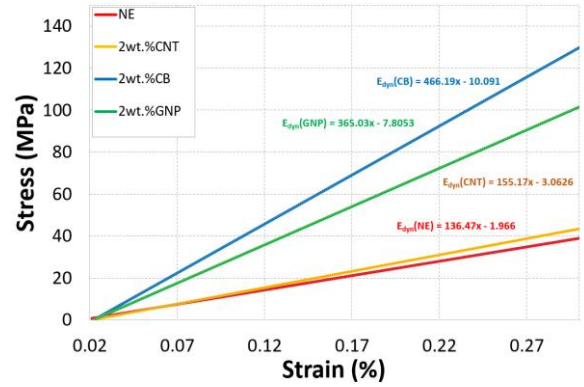
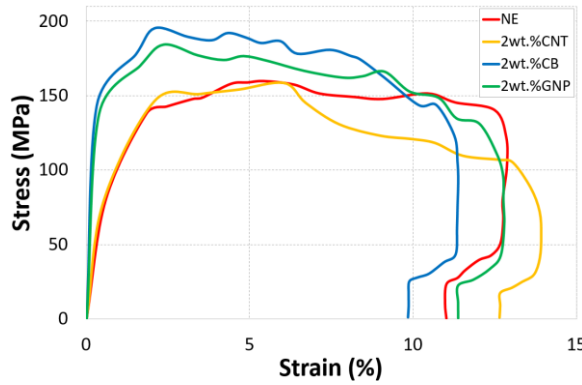
Figure V.22: Stress vs strain curves for neat adhesive and adhesive doped with 1 wt.% nanofillers



(a) 1.5 bar



(b) 2 bar



(c) 4 bar

Figure V.23: Stress vs strain curves for neat adhesive and adhesive doped with 2 wt.% nanofillers

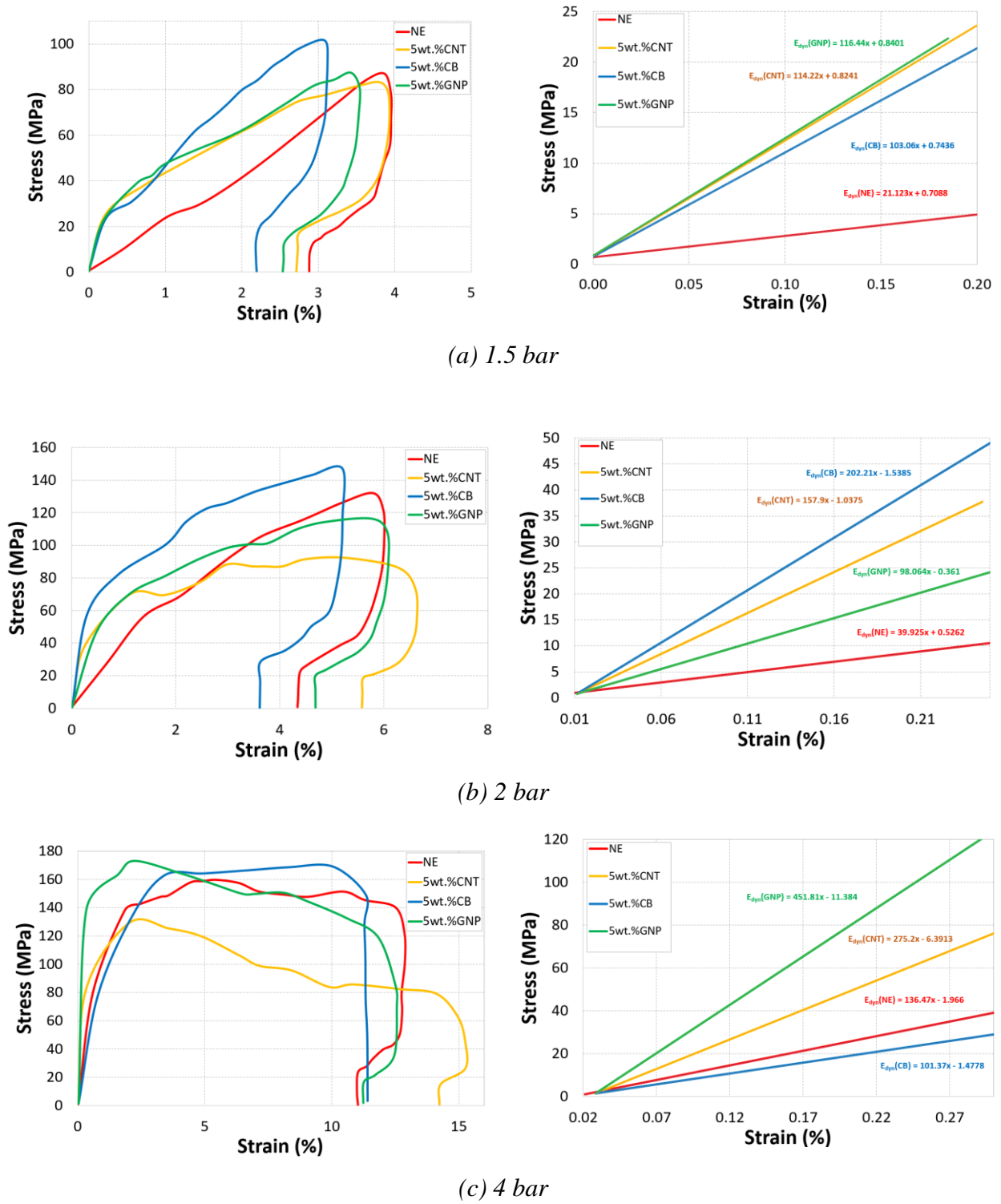


Figure V.24: Stress vs strain curves for neat adhesive and adhesive doped with 5 wt.% nanofillers

Table V.4: Dynamic mechanical parameters for neat adhesive and adhesive doped with nanofillers under 1.5 bar

1.5 BAR	NE	CNTs			GNPs			CBs		
	0	1wt.%	2wt.%	5wt.%	1wt.%	2wt.%	5wt.%	1wt.%	2wt.%	5wt.%
Dynamic Modulus E(MPa) at 0.15% Strain	3.88	19.75	14.87	17.96	12.09	16.71	18.31	17.59	20.37	16.20
<i>Percentage of progress (%)</i>	-	409.3	283.5	363.	211.	330.8	372.1	353.7	425.2	317.8
Strength (MPa)	87.01	97.29	89.77	83.14	95.07	89.78	87.36	102.32	91.18	101.78
<i>Percentage of progress (%)</i>	-	11.8	3.18	-4.44	9.27	3.19	0.41	17.60	4.79	16.97
Plastic Elongation (%)	2.88	2.04	2.54	2.71	2.26	2.28	2.53	2.15	1.76	2.19
<i>Percentage of progress (%)</i>	-	29.17	11.8	5.90	21.5	20.83	12.15	25.35	38.89	23.96
2nd Strain rate Peak (s^{-1})	201.54	158.36	175.98	222.42	168.74	168.65	194.10	164.93	130.41	145.64
<i>Percentage of progress (%)</i>	-	21.43	12.68	-10.36	16.27	16.32	3.69	18.17	35.29	27.74

Table V.5: Dynamic mechanical parameters for neat adhesive and adhesive doped with nanofillers under 2 bar

2 BAR	NE	CNTs			GNPs			CBs		
	0	1wt.%	2wt.%	5wt.%	1wt.%	2wt.%	5wt.%	1wt.%	2wt.%	5wt.%
Dynamic Modulus E(MPa) at 0.15% Strain	6.51	20.59	20.59	22.65	19.58	17.75	14.35	26.58	18	28.79
<i>Percentage of progress (%)</i>	-	216.0	216.0	247.6	200.4	172.40	120.24	307.92	176.21	341.95
Strength (MPa)	132.08	136.23	124.30	92.34	132.45	122.01	116.26	141.13	136.00	147.29
<i>Percentage of progress (%)</i>	-	3.14	-5.89	-30.09	0.29	-7.62	-11.97	6.86	2.97	11.52
Plastic Elongation (%)	4.34	3.33	3.99	5.58	3.86	4.32	4.69	3.70	4.05	3.62
<i>Percentage of progress (%)</i>	-	23.27	8.06	-28.57	11.06	0.46	-8.06	14.75	6.68	16.59
2nd Strain rate Peak (s ⁻¹)	340.16	284.81	320.77	436.58	321.96	347.61	360.71	302.70	320.69	287.98
<i>Percentage of progress (%)</i>	-	16.27	5.70	-28.35	5.35	-2.19	-6.04	11.01	5.72	15.34

Table V.6: Dynamic mechanical parameters for neat adhesive and adhesive doped with nanofillers under 4 bar

4 BAR	NE	CNTs			GNPs			CBs		
	0	1wt.%	2wt.%	5wt.%	1wt.%	2wt.%	5wt.%	1wt.%	2wt.%	5wt.%
Dynamic Modulus E(MPa) at 0.15% Strain	18.50	26.89	20.21	34.89	44.07	46.95	56.39	42.41	59.84	13.73
<i>Percentage of progress (%)</i>	-	45.34	9.23	88.54	138.1	153.71	204.72	129.21	223.37	-25.81
Strength (MPa)	159.82	163.99	124.30	130.54	177.37	122.01	173.04	194.92	136.00	168.98
<i>Percentage of progress (%)</i>	-	2.61	-0.22	-18.32	10.98	15.31	8.28	21.97	22.28	5.73
Plastic Elongation (%)	11.03	12.00	12.66	14.24	9.99	11.39	11.24	10.46	9.85	11.41
<i>Percentage of progress (%)</i>	-	-8.79	-14.78	-29.10	9.43	-3.26	-1.90	5.17	10.70	-3.45
2nd Strain rate Peak (s ⁻¹)	886.71	956.82	1014.78	1100.99	810.34	924.87	911.97	871.22	822.84	791.705
<i>Percentage of progress (%)</i>	-	-7.91	-14.44	-24.17	8.61	-4.30	-2.85	1.75	7.20	10.71

V.5 Conclusion

The damping characteristics of DGEBA adhesive, CNTs/DGEBA, GNPs/DGEBA, and CBs/DGEBA nanocomposites at different impact pressures are measured using the Split Hopkinson Pressure Bar (SHPB) in this research.

These properties are determined for DGEBA adhesive nanocomposite impregnated with various mass fractions of nanofillers and compared to those of neat DGEBA adhesive at impact pressures ranging from 1.5bar to 4bar. The test specimens' time-domain stress and strain characteristics are calculated using measurements of the incident, reflected, and transmitted, straining a Split Hopkinson Pressure Bar. Reinforced DGEBA adhesive nanocomposites are highly affected by high impact pressure, although with different increments that depend on the nanofillers nature. Furthermore, high mass fraction influences the structure morphology where at high impact pressure, the mechanical behavior tends to get plastic behavior with important elongation compared to neat DGEBA adhesive. Also, some specific conclusions are drawn from the application of several impact pressures to the loading of these materials are presented below.

Reinforced DGEBA nanocomposites:

- Increasing impact pressure generates thermal softening in the polymeric material. The adhesive plasticity and failure modes in the polymeric material under impact could cause this thermal softening. These discoveries supported the theory that the internal heat created upon impact in unreinforced and reinforced nanocomposite materials was due only to the polymeric matrix's viscoplastic behavior and failure process.
- The dynamic modulus values generally show significant, positive progress, including nanofillers with low impact pressure, whereas 1 wt.% CNTs/DGEBA shows the highest progress at 409.3%. However, in comparison to the higher impact pressures, 2wt.%

CBs/DGEBA demonstrate significant progress at 223.37%. Next in the ranking is 1wt.% CNT, which aims to enhance the DGEBA adhesive nanocomposite structure.

- The strength increases with increasing mass fraction and increasing impact pressure for CBs/DGEBA and GNPs/DGEBA; however, with CNTs/DGEBA it is reported to degrade until it becomes weaker than the neat DGEBA adhesive. This deprivation is affected by the essential quantities of the porosities presented belonging to the specimen. 5wt.% CNTs at high impact pressure 4bar generate a drop of -18.32% compared to neat DGEBA nanocomposite. At the same time, 5wt.% CBs at 4bar generate progress of 5.73% and 22.28% for 2wt.% CB.
- The appearance of a second peak over the strain rate vs. time indicates the presence of micro/macro damage. What may be more significant with this peak is the degradation of the reinforced nanocomposite. In this context, at low impact pressure, 1wt.% CNTs lead to a decrease in the strain rate of the DGEBA adhesive by 409.3%, evidencing the importance values compared to CBs/DGEBA and GNPs/DGEBA. However, at high impact pressure, 2wt.% CB generates less strain rate in the specimen compared to CNTs/DGEBA and GNPs/DGEBA nanocomposites, and following this is 1wt.% CNT.

Chapter VI:

Fracture resistance of a nanofiller- doped adhesive for bonded joints

VI. Fracture resistance of a nanofiller-doped adhesive for bonded joints

Summary

VI. Fracture resistance of a nanofiller-doped adhesive for a bonded joints 230

VI.1	Introduction	232
VI.2	Surfaces treatments	233
VI.3	Experimental procedure	236
VI.4	Analytical calculation of Strain energy release rate for Mode I (G_I)	237
VI.4.1	MBT 1 (Modified Beam Theory 1)	237
VI.4.2	MBT 2 (Modified Beam Theory 2)	238
VI.4.3	CBBM (Compliance Based Beam Method)	238
VI.4.4	CC (Compliance Calibration Method)	239
VI.5	Analytical calculation of Strain energy release rate for Mode II (G_{II})	239
VI.5.1	Simple Beam theory (SBT)	239
VI.5.2	Timoshenko Beam Theory (TBT)	240
VI.6	DCB Testing	241
VI.6.1	DCB Test Samples	241
VI.6.2	DCB test results	243
VI.6.3	Bonded joints with neat DGEBA adhesive	244
VI.6.4	Graphene nanoplatelets (GNP) reinforced adhesive for bonded joints	246
VI.6.5	Carbon nanotubes (CNT) reinforced adhesive for bonded joints	248
VI.6.6	Fracture surface analysis	252
VI.6.6.1	Fracture surface analysis of CNT reinforced adhesive for bonded joint	256
VI.6.6.2	Fracture surface analysis of GNP reinforced adhesive for bonded joint	259

Chapter VI: Fracture Resistance of a nanofiller-doped adhesive for a bonded joint

VI.6.6.3	Comparative analysis of the surface roughness parameters	261
VI.7	ENF Testing.....	262
VI.7.1	ENF Test Samples	262
VI.7.2	Experiment results.....	264
VI.7.3	Comparative analysis	270
VI.8	Numerical investigation using cohesive zone models.....	274
VI.8.1	Modeling	275
VI.8.2	Conclusion.....	283

VI.1 Introduction

Adhesively-bonded joints (ABJs) are utilized extensively in various industries, including the aerospace, automotive, and naval sectors. When compared to traditional mechanical fastener joints, ABJs offer numerous benefits. Adhesive bonding allows designers to create high-resistance joints which can withstand exhaustion loads and mechanical vibrations, as well as joints that are lightweight, low in cost, and featuring better stress distribution [339], [340]. However, ABJs do have some drawbacks, such as low temperature and humidity resistance, extended curing times in some adhesives, and the necessity for surface preparation. Researchers have suggested many strategies for improving the mechanical, electrical, and thermal properties of ABJs and composite materials, including adding micro and nanoparticles to the adhesive layer and composite matrix [128], [164], [244], [301], [341]. Zhai et al. [142], [342] improved the adhesion strength between the epoxy adhesive and the steel substrate by adding alumina nanoparticles to the epoxy adhesive. They discovered that adding 2wt.% alumina nanoparticles boosted interfacial adhesion and improved adhesion strength to a maximum. May et al. [343] investigated the strengths of single lap and butt joints using multi-walled carbon nanotubes and alumina nanoparticles in the epoxy/sol-gel adhesive at weight percentages of 0.05 and 0.71, respectively. According to the results, the introduction of these nanoparticles considerably raised the strength of adhesive connections and improved wettability on substrate surfaces. Wood et al. [344] evaluated the shear strength of overlapping glass seams after adding silica SNPs to the adhesive layer. They discovered that 0.5 wt.% of these nanoparticles in the adhesive layer significantly improved shear bond strength and interfacial adhesion. To continue on the topic of material fracture resistance, the resistance of bonded and sandwich structures will be explored. As a pertinent example, adhesives are used to attach wind turbine blades, as they are with other composite structures. They're made up of various separate components that are subsequently put together with the help of adhesives. It should be noted that, according to the

quality of manufacture, adhesive thicknesses vary from position to position in the case of environmental variables [345].

This chapter aims to see how adding nanoparticles to the adhesive layer affects the mechanical tensile and shear strength, as well as the elongation at adhesively-bonded joints failure. Two distinct toughening particles were considered for reinforcing the adhesive joints: carbon nanotubes (CNTs) and graphene (GNPs). In this study, bonded samples were formed for a bonded aluminum joint using adhesives mentioned in the previous sections and bonded composite joint with the same kind of adhesives. The surfaces of the substrates must be prepared carefully to ensure proper and correct bonding between substrates and the adhesive. This study also intends to examine the influence of substrate material contact with the reinforced adhesive. According to the fractography results, the experimental results showed that the addition of nanoparticles enhanced the failure mode from adhesive to dominant cohesive, indicating improved adhesion between the adhesive and adherents.

Furthermore, different damage mechanisms for adhesives supplemented with different toughening particles were discovered. Several researchers have proven several mechanisms, including crack development deviation, shear yielding, plastic deformation, and pull-out phenomena on the fracture surfaces of joint-reinforced with CNTs. In the instance of GNP-reinforcement, the appropriate energy-absorbing mechanisms were determined to be tensile/shear yielding, particle debonding, and subsequent void formation[346].

VI.2 Surfaces treatments

First, in the following steps, surface treatment is performed on the aluminum plate and the composite plate, where their properties are mentioned in Tables VI.1 and VI.2. Figure VI.1 shows the characterization steps of aluminum, as follows:

1. Degreasing the aluminum plate with acetone
2. Degreasing in a degreasing bath at 50°C for 15 minutes, in a water- and alkaline-based degreasing agent solution

3. Rinsing with distilled water for 5 minutes
4. Chemical stripping in a sulfuric acid bath at 52°C for 30 minutes
5. Rinsing with distilled water for 15 minutes

Figure 2 shows the characteristic steps of the composite adherent surface treatment, where:

1. Degreasing with IPA.
2. Polishing with P120 sandpaper.
3. Use of IPA for degreasing.

Table VI.1: Composite properties

$E_{11}=E_{22}$ (MPa)	E_{33} (MPa)	G_{12} (MPa)	$G_{13}=G_{23}$ (MPa)	ν_{12}	$\nu_{13}= \nu_{23}$
16022	11920	10327	3752	0.46	0.22

Table VI.2: Aluminum properties

E (MPa)	ν
70000	0.3

Finally, aluminum and composite materials' bonding joints are carefully prepared, as presented in Figure VI.3 and Figure VI.4. The main steps of this preparation are as follows:

1. Positioning PTFE tape (0.25μm thick gasket).
2. Inserting the board into the mold.
3. Applying adhesive on the surface with tape (unreinforced and reinforced).
4. Double-adhesive.
5. Buttoning the opposite side.
6. Pressing at least 20kN pressure for 16 hours.
7. Completing the polymerization reaction in an oven at 120°C for 1 hour.

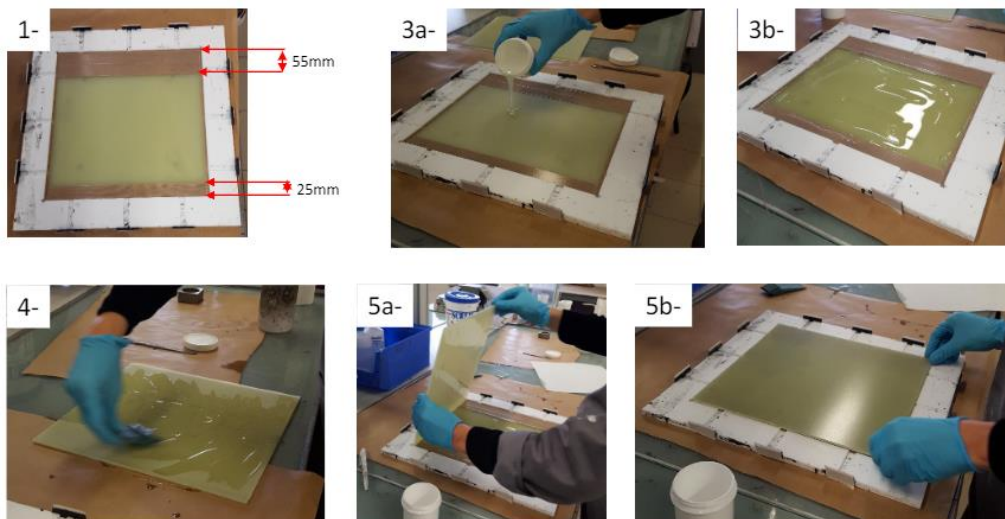
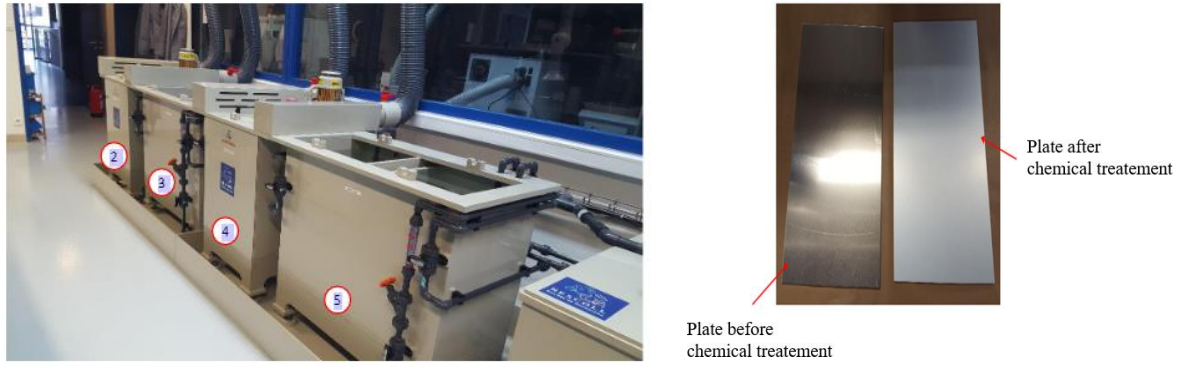


Figure VI.3: Manufacture of composite/composite bonded joints

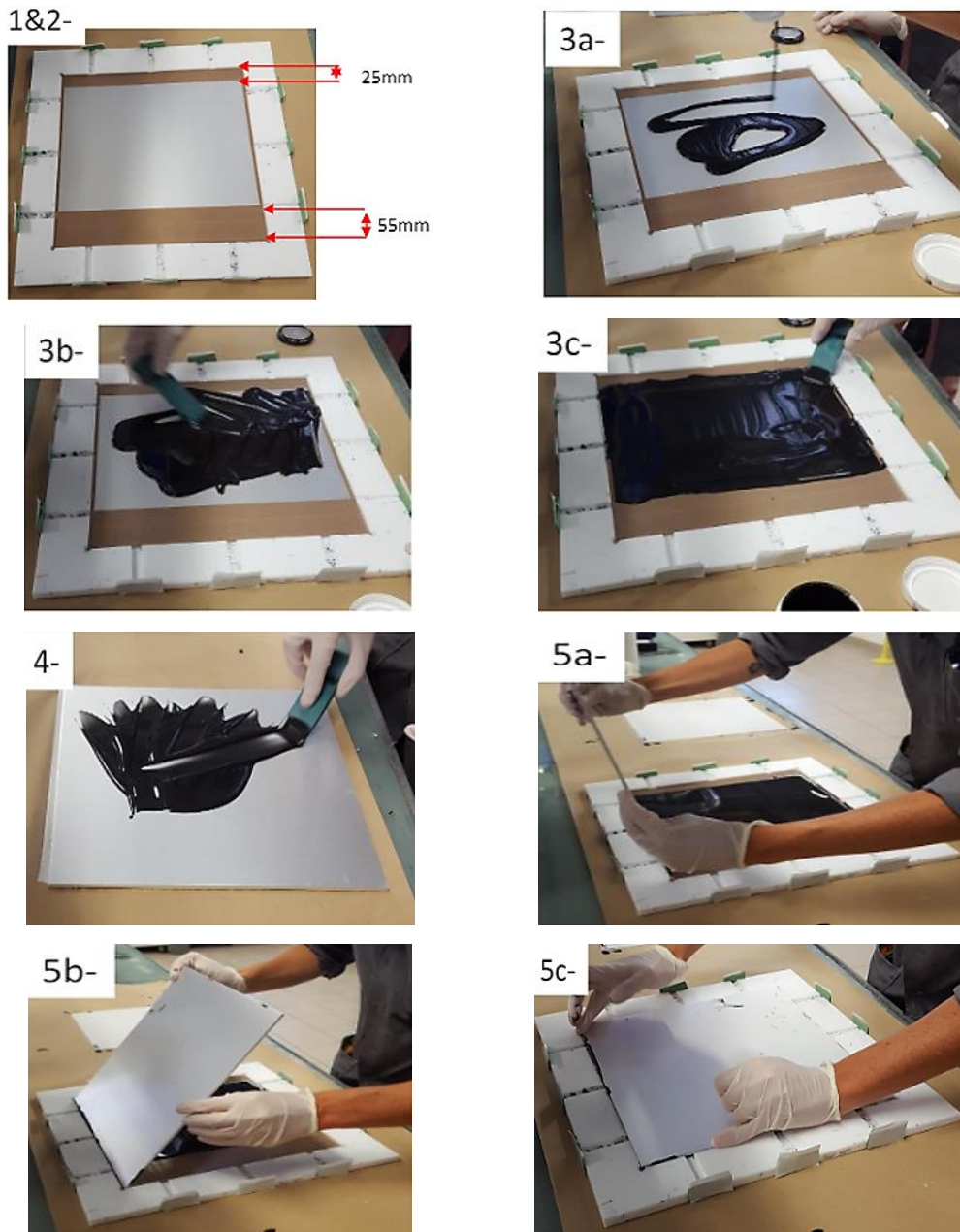


Figure VI.4: Manufacture of bonded aluminum/aluminum joints

VI.3 Experimental procedure

The following sections of the study will account for the many tests used to define the interlaminar resistance of bonded joints. These experiments are based on linear elastic fracture mechanics and call for the expression of a critical energy release rate in conjunction with the initiation and propagation of a crack in a bonded joints medium. According to certain studies,

the propagation of cracks in materials presents a combination of three modes: opening mode (Mode I), translational sliding (Mode II), and rotational sliding (Mode III), Figure VI.5. As a result, modes I, II, and III define the resistance to crack propagation [347].

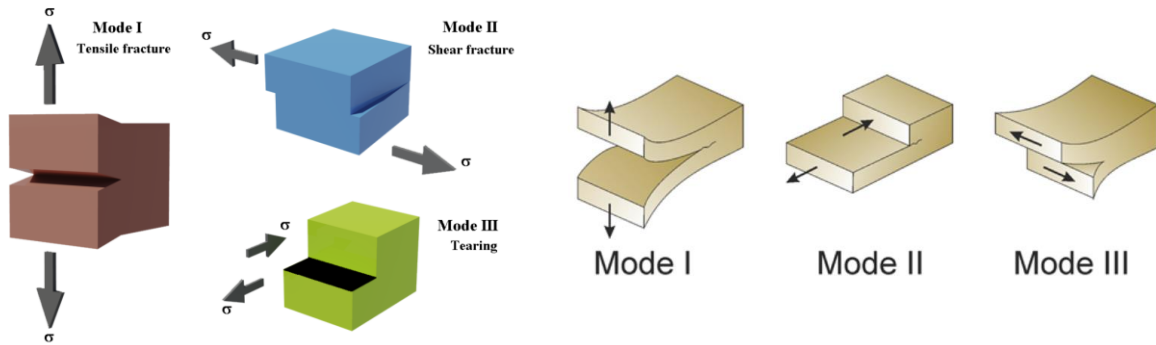


Figure VI.5: Modes of crack propagation in the material

VI.4 Analytical calculation of strain energy release rate for Mode I (G_I)

Different analytical methodologies have been formulated to calculate the strain energy release rate “ G_I ” in mode I based on beam theory.

VI.4.1 MBT 1 (Modified Beam Theory 1)

Based on the Timoshenko beam theory, the modified beam theory represents the DCB specimen as a simple cantilever beam:

$$G_I = \frac{3P\delta}{2ba} \quad (1)$$

Where “P” denotes the load required to produce a “ δ ” displacement, “b” denotes the specimen width, and “a” denotes the crack length. The G_I is calculated using this hypothesis, which takes into account the cracked beam's compliance. This fundamental law is simple to apply, but it can be erroneous on occasion.

VI.4.2 MBT 2 (Modified Beam Theory 2)

The Modified Beam Theory 2 takes into consideration the rotation of the crack front and the partially cracked interface.

$$G_I = \frac{3P\delta}{2b(a + |\Delta|)} \quad (2)$$

The rotation of the crack tip is taken into account in this theory. Also, because the DCB specimens endured considerable displacements to propagate the fracture during the trials, a correction factor should be incorporated to account for the turning effects of the U blocks.

$$N = 1 - \left(\frac{l_2}{a}\right)^3 - \frac{9}{8} \left[1 - \left(\frac{l_2}{a}\right)^2\right] \frac{l_1\delta}{a^2} - \frac{9}{35} \left(\frac{\delta}{a}\right)^2 \quad (3)$$

$$F = 1 - \frac{3}{10} \left(\frac{\delta}{a}\right)^2 - \frac{3}{2} \left(\frac{l_1\delta}{a^2}\right) \quad (4)$$

Where “P” denotes the applied force, “δ” is the displacement of the two beams, “b” is the specimen width, “a” is the crack length, “Δ” is the crack front rotation correction factor, “l₁” is the distance between the loading pin and the specimen midplane, and “l₂” is the distance between the center of the pin and the end of the U-block.

VI.4.3 CBBM (Compliance Based Beam Method)

The apparent crack length is used to formulate this approach. The changed flexural rigidity of the beam specimen is considered here:

$$\bar{E}_f = \frac{8(a_0 + |\Delta|)^3}{bh^3} \left(C_0 - \frac{12(a_0 + |\Delta|)}{5bhG_{xy}} \right) \quad (5)$$

As a result, the value of G_I can be determined as follows.

$$G_I = \frac{6P^2}{b^2h} \left(\frac{2}{\bar{E}_f} \left(\frac{a_e}{h}\right)^2 + \frac{1}{5G_{xy}} \right) \quad (6)$$

$$a_e = a_0 + |\Delta| \quad (7)$$

This approach has the benefit of not requiring the crack length to be monitored as it propagates through the specimen.

VI.4.4 CC (Compliance Calibration Method)

The compliance calibration method considers the crack beam to be a function of compliance.

$$G_I = \frac{nP^2 R a^{n-1}}{2b} \quad (8)$$

Where "R" is the anti-natural log of the intersection of "Ln(C)" and "Ln(a)" plots.

VI.5 Analytical calculation of Strain energy release rate for Mode II (G_{II})

Different analytical methodologies have been formulated to determine the strain energy release rate in mode II "G_{II}" based on beam theory.

VI.5.1 Simple Beam Theory (SBT)

Simple beam theory (SBT) is one of the most common methods used to analyze ENF test results. Assuming that the adhesive layer is rigid, the specimen compliance, C, can be calculated using the following expression [348]:

$$C = \frac{\delta}{P} = \frac{3a^3 + 2L^3}{8Bh^3E} \quad (9)$$

δ denotes the applied displacement at the loading point, P the load, "a" the crack length, L the half span length, B the sample width, h the adherent thickness, and E the elastic modulus of the adherend. The effective crack length " a_e ", which was estimated as follows, was substituted for an in Eq. (9):

$$a_e = \left[\frac{8\delta B h^3 E}{3P} - \frac{2}{3} L^3 \right]^{\frac{1}{3}} \quad (10)$$

The Irwin-Keis relation in linear elastic fracture mechanics (LEFM) can then be used to calculate the mode II fracture toughness as follows:

$$G_{II} = \frac{P^2}{2B} \frac{dC}{da} \quad (11)$$

Substituting Eq. (9) into Eq. (11) yields the following direct relationship between G_{II} and a_e :

$$G_{II} = \frac{9P^2 a_e^2}{16B^2 h^3 E} \quad (12)$$

Whereby E was replaced by E_{11} for the composite adherend.

VI.5.2 Timoshenko Beam Theory (TBT)

The specimen compliance in TBT is estimated using the expression [30]:

$$C = \frac{\delta}{P} = \frac{3a^3 + 2L^3}{8Bh^3 E_f} + \frac{3L}{10G_{23}Bh} \quad (13)$$

The adherent flexural modulus is G_{23} , while the equivalent flexural modulus is E_f . E_f is utilized instead of E_{11} in Eq. (13) to account for the adhesive layer's effect, as well as the stress concentration at the crack tip and the contact between two adherents. E_f maybe determined using Eq. (13) by substituting the initial crack length " a_0 " and initial compliance C_0 estimated at the beginning of the loading process, resulting in:

$$E_f = \frac{3a_0^3 + 2L^3}{8Bh^3} \left(C_0 - \frac{3L}{10G_{13}Bh} \right)^{-1} \quad (14)$$

Eq. (13) was used to calculate " a_0 ". Eq. (14) can be stated as a function of specimen compliance if E_f is considered:

$$a_e = \left[\frac{C_c}{C_{0c}} a_0^3 + \frac{2}{3} \left(\frac{C_c}{C_{0c}} - 1 \right) L^3 \right]^{\frac{1}{3}} \quad (15)$$

$$C_c = C - \frac{3L}{10G_{13}Bh} \quad (16)$$

$$C_{0c} = C_0 - \frac{3L}{10G_{13}Bh} \quad (17)$$

Accounting for the Irwin-Keis relation, Eq.(11), the relation between G_{II} and " a_e " can be expressed as:

$$G_{II} = \frac{9P^2 a_e^2}{16B^2 h^3 E_f} \quad (18)$$

VI.6 DCB Testing

VI.6.1 DCB Test Samples

In this section, aluminum bonded joints and composite bonded joints are used. The geometry of samples, as well as the experimental procedure, adhere to ASTM recommendations. The pre-crack is carried out with the use of a 25 μ m thickness Teflon film. The dimensions of the used specimen are provided in Figure VI.6.

A double cantilever beam (DCB) was performed to measure the Mode I interlaminar fracture toughness of reinforced bonded joints of aluminum and composite adherents. The configuration of the DCB specimen is shown in Figure VI.6. The INSTRON machine used for Mode I testing is shown in Figure VI.7. DCB tests are, as a rule, performed to obtain data on the resistance to crack propagation in mode I. This resistance is characterized by the critical energy release rate G_{Ic} . The DCB samples measure 4 mm in thickness, 20 mm in width and mm in length. A thin Teflon film is used to pre-crack the mid-plane of the substrate. The pre-crack's starting length is a_0 , Figure VI.6.

Following the TARFAOUI studies [349]–[351], it is no longer possible to propagate a crack using a typical DCB. In the case of composites, the rupture occurs at the level of the stratified upper limb. We proposed that two steel plaques be attached to the different plates on the two lips of the DCB to increase the flexion module of the arms, as shown in Figure VI.6.

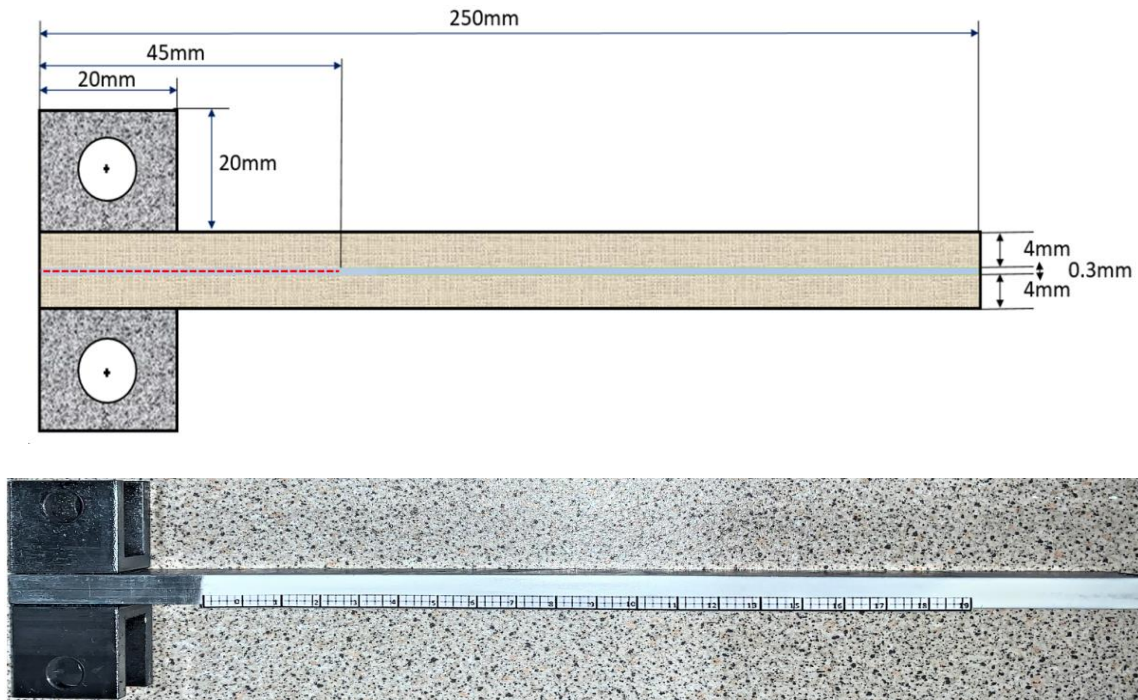


Figure VI.6: Dimensions of double cantilever beam (DCB) specimen, Mode I

As it is shown in Figure VI.7, a uniaxial testing framework attached to an INSTRON 50 kN max load testing machine is operated in displacement control mode, the crosshead speed is 1mm/min, and a computer-based information acquisition framework is utilized. The break tip movement is observed by exposing the specimen's side to a white rectification liquid, and it is then labeled at 1 mm intervals with a thin edge. During the test, the load vs displacement curve is controlled, and the break lengths are obstinately measured with an advanced RETIGA Camera.

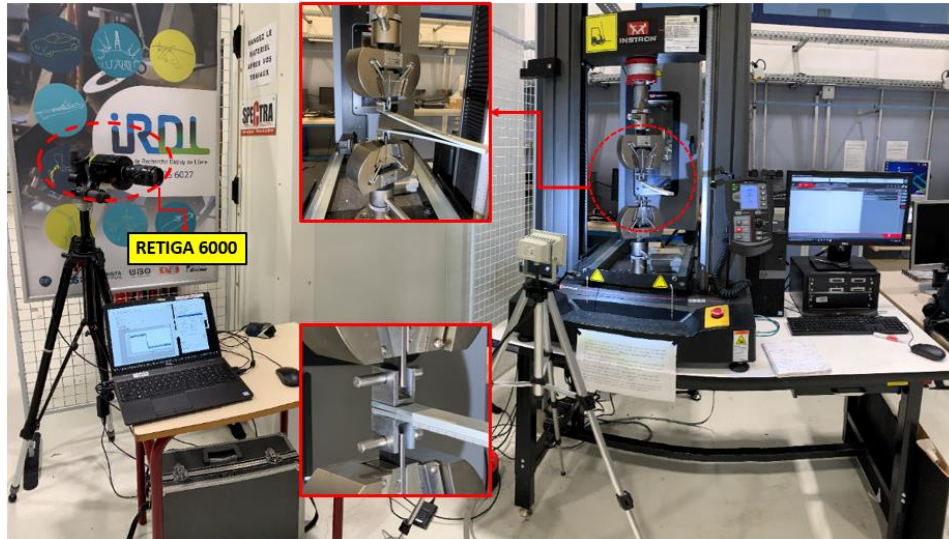


Figure VI.7: Mode I test with DCB specimen using INSTRON machine

VI.6.2 DCB test results

In this section, the details of the Mode I DCB testing, cited in Figure VI.8, will be discussed. As shown in Figure VI.9, the force-displacement curve depicts the fracture opening as photographed at each step along its propagation using a Retiga camera.

Cracking tests in Mode I are used to demonstrating the effect of a localized adhesion defect on the bonded joint resistance. The samples are shattered by force and then a stable decohesion is propagated by performing a DCB test with a 1mm/min constant opening speed.

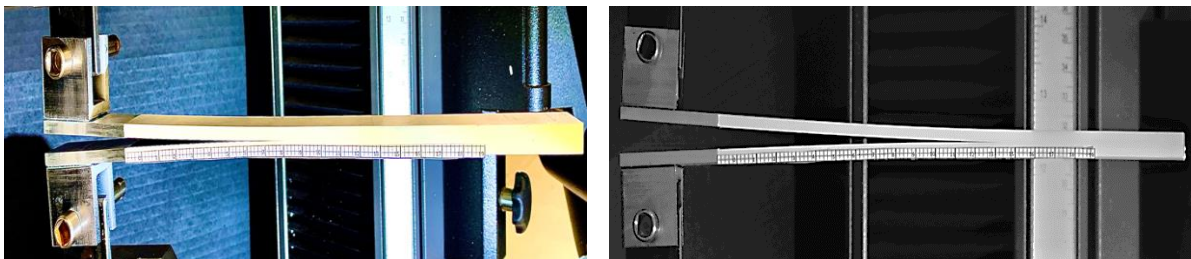
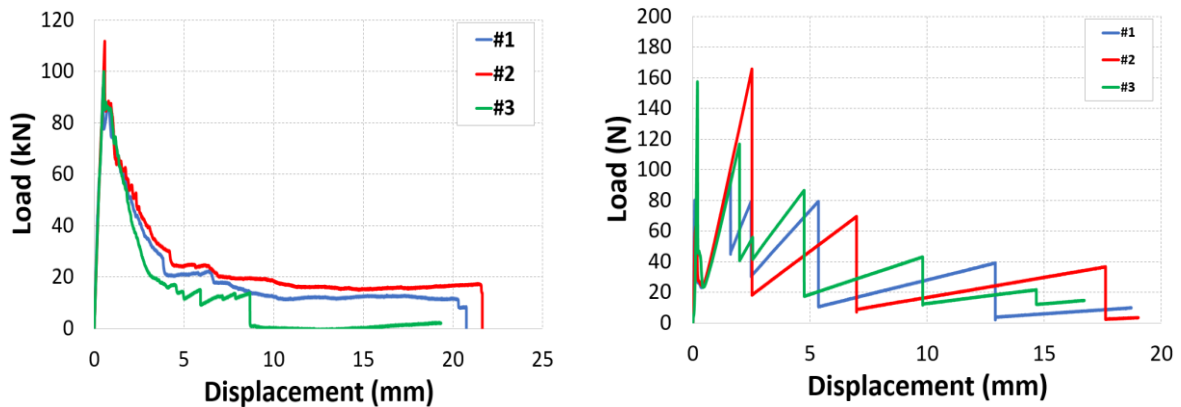


Figure VI.8: Crack propagation in a bonded joint (DCB - Mode I)

VI.6.3 Bonded joints with neat DGEBA adhesive

The experimental data is depicted in Figure VI.9 as the evolution of the applied force as a function of the opening of the imposed specimen. The energy release rate G for test pieces with different types of loaded adhesive can be calculated in terms of crack length measurements using force vs displacement curves. In this study, the energy release rate was calculated using Modified Beam Theory 1 MBT1. The reproducibility of these tests varies from specimen to specimen, as demonstrated in Figure VI.9, which depicts the reproducibility of neat DGEBA adhesive-bonded aluminum and composite joints.



(a) Aluminum/Aluminum bonded joints

(b) Composite/Composite bonded joints

Figure VI.9: Force-displacement curves of bonded joints with neat DGEBA adhesive

In Figure VI.9, the behavior of adhesive seems with weak elastic characteristics. It corresponds to a fragile elastic behavior of the adhesive. The force vs displacement response is linear during the loading phase. In the curves of adhesive bonding aluminum joints, as it is in Figure VI.9-a, the load drop is relatively "smooth", which means that the material performance gradually declines. In the first stage, the slope of the curve and the behavior of the material are linear. In the second stage, a loss of linearity is observed, which typically indicates some irreversible fracture process, such as plastic deformation or failure formation within the interface layer.

Finally, in the third stage, a major load drop was noted, which corresponds to the expansion of the Mode I crack. However, adhesive composite bonded joint as it is in Figure VI.9-b, the curve aspect is a little bit different it is seen that it has a moderate nonlinear zone around the peak force, which generates a significant crack extension as the external force decreases abruptly. As the opening displacement grows, the external force gradually increases until the critical fracture energy release rate value is reached once more. The procedure is repeated a further one or two times, until the specimen is completely separated. As a result, the change in fracture energy release rate (G_I) with equivalent crack length (a) in Figure VI.10 is discontinuous, with each peak indicating the fracture toughness value for Mode I.

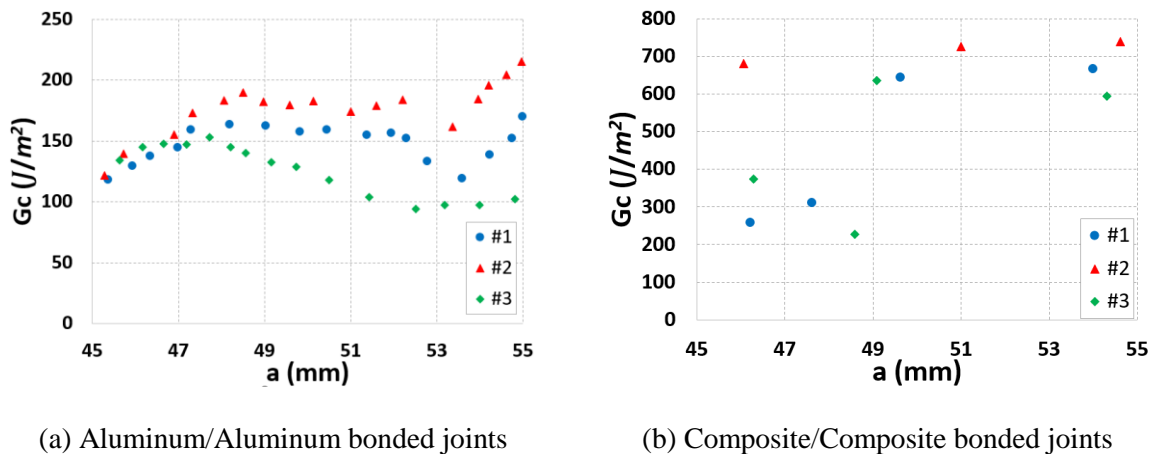


Figure VI.10: Energy release rate G_I based on the crack propagation (R curve) of bonded (a) Aluminum (b) Composite joints with neat DGEBA adhesive

These differences between the curve aspect for adhesively-bonded aluminum joint and composite joint may be due to heterogeneity within the interface and the adhesive degree of interaction of the adherent material. However, the specimens' rupture facies (fracture surface) will help us show the failure mode (cohesive, adhesive, etc.). The final tapering of the DCB test is in the form of an R-curve, on which the evolution of G as a function of the crack propagation is reported. The behavior is again similar to a fragile elastic behavior since the rate of return of

critical energy remains almost constant during the test, modulates some fluctuations associated with the intrinsic variability of the material.

The curves can be divided into two sections to explain these variances in aspect behavior. The first is the bending of the half beam up to the crack's start, and the second is the force development as the crack length grows [346]. The crack initiation with G_{II} is variable for each specimen, as can be shown in Figure VI.10, and this can be attributable to the specimens' rigidity and pre-crack condition. Due to fracture tip quality, the variances at crack initiation rise as the specimen rigidity (shape, length, and surface adhesion). The second half of the curve, which defines the G_{Ic} during the propagation stage, shows little change from specimen to specimen and has the same curvature throughout [346].

VI.6.4 Graphene nanoplatelets (GNP) reinforced adhesive for bonded joints

As shown in the force vs displacement curves for bonded aluminum joints and bonded composite joints, Figure VI.11, the inclusion of graphene nanoplatelets GNPs in the DGEBA adhesive up to 1wt.% considerably enhances joint strength, resulting in a significant increase in the mechanical behavior of the bonded joint [301].

This is compelling evidence that GNPs/ DGEBA adhesive and adherent interfaces increase the intermolecular forces that bond them together. When compared to 1wt.% GNPs, adding 2wt.% GNPs degrades performance, yet it still outperforms neat DGEBA adhesive. This effect can be seen in both adhesively-bonded aluminum joints and adhesively-bonded composite joints.

The Mode I fracture toughness of DCB specimens with neat DGEBA adhesive and varied mass fraction of nanofillers modified adhesive, including 1wt.% GNPs and 2wt.% GNPs is shown in Figures VI.12 and VI.13. The DGEBA adhesive nanocomposite reinforced with 1 wt.% GNPs increased energy release rate by nearly 9 times compared to the neat DGEBA adhesive for

bonded aluminum joints and nearly 2 times for bonded composite joints. However, compared to nanocomposites with 1wt.% GNPs, the Mode I fracture toughness (energy release rate) decreased when the GNPs mass fraction grew, while it is still higher than that of neat DGEBA adhesive. It can be asserted that 1wt.% GNPs are more effective for boosting Mode I fracture toughness than 2wt.% GNPs for both bonded aluminum/aluminum and composite/composite joints. The drop in Mode I fracture toughness as the GNPs content increase was due to GNPs aggregation in the DGEBA adhesive. The enhancement in dispersion stability and the interfacial interaction with adhesive resin also contribute to this development [352].

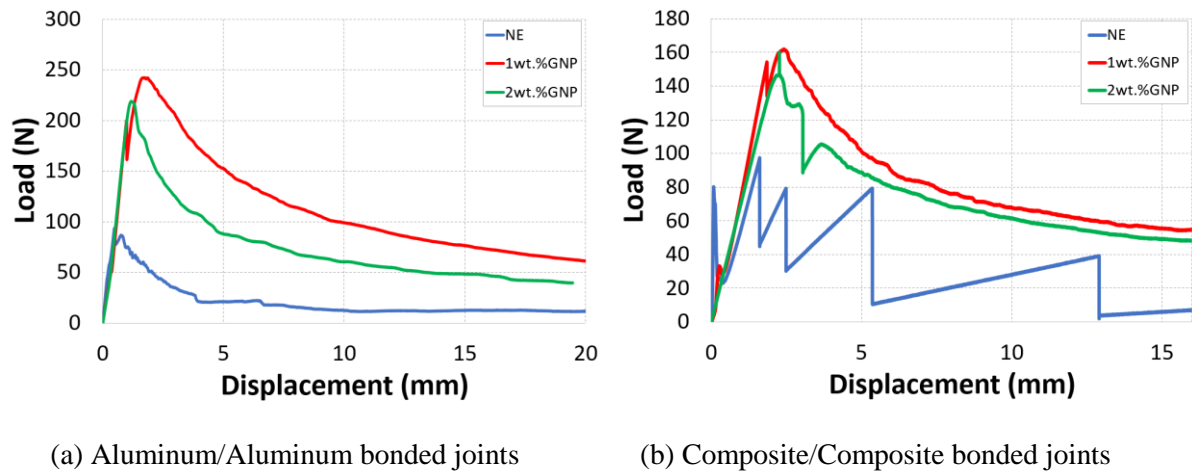


Figure VI.11: Force-displacement curves of bonded joints with DGEBA adhesive doped with 1wt.% and 2wt.% GNPs

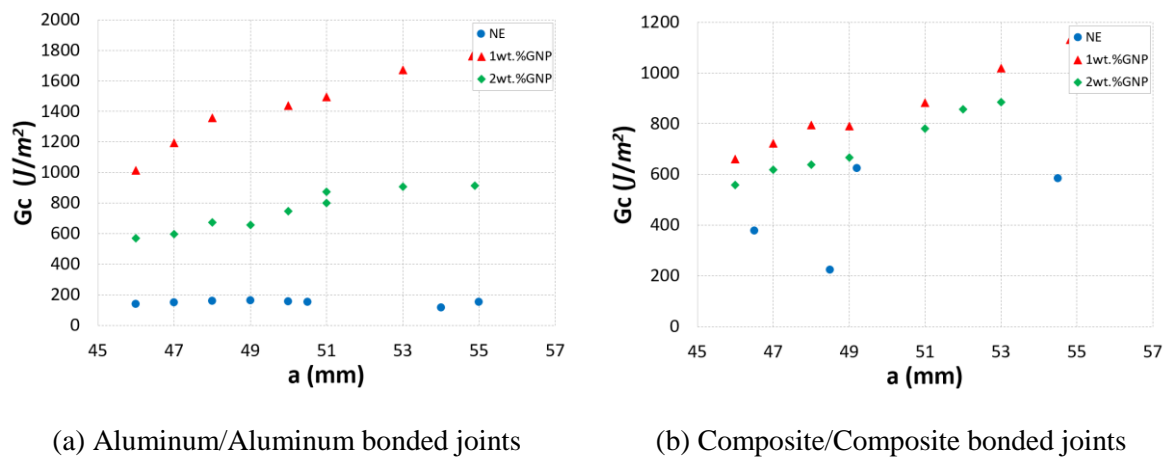
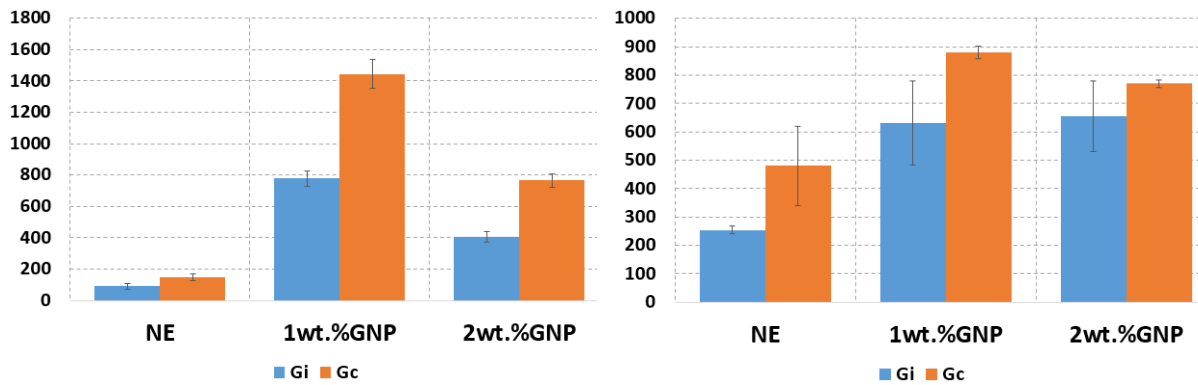


Figure VI.12: Energy release rate G_c based on the crack propagation (R curve) of bonded joints with DGEBA adhesive doped with 1wt.% and 2wt.% GNPs



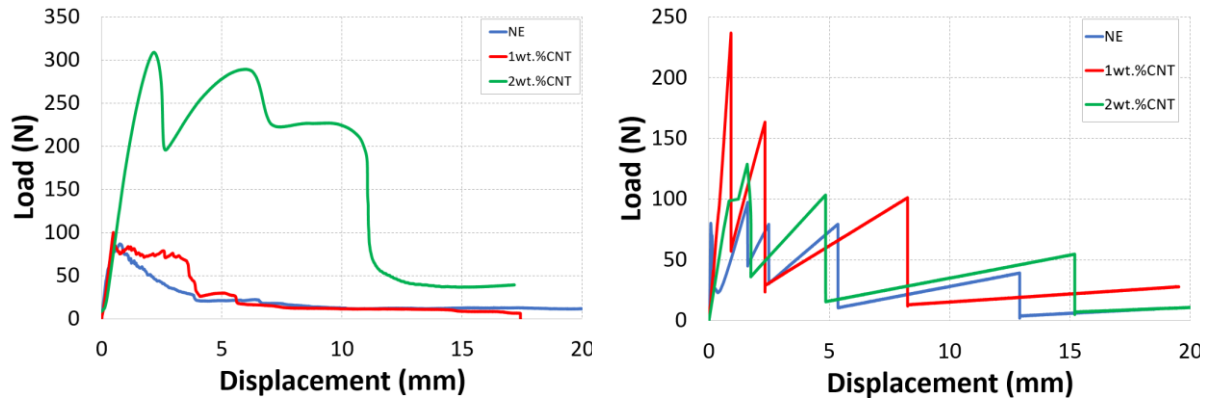
(a) Aluminum/Aluminum bonded joints

(b) Composite/Composite bonded joints

Figure VI.13: Diagram of progress initial and critical Energy release rate (J/m^2) of bonded joint with DGEBA adhesive doped with 1wt.% and 2wt.% GNPs

VI.6.5 Carbon nanotubes (CNT) reinforced adhesive for bonded joints

The force vs displacement curve in Figure VI.14 reveals that up to 2wt.% CNTs in DGEBA adhesive paste significantly enhances bonded aluminum joint strength, resulting in improved bonded joint mechanical behavior. When compared to neat DGEBA bonded composite joints, the tensile strength enhancement is noticeable at up to 1wt.% CNTs, but when raised to 2wt.%, the bonded joints start to degenerate. This behavior is most likely caused by nanofiller aggregation, driven by insufficient nanofiller dispersion in the adhesive formulation. Despite this, a larger nanofiller loading of 2wt.% CNTs aggregates of several millimeters cause significant morphological heterogeneity in the adhesive resin. The lower value of the joint's tensile strength improvement as compared to the expected value can be attributed to this incident.



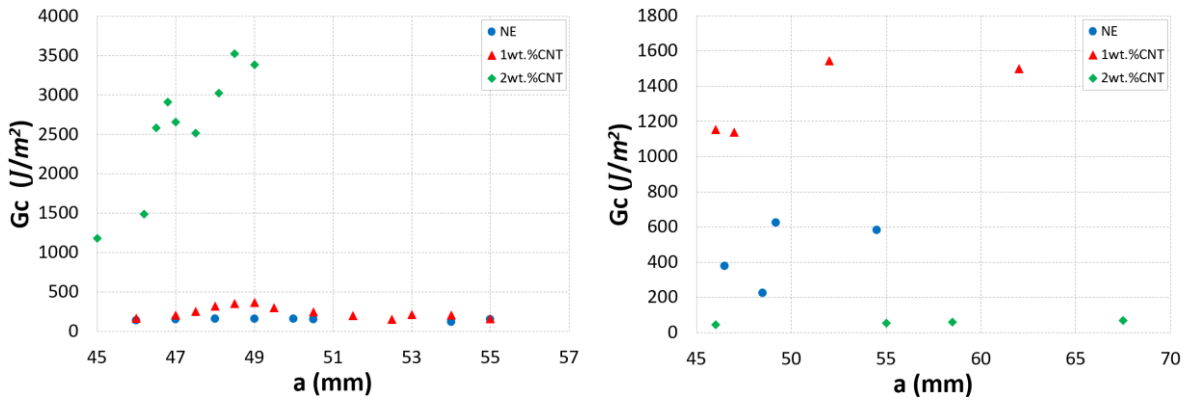
(a) Aluminum/Aluminum bonded joints

(b) Composite/Composite bonded joints

Figure VI.14: Force-displacement curves of bonded joints with DGEBA adhesive doped with 1wt.% and 2wt.% CNTs

When looking at the effect of CNT-reinforcement on energy release rate values, as seen in Figures VI.15 and VI.16, it can be realized that the 2wt.% CNT-reinforced DGEBA adhesive has a much higher prevalence for bonded aluminum joints, but the 1wt.% CNT reinforced DGEBA adhesive has a much higher prevalence for bonded composite joints [267], [268]. As a result, the adhesive's contact with the substrate's materials determines interfacial adhesion. Because the adhesive interacts way with the substrate, the attractive intermolecular interactions are strengthened.

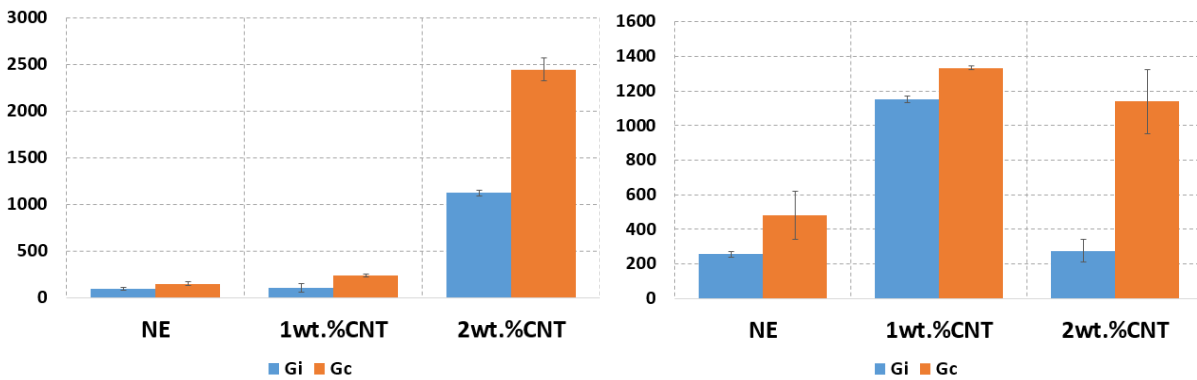
The average Mode I fracture toughness of DCB specimens with neat DGEBA adhesive, reinforced adhesive with 1wt.% CNTs, and 2wt.% CNTs is shown in Figure VI.15. The initial and critical energy release rates are shown in Figure VI.16, with the critical energy release rate appearing to be all the more surprising. When compared to neat DGEBA adhesively-bonded aluminum joint, 2wt.% CNTs enhances fracture toughness the highest. However, in bonded composite joints, 1wt.% CNTs is more effective at improving Mode I fracture toughness than 2wt.% CNTs.



(a) Aluminum/Aluminum bonded joints

(b) Composite/Composite bonded joints

Figure VI.15: Energy release rate G_I based on the crack propagation (R curve) of bonded joints with DGEBA adhesive doped with 1wt.% and 2wt.% CNTs



(a) Aluminum/Aluminum bonded joints

(b) Composite/Composite bonded joints

Figure VI.16: Diagram of progress initial and critical Energy release rate G_I (J/m^2) under DCB bonded joint with CNT-reinforced DGEBA adhesive

The uniform distribution and adhesion between the adhesive matrix and nanoparticles were used to determine the efficiency of the processes mentioned above for CNT-enhanced adhesive joints. When compared to non-reinforced joints, agglomerated particles were detected in composite joint-reinforced with the high mass fraction of CNTs created harmful stress concentration, resulting in a loss in joint strength, especially with the bonded composite joint. The presence of agglomerated particles in a bonded composite joint containing a high mass

percentage of CNTs induced local stress concentration in the adhesive layer, as can be shown in Figure VI.17 . This accelerated the degradation of the adhesive joint layer and reduced the tensile strength of the joint. Furthermore, each nanoparticle's fracture surface on a bonded joint helps in the comprehension of these numerous events.

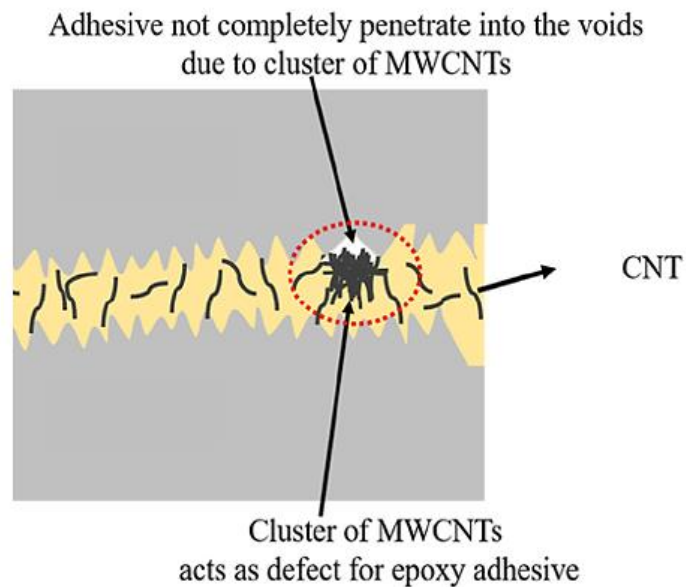


Figure VI.17: Proposed mechanism for the strengthening and toughening of adhesive joints

Table 3 summarizes the degree of progress for each reinforced adhesively-bonded joint compared to the neat adhesively-bonded joint.

Table VI.3: Energy release rate (J/m^2) under adhesive aluminum and composite bonded joints

		Aluminum Bonded Joint		Composite Bonded Joint	
		Gi	Gc	Gi	Gc
NE	Moyenne	89.74	147.59	254.15	479.79
	St-dev	16.29	21.78	15.13	140.23
1wt.% CNT	Moyenne	102.35	236.05	1149.69	1333.42
	St-dev	21.40	13.17	18.64	10.11
	Progress	x 1.14	x 1.59	x 4.52	x 2.77
2wt.% CNT	Moyenne	1120.63	2449.60	274.44	1138.88
	St-dev	18.11	125.54	65.15	184.14
	Progress	x 12.48	x 16.59	x 1.07	x 2.37
1wt.% GNP	Moyenne	776.90	1444.63	630.35	880.57
	St-dev	46.98	90.48	149.03	22.01
	Progress	x 8.65	x 9.78	x 2.48	x 1.83
2wt.% GNP	Moyenne	405.63	764.38	654.38	769.04
	St-dev	35.31	42.28	125.67	12.29
	Progress	x 4.52	x 5.17	x 2.57	x 1.60

VI.6.6 Fracture surface analysis

Understanding the failure mechanism of adhesive connections is critical for improving bonding strength; the Mode I test can, under DCB samples, provide this information as well as durability behavior.

Several revisions for adhesives made of polymer materials have been exhibited. However, the fundamentals of adhesion processes are still poorly understood or under-developed, and there

is no single, global methodology or theory to describe all adhesion phenomena or mechanisms in detail [1], [2] [3]. Despite the common use of adhesives, significant contention surrounds the concept of the bond. There are six fundamental systems or mechanisms (or theories) that can clarify the bonding procedure, and each is especially useful in understanding some of the phenomena or mechanisms involved in bonding [4]. The theories are as follows [2], [5]–[7]: (a) Mechanical interlocking theory, (b) Electronic theory or electrostatic theory, (c) Weak boundary layer theory, (d) Adsorption theory, (e) Diffusion or inter-diffusion theory, (f) Chemical bonding theory.

The mechanical interlocking theory is one of the most powerful models, as seen in the surface preparation section of this section or as discussed in detail below. One of the weaker models is the electrostatic theory, which is related to molecular attraction. The most desirable models for high strength bonding are adsorption and diffusion theories. Chemical bonding theory can be realized through bonding with polymer or polymer matrix composite materials.

According to the mechanical interlocking model or theory, which is the oldest and most widely accepted theory, adhesion is the mechanical key of the adhesive into the surface irregularities on the adherents (see Figure VI.18) [7], [8]. As a result, the means of surface treatment play an important role in the strength of the bonded structures.

Where the used chemical treatment during the surface adherent treatment creates a porous structure on the surface adherent for mechanical interlocking and provides a larger adhesion area with improved surface wettability. The wettability of the adhesive on the adherent (composite or aluminum, etc.) is a significant factor for the strength of joints, as presented briefly in Figure VI.19.

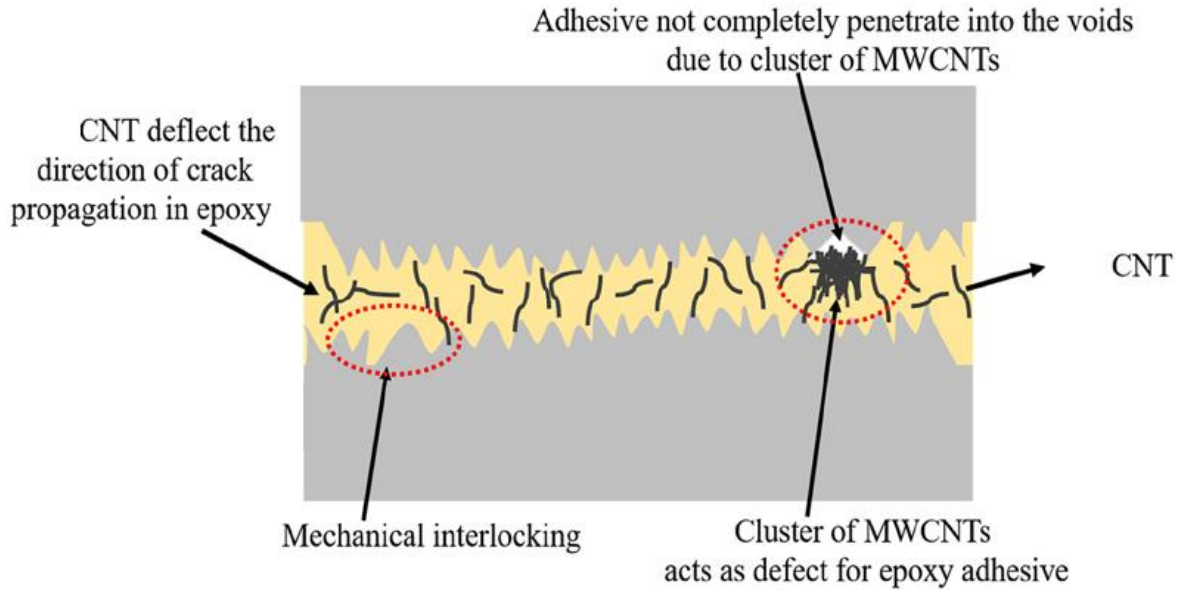


Figure VI.18: Adhesive joint interaction with adherent materials at a high mass fraction of reinforced nanofillers

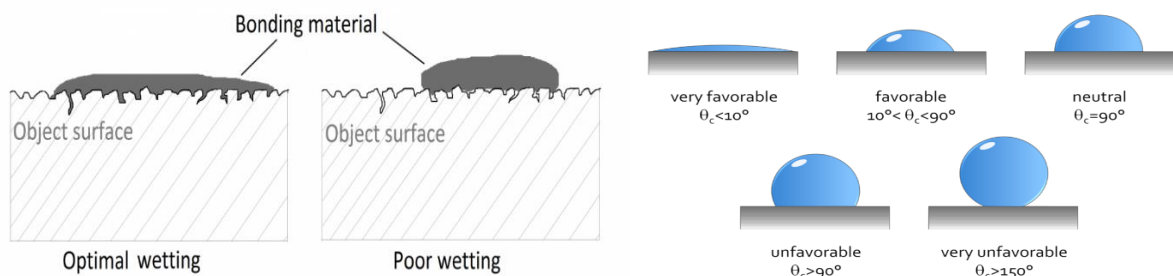


Figure VI.19: Wetting of the surface

In this mechanical interlocking theory, a polymer adhesive is filled into the pores, superficial asperities, and substrates by a wetting mechanism [4]. As a result, the roughness of the substrate surfaces is an important factor in forming enough adhesive bonds. Thereby, mechanical adhesion is determined by the roughness of the surface of the adherent. Increased surface roughness in turn increases the surface area and mechanical interlocking rates. Increased roughness also increases shear and tensile strength significantly. The main requirement for surface roughness is that it be uniform across the entire substrate.

The surface morphology, adhesion area, and wettability were all used to determine the strength of the adhesion joint in these illustrations. The chemical interaction between the surface of the adherent and the adhesive, on the other hand, plays an important role in enhancing joint strength. This variation in adhesive wettability for different faying surfaces can affect the strength of joints at applied rolling load during joint preparation.

Fundamentally, in the adhesive bonding mechanism, three areas of the adhesively-bonded joint (ABJ) can fail (adhesion to the substrate, adhesive cohesion, and the (first ply of) substrate adjacent to the adhesive), Figure VI.20.

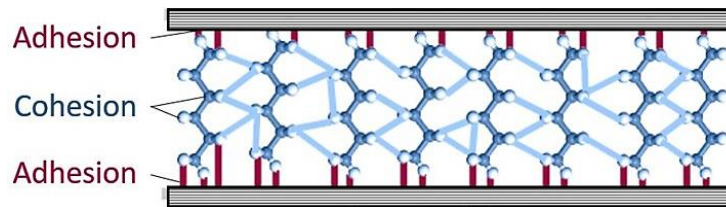


Figure VI.20: Illustration of mechanical coupling between two substrates

For this discussion, we will focus on adhesive and cohesive failures, where adhesion is the force that holds the adhesive to the substrate. Adhesion holds the adhesive to the substrate, and cohesion is the force of attachment within the adhesive itself. It is essentially the material strength of the cured adhesive material, Figure VI.21.

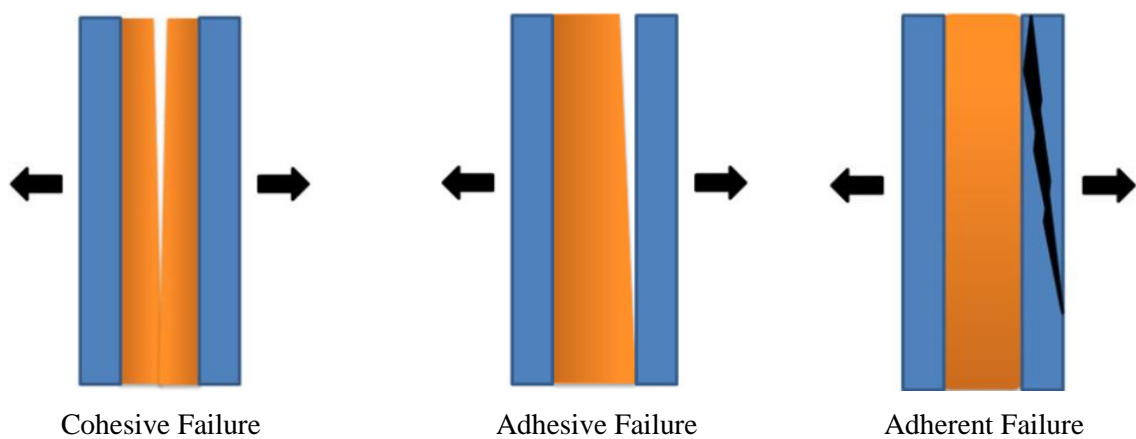


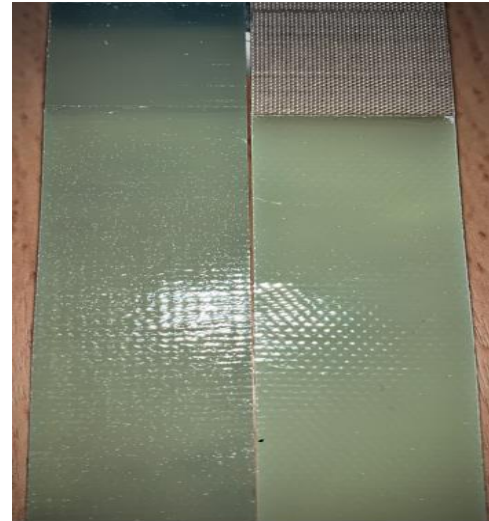
Figure VI.21: Representation of the failure modes of the adhesive joint[353]

VI.6.6.1 Fracture surface analysis of CNT reinforced adhesive for bonded joint

This section shows the fracture surfaces of a bonded joint reinforced with DGEBA/CNTs at two mass fractions of 1wt.% and 2wt.%. As illustrated in Figure VI.22, neat DGEBA bonded joints presented smooth and flat fracture surfaces in both the bonded aluminum and bonded composite joints. In other areas, the adhesive resin covered the specimen's surface, and the broken surface was relatively smooth, indicating low bonding strength. The failure occurred as adhesive failure in unreinforced bonded joints, as shown in Figure VI.18. The dominant adhesive failure zone of the neat adhesive resin on the treated surface adherent makes clear that the cracks propagate freely, with the formation of very smooth patterns. This indicates the weak ability of the neat DGEBA adhesive to avoid crack propagation, which is the typical brittle fracture of neat adhesive.



(a) Neat Adhesive Bonded Aluminum Joint



(b) Neat Adhesive Bonded Composite Joint

Figure VI.22: Fracture surfaces of DCB specimens Aluminum and Composite bonded with neat DGEBA adhesive

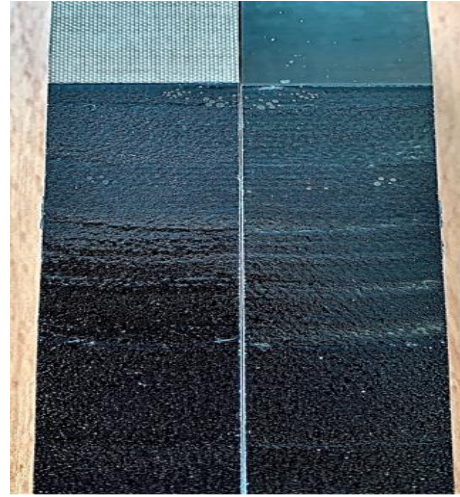
Figure VI.23 shows that adding 1wt.% CNTs to the adhesive for bonded composite joints caused more wrinkles and surface roughness in the adhesive, confirming the cohesive failure.

Thus, leading to a coarser failure surface, and the nanotubes were likely pulled out during this phase, signaling a stronger bonding strength. However, at a higher weight percentage of 2wt.% CNTs, the cohesive fracture surface of the bonded composite joints starts to become smooth again and less important than the 1wt.% CNTs due to CNTs aggregation, whereas the failure surface became less rough. As a result, the bonded composite joint with 2wt.% CNTs had lower bonding strength than the bonded composite junction with 1wt.% CNTs. The reduction in strength of joints with 2wt.% CNTs may have occurred mostly due to the existence of CNT clusters. The poor cohesive failure affected adhesive resin at a high mass fraction of CNTs, acted as weaknesses in the matrix, and resulted in quicker interaction of the stress field produced in the clusters. The debonding between the CNTs and adhesive resin in clusters displays that there is not a good interfacial interaction between the CNTs and epoxy adhesive, and the CNTs are not completely wetted by the resin in the clusters, as is presented in Figure VI.23.

Furthermore, in bonded aluminum joints, introducing 1wt.% CNTs to the adhesive caused adhesive failure (interfacial adhesive). Regarding the interface, we can assert that the strains in the joint belonging to the interface region were weaker than the cohesive region's strength at the time of testing. At the same time, adding 2wt.% CNT to the adhesive increased wrinkles and surface roughness, signaling increased bonding strength. As a result, the CNT-enhanced adhesive with 2wt.% CNTs serve to intensify the attractive intermolecular contacts between the aluminum adherents. The fracture surfaces are rougher due to the presence of these nanoparticles. Generally, more energy is dissipated for higher surface roughness. Rougher fracture surfaces indicate more complex failure mechanisms, resulting in higher energy absorption as the damage develops [354].



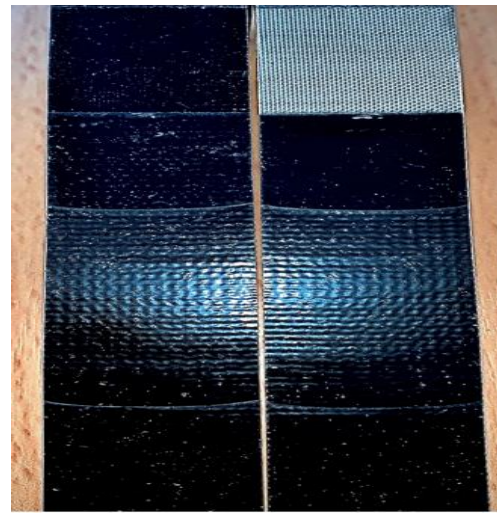
1wt.% CNTs/Adhesive Bonded Aluminum Joint



1wt.% CNTs/Adhesive Bonded Composite Joint



2wt.% CNTs/Adhesive Bonded Aluminum Joint



2wt.% CNTs/Adhesive Bonded Composite Joint

Figure VI.23: Fracture surfaces of DCB specimens bonded with CNT reinforced DGEBA adhesive under a different mass fraction

Another key mechanism that might improve the tensile strength of DCB bonded joints enhanced by particles with high aspect ratios such as nanofibers and nanotubes is the phenomenon of nanotubes being pulled out due to high tension in their surrounding matrix and also localized defects as is presented in Figure VI.24. Separating nanotubes from their matrix is usually broken down into three steps. In the first stage, the nanotube and adhesive matrix are linked together. When a distant field force is applied, shear stresses arise at the interface between the nanotubes and the adhesive matrix. Certain sections of the nanotubes begin to move along the debonding

span in the second stage [346], but a friction force stops this movement, and the remaining nanotubes bind to the matrix. In the third stage, the debonding zone extends throughout the length of the nanotubes, and all of the nanotubes initiate to slide away from their surrounding matrix [355]. It's worth noting that this phenomenon can harm the adhesive layer's shear and tensile strength due to the weak interface between the nanoparticles and the adhesive matrix.

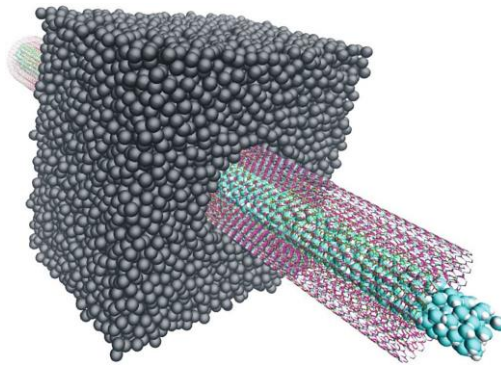


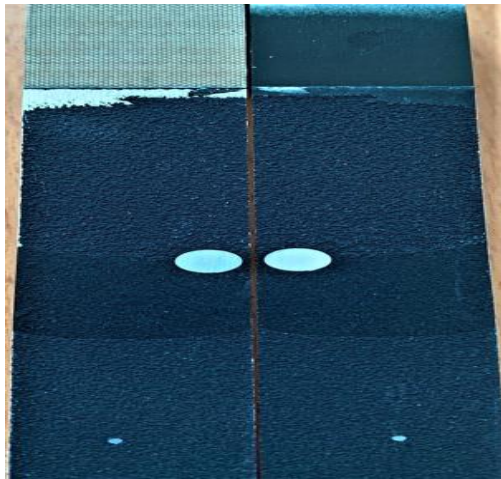
Figure VI.24: RVE showing CNT pull out under loading test

VI.6.6.2 Fracture surface analysis of GNP reinforced adhesive for bonded joint

The effect of adding GNPs to the adhesive on the fracture surfaces of DCBs under two mass fractions as 1wt.% and 2wt.% is shown in Figure VI.25. Results show rougher fracture surfaces in the DCB bonded aluminum and composite joint-reinforced with 1wt.% GNPs. The improvement in average tensile strength in reinforced DCB bonded joints has perhaps happened due to a dominant cohesive failure caused by the addition of GNPs to the adhesive and enhanced substrate adhesion forces. A high mass fraction of GNPs as 2wt.% generated local stress concentration in the adhesive layer, which allowed for local adhesive plastic deformation. The adherence of GNPs to the adhesive can potentially play a role in this. The key mechanism was the debonding of GNPs from adhesive, which was required to form plastic voids in the adhesive layer, as shown in Figure VI.25. Debonding of GNPs causes an increase in plastic voids, which

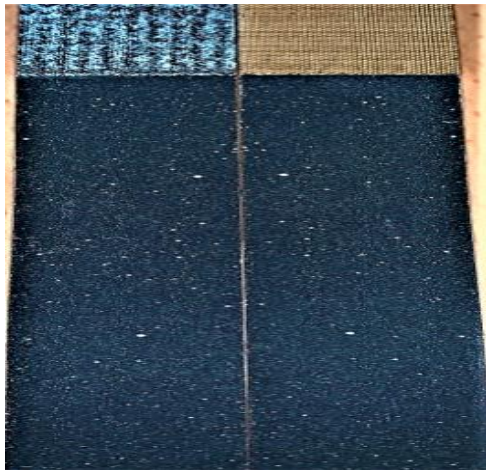
causes the adhesive layer to absorb more energy, leading to an increase in the adhesive layer's shear and tensile strength [346].

According to the precedent analysis, the fracture surfaces of DCB bonded joint-reinforced by CNTs were rougher than joint-reinforced by GNPs at exact 1wt.% mass fraction for bonded composite joints and 2wt.% for bonded aluminum joints.



1wt.% GNPs/Adhesive Bonded Aluminum Joint

1wt.% GNPs/Adhesive Bonded Composite Joint



2wt.% GNPs/Adhesive Bonded Aluminum Joint

2wt.% GNPs/Adhesive Bonded Composite Joint

Figure VI.25: Fracture surfaces of Aluminum/Aluminum and Composite/Composite bonded joints with GNP-reinforced DGEBA adhesive

VI.6.6.3 Comparative analysis of the surface roughness parameters

Figure VI.26 shows the average critical energies measurement results for the bonded aluminum and the composite joint. Following data analysis, it was determined that the aluminum alloy had the maximum fracture energies for both 1wt.% GNPs/DGEBA adhesive and 2wt.% CNTs/DGEBA adhesive. This is explained by the flexible adherent, which has a significant impact on mode I test findings. However, for bonded composite joints, 1wt.% CNTs has the highest fracture energies. This demonstrated that CNT-reinforced DGEBA adhesive was more compatible with the assembly of composite material adherents.

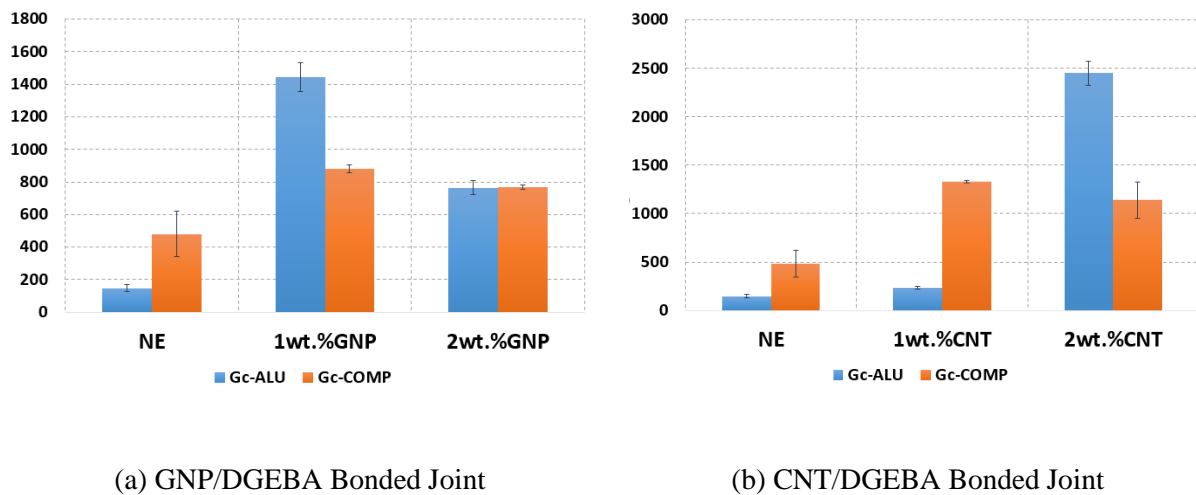


Figure VI.26: Energy release rate (J/m^2) for aluminum/aluminum and composite/composite bonded joints with DGEBA adhesive doped with nanofillers

The experimental results presented in this Figure VI.26 and VI.27 reveal that low mass fraction 1wt.% GNP-reinforced adhesively-bonded aluminum/aluminium and composite/composite joints have significant mechanical strength, and with aluminum adherents being more considerable. However, at large mass fractions, adding 2wt.% CNT resulted in the most dramatic increase in strength, with bonded aluminum joints and 1wt.% CNTs show the highest strength under adhesively-bonded composite joint. In comparison to 2wt.% CNTs/DGEBA adhesive, 2wt.% GNPs exhibits a moderate improvement in adhesive-bonded joint adherent for

both aluminum and composite adherents. In such a situation, and to sum up as in Figure VI.27, 1wt.% CNTs might be chosen as a sufficient reinforced nanoparticle for bonded composite joints. 2wt.% CNTs might be chosen as a sufficient reinforced nanoparticle for bonded aluminum joints

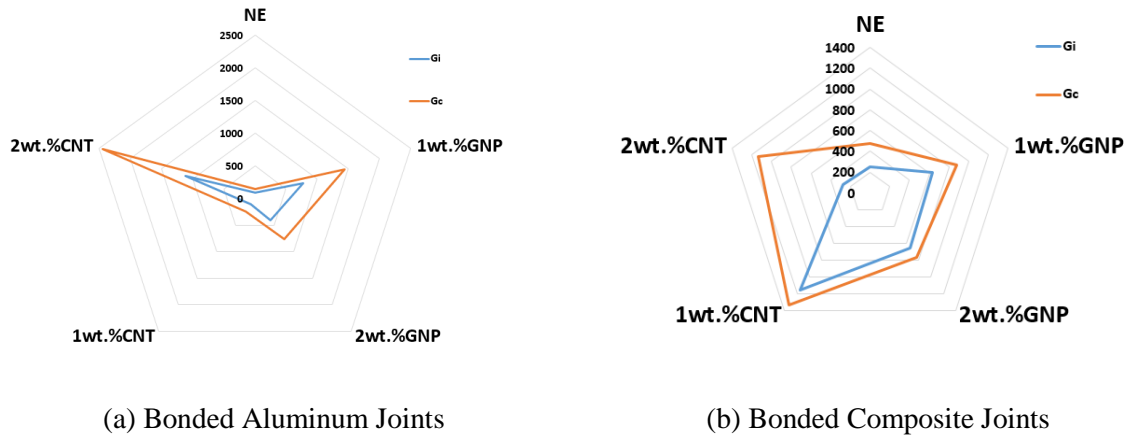


Figure VI.27: Energy release rate (J/m^2) progress among CNT/DGEBA adhesive and GNPs/DGEBA adhesively-bonded joint

VI.7 ENF Testing

VI.7.1 ENF Test Samples

The mode II fracture toughness of the adhesive with different GNPs and CNTs nanofillers was tested using the ENF specimens and the dimensions are shown in Figure VI.28. Pre-crack is made using a Teflon film with a thickness of 25 μ m, just as they are for the DCB sample. The specimen is supported on both ends and is subjected to a constant-speed movement of 1 mm/min.

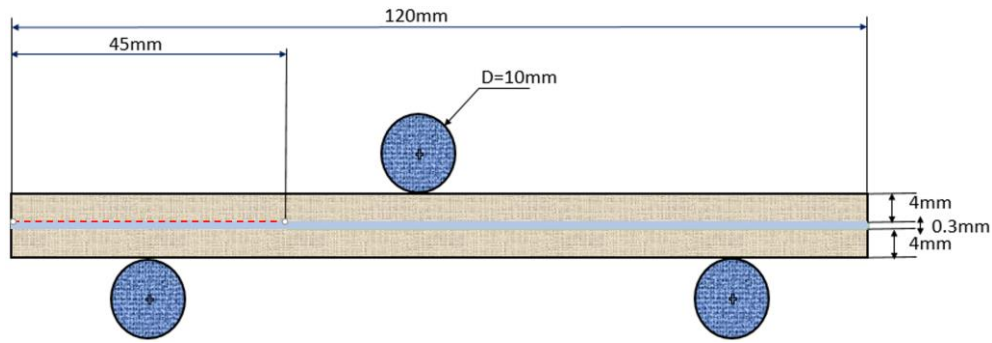


Figure VI.28: Dimensions of Notched Flexure specimen (ENF), Mode II

The vital parameter in the mode II test is the a_0/L ratio. This ratio allowed for smooth crack propagation and stable progressive crack growth. It is this last that introduces the test's stability condition. This parametric study aims to demonstrate the stability of crack propagation through experimentation. The beginning length of the crack is a factor determining the stability of this crack propagation in ENF samples under the mode II test. The zones of stability of experiments can be calculated using propagation curves based on the evolution of the applied force P and the displacement u .

For our work, $a_0/L = 0,35$ has a stable crack propagation for both bonded aluminum joint and bonded composite joint. This can be explained by the model hypotheses emitted during the establishment of this state, which is defined based on the theory of beam. This may be due to the effects of freezing and shear that were not taken into account. It will become more apparent as time goes on that shear behavior has little impact on the values of critical energy restoration rates.

The mode II fracture toughness of adhesive was determined using a data analysis method called beam theory [356]–[358]. The mode II fracture toughness of adhesive is calculated simply using the compliance of specimens, which considerably simplifies the difficulty of the tests.

This method was compared to traditional crack propagation measurement methods [356], [357], and a good agreement was found.

VI.7.2 Experiment results

To study the effect of GNPs and CNTs content on mode II fracture toughness of adhesive, experimental tests on ENF specimens were implemented under the quasi-static loadings, as shown in Figure VI.29.

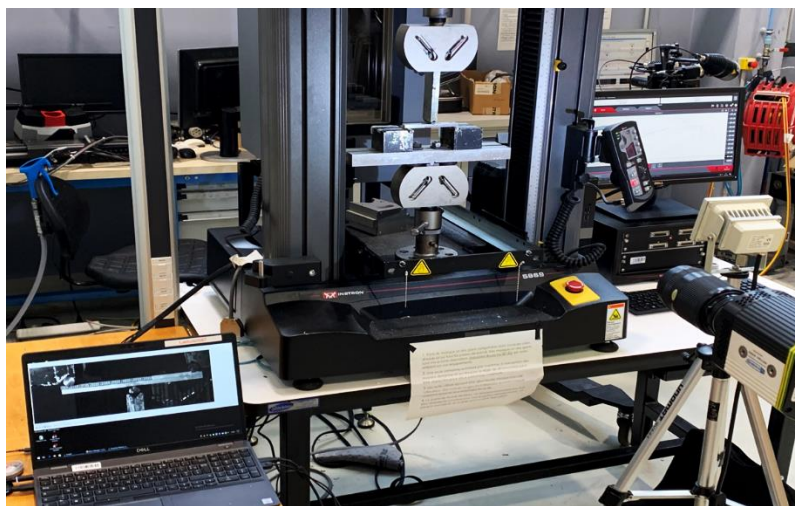
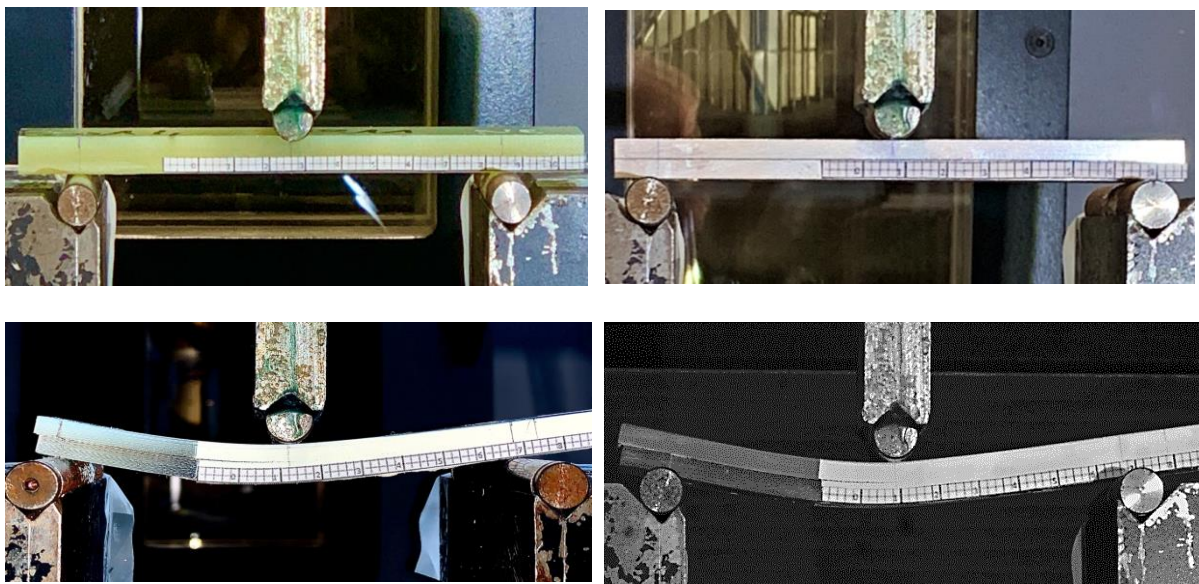


Figure VI.29: ENF specimen for mode II bonding characterization

During the experiment, force vs displacement curves were recorded. Typical force vs displacement curves of ENF specimens with neat adhesive and GNPs/DGEBA adhesive, CNTs/DGEBA adhesive nanocomposites with two different mass fractions (1wt.% and 2wt.%). At least three specimens were experimentally examined for each mass fraction to determine reproducibility, as illustrated in Figure VI.30 for a neat adhesive-bonded connection. The fracture start is considered to be indicated by the point of divergence from linearity. After the load reaches its maximum in mode II tests, it begins to decline. The load then increases again, and the majority of this section of the curves has been deleted from the Figure because it is no longer valid for G_{IIc} calculations[359][360].

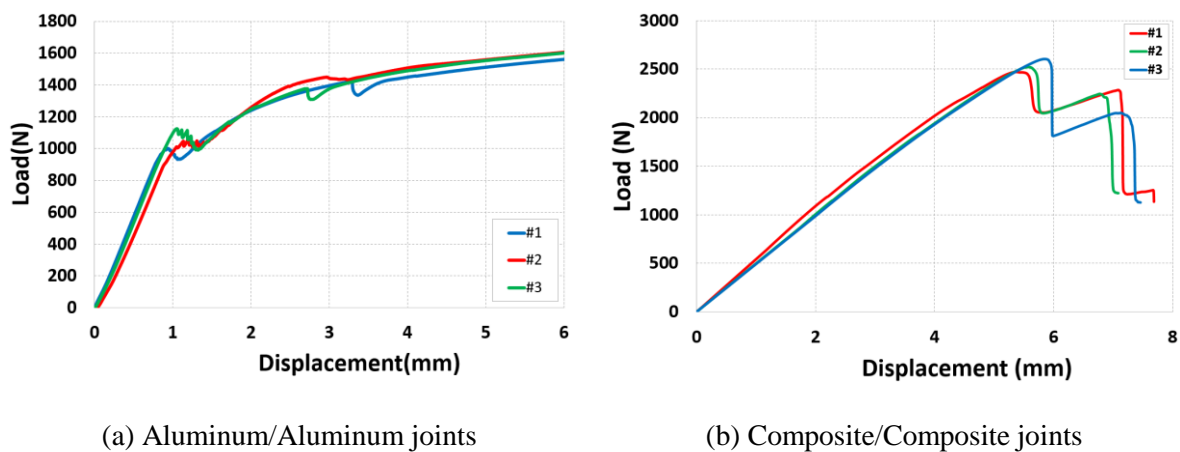


Figure VI.30: Force-displacement curves of ENF specimens bonded joints with neat DGEBA adhesive

According to several studies, the linear deformation curves, force vs displacement in Figures VI.31 and VI.32, clearly show that the increase in the mass fraction of nanoparticles of carbon nanotubes leads to a decrease of the maximum deformation. We also find that the variation of the maximum deformation is inversely proportional to the rate of nanoparticles in the epoxy adhesive. Indeed, the reinforcement adhesive by carbon nanoparticles leads to an increase in the rigidity of the adhesive joint and consequently to a decrease in the maximum deformation [361].

Figures 31 and 32 shows that the maximum load of the GNPs/adhesive and CNTs/adhesive, bonded joints are higher than that of the unreinforced adhesive. Figure VI.31 illustrates that raising the CNTs mass fraction to 1wt.% improves the tensile strength of bonded aluminum/aluminum joints as well as bonded composite/composite joints due to its high performance. However, increasing the CNTs mass fraction to 2wt.% degrades the structure performance.

It can be observed that under the mode II test, ENF specimens with nanocomposites in Figure VI.32 showed a significantly higher peak load when the GNPs content was 1 wt.% due to increasing the surface area of nanoparticles acting as loading transfer, as mentioned with GNPs in several research papers. At the same time, the peak loading decreased compared with the value for neat adhesive when GNPs content continued to increase to 2 wt.%.

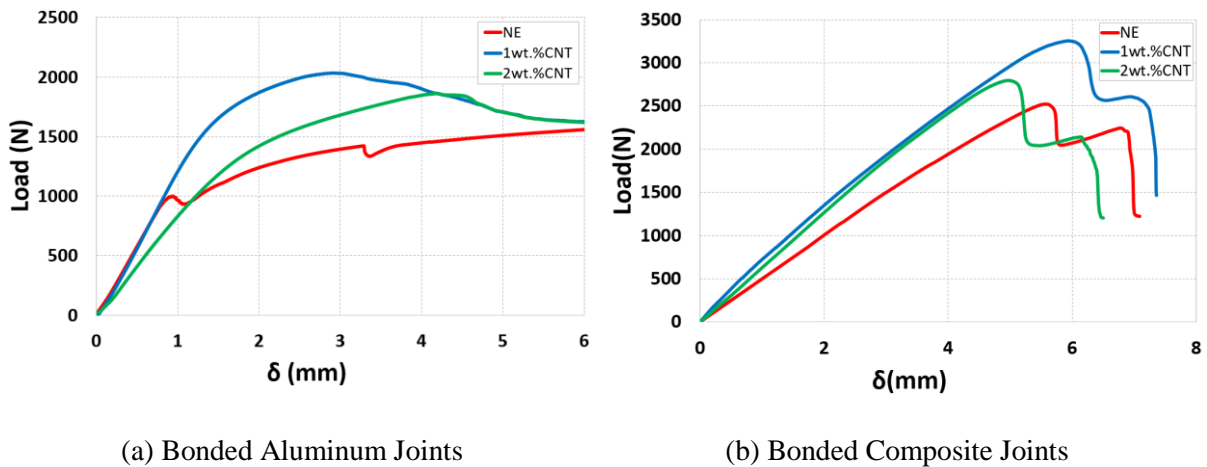


Figure VI.31: Force-displacement curves of ENF specimens bonded with DGEBA adhesive doped with CNTs

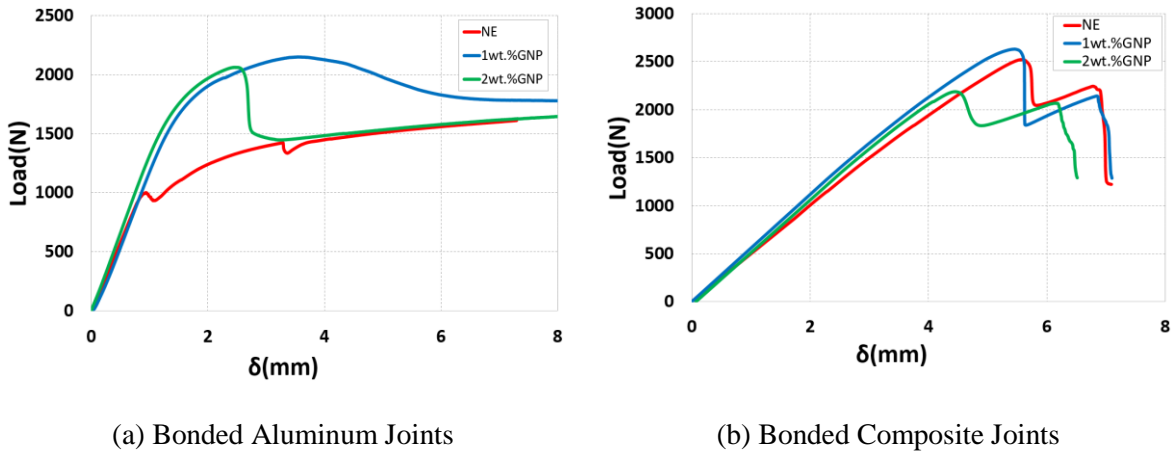


Figure VI.32: Force-displacement curves of ENF specimens bonded with DGEBA adhesive doped with GNPs

Figure VI.33 and VI.34 depicts typical R-curves for neat DGEBA adhesive and nanocomposites with varying GNPs concentration, whereas it depicts the variation trend of mode II critical and initial strain energy release rate of nanocomposites with GNPs. When compared to neat DGEBA adhesive, 1wt.% GNP is thought to have the largest improvement in fracture energy, Figure VI.33. Increasing the GNPs mass fraction to 2wt.% contributes to the onset of deterioration caused by the clusters phenomenon [362][352].

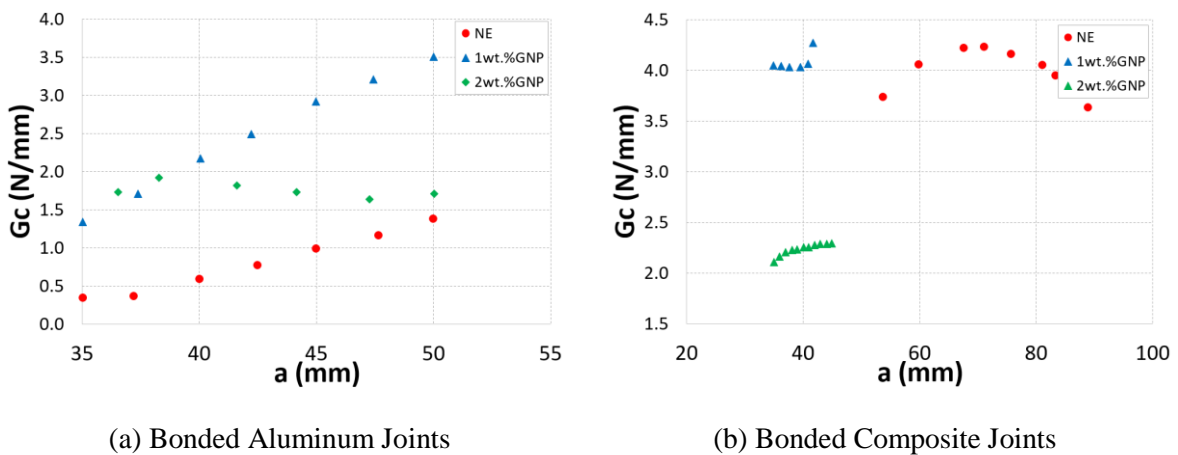


Figure VI.33: Energy release rate G_{II} based on the crack propagation of ENF specimens of bonded joints with DGEBA adhesive doped by GNPs

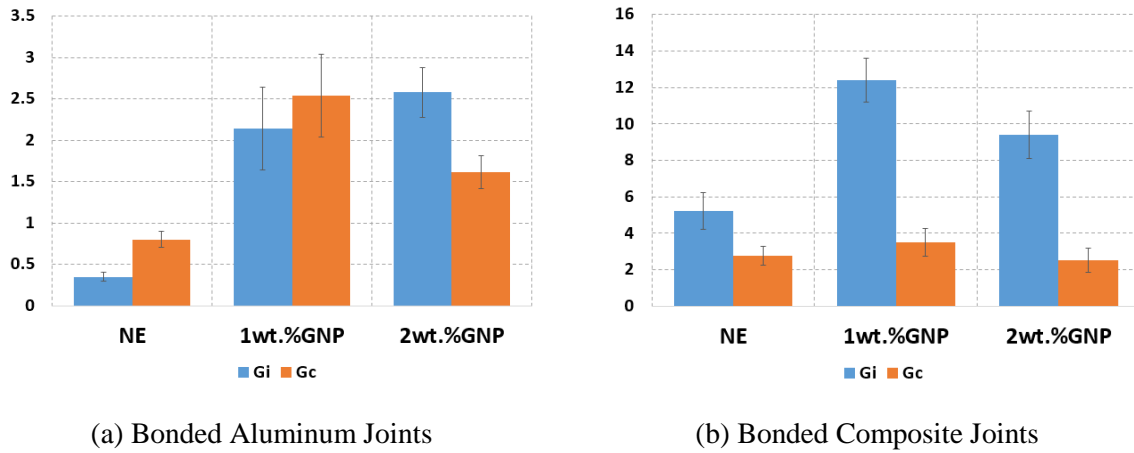
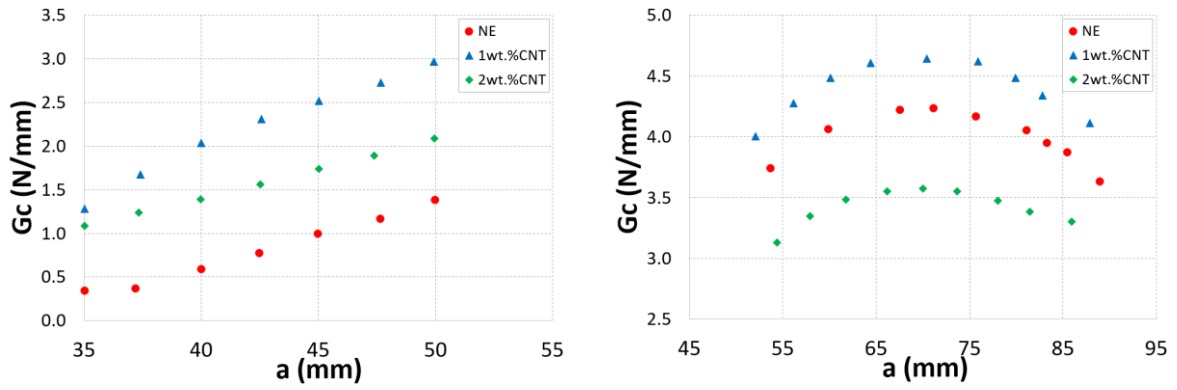


Figure VI.34: Diagram of progress initial and critical Energy release rate G_{II} (N/mm) of ENF specimen of bonded joints with DGEBA adhesive doped by GNPs

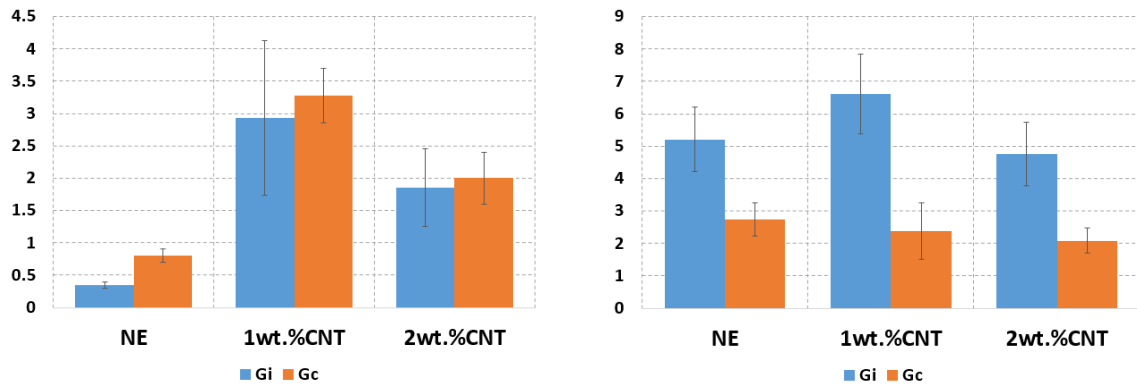
The mode II tests of CNT-reinforced adhesive-bonded aluminum/aluminum and composite/composite joints, as shown in Figure VI.35, revealed a rising R-curve behavior, with the fracture energy increasing progressively with crack length. A growing damage zone forward of the fracture tip may be the source of this [238] [363]. According to the findings, Figure VI.35 and VI.36, CNTs significantly improved the mode-II fracture toughness of the bonded aluminum joint and bonded composite joint. Under bonded aluminum joint, the G_{IIC} increased from 800J/m^2 in control to 2540J/m^2 in the 1wt.% CNT-reinforced DGEBA adhesive, then decreased to 1600J/m^2 in the 2wt.% CNT-reinforced DGEBA adhesive. Under bonded composite joints, G_{IIC} increased from 2740J/m^2 in the control to 3490J/m^2 in the 1wt.% CNT-reinforced DGEBA adhesive, then declined to 2510J/m^2 in the 2wt.% CNT-reinforced DGEBA adhesive.



(a) Bonded Aluminum Joints

(b) Bonded Composite Joints

Figure VI.35: Energy release rate G_{II} based on the crack propagation of ENF specimens bonded with CNT-reinforced DGEBA adhesive under 1wt.% and 2wt.%



(a) Bonded Aluminum Joints

(b) Bonded Composite Joints

Figure VI.36: Diagram of progress initial and critical Energy release rate G_{II} (N/mm) of ENF bonded joint with CNT-reinforced DGEBA adhesive

The reinforcing effects of high strength CNTs (ranging from 63 GPa to 500 GPa) [364] on the improved mechanical properties of the adhesive material were attributed to the improved impact bending rigidity, as shown in force vs displacement, Figure VI.37 [365]. Furthermore, including carbon nanotubes into the adhesive layer can activate nanoscale interfacial processes, which can help stop crack propagation and increase the bonded joint's local rigidity. Figure VI.34 shows how carbon nanotubes react under bending loading. This enhancement was seen when

1wt.% CNTs was added to the adhesively-bonded aluminum joints and the adhesively-bonded composite joints [366].

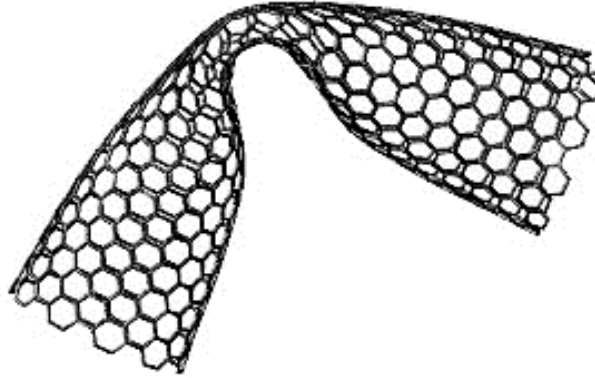


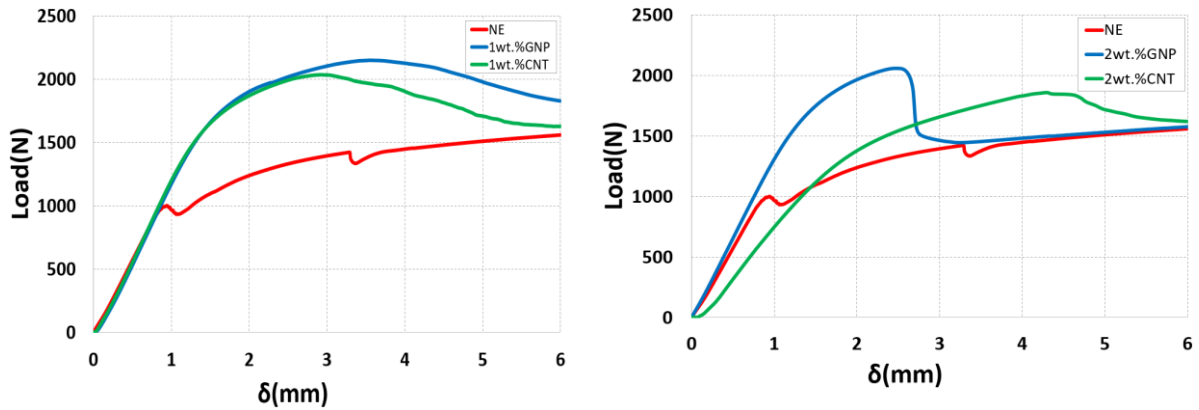
Figure VI.37: CNT deformation during bending loading

VI.7.3 Comparative analysis

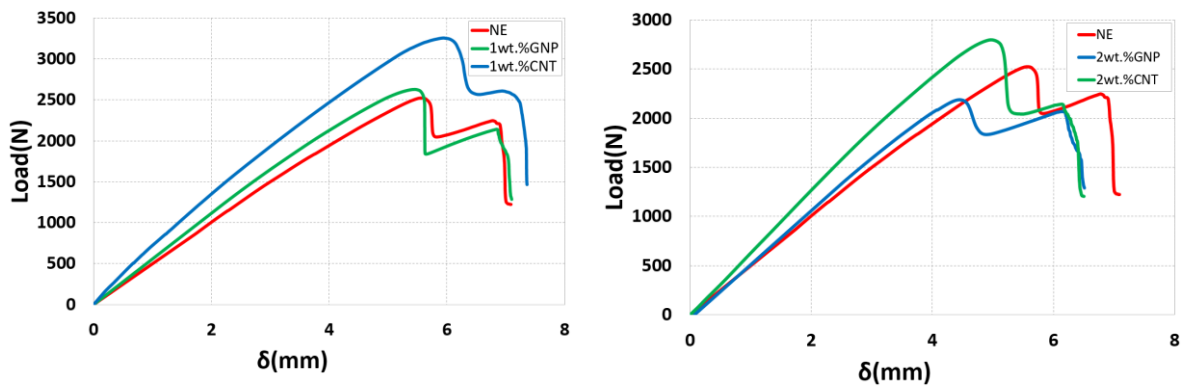
Figure VI.38 demonstrates that the best strengthening efficiency was recorded for GNPs with bonded aluminum joints, compared to CNTs. However, CNTs present a higher strengthened structure with bonded composite structure [13]. At the same time, adding CNTs indicates a large energy release rate with bonded composite joints, as seen in Figure VI.39. Though, incorporating GNPs indicates a significant rate of energy release [13].

A comparison study must be considered when selecting the appropriate adherent with suitably reinforced adhesive to obtain a more robust bonded structure. As shown in Figures VI.40 and VI.41, introducing a low mass fraction of GNPs to a bonded aluminum joint increases interface strength more than adding a low mass fraction of CNTs. Additionally, adding CNTs seeks also to improve the adhesive-bonded joint with a moderate level of enhancement. Furthermore, as compared to 1wt.% GNPs, adding 1wt.% CNTs corresponded more with a high energy release rate in bonded composite joints, Figure VI.40. Where it presents the high energy release rate.

At the same time, when compared at high mass fractions 2wt.% GNPs, 2wt.% CNTs have a higher energy release rate with only the bonded aluminum joints. Nevertheless, under bonded composite joint at high mass fraction 2wt.% of CNTs and GNPs, the energy release rate decrease where it became less than the neat DGEBA adhesive.

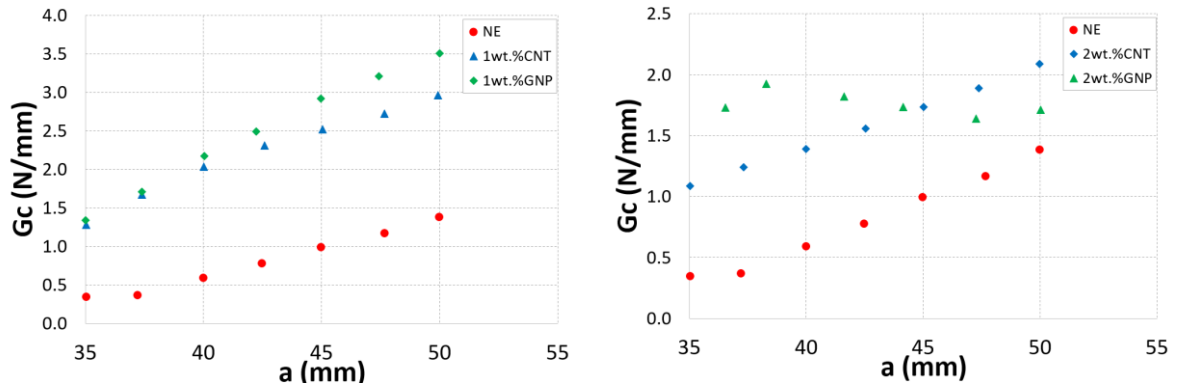


(a) Bonded Aluminum Joint

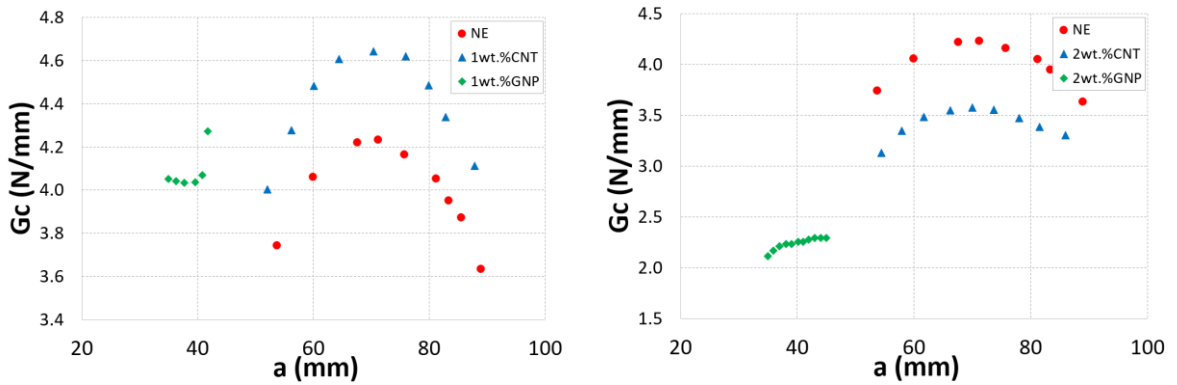


(b) Bonded Composite Joint

Figure VI.38: Comparison analysis Force-displacement curves of ENF specimens of bonded joints with CNTs/DGEBA and GNPs/DGEBA adhesive

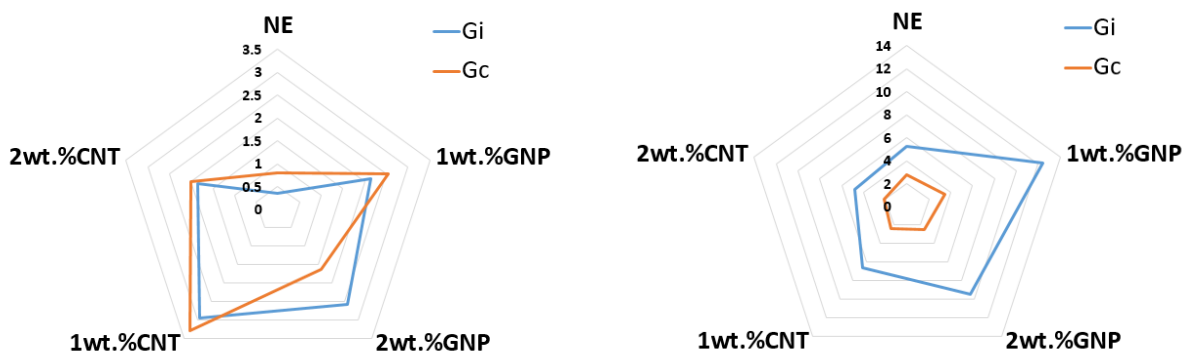


(a) Bonded Aluminum Joint



(b) Bonded Composite Joint

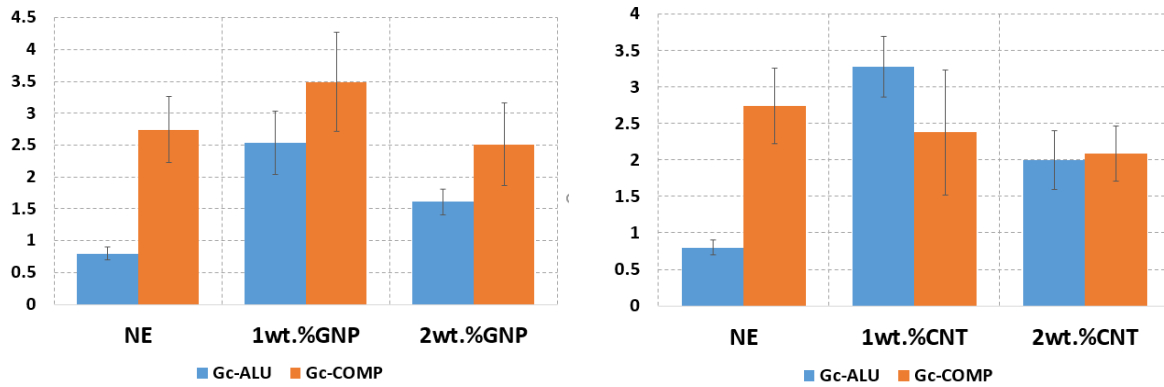
Figure VI.39: Comparison analysis energy release rate (R- curves) of ENF specimens of bonded joints with CNTs/DGEBA and GNPs/DGEBA adhesive



(a) Bonded Aluminum Joint

(b) Bonded Composite Joint

Figure VI.40: Diagram showing the Energy release rate GII difference of ENF samples bonded joint and with GNPs/DGEBA and CNTs/DGEBA adhesive (N/mm)



(a) GNPs/DGEBA Bonded Composite Joint

(b) CNTs/DGEBA Bonded Composite Joint

Figure VI.41: Diagram showing the Energy release rate G_{II} difference of ENF-aluminum bonded joint and ENF-Composite bonded joint with GNPs/DGEBA and CNTs/DGEBA adhesive

Figure VI.40 and Table VI.4 sum up that 1wt.% CNTs/DGEBA show the suitable adhesive with bonded aluminum joints, followed by 1wt.% GNPs. However, under bonded composite joints, 1wt.% GNPs/DGEBA shows the appropriate adhesive for affecting a good attachment, followed by 2wt.% GNPs/DGEBA.

Table VI.4: Energy release rate (N/mm) under adhesively-bonded Aluminum and Composite joint under ENF sample

		Aluminum Bonded Joint		Composite Bonded Joint	
		Gi	Gc	Gi	Gc
NE	Moyenne	0.35	0.80	5.21	2.74
	St-dev	0.05	0.1	1	0.52
1wt.% CNT	Moyenne	2.14	2.54	12.39	3.49
	St-dev	1.2	0.42	1.23	0.86
	Progress	x 6.11	x 3.18	x 2.37	x 1.27
2wt.% CNT	Moyenne	2.58	1.61	9.41	2.51
	St-dev	0.6	0.4	0.98	0.38
	Progress	x 7.37	x 2.01	x 1.81	x 0.92
1wt.% GNP	Moyenne	2.93	3.28	6.62	2.38
	St-dev	0.5	0.5	1.2	0.78
	Progress	x 8.38	x 4.1	x 1.27	x 0.87
2wt.% GNP	Moyenne	1.85	2.00	4.75	2.09
	St-dev	0.3	0.2	1.3	0.65
	Progress	x 5.28	x 2.5	x 0.91	x 0.76

VI.8 Numerical investigation using cohesive zone models

In the previous section, bonded joint specimens were used to determine the bond strength at crack initiation and propagation in modes I and II. In this section, we focus on the development of numerical models of the DCB and ENF tests using the ABAQUS finite element code. The comparison of final strength and, in particular, Mode I and II failure of various types of

specimens as predicted by ABAQUS and observed accurate tests , serves to validate the numerical approach.

In ABAQUS, cohesive zone models CZMs, are used to present the bonded joint structure carefully and precisely. The separation of coupled interfaces is the basis of CZM. They are based on the displacement jumps that occur when two adjacent parts separate, resulting in complete failure. The CZMs are based on the utilization of cohesive zones, which can be thought of as having zero thickness, or in other words, the entire CZM element acts as a single unit that degrades and fails at the same time. Only the interactions of the interfaces, including the traction forces at the interfaces and their relative displacements, are considered. The position of cohesive components determines the direction of crack propagation. Different traction separation rules have been devised [367]; however, they all describe the same global behavior. The traction at the cohesive zone interface grows up to a limiting value, referred to as fracture initiation traction in stress terms. The cohesive zone is then given a set amount of "softening" until the traction "stress" is at zero [368] [369].

VI.8.1 Modeling

For simplicity purposes and to save on computational resources, the specimens to be evaluated under simple mode I and mode II tests are modelled using 3D solid elements. It is critical to compare model results to experimental data to validate the model. For determining the correctness of the results, forced vs displacement curves from various experimental Mode I and Mode II tests are used. The proposed design of the DCB and ENF tests using ABAQUS was validated as a result of these findings, Figures VI.42 and VI.43. The developed 3D numerical model for crack propagation, which satisfactorily simulates the load vs displacement response of the joint up to crack propagation onset, validated the proposed design of the DCB and ENF tests using ABAQUS.

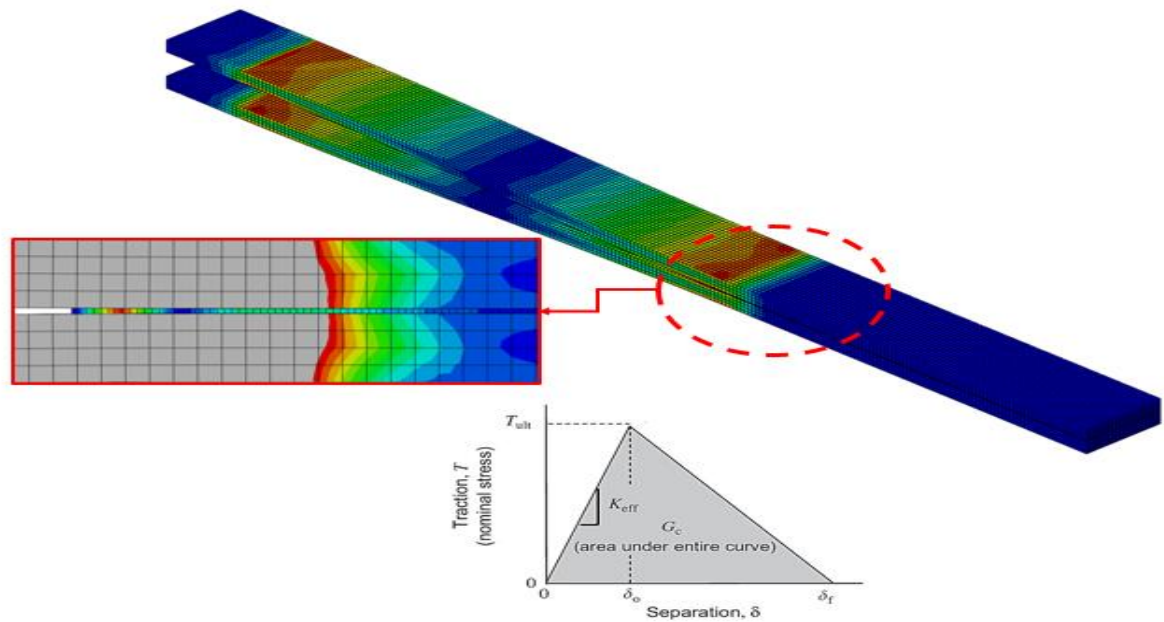


Figure VI.42: Finite element model of a double cantilever beam test

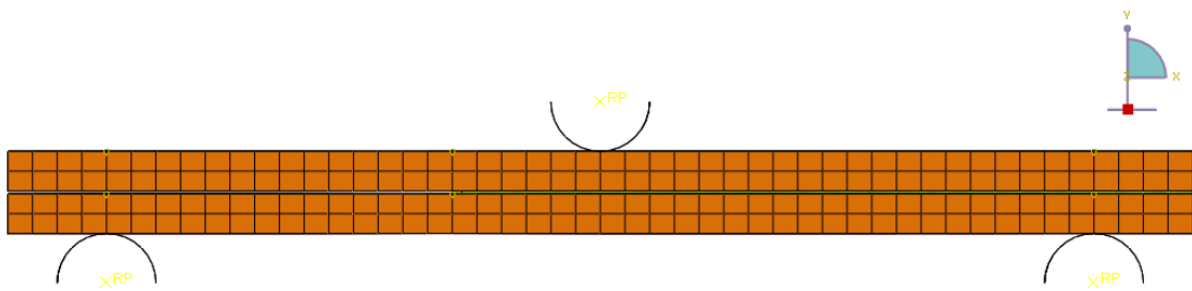


Figure VI.43: Finite element model of end notched flexure test

The CZM of the Double Cantilever Beam concept is shown schematically in Figure VI.42. The most essential metric in CZM is fracture energy [349], [370]. Experiments on unreinforced and reinforced adhesives identify it using the test procedure described in the section on test methods. To avoid the CZM from impacting the general compliance of the model before damage occurs, the initial rigidity should be as high as possible. It cannot, however, be infinite from a numerical standpoint. The value will be lower if this is not the case. After all, $10,000 \text{ N/mm}^3$ is considered as the initial rigidity. Finally, we achieved the only remaining parameter (cohesive strength) to produce the best correlation between the simulated and experimental adhesive joint force vs

displacement curve. The numerical models are performed by using Abaqus/standard finite element code.

The substrate and adhesive layers were chosen as eight-node linear brick, reduced integration, hourglass control (C3D8R), and three-dimensional cohesive elements (COH3D8), as illustrated in Figure VI.44. The traction-separation law for self-adhesive and reinforced adhesives has been established, and it applies to adhesives bonded aluminum joint and adhesives bonded composite joint including varying proportions of CNTs and GNPs. The material properties are summarized in Table V3. TEXGEN and DIGIMAT software were used to simulate the properties of the composite, as shown in Figure VI.45. Table VI.5 indicates the composite adherent parameters and Table VI.6 and VI.7 presents the reinforced adhesive. Table VI.8-VI.9-VI.10 present the different cohesive parameters.

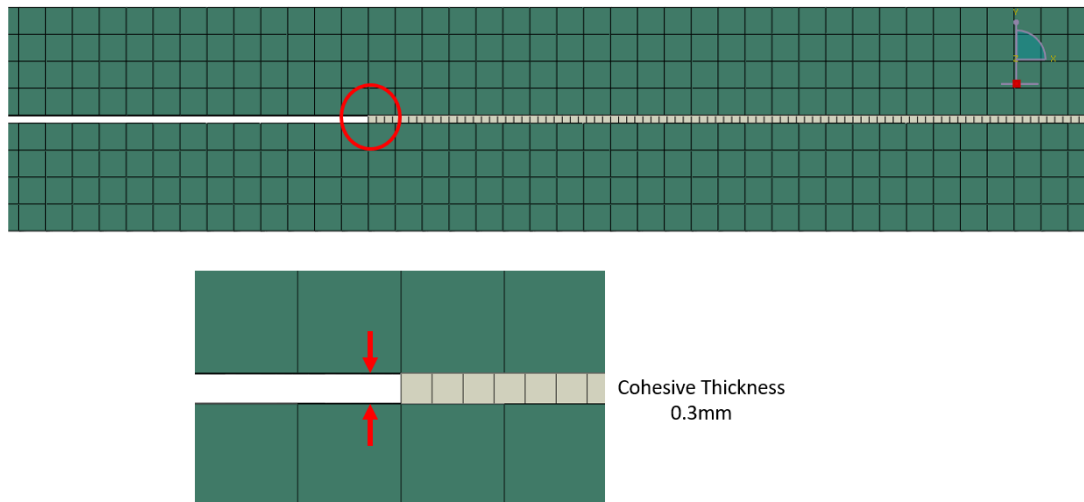


Figure VI.44: Mesh employed in the FE simulation and cohesive thickness element size

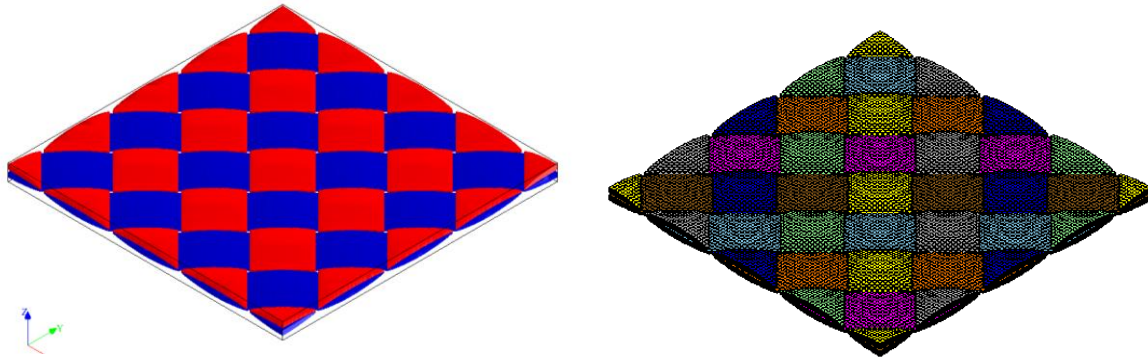


Figure VI.45: Adherent Composite laminated structure simulated with Texgen and Digimat

Table VI.5: Composite properties

$E_{11} = E_{22}$ (MPa)	E_{33} (MPa)	$\nu_{12} = \nu_{21}$	$\nu_{13} = \nu_{23}$	$\nu_{31} = \nu_{32}$	G_{12} (MPa)	$G_{13} = G_{23}$ (MPa)	ρ (Kg.m ³)
16021.7	11920.3	0.46	0.22	0.16	10327.7	3752	2.08

Table VI.6: CNTs/DGEBA properties

	E (MPa)	ν	G (MPa)	ρ (kg.m ³)
1wt.% CNT/ DGEBA	17478	0.26	6920	1509
2wt.% CNT/ DGEBA	12772	0.26	5037	1472

Table VI.7: GNPs/DGEBA properties

	E (MPa)	ν	G (MPa)	ρ (kg.m ³)
1wt.% GNPs/ DGEBA	15812	0.24	6359	1565
2wt.% GNPs/ DGEBA	17199	0.24	6927	1575

Table VI.8: Cohesive parameters of GNPs/DGEBA adhesively-bonded composite joint

	K_S (N/ mm ³)	K_n (N/mm ³)	t_1^0 (MPa)	t_2^0 (MPa)	G_{Ic} (N/mm)	G_{IIc} (N/mm)	$\Delta\tau$ (s)
NE	10 ⁶	10 ⁶	40	40	0.2	0.24	10 ⁻¹⁰
1wt.% GNP	10 ⁶	10 ⁶	60	60	0.86	2.3	10 ⁻¹⁰
2wt.% GNP	10 ⁶	10 ⁶	80	80	0.76	2.09	10 ⁻¹⁰

Table VI.9: Cohesive parameters of GNPs/DGEBA adhesively-bonded aluminum joint

	K_S (N/mm ³)	K_n (N/mm ³)	t_1^0 (MPa)	t_2^0 (MPa)	G_{Ic} (N/mm)	G_{IIc} (N/mm)	$\Delta\tau$ (s)
NE	106	106	37	37	0.08	0.3	10-10
1wt.% GNP	106	106	85	85	1.4	2.9	10-10
2wt.% GNP	106	106	75	75	0.7	1.85	10-10

Table VI.10: Cohesive parameters of CNTs/DGEBA adhesively-bonded composite joint

	K_S (N/mm ³)	K_n (N/mm ³)	t_1^0 (MPa)	t_2^0 (MPa)	G_{Ic} (N/mm)	G_{IIc} (N/mm)	$\Delta\tau$ (s)
NE	10 ⁶	10 ⁶	40	40	0.2	0.24	10 ⁻¹⁰
1wt.% CNT	10 ⁶	10 ⁶	60	60	1.3	3.4	10 ⁻¹⁰
2wt.% CNT	10 ⁶	10 ⁶	80	80	1.13	2.5	10 ⁻¹⁰

Table VI.11: Cohesive parameters of CNTs/DGEBA adhesively-bonded aluminum joint

	K_S (N/mm ³)	K_n (N/mm ³)	t_1^0 (MPa)	t_2^0 (MPa)	G_{Ic} (N/mm)	G_{IIc} (N/mm)	$\Delta\tau$ (s)
NE	106	106	37	37	0.08	0.3	10-10
1wt.% CNT	106	106	85	85	2.3	2.14	10-10
2wt.% CNT	106	106	75	75	1.1	1.61	10-10

Figures VI.46 and VI.47 indicate the mode of fracture propagation under the DCB and ENF model. It shows that the projected curve has a strong relationship with the experimental curve's peak value. Figure VI.46 also shows how the adhesive interacts with the overall structure of the mode I simulation, including the stress singularity and how the crack propagation moves about in the bonded joint. From the other side, Figure VI.47 shows how the adhesive behaves in a

mode II simulation of the whole structure, where the stress singularity belongs to the debonding zone. Figures VI.48 and VI.49 show the computational and experimental load vs displacement curves of the unreinforced and reinforced adhesively-bonded aluminum/aluminum and composite/composite joints.

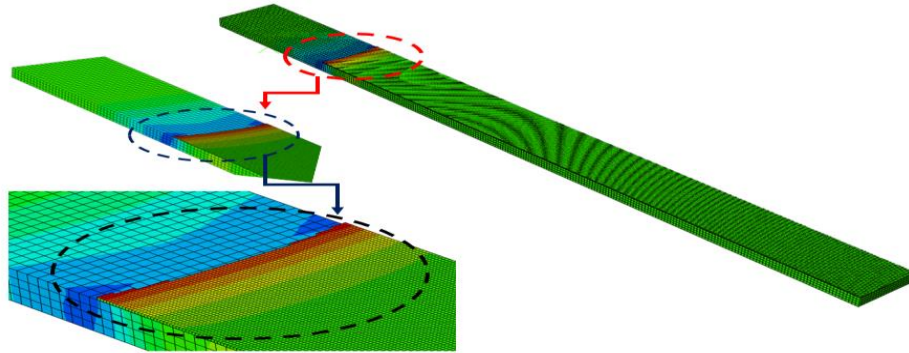


Figure VI.46: Damage of joints, DCB model

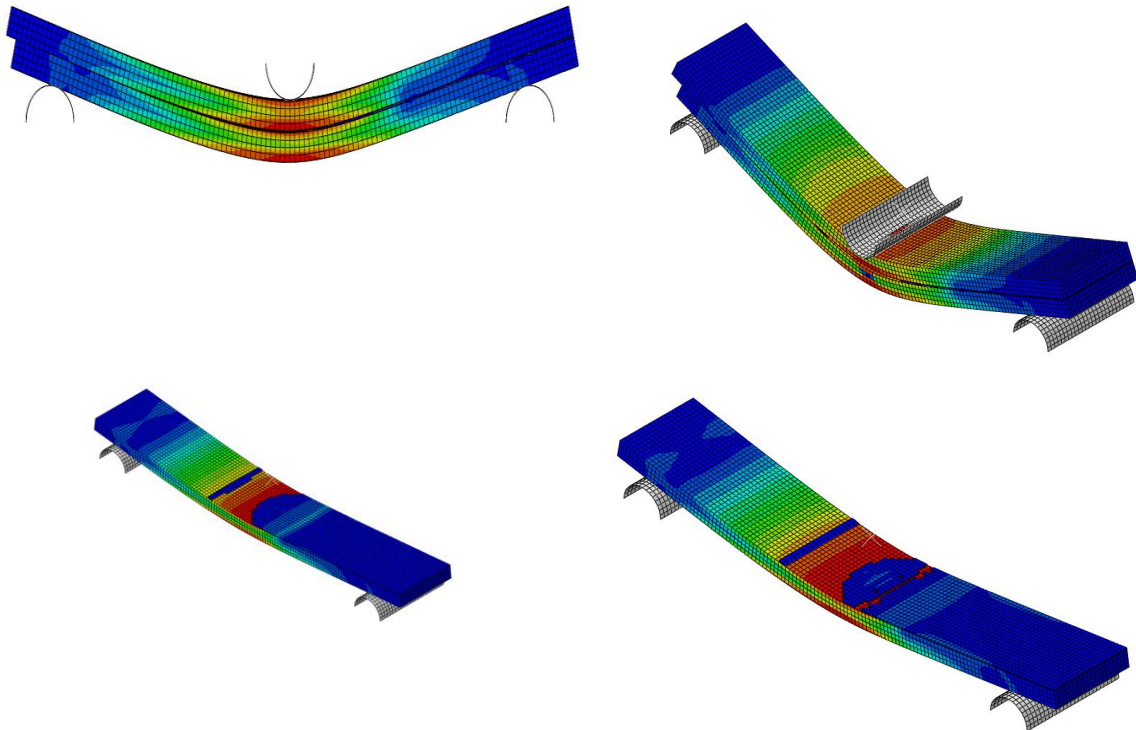
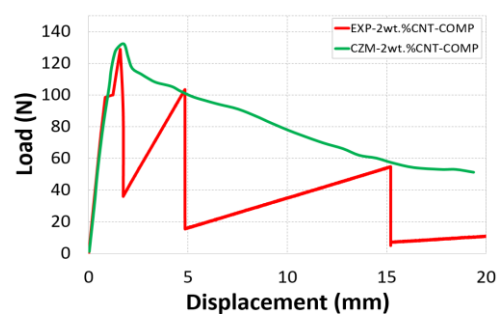
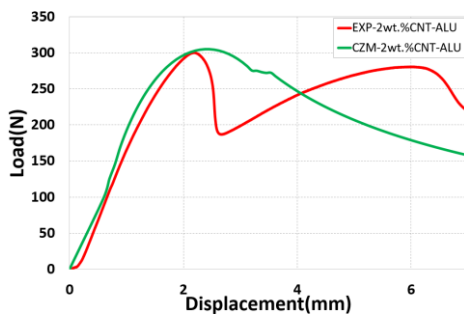
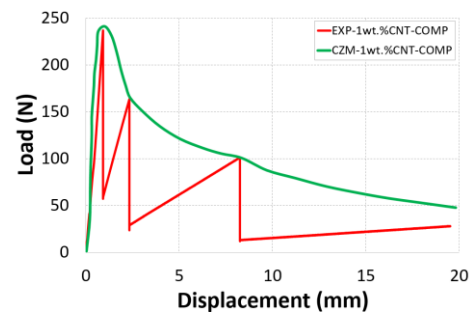
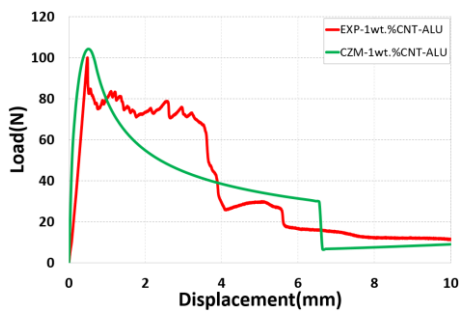
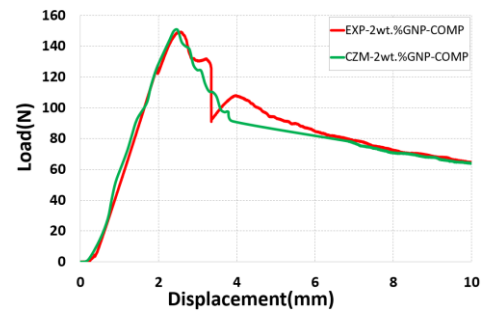
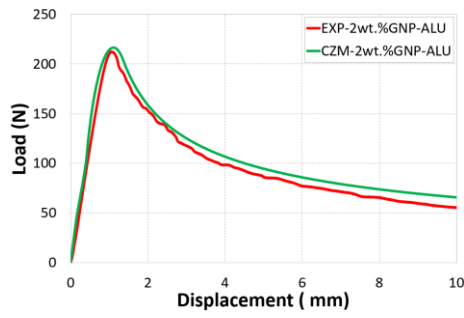
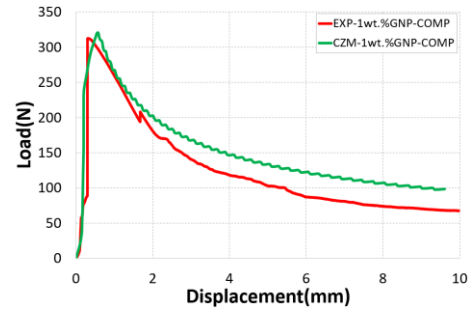
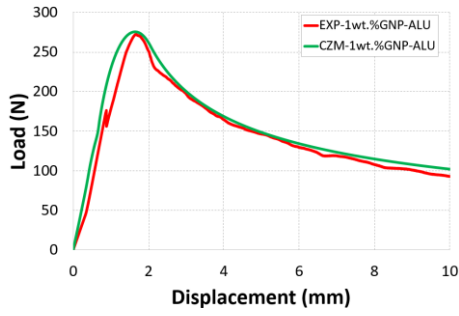
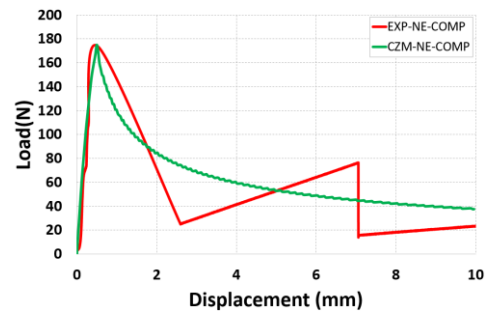
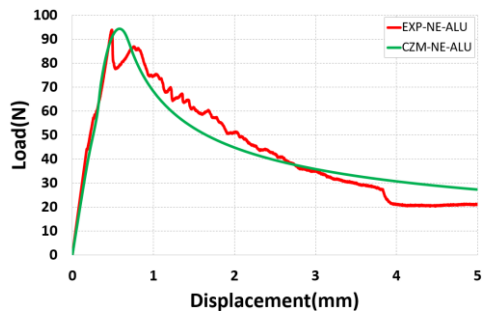


Figure VI.47: Damage of joints, ENF model

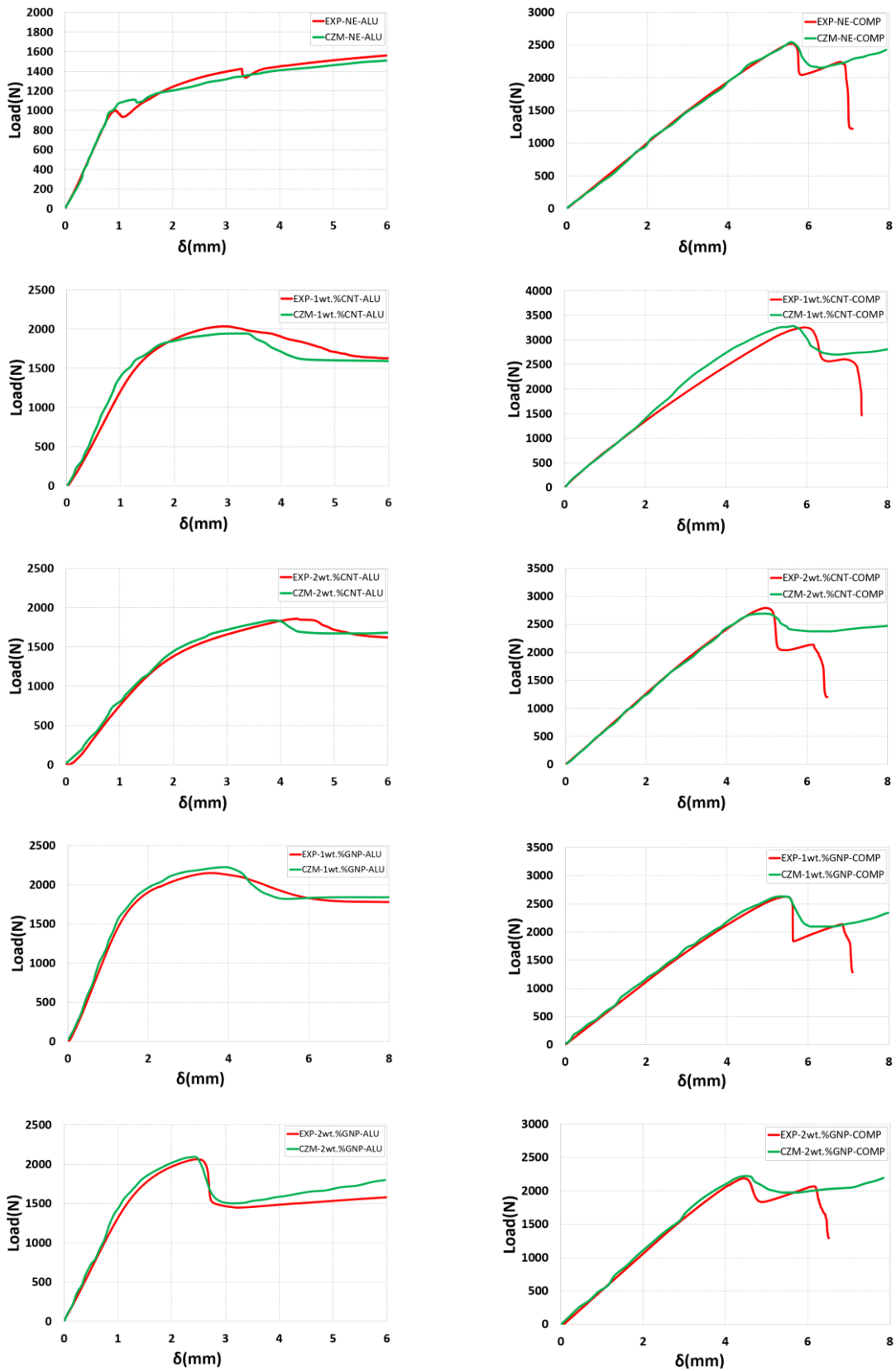
Chapter VI: Fracture Resistance of a nanofiller-doped adhesive for a bonded joint



(a) Aluminum/Aluminum bonded Joints

(b) Composite/Composite bonded Joints

Figure VI.48: Comparison of numerical and experimental force-displacement curves for DCB tests



(a) Aluminum/Aluminum bonded Joints

(b) Composite/Composite bonded Joints

Figure 49: Comparison of numerical and experimental force-displacement curves for ENF tests Conclusion

VI.8.2. Conclusion

To conclude, the presence of nanofillers improved the adhesion between the adhesive and the substrate, as the joint strength rose with the addition of CNTs or GNPs. However, as the mass fraction of CNTs or GNPs was increased, the interface worsened due to nanoparticle aggregation. Understanding why the inclusion of nanoparticles improves adhesive adhesion to substrates will require more extensive and focused studies, which might be the subject of future study. In this chapter, elements were presented to understand the effect of reinforcement according to their type and their interaction with the adherents on the resistance to crack development in mode I. Indeed, two types of reinforcement were considered (CNTs and GNPs) with two mass fractions (1wt.% and 2wt.%). However, reinforcements have a significant influence on delamination resistance.

In the second part, the focus was on Mode II, and it was possible to study it from tests under ENF samples. Particular attention was paid to the problem of unstable crack propagation in such tests. In fact, from simple models based on the theory of beams, it was possible to determine a criterion of propagation stability, the latter being found in the literature. The test campaign was conducted by conducting a study on this condition of propagation stability. A comparison of the values of critical energy return rates in Mode I and Mode II with the literature results show a particularly good agreement. As shown in previous experimental results using DCB samples under Mode I test confirmed by numerical results, reinforced 2wt.% CNTs/adhesive to a bonded aluminum joint results in a significant energy release rate. Accordingly, with adhesively-bonded composite joint, 1wt.% CNTs/DGEBA adhesive have the better interaction. In the other hand, as shown in previous experimental results using ENF samples under Mode II test, reinforced 1wt.% CNTs/DGEBA adhesive followed by 1wt.%

GNPs /DGEBA adhesive show the highest improvement of the bonded aluminum joint behavior. However, with adhesively-bonded composite joint 1wt.% GNPs/DGEBA followed by 2wt.% GNPs/DGEBA adhesive demonstrate a significant energy release rate.

General Conclusion

Today, many researchers and design engineers are inspired to use adhesive-bonded joints to achieve a high strength-to-weight ratio in modern structures. When compared to traditional mechanical fastener joints such as spot welding, riveting, and so on, the joints present distinct properties. The ability to bond dissimilar materials, significant resistance to fatigue loadings, improved stress distribution, good sealing ability, and decreased structural weight and fabrication cost are all significant advantages of adhesively-bonded joints. It has been discovered that the mechanical properties of adhesives can be improved by combining one or more reinforcing phases with varying mass fractions.

In this regard, several techniques have been used in the past to improve the mechanical behavior of epoxy adhesives as structural adhesives. We have demonstrated in this thesis that the addition of nanofillers to the adhesive layer has proven to be a highly effective technique. There are several types of nanofillers with different geometric shapes (0D, 1D, 2D,3D), each with a distinct and singular effect on the final properties of the adhesive. Carbon nanoparticles such as graphene nanoplatelets (GNP), carbon nanotubes (CNT), and carbon black (CB) were selected as reinforcement materials in our research.

However, obtaining a unique influence from all types of carbon nanoparticles to improve the mechanical properties of reinforced adhesive is difficult because this influence heavily depends on the manufacturing procedure, the dimensions of the nanofillers, etc.

In order to evaluate the extent to which carbon nanofillers influence adhesive performance in bonded joint structures, it is necessary to first examine the reinforced adhesive alone under various mechanical loading to assess its mechanical properties. Several analyses have thus been

carried out to determine the different nanofillers' influence on the adhesive's performance evolution, such as through the physico-chemical tests as described in chapter 3, the quasi-static tests as described in Chapter 4, and the dynamic tests as described in chapter 5.

In Chapter 3, the DSC study was conducted to evaluate the difference in the glass transition temperature (T_g) between the various nanoparticles incorporated. We have shown that 1wt.% CNTs/DGEBA adhesive nanocomposite structure outperforms GNPs and CBs. Foremost, this chapter demonstrated that 1 wt.% CNTs significantly increased the elastic modulus, hardness, rigidity, and other mechanical properties of reinforced specimens. This revealed a variety of mechanical properties, with the 1wt.% CNTs/DGEBA nanocomposite presenting the most preferable structure when tried to compare to GNPs/DGEBA and CBs/DGEBA.

In chapter 4, the quasi-static analysis revealed that the mechanical behavior of unreinforced and reinforced DGEBA adhesives differed depending on the nanofiller type and mass fraction level. Besides this, when compared to GNPs and CBs under tensile circumstances, 1wt.% CNTs was found to be the selecting the most suitable nanoparticles for enhancing DGEBA adhesive.

Furthermore, under compressive conditions, 1wt.% CBs were found to be suitable nanoparticles with DGEBA epoxy adhesive, although they also generated critical damage on the sample edge. This does not excuse the fact that 1wt.% CNTs helped improve the mechanical structure of DGEBA adhesive resulting in toughness-reinforced DGEBA adhesive nanocomposite samples with higher plasticity when comparison to neat DGEBA adhesive. As a result, after compressive loading, CNTs/DGEBA adhesive has an almost smooth edge, confirming its high plasticity. However, GNPs/DGEBA adhesive and CBs/DGEBA adhesive exhibits grave edge burst, indicating that there is poor plasticity. 1wt.% CBs is selected as the best option for improving adhesive DGEBA elastic effectiveness, followed by 1wt.% CNTs, which contribute to DGEBA strength and plasticity.

Chapter 5 reported an outline for performing SHPB tests, which included validity assumptions, data acquisition, basic governing equations, data processing, and typical experimental results. This chapter investigates the effect of different carbon nanofillers with varying mass fractions on DGEBA adhesive behavior. The dynamic modulus values typically display appreciable improvement, including nanofillers under low impact pressure, where 1wt.% CNTs/DGEBA showing the highest improvement by 409%. However, at higher impact pressure, 2wt.% CBs/DGEBA has significant progress of 223% over the second-ranked 1wt.% CNT/DGEBA adhesive.

Furthermore, the strength of CBs/DGEBA and GNPs/DGEBA increases with increasing mass fraction and impact pressure; however, CNTs/DGEBA degrades until it became weaker than the neat DGEBA adhesive. The essential quantities of porosities/percolations provided by the sample dramatically affect this deprivation. In comparison to neat DGEBA adhesive, 5wt.% CNTs at high impact pressure (4bar) result in a drop of -18.32 %. 5wt.% CBs at 4bar, on the other hand, generate 5.73% progress and 22.28 % for 2wt.% CBs.

Moreover, the appearance of a second peak well overstrains rate vs time curve suggests the presence of micro/macro damage, with this peak being more important followed by degradation of the reinforced nanocomposite. At low impact pressure, 1wt.% CNTs reduce the strain rate of the DGEBA adhesive by 409%, demonstrating the importance of CNTs/DGEBA. However, at high impact pressure, 2wt.% CBs generate less strain rate in the sample than CNTs/DGEBA and GNPs/DGEBA nanocomposites and 1wt.% CNTs come in the second array.

In chapter 6, knowledge implications of nanofiller'-reinforced adhesives based on their type and their interaction with adherents on crack growth resistance during mode I and mode II. Indeed, two types of reinforced adhesive (CNTs/DGEBA and GNPs/DGEBA) with under two mass fractions were considered (1wt.% and 2wt.%). At the same time, reinforcing adhesive-bonded joints have a significant impact on delamination resistance.

Under Mode I testing, reinforced 2wt.% CNTs/DGEBA adhesive w a bonded aluminum joint results in a significant energy release rate, as confirmed by numerical results. As a result, the adhesive-bonded composite joint with 1wt. % CNTs/DGEBA adhesive has the best interaction. In contrast, previous experimental results using ENF samples under the mode II test show that reinforced 1wt.% CNTs/DGEBA adhesive, followed by 1wt.% GNPs/DGEBA adhesive, improve the bonded aluminum joint behavior the most. However, the adhesive-bonded composite joint with 1wt.% GNPs/DGEBA adhesive followed by 2wt.% GNPs/DGEBA adhesive shows a significant energy release rate.

To conclude, the choice of the most appropriate carbon nanoparticle was a very delicate task, as each nanoparticle reacts in a particular way to the different types of mechanical solicitation.

Although this study has highlighted the impact of nanofillers on specific properties and characteristics for the DGEBA adhesive, it is not exhaustive and has raised some questions that require convincing answers in future work. It will be preferable to open this study to many perspectives and directions in order to advance this work:

- Tomographic examination of various- reinforced adhesive specimens.
- Adhesive analysis in an assembly: single and double lap joints.
- FE templates: traction/compression, SHPB with damage criteria introduction.

References

- [1] E. Paroissien, “Contribution aux assemblages hybrides (boulonnés/collés)-Application aux jonctions aéronautiques.” Université Paul Sabatier-Toulouse III, 2006.
- [2] M. Lafait, “Analyse du transfert de charge de joints boulonnés à simple recouvrement.” École Polytechnique de Montréal, 2015.
- [3] “No Title.” CLS orders Japan’s first LNG bunkering vessel - Offshore Energy (offshore-energy.biz).
- [4] “No Title,” [Online]. Available: Steel and Aluminium Hulls - Safe Skipper Boating & Safety Afloat Apps for phones & tablets (safe-skipper.com).
- [5] J.-H. Kweon, J.-W. Jung, T.-H. Kim, J.-H. Choi, and D.-H. Kim, “Failure of carbon composite-to-aluminum joints with combined mechanical fastening and adhesive bonding,” *Compos. Struct.*, vol. 75, no. 1–4, pp. 192–198, 2006.
- [6] “No Title,” [Online]. Available: matteana.blogspot.com.
- [7] M. Tarfaoui, A. El Moumen, and H. Ben Yahia, “Damage detection versus heat dissipation in E-glass/Epoxy laminated composites under dynamic compression at high strain rate,” *Compos. Struct.*, vol. 186, pp. 50–61, 2018.
- [8] B. Beylergil, Y. Cunedioğlu, and A. Aktas, “Experimental and numerical analysis of single lap composite joints with inter-adherent fibers,” *Compos. Part B Eng.*, vol. 42, no. 7, pp. 1885–1896, 2011.
- [9] L. F. M. Da Silva, A. Öchsner, and R. D. Adams, *Handbook of adhesion technology*. Springer Science & Business Media, 2011.
- [10] S. M. J. Razavi, M. R. Ayatollahi, E. Esmaili, and L. F. M. Da Silva, “Mixed-mode fracture response of metallic fiber-reinforced epoxy adhesive,” *Eur. J. Mech.*, vol. 65, pp. 349–359, 2017.
- [11] “No Title,” [Online]. Available: <https://www.compositesworld.com/>.

- [12] S. Yu, M. N. Tong, and G. Critchlow, "Use of carbon nanotube-reinforced epoxy as adhesives to join aluminum plates," *Mater. Des.*, vol. 31, pp. S126–S129, 2010.
- [13] P. Jojibabu, M. Jagannatham, P. Haridoss, G. D. Janaki Ram, A. P. Deshpande, and S. R. Bakshi, "Effect of different carbon nano-fillers on rheological properties and lap shear strength of epoxy adhesive joints," *Compos. Part A Appl. Sci. Manuf.*, vol. 82, pp. 53–64, 2016, doi: <https://doi.org/10.1016/j.compositesa.2015.12.003>.
- [14] S. M. J. Razavi, M. R. Ayatollahi, A. N. Giv, and H. Khoramishad, "Single lap joints bonded with structural adhesive-reinforced with a mixture of silica nanoparticles and multi walled carbon nanotubes," *Int. J. Adhes. Adhes.*, vol. 80, pp. 76–86, 2018.
- [15] D. Laporte, "Analyse de la réponse d'assemblages collés sous des sollicitations en dynamique rapide. Essais et modélisations." ISAE-ENSMA Ecole Nationale Supérieure de Mécanique et d'Aérotechnique-Poitiers, 2011.
- [16] C.-H. Kim and J.-H. Choi, "Effects of dispersion methods and surface treatment of carbon nano-tubes on defect detectability and static strengths of adhesive joints," *Compos. Struct.*, vol. 176, pp. 684–691, 2017.
- [17] M. Tarfaoui, "Prediction of the strength of the adhesively-bonded joints by the finite elements method," in *Applied Mechanics and Materials*, 2011, vol. 62, pp. 125–134.
- [18] F. Ascione, "The influence of adhesion defects on the collapse of FRP adhesive joints," *Compos. Part B Eng.*, vol. 87, pp. 291–298, 2016.
- [19] G. Di Franco and B. Zuccarello, "Analysis and optimization of hybrid double lap aluminum-GFRP joints," *Compos. Struct.*, vol. 116, pp. 682–693, 2014.
- [20] G. Marannano and B. Zuccarello, "Numerical experimental analysis of hybrid double lap aluminum-CFRP joints," *Compos. Part B Eng.*, vol. 71, pp. 28–39, 2015.
- [21] S. Akpınar, "The strength of the adhesively-bonded step-lap joints for different step numbers," *Compos. Part B Eng.*, vol. 67, pp. 170–178, 2014.

- [22] “No Title.” <https://www.techniques-ingenieur.fr/base-documentaire/archives-th12/archives-travail-des-metaux-assemblage-tiabt/archive-1/assemblages-colles-b5540/>.
- [23] P. Cognard, *Collage des composites*. Ed. Techniques Ingénieur, 2003.
- [24] G. Kelly, “Load transfer in hybrid (bonded/bolted) composite single-lap joints,” *Compos. Struct.*, vol. 69, no. 1, pp. 35–43, 2005.
- [25] M. Stewart and M. Stewart, “An experimental investigation of composite bonded and/or bolted repairs using single lap joint designs,” in *38th Structures, Structural Dynamics, and Materials Conference*, 1997, p. 1339.
- [26] G. Kelly, “Quasi-static strength and fatigue life of hybrid (bonded/bolted) composite single-lap joints,” *Compos. Struct.*, vol. 72, no. 1, pp. 119–129, 2006.
- [27] M. May, H. M. Wang, and R. Akid, “Effects of the addition of inorganic nanoparticles on the adhesive strength of a hybrid sol–gel epoxy system,” *Int. J. Adhes. Adhes.*, vol. 30, no. 6, pp. 505–512, 2010.
- [28] J. Neto, R. D. S. G. Campilho, and L. F. M. Da Silva, “Parametric study of adhesive joints with composites,” *Int. J. Adhes. Adhes.*, vol. 37, pp. 96–101, 2012.
- [29] S. Budhe, M. D. Banea, S. De Barros, and L. F. M. Da Silva, “An updated review of adhesively-bonded joints in composite materials,” *Int. J. Adhes. Adhes.*, vol. 72, pp. 30–42, 2017.
- [30] A. Baldan, “Adhesion phenomena in bonded joints,” *Int. J. Adhes. Adhes.*, vol. 38, pp. 95–116, 2012.
- [31] K. B. Katnam, A. J. Comer, D. Roy, L. F. M. Da Silva, and T. M. Young, “Composite repair in wind turbine blades: an overview,” *J. Adhes.*, vol. 91, no. 1–2, pp. 113–139, 2015.
- [32] M. D. Banea, L. F. M. da Silva, R. D. S. G. Campilho, and C. Sato, “Smart adhesive

- joints: An overview of recent developments,” *J. Adhes.*, vol. 90, no. 1, pp. 16–40, 2014.
- [33] M. Costa, G. Viana, L. F. M. Da Silva, and R. Campilho, “Environmental effect on the fatigue degradation of adhesive joints: a review,” *J. Adhes.*, vol. 93, no. 1–2, pp. 127–146, 2017.
- [34] Y. Kusano, “Atmospheric pressure plasma processing for polymer adhesion: a review,” *J. Adhes.*, vol. 90, no. 9, pp. 755–777, 2014.
- [35] E. A. S. Marques, L. F. M. da Silva, M. D. Banea, and R. J. C. Carbas, “Adhesive joints for low-and high-temperature use: an overview,” *J. Adhes.*, vol. 91, no. 7, pp. 556–585, 2015.
- [36] M. Heshmati, R. Haghani, and M. Al-Emrani, “Environmental durability of adhesively-bonded FRP/steel joints in civil engineering applications: State of the art,” *Compos. Part B Eng.*, vol. 81, pp. 259–275, 2015.
- [37] F. J. P. Chaves, L. F. M. Da Silva, M. De Moura, D. A. Dillard, and V. H. C. Esteves, “Fracture mechanics tests in adhesively-bonded joints: a literature review,” *J. Adhes.*, vol. 90, no. 12, pp. 955–992, 2014.
- [38] T. Vallée, T. Tannert, and S. Fecht, “Adhesively-bonded connections in the context of timber engineering—A Review,” *J. Adhes.*, vol. 93, no. 4, pp. 257–287, 2017.
- [39] R. M. M. Paiva, E. A. S. Marques, L. F. M. da Silva, C. A. C. Antonio, and F. Arán-Ais, “Adhesives in the footwear industry,” *Proc. Inst. Mech. Eng. Part L J. Mater. Des. Appl.*, vol. 230, no. 2, pp. 357–374, 2016.
- [40] M. M. Abdel Wahab, “Fatigue in adhesively-bonded joints: a review,” *Int. Sch. Res. Not.*, vol. 2012, 2012.
- [41] L. F. M. da Silva and C. Sato, *Design of adhesive joints under humid conditions*, vol. 461. Springer, 2013.
- [42] M. L. Williams, R. F. Landel, and J. D. Ferry, “The temperature dependence of

- relaxation mechanisms in amorphous polymers and other glass-forming liquids,” *J. Am. Chem. Soc.*, vol. 77, no. 14, pp. 3701–3707, 1955.
- [43] J. Jahn, M. Weeber, J. Boehner, and R. Steinhilper, “Assessment strategies for composite-metal joining technologies—a review,” *Procedia Cirp*, vol. 50, pp. 689–694, 2016.
- [44] M. Park, K. Frey, and L. Simon, “Modeling and analysis of composite bonded joints,” *Am. J. Mech. Ind. Eng.*, vol. 2, no. 1, p. 1, 2016.
- [45] A. J. Beck, A. Hodzic, C. Soutis, and C. W. Wilson, “Influence of implementation of composite materials in civil aircraft industry on reduction of environmental pollution and greenhouse effect,” in *IOP Conference Series: Materials Science and Engineering*, 2011, vol. 26, no. 1, p. 12015.
- [46] V. J. Law, J. Mohan, F. T. O’Neill, A. Ivankovic, and D. P. Dowling, “Air based atmospheric pressure plasma jet removal of FreKote 710-NC prior to composite-to-composite adhesive bonding,” *Int. J. Adhes. Adhes.*, vol. 54, pp. 72–81, 2014.
- [47] M. Nachtane, M. Tarfaoui, A. El Moumen, and D. Saifaoui, “Damage prediction of horizontal axis marine current turbines under hydrodynamic, hydrostatic and impacts loads,” *Compos. Struct.*, vol. 170, pp. 146–157, 2017.
- [48] L. Sohier, J.-Y. Cognard, and P. Davies, “Analysis of the mechanical behaviour of adhesively-bonded assemblies of composites under tensile–shear out-of-plane loads,” *Compos. Part A Appl. Sci. Manuf.*, vol. 53, pp. 65–74, 2013.
- [49] M. V Fernández, M. F. S. F. de Moura, L. F. M. da Silva, and A. T. Marques, “Characterization of composite bonded joints under pure mode II fatigue loading,” *Compos. Struct.*, vol. 95, pp. 222–226, 2013.
- [50] R. Hunter, J. Möller, A. Vizán, J. Pérez, J. Molina, and J. Leyrer, “Experimental study of the effect of microspheres and milled glass in the adhesive on the mechanical

- adhesion of single lap joints,” *J. Adhes.*, vol. 93, no. 11, pp. 879–895, 2017.
- [51] J. H. Tang, I. Sridhar, and N. Srikanth, “Static and fatigue failure analysis of adhesively-bonded thick composite single lap joints,” *Compos. Sci. Technol.*, vol. 86, pp. 18–25, 2013.
- [52] R. D. Adams, R. W. Atkins, J. A. Harris, and A. J. Kinloch, “Stress analysis and failure properties of carbon-fibre-reinforced-plastic/steel double-lap joints,” *J. Adhes.*, vol. 20, no. 1, pp. 29–53, 1986.
- [53] S. K. Panigrahi, “Structural design of single lap joints with delaminated FRP composite adherends,” *Compos. Part B Eng.*, vol. 51, pp. 112–120, 2013.
- [54] S. Sassi, M. Tarfaoui, and H. Ben Yahia, “An investigation of in-plane dynamic behavior of adhesively-bonded composite joints under dynamic compression at high strain rate,” *Compos. Struct.*, vol. 191, pp. 168–179, 2018.
- [55] “No Title.” <https://www.techniques-ingenieur.fr/base-documentaire/mecanique-th7/assemblage-des-materiaux-par-collage-42188210/collage-des-composites-bm7625/>.
- [56] R. A. Pethrick, “Composite to metal bonding in aerospace and other applications,” in *Welding and bonding of aerospace materials*, Elsevier, 2012, pp. 288–319.
- [57] R. M. Barker and F. Hatt, “Analysis of bonded joints in vehicular structures,” *AIAA J.*, vol. 11, no. 12, pp. 1650–1654, 1973.
- [58] H. Tang and L. Liu, “A novel metal-composite joint and its structural performance,” *Compos. Struct.*, vol. 206, pp. 33–41, 2018.
- [59] F. Erdogan and M. Ratwani, “Stress distribution in bonded joints,” *J. Compos. Mater.*, vol. 5, no. 3, pp. 378–393, 1971.
- [60] M. D. Banea and L. F. M. da Silva, “Adhesively-bonded joints in composite materials: an overview,” *Proc. Inst. Mech. Eng. Part L J. Mater. Des. Appl.*, vol. 223, no. 1, pp. 1–18, 2009.

- [61] R. A. Pethrick, “Design and ageing of adhesives for structural adhesive bonding—a review,” *Proc. Inst. Mech. Eng. Part L J. Mater. Des. Appl.*, vol. 229, no. 5, pp. 349–379, 2015.
- [62] W. Xu and Y. Wei, “Influence of adhesive thickness on local interface fracture and overall strength of metallic adhesive bonding structures,” *Int. J. Adhes. Adhes.*, vol. 40, pp. 158–167, 2013.
- [63] R. D. Adams and N. A. Peppiatt, “Stress analysis of adhesively-bonded tubular lap joints,” *J. Adhes.*, vol. 9, no. 1, pp. 1–18, 1977.
- [64] O. R. Shah and M. Tarfaoui, “Effect of adhesive thickness on the Mode I and II strain energy release rates. Comparative study between different approaches for the calculation of Mode I & II SERR’s,” *Compos. Part B Eng.*, vol. 96, pp. 354–363, 2016.
- [65] R. E. Jensen, D. C. DeSchepper, and D. P. Flanagan, “Multivariate analysis of high through-put adhesively-bonded single lap joints,” *Int. J. Adhes. Adhes.*, vol. 89, pp. 1–10, 2019.
- [66] L. D. R. Grant, R. D. Adams, and L. F. M. da Silva, “Effect of the temperature on the strength of adhesively-bonded single lap and T joints for the automotive industry,” *Int. J. Adhes. Adhes.*, vol. 29, no. 5, pp. 535–542, 2009.
- [67] D. A. Bigwood and A. D. Crocombe, “Elastic analysis and engineering design formulae for bonded joints,” *Int. J. Adhes. Adhes.*, vol. 9, no. 4, pp. 229–242, 1989.
- [68] L. F. M. Da Silva, R. J. C. Carbas, G. W. Critchlow, M. A. V Figueiredo, and K. Brown, “Effect of material, geometry, surface treatment and environment on the shear strength of single lap joints,” *Int. J. Adhes. Adhes.*, vol. 29, no. 6, pp. 621–632, 2009.
- [69] R. A. Hunter-Alarcon, J. Leyrer, E. Leal, A. Vizan, J. Perez, and L. F. M. Da Silva, “Influence of dissimilar composite adherends on the mechanical adhesion of bonded joints for small blade wind turbine applications,” *Int. J. Adhes. Adhes.*, vol. 83, pp.

- 178–183, 2018.
- [70] L. Liao, C. Huang, and T. Sawa, “Effect of adhesive thickness, adhesive type and scarf angle on the mechanical properties of scarf adhesive joints,” *Int. J. Solids Struct.*, vol. 50, no. 25–26, pp. 4333–4340, 2013.
- [71] W. K. Loh, A. D. Crocombe, M. M. A. Wahab, and I. A. Ashcroft, “Modelling anomalous moisture uptake, swelling and thermal characteristics of a rubber toughened epoxy adhesive,” *Int. J. Adhes. Adhes.*, vol. 25, no. 1, pp. 1–12, 2005.
- [72] M. Costa, G. Viana, L. F. M. da Silva, and R. Campilho, “Effect of humidity on the mechanical properties of adhesively-bonded aluminium joints,” *Proc. Inst. Mech. Eng. Part L J. Mater. Des. Appl.*, vol. 232, no. 9, pp. 733–742, 2018.
- [73] M. S. Sciolti, M. Frigione, and M. A. Aiello, “Wet lay-up manufactured FRPs for concrete and masonry repair: influence of water on the properties of composites and on their epoxy components,” *J. Compos. Constr.*, vol. 14, no. 6, pp. 823–833, 2010.
- [74] K. Aniskevich, A. Aniskevich, A. Arnautov, and J. Jansons, “Mechanical properties of pultruded glass fiber-reinforced plastic after moistening,” *Compos. Struct.*, vol. 94, no. 9, pp. 2914–2919, 2012.
- [75] X. Jiang, H. Kolstein, F. Bijlaard, and X. Qiang, “Effects of hygrothermal aging on glass-fibre reinforced polymer laminates and adhesive of FRP composite bridge: Moisture diffusion characteristics,” *Compos. Part A Appl. Sci. Manuf.*, vol. 57, pp. 49–58, 2014.
- [76] A. Zafar, F. Bertocco, J. Schjødt-Thomsen, and J. C. Rauhe, “Investigation of the long term effects of moisture on carbon fibre and epoxy matrix composites,” *Compos. Sci. Technol.*, vol. 72, no. 6, pp. 656–666, 2012.
- [77] S. Alessi, G. Pitarresi, and G. Spadaro, “Effect of hydrothermal ageing on the thermal and delamination fracture behaviour of CFRP composites,” *Compos. Part B Eng.*, vol.

- 67, pp. 145–153, 2014.
- [78] M. D. Banea and L. F. M. da Silva, “The effect of temperature on the mechanical properties of adhesives for the automotive industry,” *Proc. Inst. Mech. Eng. Part L J. Mater. Des. Appl.*, vol. 224, no. 2, pp. 51–62, 2010.
- [79] M. D. Banea, F. S. M. De Sousa, L. F. M. Da Silva, R. Campilho, and A. M. B. de Pereira, “Effects of temperature and loading rate on the mechanical properties of a high temperature epoxy adhesive,” *J. Adhes. Sci. Technol.*, vol. 25, no. 18, pp. 2461–2474, 2011.
- [80] P. Hu, X. Han, W. D. Li, L. Li, and Q. Shao, “Research on the static strength performance of adhesive single lap joints subjected to extreme temperature environment for automotive industry,” *Int. J. Adhes. Adhes.*, vol. 41, pp. 119–126, 2013.
- [81] S. Cao, W. U. Zhis, and X. Wang, “Tensile properties of CFRP and hybrid FRP composites at elevated temperatures,” *J. Compos. Mater.*, vol. 43, no. 4, pp. 315–330, 2009.
- [82] S. A. Sydlik, J.-H. Lee, J. J. Walish, E. L. Thomas, and T. M. Swager, “Epoxy functionalized multi-walled carbon nanotubes for improved adhesives,” *Carbon N. Y.*, vol. 59, pp. 109–120, 2013.
- [83] S. Bose, R. A. Khare, and P. Moldenaers, “Assessing the strengths and weaknesses of various types of pre-treatments of carbon nanotubes on the properties of polymer/carbon nanotubes composites: A critical review,” *Polymer (Guildf.)*, vol. 51, no. 5, pp. 975–993, 2010.
- [84] S. Kango, S. Kalia, A. Celli, J. Njuguna, Y. Habibi, and R. Kumar, “Surface modification of inorganic nanoparticles for development of organic–inorganic nanocomposites—A review,” *Prog. Polym. Sci.*, vol. 38, no. 8, pp. 1232–1261, 2013.

- [85] S. Pavlidou and C. D. Papaspyrides, “A review on polymer–layered silicate nanocomposites,” *Prog. Polym. Sci.*, vol. 33, no. 12, pp. 1119–1198, 2008.
- [86] A. A. Azeez, K. Y. Rhee, S. J. Park, and D. Hui, “Epoxy clay nanocomposites–processing, properties and applications: A review,” *Compos. Part B Eng.*, vol. 45, no. 1, pp. 308–320, 2013.
- [87] C.-Y. Huang, R. S. Trask, and I. P. Bond, “Characterization and analysis of carbon fibre-reinforced polymer composite laminates with embedded circular vasculature,” *J. R. Soc. Interface*, vol. 7, no. 49, pp. 1229–1241, 2010.
- [88] Y. Tao, G. Jiao, B. Wang, and Y. Chang, “Effect of Z-pins’ diameter, spacing and overlap length on connecting performance of CMC single lap joint,” *Acta Mech. Solida Sin.*, vol. 21, no. 5, pp. 461–471, 2008.
- [89] T. Löbel, B. Kolesnikov, S. Scheffler, A. Stahl, and C. Hühne, “Enhanced tensile strength of composite joints by using staple-like pins: Working principles and experimental validation,” *Compos. Struct.*, vol. 106, pp. 453–460, 2013.
- [90] H.-G. Son, Y.-B. Park, J.-H. Kweon, and J.-H. Choi, “Fatigue behaviour of metal pin-reinforced composite single-lap joints in a hygrothermal environment,” *Compos. Struct.*, vol. 108, pp. 151–160, 2014.
- [91] M.-G. Ko, J.-H. Kweon, and J.-H. Choi, “Fatigue characteristics of jagged pin-reinforced composite single-lap joints in hygrothermal environments,” *Compos. Struct.*, vol. 119, pp. 59–66, 2015.
- [92] P. Chang, A. P. Mouritz, and B. N. Cox, “Properties and failure mechanisms of pinned composite lap joints in monotonic and cyclic tension,” *Compos. Sci. Technol.*, vol. 66, no. 13, pp. 2163–2176, 2006.
- [93] Y.-B. Park, B.-H. Lee, J.-H. Kweon, J.-H. Choi, and I.-H. Choi, “The strength of composite bonded T-joints transversely reinforced by carbon pins,” *Compos. Struct.*,

- vol. 94, no. 2, pp. 625–634, 2012.
- [94] P. Chang, A. P. Mouritz, and B. N. Cox, “Elevated temperature properties of pinned composite lap joints,” *J. Compos. Mater.*, vol. 42, no. 8, pp. 741–769, 2008.
- [95] L. G. Stringer and M. J. Hiley, “Through-Thickness-reinforcement of Composite: Z-Pinning, Stitching, and 3D Weaving,” *Tech. Pap. Manuf. Eng. Ser.*, 2003.
- [96] M. Troulis, D. D. R. Cartié, L. Bartattoni, and I. K. Partridge, “Z-pinned woven laminates: interlaminar fracture results and pinning quality considerations,” in *Proceedings of the Sixth International Conference on Deformation and fracture of Composites, Manchester, UK*, 2001, pp. 447–454.
- [97] R. B. Ladani *et al.*, “Multi-scale toughening of fibre composites using carbon nanofibres and z-pins,” *Compos. Sci. Technol.*, vol. 131, pp. 98–109, 2016.
- [98] M. R. Abusrea, S.-W. Han, K. Arakawa, and N.-S. Choi, “Bending strength of CFRP laminated adhesive joints fabricated by vacuum-assisted resin transfer molding,” *Compos. Part B Eng.*, vol. 156, pp. 8–16, 2019.
- [99] J. W. Sawyer, “Effect of stitching on the strength of bonded composite single lap joints,” *AIAA J.*, vol. 23, no. 11, pp. 1744–1748, 1985.
- [100] L. K. Jain, K. H. Leong, Y.-W. Mai, and L. Tong, “Effect of through-thickness stitching on the fatigue life of composite single-lap joints,” *Appl. Compos. Mater.*, vol. 5, no. 6, pp. 399–409, 1998.
- [101] F. Aymerich, “Effect of stitching on the static and fatigue performance of co-cured composite single-lap joints,” *J. Compos. Mater.*, vol. 38, no. 3, pp. 243–257, 2004.
- [102] K. Pingkarawat, C. H. Wang, R. J. Varley, and A. P. Mouritz, “Healing of fatigue delamination cracks in carbon–epoxy composite using mendable polymer stitching,” *J. Intell. Mater. Syst. Struct.*, vol. 25, no. 1, pp. 75–86, 2014.
- [103] H. Heß and N. Himmel, “Structurally stitched NCF CFRP laminates. Part 1:

- Experimental characterization of in-plane and out-of-plane properties,” *Compos. Sci. Technol.*, vol. 71, no. 5, pp. 549–568, 2011.
- [104] K. P. Plain and L. Tong, “An experimental study on mode I and II fracture toughness of laminates stitched with a one-sided stitching technique,” *Compos. Part A Appl. Sci. Manuf.*, vol. 42, no. 2, pp. 203–210, 2011.
- [105] W.-J. An, C.-H. Kim, J.-H. Choi, and J.-H. Kweon, “Static strength of RTM composite joint with I-fiber stitching process,” *Compos. Struct.*, vol. 210, pp. 348–353, 2019.
- [106] J. Arbaoui, M. Tarfaoui, C. Bouery, and A. El Malki Alaoui, “Comparative study of mechanical properties and damage kinetics of two-and three-dimensional woven composites under high-strain rate dynamic compressive loading,” *Int. J. Damage Mech.*, vol. 25, no. 6, pp. 878–899, 2016.
- [107] M. Herrera-Alonso, A. A. Abdala, M. J. McAllister, I. A. Aksay, and R. K. Prud’homme, “Intercalation and stitching of graphite oxide with diaminoalkanes,” *Langmuir*, vol. 23, no. 21, pp. 10644–10649, 2007.
- [108] K. Dransfield, C. Baillie, and Y.-W. Mai, “Improving the delamination resistance of CFRP by stitching—a review,” *Compos. Sci. Technol.*, vol. 50, no. 3, pp. 305–317, 1994.
- [109] L. Tong and L. K. Jain, “Analysis of adhesively-bonded composite lap joints with transverse stitching,” *Appl. Compos. Mater.*, vol. 2, no. 6, pp. 343–365, 1996.
- [110] F. Aymerich, R. Onnis, and P. Priolo, “Analysis of the fracture behaviour of a stitched single-lap joint,” *Compos. Part A Appl. Sci. Manuf.*, vol. 36, no. 5, pp. 603–614, 2005.
- [111] M. Tarfaoui and L. Hamitouche, “Mode I interlaminar fracture toughness of through-thickness-reinforced laminated structures,” in *Advanced Materials Research*, 2012, vol. 423, pp. 154–165.
- [112] W. C. Chung, B. Z. Jang, T. C. Chang, L. R. Hwang, and R. C. Wilcox, “Fracture

- behavior in stitched multidirectional composites,” *Mater. Sci. Eng. A*, vol. 112, pp. 157–173, 1989.
- [113] J. Arbaoui, M. Tarfaoui, and A. E. M. Alaoui, “Mechanical behavior and damage kinetics of woven E-glass/vinylester laminate composites under high strain rate dynamic compressive loading: Experimental and numerical investigation,” *Int. J. Impact Eng.*, vol. 87, pp. 44–54, 2016.
- [114] A. Aktaş and Z. Polat, “Improving strength performance of adhesively-bonded single-lap composite joints,” *J. Compos. Mater.*, vol. 44, no. 24, pp. 2919–2928, 2010.
- [115] P. E. Rouse Jr, “A theory of the linear viscoelastic properties of dilute solutions of coiling polymers,” *J. Chem. Phys.*, vol. 21, no. 7, pp. 1272–1280, 1953.
- [116] H. R. Brown, “The adhesion between polymers,” *Annu. Rev. Mater. Sci.*, vol. 21, no. 1, pp. 463–489, 1991.
- [117] “No Title.” <https://www.intechopen.com/chapters/72636>.
- [118] I. A. Akpınar, K. Gültekin, S. Akpınar, H. Akbulut, and A. Ozel, “Experimental analysis on the single-lap joints bonded by a nanocomposite adhesives which obtained by adding nanostructures,” *Compos. Part B Eng.*, vol. 110, pp. 420–428, 2017.
- [119] F. H. Gojny, M. H. G. Wichmann, U. Köpke, B. Fiedler, and K. Schulte, “Carbon nanotube-reinforced epoxy-composites: enhanced rigidity and fracture toughness at low nanotube content,” *Compos. Sci. Technol.*, vol. 64, no. 15, pp. 2363–2371, 2004.
- [120] R. Schueler, J. Petermann, K. Schulte, and H. Wentzel, “Percolation in carbon black filled epoxy resin,” in *Macromolecular Symposia*, 1996, vol. 104, no. 1, pp. 261–268.
- [121] M. Kupke, H.-P. Wentzel, and K. Schulte, “Electrically conductive glass fibre reinforced epoxy resin,” *Mater. Res. Innov.*, vol. 2, no. 3, pp. 164–169, 1998.
- [122] M. Hassar, “Influence des nano-charges de noir de carbone sur le comportement mécanique de matériaux composites: application au blindage électromagnétique.”

- Université de Technologie de Compiègne, 2013.
- [123] M. Tarfaoui, K. Lafdi, I. Beloufa, D. Daloia, and A. Muhsan, “Effect of graphene nano-additives on the local mechanical behavior of derived polymer nanocomposites,” *Polymers (Basel)*, vol. 10, no. 6, p. 667, 2018.
- [124] Y. K. Hong, C. Y. Lee, C. K. Jeong, D. E. Lee, K. Kim, and J. Joo, “Method and apparatus to measure electromagnetic interference shielding efficiency and its shielding characteristics in broadband frequency ranges,” *Rev. Sci. Instrum.*, vol. 74, no. 2, pp. 1098–1102, 2003.
- [125] M.-F. Yu, B. S. Files, S. Arepalli, and R. S. Ruoff, “Tensile loading of ropes of single wall carbon nanotubes and their mechanical properties,” *Phys. Rev. Lett.*, vol. 84, no. 24, p. 5552, 2000.
- [126] H. Im and J. Kim, “Thermal conductivity of a graphene oxide–carbon nanotube hybrid/epoxy composite,” *Carbon N. Y.*, vol. 50, no. 15, pp. 5429–5440, 2012.
- [127] Z. A. Ghaleb, M. Mariatti, and Z. M. Ariff, “Properties of graphene nanopowder and multi-walled carbon nanotube-filled epoxy thin-film nanocomposites for electronic applications: The effect of sonication time and filler loading,” *Compos. Part A Appl. Sci. Manuf.*, vol. 58, pp. 77–83, 2014.
- [128] A. El Moumen, M. Tarfaoui, K. Lafdi, and H. Benyahia, “Dynamic properties of carbon nanotube-reinforced carbon fibers/epoxy textile composites under low velocity impact,” *Compos. Part B Eng.*, vol. 125, pp. 1–8, 2017.
- [129] L. S. Schadler, S. C. and Giannaris, and P. M. Ajayan, “Load transfer in carbon nanotube epoxy composites,” *Appl. Phys. Lett.*, vol. 73, no. 26, pp. 3842–3844, 1998.
- [130] N. G. Sahoo, S. Rana, J. W. Cho, L. Li, and S. H. Chan, “Polymer nanocomposites based on functionalized carbon nanotubes,” *Prog. Polym. Sci.*, vol. 35, no. 7, pp. 837–867, 2010.

- [131] A. El Moumen, M. Tarfaoui, and K. Lafdi, “Mechanical characterization of carbon nanotubes based polymer composites using indentation tests,” *Compos. Part B Eng.*, vol. 114, pp. 1–7, 2017.
- [132] X. Sun, H. Sun, H. Li, and H. Peng, “Developing polymer composite materials: carbon nanotubes or graphene?,” *Adv. Mater.*, vol. 25, no. 37, pp. 5153–5176, 2013.
- [133] K. Song *et al.*, “Structural polymer-based carbon nanotube composite fibers: Understanding the processing–structure–performance relationship,” *Materials (Basel)*, vol. 6, no. 6, pp. 2543–2577, 2013.
- [134] L. Bokobza, “Multiwall carbon nanotube-filled natural rubber: Electrical and mechanical properties,” *Express Polym. Lett.*, vol. 6, no. 3, 2012.
- [135] B. F. Jogi, M. Sawant, M. Kulkarni, and P. K. Brahmankar, “Dispersion and performance properties of carbon nanotubes (CNTs) based polymer composites: a review,” 2012.
- [136] H. Benyahia, M. Tarfaoui, V. Datsyuk, A. El Moumen, S. Trotsenko, and S. Reich, “Dynamic properties of hybrid composite structures based multiwalled carbon nanotubes,” *Compos. Sci. Technol.*, vol. 148, pp. 70–79, 2017.
- [137] M. Tarfaoui, A. El Moumen, and K. Lafdi, “Progressive damage modeling in carbon fibers/carbon nanotube-reinforced polymer composites,” *Compos. Part B Eng.*, vol. 112, pp. 185–195, 2017.
- [138] P. J. F. Harris, “Carbon nanotubes and related structures: new materials for the twenty-first century.” American Association of Physics Teachers, 2004.
- [139] K. Gültekin, S. Akpınar, and A. Özel, “The effect of moment and flexural rigidity of adherent on the strength of adhesively-bonded single lap joints,” *J. Adhes.*, vol. 91, no. 8, pp. 637–650, 2015.
- [140] J. Kim *et al.*, “Effect of the hydrophilic nanofiller loading on the mechanical properties

- and the microtensile bond strength of an ethanol-based one-bottle dentin adhesive,” *J. Biomed. Mater. Res. Part B Appl. Biomater. An Off. J. Soc. Biomater. Japanese Soc. Biomater. Aust. Soc. Biomater. Korean Soc. Biomater.*, vol. 72, no. 2, pp. 284–291, 2005.
- [141] M. C. M. Conde, C. H. Zanchi, S. A. Rodrigues-Junior, N. L. V Carreno, F. A. Ogliari, and E. Piva, “Nanofiller loading level: Influence on selected properties of an adhesive resin,” *J. Dent.*, vol. 37, no. 5, pp. 331–335, 2009.
- [142] L. Zhai, G. Ling, J. Li, and Y. Wang, “The effect of nanoparticles on the adhesion of epoxy adhesive,” *Mater. Lett.*, vol. 60, no. 25–26, pp. 3031–3033, 2006.
- [143] B. J. P. Jansen, K. Y. Tamminga, H. E. H. Meijer, and P. J. Lemstra, “Preparation of thermoset rubbery epoxy particles as novel toughening modifiers for glassy epoxy resins,” *Polymer (Guildf.)*, vol. 40, no. 20, pp. 5601–5607, 1999.
- [144] V. K. Srivastava, “Effect of carbon nanotubes on the strength of adhesive lap joints of C/C and C/C–SiC ceramic fibre composites,” *Int. J. Adhes. Adhes.*, vol. 31, no. 6, pp. 486–489, 2011.
- [145] R. J. Park *et al.*, “Export efficiency of black carbon aerosol in continental outflow: Global implications,” *J. Geophys. Res. Atmos.*, vol. 110, no. D11, 2005.
- [146] S. Yano, T. Furukawa, M. Kodomari, and K. Kurita, “Physical properties of poly (vinyl alcohol)/silica hybrid prepared by sol-gel process,” *Kobunshi ronbunshu (Tokyo)*, vol. 53, no. 4, pp. 218–224, 1996.
- [147] I. V Shpan’Ko, I. V Sadovaya, and A. M. Kitaigorodskii, “Effect of the Structures of Arylsulfonic Acids on the Kinetics of Oxirane Ring Opening in 4-Nitrophenyloxirane,” *Theor. Exp. Chem.*, vol. 36, no. 6, pp. 338–341, 2000.
- [148] Q. L. Ji, M. Q. Zhang, M. Z. Rong, B. Wetzel, and K. Friedrich, “Tribological properties of surface modified nano-alumina/epoxy composites,” *J. Mater. Sci.*, vol. 39,

- no. 21, pp. 6487–6493, 2004.
- [149] B. Soltannia and F. Taheri, “Influence of nano-reinforcement on the mechanical behavior of adhesively-bonded single-lap joints subjected to static, quasi-static, and impact loading,” *J. Adhes. Sci. Technol.*, vol. 29, no. 5, pp. 424–442, 2015.
- [150] R. Aradhana, S. Mohanty, and S. K. Nayak, “High performance epoxy nanocomposite adhesive: Effect of nanofillers on adhesive strength, curing and degradation kinetics,” *Int. J. Adhes. Adhes.*, vol. 84, pp. 238–249, 2018.
- [151] W. Zielecki, A. Kubit, T. Trzepieciński, U. Narkiewicz, and Z. Czech, “Impact of multiwall carbon nanotubes on the fatigue strength of adhesive joints,” *Int. J. Adhes. Adhes.*, vol. 73, pp. 16–21, 2017.
- [152] R. Mactabi, I. D. Rosca, and S. V Hoa, “Monitoring the integrity of adhesive joints during fatigue loading using carbon nanotubes,” *Compos. Sci. Technol.*, vol. 78, pp. 1–9, 2013.
- [153] T. Liu, I. Y. Phang, L. Shen, S. Y. Chow, and W.-D. Zhang, “Morphology and mechanical properties of multiwalled carbon nanotube-reinforced nylon-6 composites,” *Macromolecules*, vol. 37, no. 19, pp. 7214–7222, 2004.
- [154] F. H. Gojny, M. H. G. Wichmann, B. Fiedler, and K. Schulte, “Influence of different carbon nanotubes on the mechanical properties of epoxy matrix composites—a comparative study,” *Compos. Sci. Technol.*, vol. 65, no. 15–16, pp. 2300–2313, 2005.
- [155] M. May, H. M. Wang, and R. Akid, “Influence of adding multiwalled carbon nanotubes on the adhesive strength of composite epoxy/sol–gel materials,” *J. Coatings Technol. Res.*, vol. 13, no. 2, pp. 325–332, 2016.
- [156] E. Sancaktar and S. Kumar, “Selective use of rubber toughening to optimize lap-joint strength,” *J. Adhes. Sci. Technol.*, vol. 14, no. 10, pp. 1265–1296, 2000.
- [157] L. Guadagno, M. Sarno, U. Vietri, M. Raimondo, C. Cirillo, and P. Ciambelli,

- “Graphene-based structural adhesive to enhance adhesion performance,” *RSC Adv.*, vol. 5, no. 35, pp. 27874–27886, 2015.
- [158] A. Silva Neto, D. T. L. da Cruz, and A. F. Ávila, “Nano-modified adhesive by graphene: the single lap-joint case,” *Mater. Res.*, vol. 16, pp. 592–596, 2013.
- [159] I. A. Akpınar, K. Gültekin, S. Akpınar, H. Akbulut, and A. Ozel, “Research on strength of nanocomposite adhesively-bonded composite joints,” *Compos. Part B Eng.*, vol. 126, pp. 143–152, 2017.
- [160] B. Ahmadi-Moghadam, M. Sharafimasooleh, S. Shadlou, and F. Taheri, “Effect of functionalization of graphene nanoplatelets on the mechanical response of graphene/epoxy composites,” *Mater. Des.*, vol. 66, pp. 142–149, 2015.
- [161] Y.-J. Wan *et al.*, “Improved dispersion and interface in the graphene/epoxy composites via a facile surfactant-assisted process,” *Compos. Sci. Technol.*, vol. 82, pp. 60–68, 2013.
- [162] C. Salom, M. G. Prolongo, A. Toribio, A. J. Martínez-Martínez, I. A. de Cárcer, and S. G. Prolongo, “Mechanical properties and adhesive behavior of epoxy-graphene nanocomposites,” *Int. J. Adhes. Adhes.*, vol. 84, pp. 119–125, 2018.
- [163] M. Shioya, Y. Kuroyanagi, M. Ryu, and J. Morikawa, “Analysis of the adhesive properties of carbon nanotube-and graphene oxide nanoribbon-dispersed aliphatic epoxy resins based on the Maxwell model,” *Int. J. Adhes. Adhes.*, vol. 84, pp. 27–36, 2018.
- [164] M. Tarfaoui, K. Lafdi, and A. El Moumen, “Mechanical properties of carbon nanotubes based polymer composites,” *Compos. Part B Eng.*, vol. 103, pp. 113–121, 2016.
- [165] K. H. G. Ashbee and R. C. Wyatt, “Water damage in glass fibre/resin composites,” *Proc. R. Soc. London. A. Math. Phys. Sci.*, vol. 312, no. 1511, pp. 553–564, 1969.
- [166] B. Dewimille and A. R. Bunsell, “Vieillissement hygrothermique d’un matériau

- composite fibres de verre–résine époxyde,” *Thesis Ec. des Mines Paris*, 1981.
- [167] L. Vincent, A. Chateauinois, B. Chabert, and J. P. Soulier, “Effects of hygrothermal aging on the durability of glass/epoxy composites. Physico-chemical analysis and damage mapping in static fatigue,” *ICCM/9. Compos. Behav.*, vol. 5, pp. 593–600, 1993.
- [168] M.-B. Heman, “Contribution à l’étude des interphases et de leur comportement au vieillissement hygrothermique dans les systèmes à matrice thermodurcissable renforcés de fibres de verre.” Université du Sud Toulon Var, 2008.
- [169] S. Iijima, “Helical microtubules of graphitic carbon,” *Nature*, vol. 354, no. 6348, pp. 56–58, 1991.
- [170] S. Iijima and T. Ichihashi, “Single-shell carbon nanotubes of 1-nm diameter,” *Nature*, vol. 363, no. 6430, pp. 603–605, 1993.
- [171] D. S. Bethune *et al.*, “Cobalt-catalysed growth of carbon nanotubes with single-atomic-layer walls,” *Nature*, vol. 363, no. 6430, pp. 605–607, 1993.
- [172] M. K. Njuguna, “Characterisation of multi wall carbon nanotube–polymer composites for strain sensing applications.” Queensland University of Technology, 2012.
- [173] D. H. Robertson, D. W. Brenner, and J. W. Mintmire, “Energetics of nanoscale graphitic tubules,” *Phys. Rev. B*, vol. 45, no. 21, p. 12592, 1992.
- [174] M. M. J. Treacy, T. W. Ebbesen, and J. M. Gibson, “Exceptionally high Young’s modulus observed for individual carbon nanotubes,” *Nature*, vol. 381, no. 6584, pp. 678–680, 1996.
- [175] E. W. Wong, P. E. Sheehan, and C. M. Lieber, “Nanobeam mechanics: elasticity, strength, and toughness of nanorods and nanotubes,” *Science (80-.)*, vol. 277, no. 5334, pp. 1971–1975, 1997.
- [176] A. Krishnan, E. Dujardin, T. W. Ebbesen, P. N. Yianilos, and M. M. J. Treacy,

- “Young’s modulus of single-walled nanotubes,” *Phys. Rev. B*, vol. 58, no. 20, p. 14013, 1998.
- [177] M.-F. Yu, O. Lourie, M. J. Dyer, K. Moloni, T. F. Kelly, and R. S. Ruoff, “Strength and breaking mechanism of multiwalled carbon nanotubes under tensile load,” *Science (80-.)*, vol. 287, no. 5453, pp. 637–640, 2000.
- [178] J. P. Lu, “Elastic properties of single and multilayered nanotubes,” *J. Phys. Chem. Solids*, vol. 58, no. 11, pp. 1649–1652, 1997.
- [179] E. Hernandez, C. Goze, P. Bernier, and A. Rubio, “Elastic properties of C and B x C y N z composite nanotubes,” *Phys. Rev. Lett.*, vol. 80, no. 20, p. 4502, 1998.
- [180] B. I. Yakobson, C. J. Brabec, and J. Bernholc, “Nanomechanics of carbon tubes: instabilities beyond linear response,” *Phys. Rev. Lett.*, vol. 76, no. 14, p. 2511, 1996.
- [181] M. B. Nardelli, B. I. Yakobson, and J. Bernholc, “Brittle and ductile behavior in carbon nanotubes,” *Phys. Rev. Lett.*, vol. 81, no. 21, p. 4656, 1998.
- [182] Q. Zhao, M. B. Nardelli, and J. Bernholc, “Ultimate strength of carbon nanotubes: A theoretical study,” *Phys. Rev. B*, vol. 65, no. 14, p. 144105, 2002.
- [183] K. S. Novoselov, “Nobel lecture: Graphene: Materials in the flatland,” *Rev. Mod. Phys.*, vol. 83, no. 3, p. 837, 2011.
- [184] X. Li, “Nanocomposites graphène/polymères: rôle de la viscoélasticité, mise en oeuvre par assemblage forcé, et étude de l’interface.” Ecole nationale supérieure d’arts et métiers-ENSAM, 2015.
- [185] B. C. Brodie, “XIII. On the atomic weight of graphite,” *Philos. Trans. R. Soc. London*, no. 149, pp. 249–259, 1859.
- [186] K. S. Novoselov *et al.*, “Electric field effect in atomically thin carbon films,” *Science (80-.)*, vol. 306, no. 5696, pp. 666–669, 2004.
- [187] A. K. Geim, “Graphene: status and prospects,” *Science (80-.)*, vol. 324, no. 5934, pp.

- 1530–1534, 2009.
- [188] I. W. Frank, D. M. Tanenbaum, A. M. van der Zande, and P. L. McEuen, “Mechanical properties of suspended graphene sheets,” *J. Vac. Sci. Technol. B Microelectron. Nanom. Struct. Process. Meas. Phenom.*, vol. 25, no. 6, pp. 2558–2561, 2007.
- [189] C. Lee, X. Wei, J. W. Kysar, and J. Hone, “Measurement of the elastic properties and intrinsic strength of monolayer graphene,” *Science (80-.)*, vol. 321, no. 5887, pp. 385–388, 2008.
- [190] J. Zhang, T. P. Lodge, and C. W. Macosko, “Interfacial slip reduces polymer-polymer adhesion during coextrusion,” *J. Rheol. (N. Y. N. Y.)*, vol. 50, no. 1, pp. 41–57, 2006.
- [191] J. S. Bunch *et al.*, “Impermeable atomic membranes from graphene sheets,” *Nano Lett.*, vol. 8, no. 8, pp. 2458–2462, 2008.
- [192] A. B. Bourlinos, V. Georgakilas, R. Zboril, T. A. Steriotis, and A. K. Stubos, “Liquid-phase exfoliation of graphite towards solubilized graphenes,” *small*, vol. 5, no. 16, pp. 1841–1845, 2009.
- [193] D. Parviz, S. Das, H. S. T. Ahmed, F. Irin, S. Bhattacharia, and M. J. Green, “Dispersions of non-covalently functionalized graphene with minimal stabilizer,” *ACS Nano*, vol. 6, no. 10, pp. 8857–8867, 2012.
- [194] R. Bari, G. Tamas, F. Irin, A. J. A. Aquino, M. J. Green, and E. L. Quitevis, “Direct exfoliation of graphene in ionic liquids with aromatic groups,” *Colloids Surfaces A Physicochem. Eng. Asp.*, vol. 463, pp. 63–69, 2014.
- [195] W. S. Hummers Jr and R. E. Offeman, “Preparation of graphitic oxide,” *J. Am. Chem. Soc.*, vol. 80, no. 6, p. 1339, 1958.
- [196] X. Wang *et al.*, “Large-scale synthesis of few-layered graphene using CVD,” *Chem. Vap. Depos.*, vol. 15, no. 1-3, pp. 53–56, 2009.
- [197] X. Li *et al.*, “Large-area synthesis of high-quality and uniform graphene films on

- copper foils,” *Science* (80-.), vol. 324, no. 5932, pp. 1312–1314, 2009.
- [198] E. Rollings *et al.*, “Synthesis and characterization of atomically thin graphite films on a silicon carbide substrate,” *J. Phys. Chem. Solids*, vol. 67, no. 9–10, pp. 2172–2177, 2006.
- [199] P. W. Sutter, J.-I. Flege, and E. A. Sutter, “Epitaxial graphene on ruthenium,” *Nat. Mater.*, vol. 7, no. 5, pp. 406–411, 2008.
- [200] J. R. Potts, D. R. Dreyer, C. W. Bielawski, and R. S. Ruoff, “Graphene-based polymer nanocomposites,” *Polymer (Guildf.)*, vol. 52, no. 1, pp. 5–25, 2011.
- [201] X. Li *et al.*, “Forced assembly by multilayer coextrusion to create oriented graphene reinforced polymer nanocomposites,” *Polymer (Guildf.)*, vol. 55, no. 1, pp. 248–257, 2014.
- [202] T. Ramanathan *et al.*, “Functionalized graphene sheets for polymer nanocomposites,” *Nat. Nanotechnol.*, vol. 3, no. 6, pp. 327–331, 2008.
- [203] P. Song, Z. Cao, Y. Cai, L. Zhao, Z. Fang, and S. Fu, “Fabrication of exfoliated graphene-based polypropylene nanocomposites with enhanced mechanical and thermal properties,” *Polymer (Guildf.)*, vol. 52, no. 18, pp. 4001–4010, 2011.
- [204] T. Wei *et al.*, “The synergy of a three filler combination in the conductivity of epoxy composites,” *Mater. Lett.*, vol. 64, no. 21, pp. 2376–2379, 2010.
- [205] J. K. Oleiwi, M. S. Hamza, and N. A. Nassir, “A study of the effect of carbon black powder on the physical properties of SBR/NR blends used in passenger tire treads,” *Eng. Tech. J.*, vol. 29, no. 5, pp. 856–870, 2011.
- [206] S. K. Jebur, “Carbon black production, analyzing and characterization,” 2018.
- [207] W. Kwon, J.-M. Kim, and S.-W. Rhee, “Electrocatalytic carbonaceous materials for counter electrodes in dye-sensitized solar cells,” *J. Mater. Chem. A*, vol. 1, no. 10, pp. 3202–3215, 2013.

- [208] S. Samaržija-Jovanović, V. Jovanović, G. Marković, and M. Marinović-Cincović, “The effect of different types of carbon blacks on the rheological and thermal properties of acrylonitrile butadiene rubber,” *J. Therm. Anal. Calorim.*, vol. 98, no. 1, pp. 275–283, 2009.
- [209] L. Moulin, S. Da Silva, A. Bounaceur, M. Herblot, and Y. Soudais, “Assessment of recovered carbon black obtained by waste tires steam water thermolysis: an industrial application,” *Waste and Biomass Valorization*, vol. 8, no. 8, pp. 2757–2770, 2017.
- [210] P. Poudel and Q. Qiao, “Carbon nanostructure counter electrodes for low cost and stable dye-sensitized solar cells,” *Nano Energy*, vol. 4, pp. 157–175, 2014.
- [211] Q. Tang, J. Duan, Y. Duan, B. He, and L. Yu, “Recent advances in alloy counter electrodes for dye-sensitized solar cells. A critical review,” *Electrochim. Acta*, vol. 178, pp. 886–899, 2015.
- [212] W. B. Wiegand and W. A. Ladd, “Colloidal Carbon as Revealed by the Electron Microscope,” *Rubber Chem. Technol.*, vol. 15, no. 3, pp. 664–671, 1942.
- [213] S. Wolff and M. J. Wang, “Carbon black science & technology,” by *JB Donnet, RC Bansal, MJ Wang*, 1993.
- [214] N. Domun, H. Hadavinia, T. Zhang, T. Sainsbury, G. H. Liaghat, and S. Vahid, “Improving the fracture toughness and the strength of epoxy using nanomaterials—a review of the current status,” *Nanoscale*, vol. 7, no. 23, pp. 10294–10329, 2015.
- [215] X. Wang, J. Jin, and M. Song, “An investigation of the mechanism of graphene toughening epoxy,” *Carbon N. Y.*, vol. 65, pp. 324–333, 2013.
- [216] G. Gkikas, N.-M. Barkoula, and A. S. Paipetis, “Effect of dispersion conditions on the thermo-mechanical and toughness properties of multi walled carbon nanotubes-reinforced epoxy,” *Compos. Part B Eng.*, vol. 43, no. 6, pp. 2697–2705, 2012.
- [217] L.-C. Tang, H. Zhang, S. Sprenger, L. Ye, and Z. Zhang, “Fracture mechanisms of

- epoxy-based ternary composites filled with rigid-soft particles,” *Compos. Sci. Technol.*, vol. 72, no. 5, pp. 558–565, 2012.
- [218] H.-Y. Liu, G.-T. Wang, Y.-W. Mai, and Y. Zeng, “On fracture toughness of nano-particle modified epoxy,” *Compos. Part B Eng.*, vol. 42, no. 8, pp. 2170–2175, 2011.
- [219] L.-C. Tang *et al.*, “Fracture toughness and electrical conductivity of epoxy composites filled with carbon nanotubes and spherical particles,” *Compos. Part A Appl. Sci. Manuf.*, vol. 45, pp. 95–101, 2013.
- [220] P. Richard, T. Prasse, J.-Y. Cavaille, L. Chazeau, C. Gauthier, and J. Duchet, “Reinforcement of rubbery epoxy by carbon nanofibres,” *Mater. Sci. Eng. A*, vol. 352, no. 1–2, pp. 344–348, 2003.
- [221] T. Adachi, M. Osaki, W. Araki, and S.-C. Kwon, “Fracture toughness of nano-and micro-spherical silica-particle-filled epoxy composites,” *Acta Mater.*, vol. 56, no. 9, pp. 2101–2109, 2008.
- [222] A. J. Kinloch, S. J. Shaw, D. A. Tod, and D. L. Hunston, “Deformation and fracture behaviour of a rubber-toughened epoxy: 1. Microstructure and fracture studies,” *Polymer (Guildf.)*, vol. 24, no. 10, pp. 1341–1354, 1983.
- [223] T. H. Hsieh, A. J. Kinloch, K. Masania, A. C. Taylor, and S. Sprenger, “The mechanisms and mechanics of the toughening of epoxy polymers modified with silica nanoparticles,” *Polymer (Guildf.)*, vol. 51, no. 26, pp. 6284–6294, 2010.
- [224] C. Chen, R. S. Justice, D. W. Schaefer, and J. W. Baur, “Highly dispersed nanosilica–epoxy resins with enhanced mechanical properties,” *Polymer (Guildf.)*, vol. 49, no. 17, pp. 3805–3815, 2008.
- [225] J. Lee and A. F. Yee, “Inorganic particle toughening II: toughening mechanisms of glass bead filled epoxies,” *Polymer (Guildf.)*, vol. 42, no. 2, pp. 589–597, 2001.
- [226] M. R. Dadfar and F. Ghadami, “Effect of rubber modification on fracture toughness

- properties of glas-reinforced hot cured epoxy composites,” *Mater. Des.*, vol. 47, pp. 16–20, 2013.
- [227] R. Thomas *et al.*, “Miscibility, morphology, thermal, and mechanical properties of a DGEBA based epoxy resin toughened with a liquid rubber,” *Polymer (Guildf.)*, vol. 49, no. 1, pp. 278–294, 2008.
- [228] P. Bussi and H. Ishida, “Partially miscible blends of epoxy resin and epoxidized rubber: structural characterization of the epoxidized rubber and mechanical properties of the blends,” *J. Appl. Polym. Sci.*, vol. 53, no. 4, pp. 441–454, 1994.
- [229] J. M. Wernik and S. A. Meguid, “On the mechanical characterization of carbon nanotube reinforced epoxy adhesives,” *Mater. Des.*, vol. 59, pp. 19–32, 2014.
- [230] P. Bussi and H. Ishida, “Composition of the continuous phase in partially miscible blends of epoxy resin and epoxidized rubber by dynamic mechanical analysis,” *Polymer (Guildf.)*, vol. 35, no. 5, pp. 956–966, 1994.
- [231] X.-L. Xie, Y.-W. Mai, and X.-P. Zhou, “Dispersion and alignment of carbon nanotubes in polymer matrix: a review,” *Mater. Sci. Eng. R Reports*, vol. 49, no. 4, pp. 89–112, 2005.
- [232] C. E. Pizzutto, J. Suave, J. Bertholdi, S. H. Pezzin, L. A. F. Coelho, and S. C. Amico, “Mechanical and dilatometric properties of carboxylated swcnt/epoxy composites: effects of the dispersion in the resin and in the hardener,” *J. Reinf. Plast. Compos.*, vol. 29, no. 4, pp. 524–530, 2010.
- [233] M. Yourdkhani and P. Hubert, “A systematic study on dispersion stability of carbon nanotube-modified epoxy resins,” *Carbon N. Y.*, vol. 81, pp. 251–259, 2015.
- [234] V. Vahedi, P. Pasbakhsh, and S.-P. Chai, “Toward high performance epoxy/halloysite nanocomposites: new insights based on rheological, curing, and impact properties,” *Mater. Des.*, vol. 68, pp. 42–53, 2015.

- [235] S.-Y. Fu, Z.-K. Chen, S. Hong, and C. C. Han, “The reduction of carbon nanotube (CNT) length during the manufacture of CNT/polymer composites and a method to simultaneously determine the resulting CNT and interfacial strengths,” *Carbon N. Y.*, vol. 47, no. 14, pp. 3192–3200, 2009.
- [236] P.-C. Ma, N. A. Siddiqui, G. Marom, and J.-K. Kim, “Dispersion and functionalization of carbon nanotubes for polymer-based nanocomposites: a review,” *Compos. Part A Appl. Sci. Manuf.*, vol. 41, no. 10, pp. 1345–1367, 2010.
- [237] A. Jiménez-Suárez, M. Campo, M. Sánchez, C. Romón, and A. Ureña, “Influence of the functionalization of carbon nanotubes on calendaring dispersion effectiveness in a low viscosity resin for VARIM processes,” *Compos. Part B Eng.*, vol. 43, no. 8, pp. 3482–3490, 2012.
- [238] D. Quan, J. L. Urdániz, and A. Ivanković, “Enhancing mode-I and mode-II fracture toughness of epoxy and carbon fibre reinforced epoxy composites using multi-walled carbon nanotubes,” *Mater. Des.*, vol. 143, pp. 81–92, 2018, doi: <https://doi.org/10.1016/j.matdes.2018.01.051>.
- [239] D. Quan, D. Carolan, C. Rouge, N. Murphy, and A. Ivankovic, “Carbon nanotubes and core-shell rubber nanoparticles modified structural epoxy adhesives,” *J. Mater. Sci.*, vol. 52, no. 8, pp. 4493–4508, 2017.
- [240] W. Zhao, M. Fang, F. Wu, H. Wu, L. Wang, and G. Chen, “Preparation of graphene by exfoliation of graphite using wet ball milling,” *J. Mater. Chem.*, vol. 20, no. 28, pp. 5817–5819, 2010.
- [241] “No Title.” <https://magic-engineering.ro/uploads/2017/05/Digimat-for-Nano-Composites.pdf>.
- [242] A. El Moumen, M. Tarfaoui, M. Nachtane, and K. Lafdi, “Carbon nanotubes as a player to improve mechanical shock wave absorption,” *Compos. Part B Eng.*, vol. 164,

- pp. 67–71, 2019.
- [243] A. El Moumen, M. Tarfaoui, H. Benyahia, and K. Lafdi, “Mechanical behavior of carbon nanotubes-based polymer composites under impact tests,” *J. Compos. Mater.*, vol. 53, no. 7, pp. 925–940, 2019.
- [244] M. Chihi, M. Tarfaoui, Y. Qureshi, H. Benyahia, and C. Bouraoui, “Graphene nanofillers as a player to improve the dynamic compressive response and failure behavior of carbon/epoxy composite,” *Nanotechnology*, vol. 31, no. 42, p. 425709, 2020.
- [245] M. El Achaby, “Nanocomposites graphène-polymère thermoplastique: Fabrication et étude des propriétés structurales, thermiques, rhéologiques et mécaniques.” Université Mohammed V-Agdal, Faculté des Sciences de Rabat; Faculté des ..., 2012.
- [246] Y. Kanake, “Développement de nanocomposites à base de polymères d’origine renouvelable-optimisation des propriétés barrière et de transport.” Reims, 2016.
- [247] A. Chorfa, “Etude de la fissuration du verre par l’indentation instrumentée.” 2018.
- [248] P. J. Blau, *Microindentation Techniques in Materials Science and Engineering: A Symposium Sponsored by ASTM Committee E-4 on Metallography and by the International Metallographic Society, Philadelphia, PA, 15-18 July 1984*, no. 889. Astm International, 1986.
- [249] K. L. Johnson and K. L. Johnson, *Contact mechanics*. Cambridge university press, 1987.
- [250] P. Kaszinski, “Indentation cyclique et déformation progressive: étude expérimentale et simulation des contacts internes à des implants chirurgicaux.” Cachan, Ecole normale supérieure, 1999.
- [251] H. Kolsky, “An investigation of the mechanical properties of materials at very high rates of loading,” *Proc. Phys. Soc. Sect. B*, vol. 62, no. 11, p. 676, 1949.

- [252] K. M. Kpenyigba, “Etude du comportement dynamique et modélisation thermoviscoplastique de nuances d’acier soumises à un impact balistique.” Université de Lorraine, 2013.
- [253] W. W. Chen and B. Song, *Split Hopkinson (Kolsky) bar: design, testing and applications*. Springer Science & Business Media, 2010.
- [254] manel chihi and M. T. and Y. Q. and C. B. and H. B. E. N. YAHYA, “Effect of Carbon Nanotubes on the In-plane Dynamic Behavior of a Carbon/Epoxy Composite under high strain rate compression using SPHB,” *Smart Mater. Struct.*, 2020, [Online]. Available: <http://iopscience.iop.org/10.1088/1361-665X/ab83cd>.
- [255] S. Sassi, M. Tarfaoui, M. Nachtane, and H. Ben Yahia, “Strain rate effects on the dynamic compressive response and the failure behavior of polyester matrix,” *Compos. Part B Eng.*, vol. 174, p. 107040, 2019.
- [256] S. Khammassi, M. Tarfaoui, and K. Lafdi, “Study of mechanical performance of polymer nanocomposite-reinforced with exfoliated graphite of different mesh sizes using micro-indentation,” *J. Compos. Mater.*, p. 0021998321993211, 2021.
- [257] G. Gary and H. Zhao, “Étude expérimentale du comportement dynamique des matériaux,” *Mécanique Ind.*, vol. 1, no. 1, pp. 15–26, 2000.
- [258] W. E. Jahsman, “Reexamination of the Kolsky technique for measuring dynamic material behavior,” 1971.
- [259] J. F. Bell, “An experimental diffraction grating study of the quasi-static hypothesis of the split Hopkinson bar experiment,” *J. Mech. Phys. Solids*, vol. 14, no. 6, pp. 309–327, 1966.
- [260] H. D. Bui, “Introduction aux problèmes inverses en mécanique des matériaux,” 1993.
- [261] K. T. Ramesh, “Handbook of experimental solid mechanics.” Springer New York, 2008.

- [262] M. Considère, *Mémoire sur l'emploi du fer et de l'acier dans les constructions*. Vue Ch. Dunod, 1885.
- [263] T. Jankowiak, A. Rusinek, and T. Lodygowski, "Validation of the Klepaczko–Malinowski model for friction correction and recommendations on Split Hopkinson Pressure Bar," *Finite Elem. Anal. Des.*, vol. 47, no. 10, pp. 1191–1208, 2011.
- [264] K. Safa and G. Gary, "Displacement correction for punching at a dynamically loaded bar end," *Int. J. Impact Eng.*, vol. 37, no. 4, pp. 371–384, 2010.
- [265] M. A. S. Anwer, J. Wang, A. Q. Guan, and H. E. Naguib, "Chitin nano-whiskers (CNWs) as a bio-based bio-degradable reinforcement for epoxy: Evaluation of the impact of CNWs on the morphological, fracture, mechanical, dynamic mechanical, and thermal characteristics of DGEBA epoxy resin," *RSC Adv.*, vol. 9, no. 20, pp. 11063–11076, 2019.
- [266] M. Pyda and B. Wunderlich, "Reversing and nonreversing heat capacity of poly (lactic acid) in the glass transition region by TMDSC," *Macromolecules*, vol. 38, no. 25, pp. 10472–10479, 2005.
- [267] M. Tarfaoui, K. Lafdi, and A. El Moumen, "Performance of polymer composite-reinforced with carbon nanotubes," 2017.
- [268] A. El Moumen, M. Tarfaoui, and K. Lafdi, "Computational homogenization of mechanical properties for laminate composite-reinforced with thin film made of carbon nanotubes," *Appl. Compos. Mater.*, vol. 25, no. 3, pp. 569–588, 2018.
- [269] Y.-T. Lin *et al.*, "Improvement of mechanical properties and anticorrosion performance of epoxy coatings by the introduction of polyaniline/graphene composite," *Surf. Coatings Technol.*, vol. 374, pp. 1128–1138, 2019.
- [270] A. T. Mou'ad *et al.*, "Mechanical reinforcement with enhanced electrical and heat conduction of epoxy resin by polyaniline and graphene nanoplatelets," *Nanotechnol.*

- Rev.*, vol. 9, no. 1, pp. 1550–1561, 2020.
- [271] N. Norhakim, S. H. Ahmad, C. H. Chia, and N. M. Huang, “Mechanical and thermal properties of graphene oxide filled epoxy nanocomposites,” *Sains Malaysiana*, vol. 43, no. 4, pp. 603–609, 2014.
- [272] S. Khammassi and M. Tarfaoui, “Influence of exfoliated graphite filler size on the electrical, thermal, and mechanical polymer properties,” *J. Compos. Mater.*, 2020, doi: 10.1177/0021998320918639.
- [273] T. A. Vilgis, G. Heinrich, and M. Klüppel, *Reinforcement of polymer nano-composites: theory, experiments and applications*. Cambridge University Press, 2009.
- [274] X. Li *et al.*, “Nanomechanical characterization of single-walled carbon nanotube reinforced epoxy composites,” *Nanotechnology*, vol. 15, no. 11, p. 1416, 2004.
- [275] M. L. Oyen and R. F. Cook, “Load–displacement behavior during sharp indentation of viscous–elastic–plastic materials,” *J. Mater. Res.*, vol. 18, no. 1, pp. 139–150, 2003.
- [276] M. Lei, B. Xu, Y. Pei, H. Lu, and Y. Q. Fu, “Micro-mechanics of nanostructured carbon/shape memory polymer hybrid thin film,” *Soft Matter*, vol. 12, no. 1, pp. 106–114, 2016.
- [277] K. Yu, Q. Ge, and H. J. Qi, “Effects of stretch induced softening to the free recovery behavior of shape memory polymer composites,” *Polymer (Guildf.)*, vol. 55, no. 23, pp. 5938–5947, 2014, doi: <https://doi.org/10.1016/j.polymer.2014.06.050>.
- [278] Q. Zia, R. Androsch, H.-J. Radusch, and S. Piccarolo, “Morphology, reorganization and stability of mesomorphic nanocrystals in isotactic polypropylene,” *Polymer (Guildf.)*, vol. 47, no. 24, pp. 8163–8172, 2006, doi: <https://doi.org/10.1016/j.polymer.2006.09.038>.
- [279] M. T. Demirci, N. Tarakçioğlu, A. Avcı, A. Akdemir, and I. Demirci, “Fracture toughness (Mode I) characterization of SiO₂ nanoparticle filled basalt/epoxy filament

- wound composite ring with split-disk test method,” *Compos. Part B Eng.*, vol. 119, pp. 114–124, 2017.
- [280] M. Taşyürek and N. Tarakçıoğlu, “Enhanced fatigue behavior under internal pressure of CNT reinforced filament wound cracked pipes,” *Compos. Part B Eng.*, vol. 124, pp. 23–30, 2017.
- [281] Y.-P. Zheng, J.-X. Zhang, Q. Li, W. Chen, and X. Zhang, “The influence of high content nano-Al₂O₃ on the properties of epoxy resin composites,” *Polym. Plast. Technol. Eng.*, vol. 48, no. 4, pp. 384–388, 2009.
- [282] M. Uyaner and M. Kara, “Dynamic response of laminated composites subjected to low-velocity impact,” *J. Compos. Mater.*, vol. 41, no. 24, pp. 2877–2896, 2007.
- [283] C. Evcı and M. Gülgeç, “An experimental investigation on the impact response of composite materials,” *Int. J. Impact Eng.*, vol. 43, pp. 40–51, 2012.
- [284] H. B. Kaybal, H. Ulus, O. Demir, Ö. S. Şahin, and A. Avcı, “Effects of alumina nanoparticles on dynamic impact responses of carbon fiber reinforced epoxy matrix nanocomposites,” *Eng. Sci. Technol. an Int. J.*, vol. 21, no. 3, pp. 399–407, 2018, doi: <https://doi.org/10.1016/j.jestch.2018.03.011>.
- [285] E. Dal Lago, E. Cagnin, C. Boaretti, M. Roso, A. Lorenzetti, and M. Modesti, “Influence of Different Carbon-Based Fillers on Electrical and Mechanical Properties of a PC/ABS Blend,” *Polymers (Basel)*, vol. 12, no. 1, p. 29, 2020.
- [286] C. DeArmitt and K. Breese, “Filled polypropylene: a cost-performance comparison of common fillers,” *Plast. Addit. Compd.*, vol. 3, no. 9, pp. 28–33, 2001, doi: [https://doi.org/10.1016/S1464-391X\(01\)80252-X](https://doi.org/10.1016/S1464-391X(01)80252-X).
- [287] S.-Y. Fu, X.-Q. Feng, B. Lauke, and Y.-W. Mai, “Effects of particle size, particle/matrix interface adhesion and particle loading on mechanical properties of particulate–polymer composites,” *Compos. Part B Eng.*, vol. 39, no. 6, pp. 933–961,

- 2008, doi: <https://doi.org/10.1016/j.compositesb.2008.01.002>.
- [288] S. Aktaş and E. A. Diler, “A review on the effects of micro-nano particle size and volume fraction on microstructure and mechanical properties of metal matrix composites manufactured via mechanical alloying,” *Int. Adv. Res. Eng. J.*, vol. 2, no. 1, pp. 68–74, 2018.
- [289] L.-C. Tang *et al.*, “The effect of graphene dispersion on the mechanical properties of graphene/epoxy composites,” *Carbon N. Y.*, vol. 60, pp. 16–27, 2013.
- [290] B. Jiang, C. Liu, C. Zhang, B. Wang, and Z. Wang, “The effect of non-symmetric distribution of fiber orientation and aspect ratio on elastic properties of composites,” *Compos. Part B Eng.*, vol. 38, no. 1, pp. 24–34, 2007, doi: <https://doi.org/10.1016/j.compositesb.2006.05.002>.
- [291] S. Pradhan, R. Lach, H. H. Le, W. Grellmann, H.-J. Radusch, and R. Adhikari, “Effect of filler dimensionality on mechanical properties of nanofiller reinforced polyolefin elastomers,” *Int. Sch. Res. Not.*, vol. 2013, 2013.
- [292] H. Saghafi, M. Fotouhi, and G. Minak, “Improvement of the impact properties of composite laminates by means of nano-modification of the matrix—A review,” *Appl. Sci.*, vol. 8, no. 12, p. 2406, 2018.
- [293] J. Zhu *et al.*, “Reinforcing epoxy polymer composites through covalent integration of functionalized nanotubes,” *Adv. Funct. Mater.*, vol. 14, no. 7, pp. 643–648, 2004.
- [294] M. D. Frogley, D. Ravich, and H. D. Wagner, “Mechanical properties of carbon nanoparticle-reinforced elastomers,” *Compos. Sci. Technol.*, vol. 63, no. 11, pp. 1647–1654, 2003.
- [295] B. Ahmadi Moghadam, “Development of a Highly Resilient Graphene Nanoplatelet Resin/Adhesive,” 2015.
- [296] R. Atchudan, A. Pandurangan, and J. Joo, “Effects of nanofillers on the thermo-

- mechanical properties and chemical resistivity of epoxy nanocomposites,” *J. Nanosci. Nanotechnol.*, vol. 15, no. 6, pp. 4255–4267, 2015.
- [297] Y. S. Song and J. R. Youn, “Modeling of effective elastic properties for polymer based carbon nanotube composites,” *Polymer (Guildf)*, vol. 47, no. 5, pp. 1741–1748, 2006.
- [298] S. K. Lee, B. C. Bai, J. S. Im, S. J. In, and Y.-S. Lee, “Flame retardant epoxy complex produced by addition of montmorillonite and carbon nanotube,” *J. Ind. Eng. Chem.*, vol. 16, no. 6, pp. 891–895, 2010.
- [299] Y. S. Song and J. R. Youn, “Influence of dispersion states of carbon nanotubes on physical properties of epoxy nanocomposites,” *Carbon N. Y.*, vol. 43, no. 7, pp. 1378–1385, 2005.
- [300] M. M. Gallego, “Development of epoxy nanocomposites based on carbon nanostructures.” Universidad Rey Juan Carlos, 2015.
- [301] S. Khammassi, M. Tarfaoui, Y. Qureshi, and H. Benyahia, “Mechanical properties of graphene nanoplatelet-reinforced epikote 828 under dynamic compression,” *Mech. Mater.*, vol. 158, p. 103873, 2021, doi: <https://doi.org/10.1016/j.mechmat.2021.103873>.
- [302] W. Han, H.-P. Zhang, J. Tavakoli, J. Campbell, and Y. Tang, “Polydopamine as sizing on carbon fiber surfaces for enhancement of epoxy laminated composites,” *Compos. Part A Appl. Sci. Manuf.*, vol. 107, pp. 626–632, 2018, doi: <https://doi.org/10.1016/j.compositesa.2018.02.003>.
- [303] S. Han, Q. Meng, S. Araby, T. Liu, and M. Demiral, “Mechanical and electrical properties of graphene and carbon nanotube reinforced epoxy adhesives: experimental and numerical analysis,” *Compos. Part A Appl. Sci. Manuf.*, vol. 120, pp. 116–126, 2019.
- [304] S.-Y. Yang *et al.*, “Synergetic effects of graphene platelets and carbon nanotubes on

- the mechanical and thermal properties of epoxy composites,” *Carbon N. Y.*, vol. 49, no. 3, pp. 793–803, 2011.
- [305] C. E. Corcione, F. Freuli, and A. Maffezzoli, “The aspect ratio of epoxy matrix nanocomposite-reinforced with graphene stacks,” *Polym. Eng. Sci.*, vol. 53, no. 3, pp. 531–539, 2013.
- [306] J. A. King, D. R. Klimek, I. Miskioglu, and G. M. Odegard, “Mechanical properties of graphene nanoplatelet/epoxy composites,” *J. Appl. Polym. Sci.*, vol. 128, no. 6, pp. 4217–4223, 2013.
- [307] I. Zaman *et al.*, “Epoxy/graphene platelets nanocomposites with two levels of interface strength,” *Polymer (Guildf)*, vol. 52, no. 7, pp. 1603–1611, 2011.
- [308] M. R. Zakaria, M. H. A. Kudus, H. M. Akil, and M. Z. M. Thirmizir, “Comparative study of graphene nanoparticle and multiwall carbon nanotube filled epoxy nanocomposites based on mechanical, thermal and dielectric properties,” *Compos. Part B Eng.*, vol. 119, pp. 57–66, 2017.
- [309] M. Saberian, F. A. Ghasemi, I. Ghasemi, and S. Daneshpayeh, “Investigation on tensile properties of epoxy/graphene nano-platelets/carboxylated nitrile butadiene rubber ternary nanocomposites using response surface methodology,” *Nanomater. Nanotechnol.*, vol. 9, p. 1847980419855842, 2019.
- [310] M. Wang, H. Xue, Z. Feng, B. Cheng, and H. Yang, “Increase of tensile strength and toughness of bio-based diglycidyl ether of bisphenol A with chitin nanowhiskers,” *PLoS One*, vol. 12, no. 6, p. e0177673, 2017.
- [311] B. Wetzal, F. Hauptert, and M. Q. Zhang, “Epoxy nanocomposites with high mechanical and tribological performance,” *Compos. Sci. Technol.*, vol. 63, no. 14, pp. 2055–2067, 2003.
- [312] Y. Zhou, E. White, M. Hosur, and S. Jeelani, “Effect of particle size and weight

- fraction on the flexural strength and failure mode of TiO₂ particle-reinforced epoxy,” *Mater. Lett.*, vol. 64, no. 7, pp. 806–809, 2010.
- [313] D. Tzetzis and G. Mansour, “Nanoindentation, compression and fractural characterization of highly dispersed epoxy silica nanocomposites,” *J. Reinf. Plast. Compos.*, vol. 35, no. 7, pp. 541–555, 2016.
- [314] A. H. Majeed, “Effect of Ading Nanocarbon Black on The Mechanical Properties of Epoxy,” *Diyala J. Eng. Sci.*, vol. 7, no. 1, pp. 94–108, 2014.
- [315] J.-C. Lin, “Compression and wear behavior of composites filled with various nanoparticles,” *Compos. Part B Eng.*, vol. 38, no. 1, pp. 79–85, 2007.
- [316] M. Nachtane, M. Tarfaoui, Y. Ledoux, S. Khammassi, E. Leneveu, and J. Pelleter, “Experimental investigation on the dynamic behavior of 3D printed CF-PEKK composite under cyclic uniaxial compression,” *Compos. Struct.*, vol. 247, 2020, doi: 10.1016/j.compstruct.2020.112474.
- [317] M. Chihi, M. Tarfaoui, C. Bouraoui, and A. El Moumen, “Effect of CNTs additives on the energy balance of carbon/epoxy nanocomposites during dynamic compression test,” *Polymers (Basel)*, vol. 12, no. 1, p. 194, 2020.
- [318] M. Nachtane, M. Tarfaoui, S. Sassi, A. El Moumen, and D. Saifaoui, “An investigation of hygrothermal aging effects on high strain rate behaviour of adhesively-bonded composite joints,” *Compos. Part B Eng.*, vol. 172, pp. 111–120, 2019.
- [319] M. Tarfaoui, S. Choukri, and A. Nême, “Dynamic response of symmetric and asymmetric e-glass/epoxy laminates at high strain rates,” in *Key Engineering Materials*, 2010, vol. 446, pp. 73–82.
- [320] M. Tarfaoui, S. Choukri, and A. Nême, “Effect of fibre orientation on mechanical properties of the laminated polymer composites subjected to out-of-plane high strain rate compressive loadings,” *Compos. Sci. Technol.*, vol. 68, no. 2, pp. 477–485, 2008.

- [321] M. Tarfaoui, “Static and dynamic behavior of nano filled polymer based composites,” 2017.
- [322] Y. Tian *et al.*, “High strain rate compression of epoxy based nanocomposites,” *Compos. Part A Appl. Sci. Manuf.*, vol. 90, pp. 62–70, 2016, doi: <https://doi.org/10.1016/j.compositesa.2016.06.008>.
- [323] S. Rose, A. Dizeux, T. Narita, D. Hourdet, and A. Marcellan, “Time dependence of dissipative and recovery processes in nanohybrid hydrogels,” *Macromolecules*, vol. 46, no. 10, pp. 4095–4104, 2013.
- [324] N. K. Naik, K. S. Pandya, V. R. Kavala, W. Zhang, and N. A. Koratkar, “Alumina nanoparticle filled epoxy resin: High strain rate compressive behavior,” *Polym. Eng. Sci.*, vol. 54, no. 12, pp. 2896–2901, 2014.
- [325] Y. Guo and Y. Li, “Quasi-static/dynamic response of SiO₂–epoxy nanocomposites,” *Mater. Sci. Eng. A*, vol. 458, no. 1–2, pp. 330–335, 2007.
- [326] Qian Dong, and Wagner Gregory J, W. K. Liu, M.-F. Yu, and R. S. Ruoff, “Mechanics of carbon nanotubes ,” *Appl. Mech. Rev.*, vol. 55, no. 6, pp. 495–533, Oct. 2002, doi: 10.1115/1.1490129.
- [327] T. Gómez-del Río and J. Rodríguez, “Compression yielding of epoxy: Strain rate and temperature effect,” *Mater. Des.*, vol. 35, pp. 369–373, 2012.
- [328] S. Shadlou, B. Ahmadi-Moghadam, and F. Taheri, “The effect of strain-rate on the tensile and compressive behavior of graphene reinforced epoxy/nanocomposites,” *Mater. Des.*, vol. 59, pp. 439–447, 2014.
- [329] A. Taşdemirci, S. Yüksel, D. Karsu, E. Gültürk, I. W. Hall, and M. Güden, “Diatom frustule-filled epoxy: Experimental and numerical study of the quasi-static and high strain rate compression behavior,” *Mater. Sci. Eng. A*, vol. 480, no. 1–2, pp. 373–382, 2008.

- [330] J. Seaglar and C.-E. Rousseau, “Compressive evaluation of homogeneous and graded epoxy–glass particulate composites,” *Mater. Sci. Eng. C*, vol. 49, pp. 727–734, 2015.
- [331] C. Uzunpinar, “Effect of dispersion of swents on the viscoelastic and final properties of epoxy based nanocomposites.” 2010.
- [332] G. S. Lohar and B. F. Jogi, “Influence of carbon black (CB) on Mechanical Behaviour and Microscopic Analysis of Poly-propylene (PP)/ Acrylonitrile-butadiene- styrene (ABS) Nanocomposites,” *Procedia Manuf.*, vol. 20, pp. 85–90, 2018, doi: <https://doi.org/10.1016/j.promfg.2018.02.012>.
- [333] A. Jadhav, “High strain rate properties of polymer matrix composites,” 2003.
- [334] H. M. Hsiao, I. M. Daniel, and R. D. Cordes, “Strain rate effects on the transverse compressive and shear behavior of unidirectional composites,” *J. Compos. Mater.*, vol. 33, no. 17, pp. 1620–1642, 1999.
- [335] Ö. U. Colak, N. Bahlouli, D. Uzunsoy, and C. Francart, “High strain rate behavior of graphene-epoxy nanocomposites,” *Polym. Test.*, vol. 81, p. 106219, 2020, doi: <https://doi.org/10.1016/j.polymertesting.2019.106219>.
- [336] H. Eyring, “Viscosity, plasticity, and diffusion as examples of absolute reaction rates,” *J. Chem. Phys.*, vol. 4, no. 4, pp. 283–291, 1936.
- [337] E. M. Arruda, M. C. Boyce, and R. Jayachandran, “Effects of strain rate, temperature and thermomechanical coupling on the finite strain deformation of glassy polymers,” *Mech. Mater.*, vol. 19, no. 2–3, pp. 193–212, 1995.
- [338] S. Sassi, M. Tarfaoui, and H. Ben Yahia, “Dynamic thermomechanical behavior of adhesively-bonded composite joints,” 2017.
- [339] O. R. Shah, “Identification and characterization of mechanical and structural properties against static damage and fatigue of a composite floating wind turbine blade.” Brest, 2014.

- [340] L. Hamitouche, “Endommagement et rupture des assemblages en T de structures composites pour des applications navales.” Brest, 2008.
- [341] N. Al Habis, A. El Moumen, M. Tarfaoui, and K. Lafdi, “Mechanical properties of carbon black/poly (ϵ -caprolactone)-based tissue scaffolds,” *Arab. J. Chem.*, vol. 13, no. 1, pp. 3210–3217, 2020.
- [342] L. L. Zhai, G. P. Ling, and Y. W. Wang, “Effect of nano-Al₂O₃ on adhesion strength of epoxy adhesive and steel,” *Int. J. Adhes. Adhes.*, vol. 28, no. 1–2, pp. 23–28, 2008.
- [343] L. F. M. Da Silva and M. J. C. Q. Lopes, “Joint strength optimization by the mixed-adhesive technique,” *Int. J. Adhes. Adhes.*, vol. 29, no. 5, pp. 509–514, 2009.
- [344] S. M. J. Razavi, L. Sandnes, J. Torgersen, and F. Berto, “The effect of fiber orientation on fracture response of metallic fiber-reinforced adhesive thin films,” *Theor. Appl. Mech. Lett.*, vol. 8, no. 1, pp. 43–47, 2018.
- [345] Q. Rao, Z. Ouyang, and X. Peng, “Enhancing mode I fracture toughness of adhesively-bonded unidirectional composite joints using surfactant-stabilized multi-walled carbon nanotube and graphene nanoplate,” *Polym. Test.*, vol. 96, p. 107110, 2021, doi: <https://doi.org/10.1016/j.polymertesting.2021.107110>.
- [346] M. R. Ayatollahi, A. Nemati Giv, S. M. J. Razavi, and H. Khoramishad, “Mechanical properties of adhesively single lap-bonded joint-reinforced with multi-walled carbon nanotubes and silica nanoparticles,” *J. Adhes.*, vol. 93, no. 11, pp. 896–913, 2017.
- [347] O. R. Shah and M. Tarfaoui, “Determination of mode I & II strain energy release rates in composite foam core sandwiches. An experimental study of the composite foam core interfacial fracture resistance,” *Compos. Part B Eng.*, vol. 111, pp. 134–142, 2017, doi: <https://doi.org/10.1016/j.compositesb.2016.11.044>.
- [348] P. Davies *et al.*, “Comparison of test configurations for the determination of GIIC of unidirectional carbon/epoxy composites, an international round robin,” *Plast Rubber*

- Compos*, vol. 28, no. 9, pp. 432–437, 1999.
- [349] M. C. Ezzine, A. Amiri, M. Tarfaoui, and K. Madani, “Damage of bonded, riveted and hybrid (bonded/riveted) joints, Experimental and numerical study using CZM and XFEM methods,” *Adv. Aircr. Spacecr. Sci.*, vol. 5, no. 5, p. 595, 2018.
- [350] O. Essersi, M. Tarfaoui, S. W. Boyd, F. Meraghni, and R. A. Shenoi, “Dynamic study of adhesively-bonded double lap composite joints,” 2009.
- [351] E. Oussama, T. Mostapha, M. Fodil, B. Steven, and S. Ajit, “Experimental study of the strength of Aluminum/Aluminum and Composite/Composite adhesively-bonded joints under dynamic loading.”
- [352] Z. Jia, X. Feng, and Y. Zou, “Graphene Reinforced Epoxy Adhesive For Fracture Resistance,” *Compos. Part B Eng.*, vol. 155, pp. 457–462, 2018, doi: <https://doi.org/10.1016/j.compositesb.2018.09.093>.
- [353] “No Title.” <https://www.thomasnet.com/articles/adhesives-sealants/overview-of-adhesives/>.
- [354] S. Yu, M. N. Tong, and G. Critchlow, “Wedge test of carbon-nanotube-reinforced epoxy adhesive joints,” *J. Appl. Polym. Sci.*, vol. 111, no. 6, pp. 2957–2962, 2009.
- [355] X. Chen, I. J. Beyerlein, and L. C. Brinson, “Curved-fiber pull-out model for nanocomposites. Part 1: Bonded stage formulation,” *Mech. Mater.*, vol. 41, no. 3, pp. 279–292, 2009.
- [356] R. Campilho, D. C. Moura, D. J. S. Gonçalves, J. Da Silva, M. D. Banea, and L. F. M. da Silva, “Fracture toughness determination of adhesive and co-cured joints in natural fibre composites,” *Compos. Part B Eng.*, vol. 50, pp. 120–126, 2013.
- [357] M. De Moura, R. Campilho, and J. P. M. Gonçalves, “Crack equivalent concept applied to the fracture characterization of bonded joints under pure mode I loading,” *Compos. Sci. Technol.*, vol. 68, no. 10–11, pp. 2224–2230, 2008.

- [358] M. De Moura, J. P. M. Gonçalves, J. A. G. Chousal, and R. Campilho, “Cohesive and continuum mixed-mode damage models applied to the simulation of the mechanical behaviour of bonded joints,” *Int. J. Adhes. Adhes.*, vol. 28, no. 8, pp. 419–426, 2008.
- [359] J. P. R. Monteiro, R. Campilho, E. A. S. Marques, and L. F. M. Da Silva, “Experimental estimation of the mechanical and fracture properties of a new epoxy adhesive,” *Appl. Adhes. Sci.*, vol. 3, no. 1, pp. 1–17, 2015.
- [360] A. Dadian, S. Rahnama, and A. Zolfaghari, “Experimental study of the CTBN effect on mechanical properties and mode I and II fracture toughness of a new epoxy resin,” *J. Adhes. Sci. Technol.*, vol. 34, no. 22, pp. 2389–2404, 2020.
- [361] K. Zafeiropoulou, C. Kostagiannakopoulou, G. Sotiriadis, and V. Kostopoulos, “A Preliminary Study of the Influence of Graphene Nanoplatelet Specific Surface Area on the Interlaminar Fracture Properties of Carbon Fiber/Epoxy Composites,” *Polymers (Basel)*, vol. 12, no. 12, p. 3060, 2020.
- [362] Z. Jia, X. Feng, and Y. Zou, “An investigation on mode II fracture toughness enhancement of epoxy adhesive using graphene nanoplatelets,” *Compos. Part B Eng.*, vol. 155, pp. 452–456, 2018.
- [363] B. R. K. Blackman, A. J. Kinloch, and M. Paraschi, “The determination of the mode II adhesive fracture resistance, GIIC, of structural adhesive joints: an effective crack length approach,” *Eng. Fract. Mech.*, vol. 72, no. 6, pp. 877–897, 2005.
- [364] U. A. Khashaba, R. Othman, and I. M. R. Najjar, “Experimental analysis of composite scarf adhesive joints modified with multiwalled carbon nanotubes under bending and thermomechanical impact loads,” *Proc. Inst. Mech. Eng. Part L J. Mater. Des. Appl.*, vol. 234, no. 1, pp. 48–64, 2020.
- [365] A. H. Korayem, C. Y. Li, Q. H. Zhang, X. L. Zhao, and W. H. Duan, “Effect of carbon nanotube modified epoxy adhesive on CFRP-to-steel interface,” *Compos. Part B Eng.*,

- vol. 79, pp. 95–104, 2015.
- [366] G. Gkikas, D. Sioulas, A. Lekatou, N. M. Barkoula, and A. S. Paipetis, “Enhanced bonded aircraft repair using nano-modified adhesives,” *Mater. Des.*, vol. 41, pp. 394–402, 2012.
- [367] K. Park and G. H. Paulino, “Cohesive zone models: a critical review of traction-separation relationships across fracture surfaces,” *Appl. Mech. Rev.*, vol. 64, no. 6, 2011.
- [368] R. Kregting, “Cohesive zone models,” *preprint*, 2005.
- [369] L. Hamitouche, M. Tarfaoui, and A. Vautrin, “An interface debonding law subject to viscous regularization for avoiding instability: Application to the delamination problems,” *Eng. Fract. Mech.*, vol. 75, no. 10, pp. 3084–3100, 2008, doi: <https://doi.org/10.1016/j.engfracmech.2007.12.014>.
- [370] M. Tarfaoui, L. Hamitouche, S. Khammassi, and O. Shah, “Examination of the Delamination of a Stitched Laminated Composite with Experimental and Numerical Analysis Using Mode I Interlaminar,” *Arab. J. Sci. Eng.*, 2020, doi: 10.1007/s13369-020-04599-z.

Title: Nanotechnology and bonded joints: an investigation of the mechanical performance of an adhesive doped with nanofillers

Abstract: Adhesively bonded joint is a joining technique that is increasingly in a request today in many fields such as the automotive, aerospace, and naval. The adhesive selection is an important parameter to guarantee the reliability and durability of an adhesively bonded joint. It is well known that the wrong design of a bonded joint, the wrong choice of adhesive, or even a poorly executed surface treatment can have dramatic consequences. In terms of performance, the incorporation of carbon-based nanoparticles into the adhesive improves the performance of bonded joints. In this study, DGEBA adhesive doped by three kinds of nanofillers is established. Indeed, the adhesive has been doped with carbon nanotubes (CNT), graphene nanoplatelets (GNP), and carbon black (CB) with different mass fractions (1wt.%, 2wt.%, and 5wt.%). The overall objective is to study the influence of the type, mass fraction, and dimensions of the nanofillers on the mechanical behavior of the adhesive and the bonded joint. The results showed that each type of adhesive reinforced with nanofillers has a good potential in terms of mechanical behavior under static and dynamic loadings. However, the presence of a high mass fraction of nanoparticles tends to lead to degradation compared to the neat adhesive due to the transformation in microstructure morphology and physicochemical interactions. In addition, to quantify the damage resistance of the nanofiller-doped adhesive and demonstrate the adhesion compatibility with various kinds of substrates; DCB and ENF tests were performed on aluminum/aluminum and composite/composite bonded joints. Besides, numerical models taking into account the damage of the doped adhesive were developed and validated with the experimental results. This study demonstrates that the type, mass fraction, size, and shape of nanofillers play an important role in improving the performance of the adhesively bonded joints.

Keyword: Adhesive performance, Nanofillers, Adhesively bonded joint, Mechanical behavior, Damage, FE modeling

Titre: Nanotechnologie et assemblages collés: étude des performances mécaniques d'un adhésif dopé par des nanocharges

Résumé: Le collage structural est une technique d'assemblage de plus en plus demandée aujourd'hui dans beaucoup de domaines comme l'automobile, l'aéronautique, l'aérospatial, l'industrie navale et ferroviaire. La qualité d'un adhésif est un important paramètre pour garantir la fiabilité et la durabilité d'un assemblage collé. On sait qu'une fausse conception d'un joint collé, un mauvais choix d'adhésif ou même un traitement de surface mal réalisé pourra avoir des conséquences spectaculaires voire dramatiques. En termes de performance, l'ajout de nanoparticules à base de carbone à l'adhésif peut contribuer à améliorer les performances des assemblages collés. Dans cette étude, des adhésifs renforcés par trois types de nanocharges sont développés. En effet, l'adhésif DGEBA a été renforcé avec des nanotubes de carbone (CNT), des nanoplaquettes de graphène (GNP) et du noir de carbone (CB) avec différentes fractions massiques (1wt.%, 2wt.% et 5wt.%). L'objectif global est l'étude de l'influence du type, de la fraction massique et des dimensions des nanocharges sur le comportement mécanique de la colle et de l'assemblage collé. Les résultats ont montré que chaque type d'adhésif renforcé par des nanocharges possède un bon potentiel en termes de comportement mécanique sous des sollicitations statiques et dynamiques. Cependant, la présence d'une fraction massique élevée de nanoparticules a tendance à entraîner une dégradation par rapport à l'adhésif pur en raison du changement de morphologie de la microstructure et des interactions physico-chimiques. Et afin de quantifier la résistance à l'endommagement de l'adhésif dopé par des nanocharges et démontrer la compatibilité de l'adhésion avec divers substrats, des essais DCB et ENF ont été réalisés sur des assemblages Aluminium/aluminium et Composite/composite. De plus, des modèles numériques avec prise en compte de l'endommagement de la colle dopée ont été développés et validés avec les résultats expérimentaux. Cette étude démontre que le type, la fraction massique, la taille et la forme des nanocharges jouent un rôle important dans l'amélioration des performances des assemblages collés.

Mots clés: Adhésif, Assemblage Collé, Nanoparticules, Comportement Statique, Comportement Dynamique, Endommagement, Modélisation EF.